Kinetics and regulation of the chromaffin granule proton pump

Lorna Christina Webster

Thesis submitted for the degree of Doctor of Philosophy
University of Edinburgh
November 1995

Contents.

Chapter 4. Kinetics of H^+-translocation and ATP hydrolysis.

Chapter 5. Kinetics of N-ethylmaleimide inactivation of V-ATPases.

Declaration.

This thesis was composed by myself and the work presented herein was carried out by myself while a member of a research group directed and supervised by Dr. D.K. Apps. Some of the results presented have already been published.

Lorna Christina Webster
Department of Biochemistry,
University of Edinburgh Medical School,
Hugh Robson Building,
George Square,
Edinburgh.
EH8 9XD.

November 1995.

Acknowledgments.

First and foremost I would like to thank my supervisor, Dr. D.K. Apps for his invaluable advice, encouragement and friendship throughout the last three years as well as during my undergraduate studies.

Many thanks to Fariha Getlawi, Ian Thomson and Jan Mackintosh for help with membrane preparations, Dr. G.L. Atkins for running the computer optimisation programs, Dr M.B. Dutia for help with setting up the data collection system and Leo Cuifo for help with molecular biology techniques.

Special thanks also to Leo, Jan and Shahida Nasim for their constant friendship and advice.

Finally I am indebted to my family, Ian and Troyshin who are always around to keep me going.

Abstract.

Proton-translocating ATPases belong to three broad and distinct classes, termed P-, F- and V-types. The V-type (vacuolar) ATPases are present in intracellular membranes surrounding acidic compartments such as secretory granules and in the plasma membranes of certain specialised cell types. The secretory granule V-ATPase utilises the energy of ATP hydrolysis to generate an electrochemical gradient of protons that drives the secondary transport of small molecules across the granule membrane.

The ATPase from bovine adrenal secretory granules (chromaffin granules) was purified and reconstituted into proteoliposomes. The kinetics of ATP-dependent proton translocation were studied and a fluorimetric assay to allow accurate estimations of initial rates was developed. Rate analysis showed that the ATPase is allosterically regulated by MgADP: modelling studies predicted that it exists in two conformational states, with different activities and affinities for MgATP. Both conformational states have three binding sites for MgATP which bind MgADP competitively. MgADP also binds to a single regulatory site on the inactive conformational state. Other nucleotide diphosphates show the same properties as MgADP but have lower affinities.

It was shown that the covalently-reacting inhibitor N-ethylmaleimide (NEM) inactivates the ATPase in a pseudo-first order reaction. This inactivation was inhibited by the presence of micromolar concentrations of MgADP and other nucleotide diphosphates in a way that correlated with their regulatory features in proton translocation. The kinetics of protection were consistent with the two states of the enzyme being inactivated at different rates and also confirmed the existence of different types of binding site for MgADP. The three 72kDa (catalytic) subunits had the same rate constant for alkylation by NEM, suggesting that the enzyme is symmetrical.

Direct binding analysis confirmed the results of both the kinetics of proton translocation and protection from NEM. MgADP was shown to bind to the enzyme with a submicromolar dissociation constant and with a stoichiometry confirming the existence of a single regulatory site. Overall the results suggest that MgADP and other nucleotide diphosphates may be important physiological regulators of this enzyme.

The inhibitory effects of tributyltin and fluorescent tin complexes were studied and attempts were made to determine their site of binding. The fluorescent compounds exhibited fluorescent enhancement on binding to a dissociable subunit of the ATPase. This subunit was expressed in *E. coli* as a hexahistidine-tagged fusion protein, and its interaction with tin complexes studied. The fluorescence of the ATPase-tin complex was not altered on the addition of MgADP suggesting that the binding site is distant from any induced conformation changes.

Abbreviations.

ACA:	amino caproic acid
ACMA:	9-amino-6-chloro-2methoxyacridine
ADP:	adenosine-5′-diphosphate
ADPβS:	adenosine-5′-0-(2-thiodiphosphate)
ATP:	adenosine-5′-triphosphate
ATPase:	adenosine-5′-triphosphatase
BN-PAGE:	blue native polyacrylamide gel electrophoresis
BisTris:	bis(2-hydroxyethyl)imino-tris(hydroxymethyl)methane
BzBzATP:	2′-3′-0-(4-Benzoylbenzoyl)-adenosine-5′-triphosphate
BSA:	bovine serum albumin
$C_{12}E_8$:	octa-ethyleneglycol mono-n-dodecyl ether
$C_{12}E_9$:	polyoxyethylene-9-laurylether (Thesit)
CTP:	cytosine -5'-triphosphate
ΔμH+:	proton electrochemical gradient
ΔpH:	transmembrane pH difference (pH_{out}-pH_{in})
ΔΨ:	tramsmembrane potential
DBM:	dopamine-β-monooxygenase
DCCD:	N,N′-dicyclohexylcarbodiimide
DTT:	dithiothreitol
EDTA:	ethylenediamine tetraacetic acid
FCCP:	carbonyl cyanide p-trifluoromethoxyphenyl-hydrazone
GDP:	guanosine-5′-diphosphate
GTP:	guanosine-5′-triphosphate
H^+-ATPase:	proton translocating adenosine triphosphatase
HEPES:	N-(2-hydroxyethyl)piperizine-N′-2-ethanesulphonic acid
IDP:	inosine-5′-diphosphate
ITP:	inosine-5′-triphosphate
kDa:	Kilodalton
μCi:	microcurie
MBq:	Megabecquerel
Nbf-Cl:	4-chloro-7-nitrobenzofurazan (7-chloro-4-nitrobenzo-2-oxa-1,3-diazole)
NEM:	N-ethylmaleimide
n-OG:	n-octyl-β-D-glucopyranoside
PC:	phosphatidyl choline

PE:	phosphatidyl ethanolamine
PS:	phosphatidyl serine
PMSF:	phenylmethylsulphonyl fluoride
rpm:	revolutions per minute
SDS:	sodium dodecyl sulphate
SDS-PAGE:	sodium dodecyl sulphate polyacrylamide gel electrophoresis
TBS:	tris-buffered saline
TBq:	terabecquerel
TCA:	trichloroacetic acid
TEMED:	N,N,N'N'-tetramethylethylenediamine
TID:	3-(trifluoromethyl)-3-(imiodophenyldiazirine)
TLCK:	Na-p-tosyl-L-lysine chloromethylketone
TNP-ATP:	2'-3'-0-(2,4,6-trinitrophenyl)adenosine-5'-triphosphate
TPCK:	N-tosyl-L-phenylalanine chloromethylketone
Tris:	tris(hydroxymethyl)aminomethane
UTP:	uridine-5'-triphosphate

Chapter 1. Introduction.

1.1 The adrenal medulla.

The adrenal glands are located on the top of the kidneys and consist of the adrenal cortex and the adrenal medulla. These are distinct organs although evidence is accumulating of hormonal interaction between the two. The adrenal cortex contains several cell types, which synthesise and secrete into the plasma several steroids of two main classes: the glucocorticoids and the mineralocorticoids. The cells of the adrenal medulla secrete catecholamines (adrenalin and noradrenalin) and other components in response to stimulation of the splanchnic nerve. Histochemical studies have shown that adrenalin and noradrenalin occur in separate types of adrenal medullary cell and that these cell types have separate innervations. These cells contain secretory granules that stain brown with chromium salts and are known as chromaffin cells. The chromaffin granules are responsible for the synthesis, storage and secretion of catecholamines. Secretion occurs by the process of regulated exocytosis in which the granules undergo Ca^{2+}-triggered fusion with the plasma membrane and release their contents into the bloodstream (Burgoyne, 1991).

1.2 The chromaffin granule.

The chromaffin granule is composed of a single membrane bounding an inner acidic (pH5.5) soluble phase (Johnson and Scarpa, 1976) called the granule matrix.

1.2.1 The chromaffin granule matrix.

The non-protein components of the chromaffin granule matrix are catecholamines (550mM), nucleotides (mostly ATP, total 180mM), ascorbate (23mM), and cations such as Ca^{2+} (20mM), Mg^{2+} (5mM) and Na^{+} (22mM) (Winkler, 1976). The high concentration of catecholamines presents the problem of water entry by osmosis into the granule. It is thought that the nucleotides and proteins of the matrix interact with the catecholamines to lower their activity and avert this process (Carmichael and Winkler, 1985). Ascorbate is necessary for the synthesis of noradrenaline by hydroxylation of dopamine, a reaction catalysed by dopamine β-monooxygenase (EC.1.14.17.1).

The protein content of the matrix mainly consists of a family of acidic glycoproteins called the chromogranins or secretogranins. Chromogranin A (polypeptide M_r =48kDa, Iacangelo *et al*, 1986) is the major matrix protein in bovine chromaffin cells and has extensive O-linked glycosylation. It therefore does not bind mannose-specific lectins like Concanavalin A but after desialylation reacts with

galactose-specific lectins such as peanut agglutinin. Other members of this family present in the granule matrix are chromogranins B and C (sectretogranins I and II respectively) (Winkler *et al*, 1986). The chromogranins undergo significant proteolysis inside the granule resulting in the formation of small peptides. The function of these acidic glycoproteins is as yet unknown. Although it has been speculated that they may be involved in stabilising the granule, binding the large amounts of calcium or providing buffering capacity (chromogranin B has a pI significantly higher than the pH of the matrix) (Winkler *et al*, 1986); it is now thought that the proteolysis products of the chromogranins may function as neuropeptides. Other glycoproteins in the matrix include glycoproteins III, J and K. The function of glycoprotein III has not been determined (Palmer and Christie, 1990) but glycoproteins J and K have been identified as carboxypeptidases involved in protein processing (Hook *et al*, 1985). The enzyme dopamine β-monooxygenase (DBM) which is necessary for the synthesis of noradrenaline from dopamine is present in the matrix in a soluble form and also exists attached to the membrane of the granule perhaps via an anchor of hydrophobic amino acids such as an uncleaved signal sequence (Taljanidisz *et al*, 1989). Various small peptides are also present in the granule matrix, the major ones being the neuropeptides, enkephalins (Winkler *et al*, 1986). Soluble proteoglycans constitute about 3-4% of the total soluble proteins (Kiang *et al*, 1982) and again the function of these molecules is unknown.

1.2.2 The chromaffin granule membrane.

The major membrane proteins are dopamine monooxygenase, cytochrome-b561 and the proton translocating ATPase (H^+-ATPase). The functions of these proteins will be discussed at length later. Other proteins in the granule membrane include the glycoproteins II, III, J and K (Gavine *et al*, 1984; Pryde and Phillips, 1986), carriers for catecholamines, nucleotides and calcium, and the membrane-bound form of the carboxypeptidase B-like enzyme (Supattapone *et al*, 1984). Several proteins are present which may be involved in the process of exocytosis. These include synaptobrevin, synaptotagmin (p65), synaptophysin (p38) and SV2 (Schmidle *et al*, 1991). The functions of these proteins is still the subject of intense speculation: synaptobrevin is thought to be the V-SNARE involved in the fusion event; synaptotagmin, a calmodulin-binding protein, may be a calcium sensor for the exocytosis signal or a docking protein; synaptophysin has been speculated to be involved in the formation of a fusion pore/channel (Betz, 1990); and SV2 has a sequence which suggests a role in the transport of molecules across the granule membrane (Jahn and Südhof, 1994) although its substrate is unidentified.

1.2.2.1 Dopamine β-monooxygenase and cytochrome-b561.

Dopamine β-monooxygenase (DBM) was long ago identified as a major component of the chromaffin granule membrane. Membrane-bound dopamine monooxygenase accounts for 25-30% of the total membrane protein (Winkler and Westhead, 1990). As mentioned before this protein is the enzyme responsible for the synthesis of noradrenaline from dopamine and is a tetramer of subunits of molecular weight 70-75kDa (Winkler and Westhead, 1980). Cytochrome-b561 was recognised as a component of the chromaffin granule membrane more than twenty years ago (Flatmark *et al*, 1971) but it was not until much later that the function of this protein was elucidated. It had long been known that dopamine β-monooxygenase requires reducing equivalents to carry out the hydroxylation of dopamine to noradrenaline and that ascorbate was the likely source of these reducing equivalents in view of its presence in the granules (Ingebretsen *et al*, 1980). Since chromaffin granules have no mechanisms for importing ascorbate (Tirrel and Westhead, 1979) it seemed evident that they must have some mechanism for regenerating intravesicular ascorbate. It was shown that the electrons necessary for the hydroxylation of dopamine actually come from the oxidation of extravesicular ascorbate to semidehydroascorbate by cytochrome b-561 in the granule membrane. The electron from extravesicular ascorbate is carried on the cytochrome and then passed on to semidehydroascorbate in the granule matrix to regenerate ascorbate and it is this intravesicular ascorbate which becomes the substrate and electron donor for dopamine monooxygenase (Njus *et al*, 1986). Cytoplasmic semidehydroascorbate generated in this procedure is reduced to ascorbate by mitochondrial semidehydroascorbate oxidoreductase (Diliberto *et al*, 1987; Wakefield *et al*, 1986):

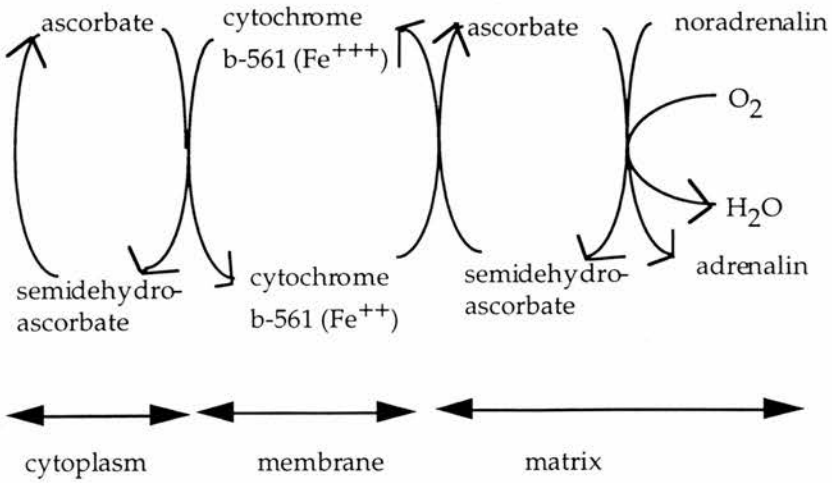

From cloning and sequencing of chromaffin granule cytochrome b-561 it has been suggested that there are six transmembrane helices (Perin *et al*, 1988). Clusters of positively charged amino acids have been shown to be present in the hydrophilic

loops on either side of the membrane which may facilitate interaction and electron flow between cytochrome b-561 and negatively-charged ascorbate and semidehydroascorbate (Kent *et al*, 1990).

1.2.2.2 ATPases of the chromaffin granule membrane.

The ATPases of the granule membrane comprise about 10% of the total membrane protein. ATPase I (H^+-ATPase) functions in the generation of an electrochemical proton gradient (positive and acidic inside) using the energy of ATP hydrolysis. This gradient is then used to drive the secondary active transport of some matrix components and is particularly important in the transport of catecholamines against a huge concentration gradient (Njus *et al*, 1981). Another ATPase, ATPase II has been identified in the chromaffin granule membrane (Percy *et al*, 1985). This enzyme has been shown to be distinct from the H^+-ATPase by its sensitivity to the inhibitor vanadate which has no effect on the H^+-ATPase and by insensitivity to dicyclohexylcarbodiimide and alkylating agents, which strongly inhibit ATPase I (Apps *et al*, 1983). ATPase II contributes approximately 30-40% of the total ATP hydrolysis capacity of the chromaffin granule membrane (Percy *et al*, 1985). The structure and function of ATPase II remains a mystery, although one possibility is that it catalyses the translocation of phospholipid from one side of the bilayer to the other (Zachowski *et al*, 1989; Zachowski, 1993). Its sensitivity to vanadate suggests that it is a member of the P-type class of ATPases. However since the elucidation of the role of ATPase I most research has concentrated on the biochemical and structural properties of this protein.

1.3 Ion-translocating ATPases.

The separation of prokaryotic cells from the external environment and the compartmentalisation of eukaryotic cells has dictated the need for transfer of material across biological lipid bilayers. The permeation of ions and other small molecules occurs through channels that are regulated by conversion between open and closed states or through permeases which are regulated in a more complex way. The proteins which carry out this transport are classified as either uniporters, where only one molecule is transported, or cotransporters which transport more than one molecule across the lipid bilayer. The cotransporters are further classified into two distinct types: symporters which transport all substrates in the same direction; and antiporters where substrates move in opposite directions. Often the transport of molecules requires the input of energy, for example when transport is directed against a concentration gradient or when the membrane potential is unfavourable to movement of charged substrates. Energy input is ultimately in the form of ATP,

either directly, where the transporter hydrolyses ATP and transports the ion or small molecule simultaneously, or indirectly, through secondary active transport. Secondary active transport involves two transporters: one hydrolyses ATP, generating a gradient of ion concentration (usually H^+) and usually of charge. This electrochemical gradient represents a store of energy which can be used by the second transporter, allowing the ions to flow back down the gradient. The energy generated is coupled to the movement of the principal ion or molecule against its concentration gradient. Protons migrate much faster than other ions through water because of their size and because they participate in hydrogen bonding and H^+/H_2O exchange (Harvey, 1992). It is not surprising then that it is protons which are the major ions transported to energise biological membranes.

1.3.1 Intravesicular acidification.

In the last two decades Mitchell's radical statement of the role of the proton motive force in bioenergetics (Mitchell, 1968) has clearly been vindicated. Proton-translocating adenosine triphosphatases are responsible for many proton-dependent processes including:
(1) pH control - both whole-body and cellular proton balance are to some extent maintained by the action of these enzymes;
(2) energy conservation through ATP synthesis at the expense of a proton motive force created by electron transport chains;
(3) the generation of a proton motive force at the expense of ATP which is used in the transport of small molecules;
(4) maintenance of the low pH in some subcellular compartments. In lysosomes and vacuoles this provides the optimal environment for the activity of acid hydrolases - the near neutral pH of the cytoplasm then prevents any "escaped" lysosomal hydrolases degrading the entire cell. In endosomes this low pH dissociates endocytosed ligands from their receptors.
Considerable evidence has accumulated over the last twenty years that the interior of both the endocytic and exocytic vacuolar apparatus in cells is maintained at a low pH (Mellman *et al*, 1986). The lumens of endocytic vesicles (Anderson *et al*, 1984), lysosomes (Poole and Ohkuma, 1981), portions of the trans-Golgi apparatus (Anderson and Pathak, 1985), some secretory vesicles (Johnson and Scarpa, 1984) and plant tonoplasts (Boller and Wienken, 1986) are acidic.

Several techniques have been used to study the function of low pH in these organelles. Some mutant cell lines that are defective in proton pumping are resistant to certain toxins and viruses that normally enter the cell by receptor-mediated endocytosis (Merion *et al*, 1983). Reagents that neutralise acidic compartments or

dissipate the proton gradient inhibit a variety of endocytic and exocytic activities including receptor recycling in receptor-mediated endocytosis (Brown *et al*, 1983), sorting of luminal and membrane proteins during exocytosis (Griffiths and Simons, 1986) and the post-translational processing of macromolecules that pass through the Golgi apparatus (Orci *et al*, 1985). pH indicators have been extensively used. Acridine orange and neutral red are basic dyes which accumulate in low pH compartments (Allison and Young, 1969) and allow visualisation of these compartments by fluorescence microscopy. Fluorescein-tagged molecules can be used to determine an actual pH value of these organelles since the spectrum of fluorescein is responsive to pH (Ohkuma and Poole, 1978). The first measurement of lysosomal pH in situ (pH 4.7-4.8) was made using fluorescein-tagged dextran (Ohkuma and Poole, 1978) and the luminal pH of fibroblast endosomes (pH 5.5) was determined using fluorescein-tagged α2-macroglobulin (Tyko and Maxfield, 1982). In the pathway of receptor-mediated endocytosis early endosomes are generally found to have a pH value between 5.5 and 6.3 while later endosomes generally have a pH of less than 5.5 (Mellman, 1992) Hence as incoming ligands and receptors progress through the endocytic pathway they encounter progressively more acidic conditions. Moreover, as the pH decreases the activity of acid-hydrolases increases so the recycling of receptors to the plasma membrane probably takes place before they reach the late endosomes and lysosomes to prevent their degradation.

Light microscopy is not of high enough resolution to study in detail the morphology of these acidic compartments. However the accumulation of weak bases in acidic compartments was used as the first step in developing a system for studying acidic compartments in the electron microscope. The weak base 3-[2,4,-dinitroanilino]3'amino-N-methyldipropylamine (DAMP) accumulates in acidic compartments, and can be fixed by formaldehyde or glutaraldehyde. Furthermore it contains a dinitrophenyl group, permitting easy detection in the electron microscope by a suitable monoclonal antibody tagged with gold. This technique has been used to identify various acidic compartments in several types of cell including CURL (compartment for uncoupling of ligand and receptor) apparatus in fibroblasts, lysosomes, a subpopulation of coated vesicles in fibroblasts, trans-Golgi vesicles, and secretory vesicles in insulin-secreting β cells (Anderson and Orci, 1988 and references therein). Some interesting insights were gained: individual endosomes in the same cell varied in their extent of acidification; the CURL does not have a uniform pH but is more acidic in the region where ligand receptor dissociation appears to occur than in the rest of the vesicular body (Anderson and Orci, 1988). In general, signals from fluorescein conjugate or DAMP experiments show that the extent of acidification increases in the order early endosomes<late

endosomes<lysosomes. Since the other ion permeabilities in these membranes do not vary in the same way as the pH does it seems that the differing pH values depend on the activity of a proton pump (Mellman, 1992). The existence of an active Na^+/K^+-ATPase in early endosomes may contribute to their mild pH (Fuchs *et al*, 1989) by increasing the negative membrane potential thereby limiting proton influx. Even though coated vesicles isolated from brain have been shown to contain a proton-translocating ATPase, this enzyme is probably a "passenger" en route from the plasma membrane back to neurosecretory vesicles and it has been shown that they do not translocate protons (Fuchs *et al*, 1994), possibly because of the absence of one or more of the vacuolar ATPase subunits. These observations illustrate the need for some form of regulation of the acidity of these intracellular organelles. This regulation may involve the proteins of the membranes of these organelles which transport protons from one side of the membrane to the other and it is also becoming apparent that anion transport (particularly chloride ions) across endomembranes has a role in regulation of ΔpH. If there were no transport of counteranions a rapid build up of membrane potential generated by proton translocation would limit further proton pumping thus inhibiting the generation of ΔpH (Al-Awqati *et al*, 1992).

The existence of three main classes of proton translocating ATPases termed P-, F- and V-type ATPases (Table 1.1), distinguished by their structure, function, mechanism of action and evolution is now accepted (Pedersen and Carafoli, 1987).

1.3.2 The P-type ATPases.

ATPases of the P-type are defined as those which form a phosphorylated intermediate as part of their reaction cycle. Examples of the type include the Na^+/K^+-ATPase (Forgac and Chin, 1985); the Ca^{2+}-ATPase of both the sarcoplasmic reticulum (Forgac and Chin, 1985) and the plasma membrane (Caroni *et al*, 1983); the gastric H^+/K^+-ATPase (Rabon *et al*, 1985); the plasma membrane H^+-ATPases of plants (Serrano, 1988), *Neurospora* (Perlin *et al*, 1984) and yeast (Malpartida and Serrano, 1981); and the K^+-ATPase of *Escherichia coli* (Laimins *et al*, 1978). Two of these enzymes are of particular pharmacological significance. The Na^+/K^+-ATPase plays a major role in the energisation of the plasma membrane of mammalian cells necessary for neurotransmitter uptake and presynaptic responses. The gastric H^+/K^+-ATPase is necessary for the production of gastric acid in the stomach and its overactivity can lead to the overproduction of acid and gastric ulcer formation (Nelson, 1991).

Most of the P-type ATPases have a major membrane-embedded subunit of 90-140kDa, (usually close to 100kDa, Figure 1.1). Normally this is the only subunit required for ATP-driven transport with the exceptions being the Na^+/K^+-ATPase,

ion	Source	Membrane	Class
H^+	Lower Eukaryotes (Yeast/fungi)	Plasma	P
K^+	Eubacteria:*E. coli, S. faecalis*	Inner	P
H^+/K^+	Higher eukaryotes (animals)	Plasma (intestine)	P
Na^+/K^+	Higher eukaryotes (animals)	Plasma	P
Ca^{2+}	Higher eukaryotes (animals)	Plasma	P
Ca^{2+}	Higher eukaryotes (animals)	Sarcoplasmic reticulum	P
Ca^{2+}	Higher eukaryotes (animals)	Lysosomes/Golgi	P
H^+	Lower eukaryotes	Vacuolar	V
H^+	Higher eukaryotes (plants)	Tonoplast	V
H^+	Higher eukaryotes (animals)	Lysosomes	V
H^+	Higher eukaryotes (animals)	Endosomes	V
H^+	Higher eukaryotes (animals)	Secretory granules	V
H^+	Higher eukaryotes (animals)	Storage granules	V
H^+	Higher eukaryotes (animals)	Clathrin-coated vesicles	V
$^*Na^+$	*E. hirae*	Inner	V
H^+	Bacteria	Inner	F
H^+	Eukaryotes (animal/fungi)	Mitochondrial inner	F
H^+	Plants	Chloroplast thylakoid	F
$^{**}H^+$	Archaebacteria	Inner	A

Table 1.1 Examples of some ion translocating ATPases discovered to date. The archaebacterial ATPase is a special case and is classed as an A-type ATPase. See reviews: Forgac, 1989; Pedersen and Carafoli, 1987; *Takase *et al*, 1993; **Ihara *et al*, 1992.

which also has a 50kDa glycosylated subunit required for activity (Forgac and Chin, 1985) and the E.*coli* K^+-ATPase which requires an additional two subunits for activity (Laimins *et al*, 1978). In all cases it is the large transmembrane 100kDa subunit which becomes phosphorylated by the γ-phosphate of ATP during the reaction cycle. Phosphorylation is stimulated by the presence of the ion to be translocated at the extracytoplasmic side (Forgac and Chin, 1985). The terminal phosphate of ATP is transferred to an aspartate residue in the active site before its transfer to a water molecule. This phosphorylation/dephosphorylation cycle is accompanied by conformational changes, linked to the transfer of ions through the enzyme. Due to the existence of two conformation states of the P-type enzymes they are often referred to as E_1E_2-type ATPases (Benaim *et al*, 1986). Some groups believe that the enzymes function as dimers (Hymel *et al*, 1984) while there is also evidence that they act as monomers (Pedersen and Carafoli, 1987). All the members of this class are inhibited by vanadate at concentrations of 100μM or less (Serrano, 1988). This inhibition is thought to be due to the fact that vanadate is an analogue of phosphate in the transition state. Other inhibitors of this class of enzyme include ouabain (Na^+/K^+-ATPase), dicyclohexyl carbodiimide, diethylstilbestrol (plasma membrane H^+-ATPase) and alkyltins (gastric H^+/K^+-ATPase) (Pedersen and Carafoli, 1987).

Many members of the P-type ATPase class have been cloned and sequenced and the primary sequences show significant homology indicating that the genes encoding these proteins have a common evolutionary origin. Extensive regions of the Na^+/K^+-ATPase and the sarcoplasmic reticulum Ca^{2+}-ATPase show greater than 50% homology, and the Ca^{2+}-ATPase and E. *coli* K^+-ATPase show greater than 40% homology in certain regions (Maclennan *et al*, 1985). The hydropathy plots are also very similar and indicate that the polypeptide chain traverses the membrane 8-10 times (Serrano, 1988). The most highly-conserved regions are, not surprisingly, those involved in ATP binding, phosphorylation, and coupling of transport to ATP hydrolysis. Regions dictating the specificity of ion binding appear to show the greatest divergence. It is quite striking in view of the overall similarity of these pumps that the family includes cotransporters of the antiport type (Na^+/K^+-ATPase, H^+/K^+-ATPase and the plasma membrane Ca^{2+}-ATPase which carries out H^+ antiport) (Forgac and Chin, 1985; Rabon *et al*, 1985) and uniporters (the plasma membrane H^+-ATPases of *Neurospora* and yeast) (Perlin *et al*, 1984; Malpartida and Serrano, 1981).

To date there have been no published high-resolution structures of P-type ion pumps, reflecting the difficulty in crystallising integral membrane proteins. Despite this problem electron microscopy has been used to determine structures to 14Å

resolution of the Ca^{2+}-ATPase (Stokes *et al*, 1994) but this is still not of high enough resolution to obtain direct evidence of the number and arrangement of transmembrane helices. Efforts are constantly being made to obtain crystals of better quality .

1.3.3 The F-type ATPases.

F- or F_1F_O-type ATPases (more accurately, ATP synthases) are found widely distributed in archaebacteria, aerobic and photosynthetic bacteria, and in mitochondria and chloroplasts. They are responsible for the generation of ATP from ADP and inorganic phosphate at the expense of an electrochemical gradient of protons generated by electron transport chains (Penefsky and Cross, 1991). F-type ATPases operate close to thermodynamic equilibrium and therefore, depending on the magnitude of the electrochemical gradient, they can function either in the synthesis of ATP or act in the reverse to hydrolyse ATP and create an electrochemical gradient of protons (Penefsky and Cross, 1991).

Under the electron microscope ATP synthase molecules have a tripartite "mushroom-like" appearance. Morphologically they consist of three distinct parts, a headpiece, a basepiece (the membrane sector) and a stalk connecting the other two. The head of the ATP synthases appears as a knob-like structures of around 10nm diameter sitting on the membrane surface (Pedersen and Amzel, 1993). Intact ATP synthases molecules are therefore composed of three parts morphologically but can be separated in biochemical experiments into two parts: a water-soluble, ATP-hydrolysing entity called F_1 and a detergent-soluble moiety called F_O through which the passive transport of protons can take place. The head is predominantly F_1 with the base being predominantly F_O. The stalk is distributed between both F_1 and F_O. F_O directs the electrochemical gradient of protons while F_1 utilises the energy from dissipation of the gradient in ATP hydrolysis (Penefsky and Cross, 1991).

F_1 from most species is composed of five different subunit types (Figure 1.1), $\alpha,\beta,\gamma,\delta$ and ε with molecular weights of around 55, 51, 30, 20 and 15kDa respectively (Foster and Fillingame, 1982). There is some variation in the subunit size in F-ATPases purified from different sources but this is very slight. The subunit stoichiometry is thought to be $\alpha_3\beta_3\gamma\delta\varepsilon$ (Schneider and Altendorf, 1987), giving a molecular mass for F_1 from mitochondria, chloroplasts and bacteria of around 400kDa. In *E.coli*, chloroplast and mitochondrial F-ATPases the α, β and γ subunits are highly homologous but the other subunits show variation between enzymes from different sources: the δ subunit of F_1 in chloroplasts and *E.coli* is the homologue of the OSCP subunit in the F_O portion of mitochondrial F-ATPase while the ε

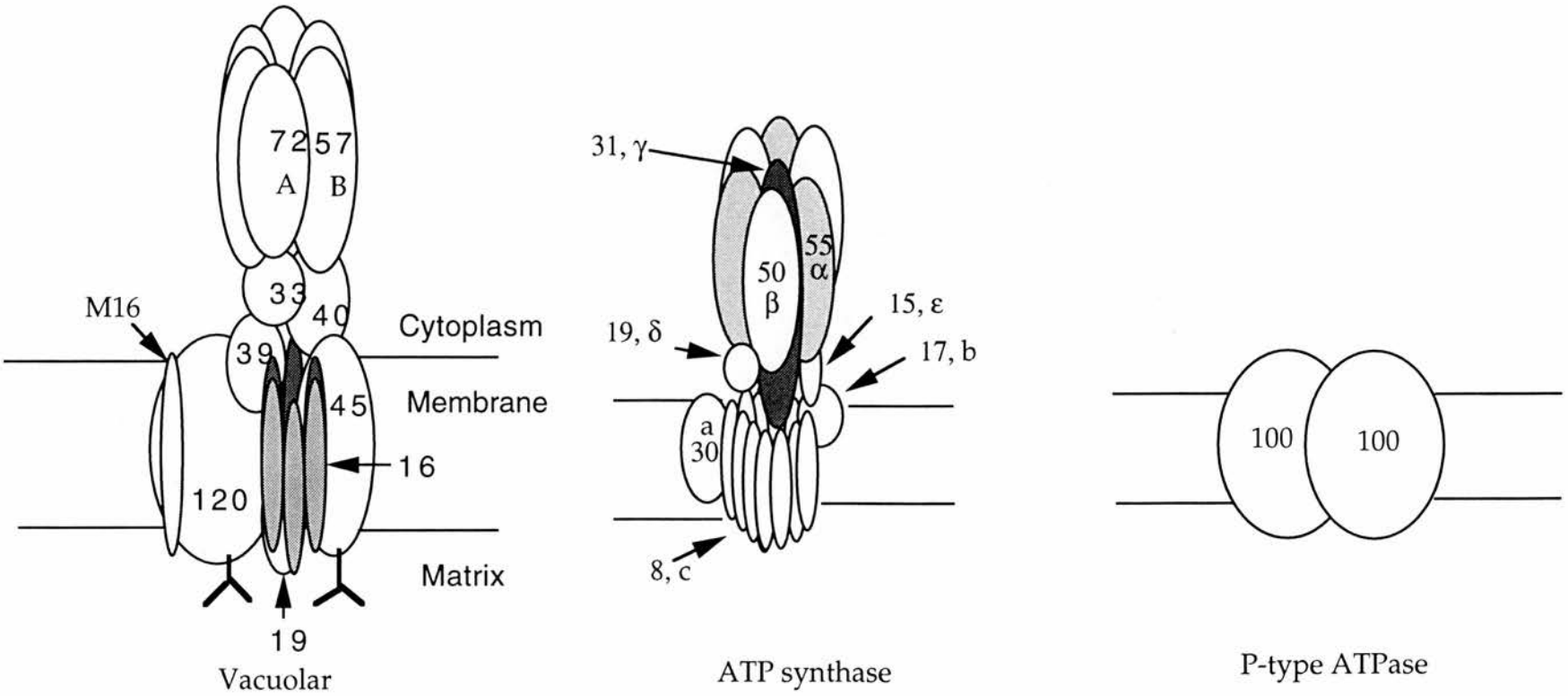

Figure 1.1 Diagrammatic representation of structures of the ion translocating ATPase classes. Molecular masses and corresponding nomenclature for the subunits are shown.

subunit in *E.coli* and chloroplasts is the homologue of the mitochondrial δ subunit (Walker *et al*, 1985). Despite the confusing nomenclature, the mitochondrial ε subunit has no counterpart in the chloroplast or *E. coli* enzymes (Pedersen, 1994). There is also extensive homology between the α and β subunits consistent with a common evolutionary origin (Walker *et al*, 1984; 1985). In mitochondrial ATP synthase there are often additional subunits associated with F_1. These are small peptides of around 12kDa called IF_1 which have been shown to inhibit the ATP hydrolysing activity of isolated F_1 (Pedersen and Amzel, 1993).

F-ATPases of E.*coli*, chloroplasts and mitochondria all have a common core of F_O consisting of three subunits termed a, b and c arranged in the stoichiometric ratio ab_2c_n. There is still controversy as to the value of n which ranges from 8-12 in the literature (Senior, 1988; Graber *et al*, 1990; Pedersen and Amzel, 1993). The molecular weights of the a, b and c subunits do not vary much between species and are around 30, 17, and 8kDa respectively (Foster and Fillingame, 1982). The E.*coli* F_O is the simplest membrane core of the F-ATPases while chloroplast F_O has an additional subunit called b'. At least an additional five subunits called d, e, OSCP, Factor 6 and A6L have been found in animal mitochondrial F_O (Pedersen and Amzel, 1993) with the presence of a sixth subunit called Factor B remaining controversial (Joshi and Hughes, 1981).

Subunit arrangement in the F-ATPases has been examined extensively with electron microscopic studies first revealing the presence of 6 or 7 distinct masses arranged in a hexagonal array (now known to represent alternating α and β subunits) around a central cavity (Gogol *et al*, 1989). The central cavity appeared to contain two α-helices (the seventh electron dense mass) running perpendicularly from the top of the hexagonal array into the stalk region of the structure now known to be the γ subunit (Abrahams *et al*, 1994; Capaldi *et al*, 1994). Recently the structure of F_1-ATPase was published (Abrahams *et al*, 1994) and illustrates the importance of the γ subunit in interacting with individual pairs of α and β subunits in the mechanism of rotational catalysis. The subunit arrangement of the F_O portion is still very much a matter of controversy. In general there is agreement that the copies of subunit c are arranged in an oligomeric array with a central pore through which protons are thought to move but the position of the other subunits is still the matter of intense speculation.

Inhibitors of F-ATPases (Table 1.2) have been reviewed in depth (Linnet and Beechey, 1979). F-ATPases are inhibited specifically by oligomycin only if the OSCP (oligomycin sensitivity-conferring protein) subunit of the stalk and also subunit 9 of F_O are present. Venturicidin (which binds to F_O) and aurovertin (which binds to the

Inhibitor	ATPase class		
Nbf-Cl	P	V	F
Quercetin	P	V	F
Trialkyltins	P	V	F
DCCD		V	F
Diethylstilbestrol		V	F
NEM	P	V	
Omeprazole	P	V	
Vanadate	P		
Oligomycin			F
Venturicidin			F
Efrapeptin			F
Aurovertin			F
Fusidic acid		V	
Suramin		V	
Bafilomycin A1		V	
Concanamycin		V	

Table 1.2 Classification of ion-translocating ATPase by inhibitor specificity. Although all classes have specific inhibitors there are several which inhibit two or all of the classes but with differing affinity.

β subunit of F1) also inhibit F-ATPases in a specific manner. The lipophilic polypeptide efrapeptin appears to bind to F_1, preventing binding of inorganic phosphate and thus inhibiting ATP synthesis. Other inhibitors of ATP synthases are less specific and include NN'-dicyclohexylcarbodiimide (DCCD), diethylstilbestrol (DES), trialkyltins and 4-chloro-7-nitrobenzofurazan (Nbf-Cl). DCCD inhibits proton translocation by reacting covalently with a single carboxyl group (glutamic or aspartic acid) located in a stretch of hydrophobic amino acids on the c subunit in F_O. This inhibitor was the main tool in determining the importance of this subunit in the transport of protons. The sensitivity of V-ATPases to DCCD provided the first clue that the mechanisms of proton translocation in the V- and F-ATPases may be related via subunit homologues. At neutral pH Nbf-Cl inhibits ATP hydrolysis by F_1 by modifying a tyrosine residue on the β subunit whereas at higher pH its reaction is with thiol groups and can be reversed with sulphydryl reagents, but migration of the inhibitor within the enzyme structure may cause irreversible inhibition by reaction with a lysine residue. The site of interaction of trialkyltins (Usta and Griffiths, 1993) and DES (McEnery and Pedersen, 1986) is likely to be on F_O.

Subunit function and the mechanism of ATP hydrolysis/synthesis and proton translocation in F-ATPases have been the subject of intensive research. Nucleotide binding by the ATP synthases has been studied in many laboratories. The F_1 moiety contains 6 adenine nucleotide-binding sites, of which 3 exchange readily with medium nucleotides during ATP hydrolysis (Cross and Nalin, 1982). Nucleotides bound at the 3 remaining non-exchanging sites may have a regulatory or structural role. Nucleotide binding sites are at the interfaces between the α and β subunits (Abrahams *et al*, 1994). The catalytic sites are predominantly formed by β subunits with some α subunit side chains contributing to the binding site and the converse holds true for the non-exchangeable, non-catalytic sites. F_1 preparations have also been shown to have a very tight binding site for Mg^{2+} and 2 or more inorganic phosphate binding sites (Pedersen and Carafoli, 1987) although the subunit location of these binding sites has not been clearly demonstrated. The recent X-ray structure of F_1 suggests that movement of the γ subunit is fundamentally important in the mechanism of rotational catalysis proposed for ATP hydrolysis/synthesis (Abrahams *et al*, 1994). Probably, rather than the $\alpha_3\beta_3$ complex rotating around a central core, the γ subunit rotates inside this core to interact with αβ pairs and alter their binding capacity. This mechanism would prevent hindrance to rotation by friction with the medium: the central core of F1 is thought to be lined with hydrophobic amino acid side chains to allow almost frictionless rotation of the γ subunit (Abrahams *et al*, 1994). Other evidence for conformational changes in the γ

subunit on ATP binding also supports this role (Turina and Capaldi, 1994). The function of the other subunits in F_1 is still a matter of controversy and there is much speculation as to their role in energy/information transfer to the membrane sector through conformation change.

The function of the subunits of the membrane sector has also been studied extensively but their very nature as integral membrane proteins makes their study intrinsically more difficult than that of F_1. The importance of the proteolipid subunit c in proton conduction has been mentioned above but oligomeric arrangements of this subunit in *E. coli* cannot support proton transport alone, indicating that subunits a and b must have some role in opening/regulation of the channel (Schneider and Altendorf, 1985). In eukaryotes the other subunits of F_O are also necessary for proton transport.

The generally-accepted mechanism for ATP synthesis by the F-ATPases is the binding-change mechanism recently critically reviewed by Boyer (1993). This mechanism assumes that the three catalytic sites are always in different states, either open, loose or tight, and the sites alternate in sequence between these states to perform synthesis of ATP (Figure 1.2). The open site has very low affinity for ligands, is catalytically inactive, and after a conformational change becomes the loose site which binds the ligands ADP and inorganic phosphate still with low affinity and still catalytically inactive. The loose site with the substrates bound then becomes the tight site, which has very high affinity for ligands, and is catalytically active, forming ATP with the release of a water molecule. To complete the cycle the tight site becomes open, resulting in release of ATP. The obvious asymmetry required for this type of mechanism has been confirmed by X-ray crystallography. Some variations on this model have been proposed which combine asymmetrical and symmetrical structures of the ATPase since some groups are insistent that the F-ATPase shows three fold symmetry (Pedersen, 1994). Clearly it will be some time before a consensus of opinion is reached.

The mechanism of coupling of the energy of proton translocation to ATP synthesis in the F-ATPases is increasingly becoming the subject of intense research as a result of the detailed mechanism put forward for nucleotide binding and rotational catalysis. Catalytic sites are approximately 35Å from the bottom of F_1; including the length of the stalk they are 75Å away from the F_O portion (Capaldi, 1994). In view of this distance and the difficulty of creating a proton pore in the narrow stalk, direct proton transfer seems unlikely. Evidence to support this comes from the bacterium *Propionigenium modestum* F_1F_O-ATPase which can easily interchange Na^+ or H^+ ions (Laubinger and Dimroth, 1989). It seem likely therefore that the energy from translocation is communicated to F_1 through conformation changes in the subunits

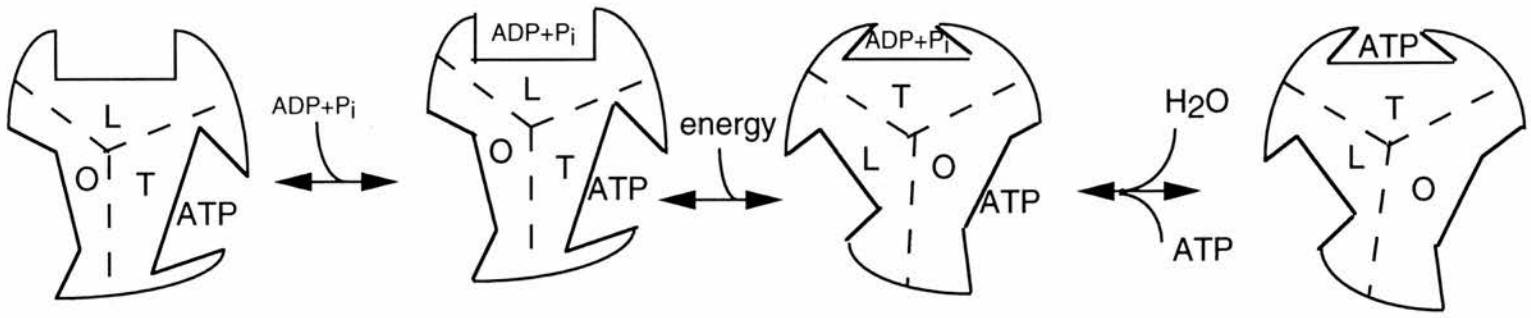

Figure 1.2 Diagramattic representation of the asymmetric binding change mechanism for ATP synthesis by mitochondrial ATP synthase.The open (O), loose (L) and tight (T) sites are indicated. Energy is required to produce the conformation change resulting in the conversion of loose to tight sites.

of the stalk. A recent model (Figure 1.3) was proposed for the mechanism of ATP synthesis driven by a proton motor (Walker J.E., personal communication). In this model the a and b subunits of F_O represent the points of entry and exit of protons. After entry to F_O the protons must interact with a subunit c moiety arranged in a circular array of c subunits with the γ subunit in the central core. Rotation around 360° of the c subunit arrangement drives the γ subunit through 360° and is necessary to allow the proton to exit at the opposite site of the membrane. This rotation will allow synthesis of 3 ATP molecules according to the binding change model and the H^+/ATP stoichiometry assuming the absence of proton slip, will depend on the number of c subunits in the motor: 12 subunits will give a stoichiometry of 4 while 9 c subunit should give $3H^+$/ATP. Ultimately a high resolution structure of F_O or of F_1 with stalk attached may be the only way to test this model.

1.3.4 The V-ATPases.

Vacuolar ATPases have been identified in a diverse range of organisms and cellular locations. Examples of V-ATPases include those found in eukaryotic endomembranes such as chromaffin granule membranes (Cidon and Nelson, 1983), synaptic vesicle (Cidon and Sihra, 1989; Moriyama and Futai, 1990) and coated vesicle membranes (Xie *et al*, 1984; Xie and Stone, 1986), lysosomal (Schneider, 1981; Arai *et al*, 1993), and Golgi membranes (Moriyama and Nelson, 1989), the vacuolar membranes of *Neurospora crassa* (Bowman and Bowman, 1982)and *Saccharomyces cerevisiae* (Kane *et al*, 1989) and the tonoplast of plants (Randall and Sze, 1986; Warren *et al*, 1992). Although once thought to occur only in endomembranes more recently these enzymes have been found in the plasma membranes of various cell types and in different species. Examples of this type of V-ATPase include those found in the plasma membranes of bovine kidney cells (Gluck and Caldwell, 1987), osteoclasts (Väänänen *et al*, 1990), tobacco hornworm (*Manduca sexta*) midgut cells (Wieczorek *et al*, 1989), eubacteria (Takase *et al*, 1993; Yokoyama *et al*, 1994) and archaebacteria (Inatomi, 1986; Konishi *et al*, 1987; Ihara and Mukohata, 1991). The method of independent regulation of this diverse range of V-ATPases, which are often present in different locations in the same cell, is not understood, but it is thought that the presence or absence of accessory subunits will be a distinguishing feature and may also be responsible for targetting of enzymes in the same cell to different locations. A novel 14kDa subunit has been identified in the V-ATPase complex in Tobacco hornworm midgut which may be a candidate for this role (Gräf *et al*, 1994).

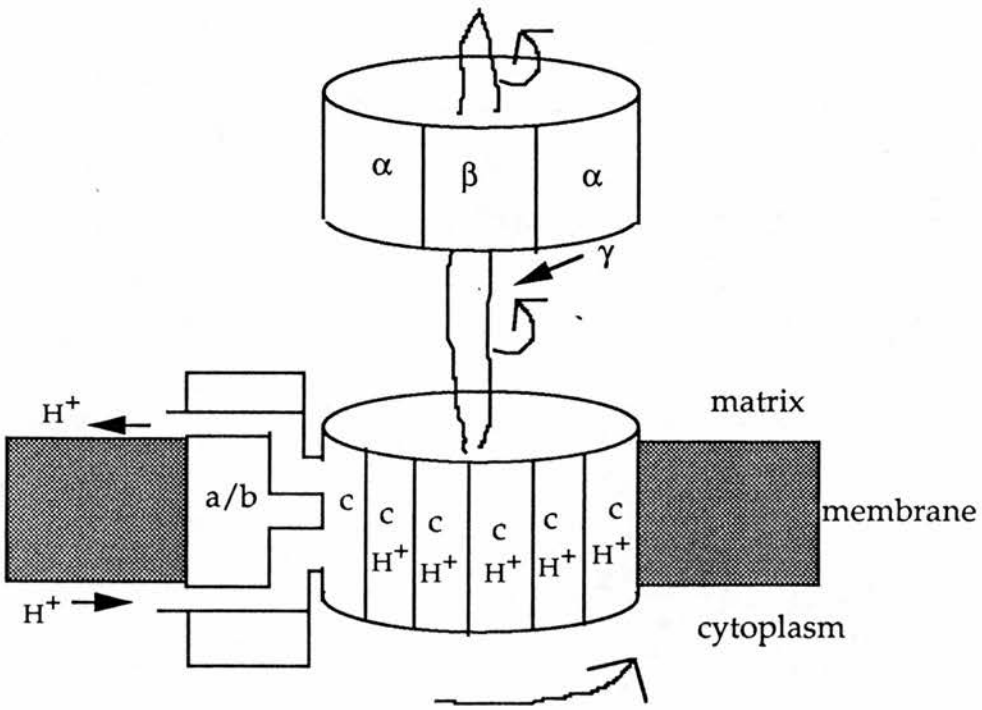

Figure 1.3 Diagrammatic representation of a model proposed for coupling of proton translocation to ATP synthesis.

1.3.4.1 Morphology, subunit composition, arrangement and topology.

Viewed by electron microscopy the V-ATPase enzymes have a similar morphology the F-type ATP synthases. A "ball and stalk" structure is seen on the surface of the lipid bilayer with the diameter of the "ball" being about 10nm, comparable to the 9nm F_1 particle (Taiz *et al*, 1989; Bowman *et al*, 1989; Moriyama *et al*, 1991). The use of phosphotungstic acid as a stain causes dissociation of the "ball" from the membrane (Taiz *et al*, 1989) as does treatment with nitrate (or high concentrations of various salts) and MgATP at 0°C (Bowman *et al*, 1989; Moriyama *et al*, 1991)which suggested that the "ball" represented the V_1 component of the V-ATPases. This was confirmed by the use of antibodies against the 72 and 57kDa subunits of the chromaffin granule ATPase (Moriyama *et al*, 1991) and by direct identification of the release of six polypeptides from the *Neurospora crassa* ATPase of 69, 59, 48, 30, and 17kDa (Bowman *et al*, 1989). F-type ATPases differ in that F_1 is not released from its membrane sector under these conditions. The integral membrane component of the V-ATPases is known as V_O by analogy with F_O although it is not, of course, inhibited by oligomycin.

Although V-type ATPases have now been purified from various sources and the subunit composition studied extensively there is still much controversy regarding this feature (Table 1.3). Initially three major subunits were identified as being common to all V-ATPases (Table 1.3). These were around 70, 60 and 16kDa (Bowman *et al*, 1986; Manolson *et al*, 1985; Randall and Sze, 1986; Uchida *et al*, 1985; Forgac, 1989). Immunological evidence has shown these subunits to be highly conserved: antibodies against the 57 and 67kDa subunits of beet tonoplasts were shown to cross-react with subunits of similar masses in clathrin-coated vesicles, yeast vacuolar and chromaffin granule membranes (Moriyama and Nelson, 1989b, c; Manolson *et al*, 1989). It is now apparent however, that all V-ATPases studied are much more complicated than this, and have many additional subunits. In V-ATPases from higher plants seven (Parry *et al*, 1983), eight (Kane *et al*, 1989) and ten (Matsuura-Endo *et al*, 1990) subunits have been reported. Animal cell V-type ATPases are similar with nine, and ten subunits reported in clathrin-coated vesicles (Forgac, 1992) and kidney epithelial cell plasma membrane V-ATPase (Gluck and Caldwell, 1987) respectively. Other endomembrane V-ATPases such as those from lysosomal and Golgi membranes have been shown to consist of a similar number of subunits (Table 1.3). It should be noted that the V-ATPase in clathrin-coated vesicles is inactive and is probably a "passenger", and has arisen from membrane retrieval after neurosecretory vesicle exocytosis (Fuchs *et al*, 1994).

A consensus for the subunit composition of the V-ATPase from chromaffin granule membranes has still to be reached. At least five subunits have been shown

Endomembrane V-ATPases	**Subunit composition**									**Reference**
Source	**Mr(kDa)**									
Bovine chromaffin granules	115	72	57	45	40	39	33	19	16	1,2
Bovine clathrin-coated vesicles	100	73	58		40	38	34/33	19	17	3
Bovine brain synaptic vesicles	115	72	57		41		34/33			4,5
Lysosomal membranes		72	57		41		34/33	18	15	6
Golgi membranes		72	57		41		34/33	30	16	7
Saccharomyces cerevisiae vacuole	100	69	60	42	36	32	27		17	8
Neurospora crassa vacuole	100	67	57	48	40	30	20	17	16	9
Red beet tonoplast	100	67	55	52	44	32			16	10
Oat root tonoplast		70	60	44	42	36	32	29	16	11
Mung bean tonoplast		68	57	44	38	37	32		16	12
Plasma membrane V-ATPases										
Kidney epithelial cells		70	56	45	42	38	33/31	15	14	13,14
Osteoclasts	115	63	57			39			16	15
Tobacco hornworm midgut		67	56	43	40	28	20	17	16	16
Eubacterial (*T. thermophilus*)	100	66	56		38	30	24	12	13	17
Archaebacterial (*S. acidocaldarius*)		69	54				28		8	18

References.

1 Moriyama and Nelson, 1987a
2 Percy and Apps, 1985
3 Arai *et al*, 1987b
4 Moriyama and Futai, 1990
5 Cidon and Sihra, 1989
6 Moriyama and Nelson, 1989a
7Moriyama and Nelson, 1989b
8 Kane *et al*, 1989
9 Bowman *et al*, 1992
10 Parry *et al*, 1989
11 Randall and Sze, 1986
12 Matsuura-Endo *et al*, 1990
13 Gluck and Caldwell, 1987
14 Wang and Gluck, 1990
15 Chatterjee *et al*, 1992
16 Wieczorek, 1992
17 Yokoyama *et al*, 1994
18 Konishi *et al*, 1987

Table 1.3 Subunit composition of Vacuolar ATPases from various sources.

to be essential for activity. These are of molecular masses 115, 72, 57, 40, and 16kDa (Cidon and Nelson, 1983, 1986; Moriyama and Nelson, 1987a, b; Percy *et al*, 1985). A subunit of molecular weight 33kDa at first seen only by one group studying the chromaffin granule ATPase (Percy *et al*, 1985) is now accepted as a *bona fide* part of the enzyme complex. More recently subunits of apparent molecular mass 45 (Supek *et al*, 1994) and 39kDa (Siebert *et al*, 1994) have been identified as accessory subunits with the 45kDa subunit being found to be glycosylated. Immunological cross-reactivity was observed with the 45kDa in purified bovine kidney microsomes but not in the plasma membranes of kidney epithelial cells suggesting that this subunit may have a function in subcellular localisation of the V-ATPases within the same cell. Even more recently another subunit named M16, distinct from the 16kDa subunit previously identified, was also identified in the chromaffin granule V-ATPase complex (Supekova *et al*, 1995). These three accessory subunits are thought to be part of the membrane sector of the ATPase .

The subunit stoichiometry has been determined in the V-ATPase isolated from bovine brain clathrin-coated vesicles by use of quantitative amino acid analysis (Arai *et al*, 1988). Results suggested that each complex consists of three of each of the 70 and 60kDa subunits, six copies of the 16kDa subunit and one each of the other subunits. Densitometric analysis of the ATPase from higher plants (Parry *et al*, 1989; Ward *et al*, 1992) is consistent with the results of amino acid analysis. This stoichiometry would give a molecular mass for the entire ATPase complex of around 750kDa although the real value is probably greater than 900kDa which is consistent with that seen in gel filtration studies (Arai *et al*, 1988; Gluck and Caldwell, 1987; Moriyama and Nelson, 1989a; Bowman *et al*, 1989; Kane *et al*, 1989; Parry *et al*, 1989) suggesting that additional subunits remain to be identified.

Topographical studies on chromaffin granules (Apps *et al*, 1989) and on reconstituted ATPase from clathrin-coated vesicles (Arai *et al*, 1988; Adachi *et al*, 1990a) show that polypeptides of the peripheral membrane sector V_1 are labelled by membrane-impermeant reagents and are thus oriented to face the cytoplasmic side of the membrane as had been indicated in the electron microscopic studies. Proteolytic cleavage of the V_1 subunits of the reconstituted enzyme by trypsin was also consistent with this orientation (Adachi *et al*, 1990a). Detergent permeabilisation of intact vesicles caused increased labelling and proteolysis of the large 100kDa subunit and the 19 and 17kDa subunits of the membrane sector suggesting that they are likely to possess some luminally-oriented peptide chain. The sialic acid glycosylation of the 100-116kDa subunit detected by neuraminidase digestion and binding to peanut lectin provided further evidence of exposure to the luminal side since this carbohydrate is found exclusively on the extra-cytoplasmic side of

biological membranes (Adachi *et al*, 1990b). The interaction of subunits with components of the lipid bilayer was studied using the photoactivable reagent [^{125}I]-3-(trifluoromethyl)-3-(imidophenyldiazirine) ([^{125}I]-TID). Extensive labelling of the hydrophobic 16kDa subunit was seen suggesting major contacts with the lipid bilayer and while there was some labelling of the 100kDa subunit there was no labelling of the 38 and 19kDa subunits which suggests that these subunits remain attached to the membrane sector on chaotropic treatment through protein-protein interaction (Arai *et al*, 1988). Cloning and sequencing of the 100kDa subunit suggests the presence of six putative transmembrane helices (Perin *et al*, 1991) consistent with the [^{125}I]-TID labelling. The homologue of the 38kDa subunit in chromaffin granules has also been cloned and sequenced and the absence of any putative transmembrane helices confirms the above observations (Wang *et al*, 1988).

1.3.4.2 Subunit function .

1.3.4.2.1 Nucleotide binding subunits.

The 67-72kDa subunit identified as a component of the peripheral V_1 sector in all V-ATPases studied to date has been shown to be labelled with [^{3}H]-N-ethylmaleimide and [^{14}C]-Nbf-Cl. Labelling and inactivation occurs in an ATP-protectable manner in the V-ATPase from chromaffin granule membranes (Moriyama and Nelson, 1987b; Percy and Apps, 1986), coated vesicles (Arai *et al*, 1987b, *Neurospora crassa* vacuoles (Bowman *et al*, 1986), plants (Mandala and Taiz, 1986; Randall and Sze, 1987) and yeast (Uchida *et al*, 1988). This was the first indication (and is still the best evidence) that this subunit is the location of the catalytic site. The cysteine residue responsible for inactivation by NEM is found in a known nucleotide binding motif, the "Walker consensus sequence" (Walker *et al*, 1985) consistent with the nucleotide protection data. Further evidence for the function of the 73kDa subunit in nucleotide binding comes from interaction with the nucleotide analogue TNP-ATP. This analogue appears to bind to the V-ATPase of coated vesicles at two distinct sites with K_D values of 50nM and 3μM and is able to protect both the 73 and 58kDa subunits from tryptic cleavage (Adachi *et al*, 1990a). Very recently a recombinant 73kDa subunit from coated vesicles was shown to be photoaffinity labelled with [α^{32}P]-ATP on UV irradiation and although the recombinant subunit alone could not support ATP hydrolysis when added back to the membrane sector with the additional head subunits an active complex was formed (Peng *et al*, 1994b). This suggests that ATP hydrolysis is dependent on the 73kDa subunit and its inter-subunit interactions.

An interesting feature of the nucleotide-binding subunit in yeast (69kDa) is its generation from self-splicing of a larger 119kDa precursor protein with the excision of a 50kDa spacer protein ("intrein") and reformation of a peptide bond (Cooper *et al*

1993). This is one of the few instances where intervening sequences are excised at the protein rather than the RNA level and may represent a regulatory feature of the V-ATPases.

The 57kDa subunit has also been implicated in nucleotide binding based on its labelling with the photoactivable analogue 3-O-(4-benzoyl)-benzoyladenosine-5'-triphosphate (Manolson *et al*, 1985). Further evidence comes from labelling of a recombinant 58kDa subunit from coated vesicle V-ATPase. The recombinant subunit was labelled by [α^{32}P]-ATP, [^{14}C]-ADP and [^{35}S]-ADP after UV irradiation and it could be shown that ATP and ADP compete for binding at the same site which has an apparent K_D for ATP and ADP of 4μM (Peng, 1995). Like the 73kDa subunit the 58kDa subunit was shown to be essential for activity in reconstitution of the holoenzyme complex. Cross-linking studies suggest that these nucleotide binding subunits are in close proximity on the cytoplasmic surface of the coated vesicle enzyme (Adachi *et al*, 1990b) and have led to a model of a hexameric arrangement of alternating 73 and 58kDa subunits (Figure 1.1).

1.3.4.2.2 Stalk region subunits.

The ability to split V-ATPases into two domains by cold inactivation (Moriyama and Nelson, 1989a) has been extremely useful in identifying the subunit components of the membrane and peripheral sectors and the function of these domains. The ATPase is incubated at 4°C in the presence of high concentrations of salt (0.2M NaCl) and MgATP. Unlike F_1 the dissociated peripheral sector of V-ATPases is unable to catalyse ATP hydrolysis (Forgac 1989). Proton transport through the V_O sector of the ATPase with the V_1 sector removed was originally thought to be absent (Zhang *et al*, 1992) but recent evidence has now shown that the V_O sector of the enzyme is able to transport protons passively when a pH gradient (Crider *et al*, 1994) or K^+/valinomycin membrane potential (Zhang *et al*, 1994) is imposed.

Several subunits around 30-45kDa are seen in V-ATPases from all sources (Table 1.3) and are thought to constitute parts of the stalk connecting V_1 and V_O sectors in the intact enzyme. Some of these subunits are found associated with the membrane sector (45 and 39kDa in the chromaffin granule ATPase) while others are found associated with V_1 (33 and 40kDa in the chromaffin granule ATPase) on cold inactivation of the enzyme (Supek *et al*, 1994). These subunits are not labelled with nucleotide analogues and are therefore thought to have functions other than nucleotide binding.

The technique of cold inactivation combined with the reconstitution of the ATPase with or without certain subunits has also proved useful in identifying which subunits are essential for activity of the enzyme and studies on how the ATPase V_1

subunits might assemble into a functional V_1V_O holoenzyme complex. The coated vesicle ATPase V_1 subunits (73, 58, 40, 34, and 33kDa) can reassemble with stripped membrane bound V_O domains into a functional complex able to catalyse ATP-dependent proton translocation with restoration of 50-60% or the original activity (Puopolo and Forgac, 1990). It was found that the 40kDa subunit was not necessary for functional reconstitution of activity and therefore of the holoenzyme complex but that the inclusion of this subunit during the reconstitution enhances the final ATP-dependent proton translocation activity obtained (Puopolo *et al*, 1992). When the same technique was applied to a recombinant 33kDa subunit it was suggested that this subunit was essential for reconstitution of activity (Peng *et al*, 1994b) although there was some activity obtained on addition of 40kDa subunit to a V_1 core lacking only the 33 and 40kDa subunits. This residual activity was explained by the presence of contaminating cores containing 33kDa subunit. Hence it appears that the accessory subunits may have a role in assembly of the complex but also are necessary for the regulation of catalytic activity. This regulation may come from the ability of these subunits to alter their conformation on ATP hydrolysis as energy is transferred to the membrane sector for translocation of protons but experimental evidence for this is lacking.

1.3.4.2.3 Functions of V_O subunits.

The sensitivity of the largest membrane-bound subunit (100-116)kDa to proteases resulted in controversy about its presence in V-ATPases from different sources. First found in chromaffin granule (Percy *et al*, 1985) and clathrin-coated vesicle V-ATPases, homologues of this subunit have now been identified in yeast (Kane *et al*, 1989), higher plants (Parry *et al*, 1989) and renal tubules (Gillespie *et al*, 1991). It has been speculated that this subunit contains nucleotide binding sites (Moriyama and Nelson, 1987b) and that it may be necessary for the ability of the coated vesicle ATPase to catalyse both Ca^{2+}- and Mg^{2+}- dependent ATP hydrolysis since removal of the 116 and 17kDa subunits abolishes the latter activity (Xie and Stone, 1988). Hard evidence for these functions is lacking at present as is the role of the single 17-19kDa subunit also found as part of V_O which remains elusive.

The oligomeric 16kDa subunit of V_O is the only component of the membrane sector with an unambiguous function. This subunit is often called the proteolipid due to its highly hydrophobic sequence which enabled its purification by organic solvent extraction (Sutton and Apps, 1981). The inhibitor dicyclohexylcarbodiimide (DCCD) inhibits proton translocation by covalent modification of the 17kDa subunit from the coated vesicle ATPase (Arai *et al*, 1987a; Sun *et al*, 1987) and of the 16kDa subunit from chromaffin granule membrane (Sutton and Apps, 1981), *Neurospora* (Bowman and Bowman, 1982), higher plant (Manolson *et al*, 1985; Mandala and Taiz,

1986; Rea *et al*, 1987) and yeast (Uchida *et al*, 1985) V-ATPases. When the stoichiometry of DCCD labelling is compared with the degree of inhibition it is seen that complete blockage of proton translocation occurs after only one-sixth of the proteolipid subunits has reacted (Arai *et al*, 1987a). This suggests that proton translocation requires the cooperative interaction of all six subunits possibly in the formation of a pore-type structure (Arai *et al*, 1988) and it has also been suggested that the hexameric structure alone is not able to form a functional pore but requires the presence of the additional 100 and 19kDa subunits (Sun *et al*, 1987), the functions of which are unknown. However this large transmembrane-subunit has been reported to be absent from V-ATPases of plants (Warren *et al*, 1992; Ward *et al*, 1992), insect midgut epithelial cell membranes (Wieczorek *et al*, 1991) and the plasma membrane of kidney cells (Gluck and Caldwell, 1987) and therefore it may not be necessary for proton transport in all V-ATPases but serve a regulatory role when present. As noted above, this subunit is very protease-sensitive; it also stains poorly with Coomassie Blue, and has a tendency to aggregate. It is therefore difficult to prove conclusively that a given V-ATPase does not contain such a subunit, and indeed has since been found in renal tubule epithelial cells (Gillespie *et al*, 1991).

Cloning and sequencing of the chromaffin granule 16kDa DCCD-reactive subunit has revealed four putative transmembrane domains. One of these helices contains a single glutamate residue which is the likely candidate for the DCCD-reactive site (Mandel *et al*, 1988) and may facilitate proton transfer. The amino acid sequence of the 16kDa subunit is highly conserved with 80% homology between the different examples sequenced to date (Nelson, 1992a) consistent with its importance in the physiological function of the enzyme. Homology also exists between the 16kDa subunit from V-ATPases and the 8kDa subunit of F_O which has led to a theory of gene duplication in evolution as will be described later (Nelson, 1992a). Interestingly the proteins which make up gap junction-like structures in the plasma membranes of *Nephrops norvegicus* (Finbow *et al*, 1984) or mediatophore preparations of *Torpedo* electric organ (Birman *et al*, 1990) appear to also be a form of stripped V-ATPase containing only the proton pore 16kDa subunits arranged in hexagonal arrays. The 16kDa protein from gap junctions has been shown to be identical to that in the ATPase complex although the mechanism of bulk flow through this pore is likely to be very different to the mechanism of selective proton transport that occurs in the ATPase (Finbow *et al*, 1984; Finbow *et al*, 1994).

1.3.4.3 Inhibitor specificity.

Inhibitor sensitivity was the major property by which the three ion-translocating ATPase classes were originally distinguished (Table 1.2). V-ATPases are insensitive to vanadate suggesting that they do not catalyse ATP hydrolysis via a

phosphoenzyme intermediate (Forgac, 1989, Pedersen and Carafoli, 1987; Moriyama and Nelson, 1988a). In addition the V-ATPases can be distinguished from those of the F-type by their resistance to oligomycin, azide , efrapeptin and aurovertin (Forgac *et al*, 1983). The macrolide antibiotic bafilomycin A_1 (Bowman *et al*, 1988; Hanada *et al*, 1990) and the related concanamycins (Dröse *et al*, 1993) are the only inhibitors to date that have been found to be highly specific to the V-type enzymes with complete inhibition at nanomolar concentrations. Bafilomycin has been shown to inhibit acid secretion by mantle epithelial cells in freshwater clams (Hudson, 1993) and bone resorption by osteoclasts (Sundquist *et al*, 1990). Very recently it has been demonstrated that this inhibitor interacts with the V_O part of the enzyme and blocks proton transport (Crider *et al*, 1994; Zhang *et al*, 1994) but the subunit location of the binding site has still to be identified.

Other inhibitors are far less specific and interact with all or at least two of the ATPase classes (Bowman, 1983). DCCD, Nbf-Cl, NEM and trialkyltin compounds, are examples of such inhibitors. DCCD is more reactive with F-ATPases than with the V-ATPases and although DCCD also inhibits ATPases of the P-type, ten times greater concentrations are required compared to inhibition of the V-type enzyme (Forgac, 1989). Nbf-Cl, like DCCD, inhibits all three classes of enzyme but again the sensitivity varies, and concentrations needed to inhibit the V-ATPases are much lower than those required for the same degree of inhibition of the F- and P-type enzymes. The alkylating reagent NEM inhibits only P- and V-type enzymes, with ten times higher potency against the V- than the P-type, while trialkyltin compounds inhibit the F and V-ATPases with similar affinity. Omeprazole, a known inhibitor of the gastric H^+/K^+-ATPase, was found recently to inhibit the V-ATPase from chromaffin granules by interacting with the same site as NEM (Moriyama *et al*, 1993). This reflects the presence of a catalytic-site cysteine in V-ATPases, but not in other types. Diethylstilbestrol, a synthetic oestrogen that has been shown to inhibit ATP hydrolysis and proton translocation in chromaffin granule ghosts (Grønberg and Flatmark, 1988), is also an inhibitor of other ATPases (Pedersen and Carafoli, 1987). Other inhibitors of V-ATPases include fusidic acid, suramin (Moriyama and Nelson, 1988b) and nitrate (Griffith *et al*, 1986) while chloride ions have been seen to stimulate the V-ATPases (Griffith *et al*, 1986).

1.3.5 Relationships between V-, F-type and archaebacterial ATPases.

Claims of similarities between F- and V-type ATPases were initially based mainly on morphological studies using electron microscopy and cold inactivation procedures as described in previous sections. Other evidence for their similarity came from their shared sensitivity to various inhibitors. As far as catalytic function

is concerned they share the same reactions but with the physiological roles reversed. More recently the application of molecular biological techniques has resulted in the cloning and sequencing of almost all V-ATPase subunits identified to date and has further revealed homologies which suggests that these enzymes may have a common evolutionary origin.

The cDNAs encoding the large subunits of the V_1 sector of around 70 and 60kDa (termed subunits A and B respectively) were first cloned from plant and fungal sources (Zimniak *et al*, 1988; Bowman *et al*, 1988b; Bowman *et al*, 1988c; Hirata *et al*, 1990; Manolson *et al*, 1988) and later from bovine chromaffin granules and brain clathrin-coated vesicles (Pan *et al*, 1991; Puopolo *et al*, 1991). Comparison of the sequences from these different sources revealed approximately 60% and 70% homology in the A and B subunits respectively. This extensive conservation between ATPases from different species and intracellular locations is consistent with the important catalytic role of these subunits. The catalytic A subunit was also seen to exhibit significant sequence homology (20-25%) to the catalytic β subunit of F-ATPases (Bowman *et al*, 1988c). Both of these subunits contain a putative nucleotide-binding motif called the P-loop or the Walker consensus sequence (Walker *et al*, 1982) and the region around this consensus sequence is that of highest homology. The sensitivity of V-ATPases to NEM has been attributed to a cysteine residue in this region thought to be present in the binding site for nucleotide (Feng and Forgac, 1992a). F-ATPases do not have a cysteine residue in a corresponding position explaining their resistance to this reagent but can be engineered using site directed mutagenesis to behave like V-ATPases by point mutation of valine 153 to a cysteine (Iwamoto *et al*, 1994). Similarly the conserved cysteine residue in the V-ATPases can be point mutated to a serine without loss of activity but the enzyme adopts the inhibitor sensitivity characteristics of F-type ATPases (Cutler *et al*, 1992). A sequence of about 100 amino acid residues was found to be present in V-ATPase enzymes and absent from those of the F-type. This region is highly conserved in all V-ATPases (Zimniak *et al*, 1988) and is also present in the related archaebacterial ATPases; consequently the overall sequence similarity in the A subunit is stronger between V- and archaebacterial ATPases (50% homology) than it is between V- and F-types (Kibak *et al*, 1992).

Subunit B in the V-ATPases sequenced to date does not appear to contain the Walker consensus sequence so the binding of nucleotides observed by this subunit (Manolson *et al*, 1985) is likely to occur in a different way. The high degree of conservation, even greater than that for the A subunit, is strongly suggestive of an important functional role, and it may be that the areas which are conserved are those in the contact regions between the proposed alternating A/B pairs. This role would

be consistent with the sequence homology between the B subunit and the α subunit of F-ATPases which is known to have a noncatalytic, functional role at the interface of the α and β subunits (Abrahams *et al*, 1994).

The 16kDa "proteolipid" from various sources has also been cloned and sequenced and four putative membrane spanning helices were identified (Mandel *et al*, 1988; Nelson and Nelson, 1989; Birman *et al*, 1990; Lai *et al*, 1991; Hanada *et al*, 1991; Sista *et al*, 1994). Searching a DNA data bank revealed that the first two helices were similar to the F-ATPase 8kDa proteolipid. The high content of hydrophobic residues means that, although the degree of identity between residues was low, conservative substitutions are tolerated and similarity is higher from a functional view point. Also functionally significant was the presence of a buried glutamate residue (the site of DCCD inhibition) in the last of the four transmembrane helices which corresponded to an aspartate in the F-type enzyme from *E. coli* (Nelson, 1992b). Site-directed mutagenesis studies on the F-type enzyme have shown that all replacements of the aspartate residue except glutamate inactivate the proton pump suggesting the importance of the acidic side chain in proton transport.

A recent theory is that V-ATPases emerged after a gene duplication event took place giving rise to "proteolipid" twice the size of that seen in the archaebacterial and F-type ATPases (Nelson and Nelson, 1989). This event was thought to be due to evolutionary pressure for an alteration of H^+/ATP stoichiometries in the different evolutionary forms of the ATPases (Cross and Taiz, 1990). According to the theory the original ancestor of both F and V-type enzymes had six copies of a catalytic subunit A and 12 copies of the "proteolipid", subunit c and 12 protons were pumped for 6 ATP hydrolysed (a stoichiometry of $2H^+$/ATP). The evolution into an ATP synthase and reversal of direction of proton flow might have necessitated the need for altered stoichiometry for the maintenance of a proper phosphorylation potential to allow a given H^+-electrochemical gradient to drive ATP synthesis against a large free energy barrier. To accomplish this the ATP synthases evolved to have three catalytic sites, with the other sites becoming non-catalytic. This results in a stoichiometry of $4H^+$/ATP (although a value close to 3 is found in most experimental measurements) and also allows enhanced rates of mutation of the noncatalytic subunit to occur.

At a point later in evolution it is thought that the second change in direction of proton flow came when the progenitor of archaebacteria gave rise to the ancestors of the V-ATPases by gene duplication of the proteolipid thereby acquiring the low H^+/ATP required for transport in this direction. The main evidence for these proposals comes from the different subunit stoichiometries found in the ATP synthases and V-ATPases and the presence of noncatalytic subunits which are still

highly homologous to their catalytic counterparts. It should be noted however that a consensus for the stoichiometry of proteolipid in the F-type enzymes is still lacking and estimates vary between 9 and 12 copies (Foster and Fillingame 1982).

As far as accessory subunits of the V-ATPases are concerned several have now been cloned and sequenced. Subunits C (Mr=40kDa, calculated molecular weight=44kDa) and E (Mr = 33kDa, calculated molecular weight = 26kDa) were cloned from bovine chromaffin granules (Nelson, *et al*, 1990) and bovine kidney (Hirsch *et al*, 1988) respectively. The discrepancy in molecular weights seen in denaturing electrophoresis in thought to be due to the highly hydrophilic nature of these peptides since they do not appear to be glycosylated. Database searches revealed no homology to subunits γ, δ and ε of the F-ATPases but it was suggested that possibly subunit C is analogous (but not homologous) to the γ subunit of the F-type enzyme. Subunits C and E appear to be conserved in the V-ATPases but the level of conservation is low (about 40%) compared to that for the A (60%) and B (70%) subunits. More recently sequence data have been obtained for accessory subunits of 45kDa (Supek *et al*, 1994) and 39kDa (Wang *et al*, 1988; Nelson N., personal communication) in SDS-PAGE. The 39kDa subunit appears to be hydrophilic with no transmembrane helices, while the 45kDa subunit is glycosylated at some or all of the seven possible glycosylation sites and a putative transmembrane domain at the C-terminus has been identified. The 45kDa subunit is know to be identical to chromaffin granule glycoprotein IV which until now had had an unknown function. Again there is no homology between these subunits and those of the F-type but immunological cross reactivity with antibodies to the 45kDa subunit indicate conservation in V-ATPases from different sources (Supek *et al*, 1994). Lack of sequence data for the corresponding accessory subunits from other V-ATPase sources prevents study of actual amino acid homology.

Although overall similarity between V- and F-ATPases is obvious in their morphology, at the amino acid level it is confined to regions involved in nucleotide binding and proton conduction. The overall subunit composition is very different and novel subunits continue to be identified in the V-ATPases. Regulation by the intracellular assembly of V_1 segments onto excess membrane-bound V_O may also be a feature that is not seen in the ATP synthases. Different V-ATPase B subunit isoforms have been detected in higher plants (Berkelman *et al*, 1994) and human brain (Bernasconi *et al*, 1990). This data should be analysed with respect to the possible function of the isoforms (tissue specific or organelle specific) and with respect to the point in evolution when gene duplication giving rise to isoforms occurred. Cloning and northern blot analysis of the tissue distribution of accessory subunit C, D and E of the human vacuolar ATPase showed that there is a constant

level of transcription in all cell types regardless of their enrichment in V-ATPases suggesting regulation of V-ATPase activity is downstream of mRNA production (van Hille *et al*, 1993). The complexity of the V-ATPase enzymes may reflect their diverse roles and locations within the cell and the presence/absence of the accessory subunits identified may have a role in this regulation.

1.4 Aim of the project.

Although much work has been carried out on the structure of the V-ATPases, the lack of information about the regulation of these complex enzymes means that they still represent the least well studied class of proton-translocating ATPases. Morphological studies and the recent cloning and sequencing of several subunits has provided evidence of their structural similarity to F-type ATP synthases, although sequence homology exists only in those subunits implicated in nucleotide binding and proton translocation. Extensive studies of the mechanism of action of mitochondrial ATP synthases have been carried out and a detailed mechanistic scheme consistent with detailed structural information is now available; in contrast, very little kinetic work has been performed on the V-ATPases.

The development of a method for rapid purification and reconstitution has facilitated the study of the V-ATPase from bovine chromaffin granules in a pure form, reconstituted in a bilayer of physiological lipid content. The overall aim of the current project is to study extensively the mechanism of kinetic regulation of the V-ATPase of chromaffin granules with particular reference to its nucleotide binding sites. Since the physiological function of the enzyme is to translocate protons this aspect of catalysis was assayed in detail. Kinetic model fitting using a wide range of nucleoside di- and triphosphates should provide information on how these enzymes are physiologically regulated as well as providing detailed information on the actual mechanism such as numbers and types of nucleotide binding sites and their dissociation constants. This information will be needed to further compare the V-type enzyme to the F-type and it is shown that mechanistically the enzymes are less similar than the current consensus of opinion, based largely on structural studies, would suggest.

Chapter 2. Materials and methods.

2.1 Materials.

All reagents used were of analytical grade.

2.1.1 Chemicals and biochemicals.

Bovine brain phosphatidyl choline, bovine spinal cord phosphatidyl serine and egg phosphatidyl ethanolamine were obtained from Lipid Products, Nutfield, Surrey. Cholesterol, n-octyl-β-glucoside, thesit ($C_{12}E_9$) and nucleotides were purchased from Boehringer Mannheim, Sussex. All nucleotides were supplied as the disodium salt except ADPβS which was the trilithium salt and were neutralised if necessary with sodium hydroxide once dissolved. $C_{12}E_8$ was purchased fron the Nikko Chemical Company, Tokyo. Triton-X114 was purchased from Fluka A.G., Switzerland. Serva blue G was supplied by Serva, Heidelberg. Biogel-P6DG and Sephadex G-25 and G-50 were obtained fron Biorad and Pharmacia respectively. Calbiosorb absorbent was supplied by Calbiochem, Nottingham. Dibutyltin dibromide, diphenyltin bromide and tributyltin chloride were obtained from Aldrich, Dorset as were the flavones, 3-hydroxyflavone, galangin, apigenin and morin. Alkyl tin flavone complexes were the kind gift of Dr. David E. Griffiths, University of Warwick until such time as we synthesised our own complexes. Acrylamide and bisacrylamide were purchased from BDH and were of electran grade. Ultima Gold scintillant was obtained from Packard. All other general laboratory chemicals were purchased from either BDH laboratory supplies and Fisons both of Leicestershire or the Sigma Chemical Company, Dorset.

2.1.2 Radiochemicals.

All radiochemicals were purchased from New England Nuclear, Du Pont(UK) Ltd. Hertfordshire. Specific activities were; [^{3}H]-ADP, 0.99TBq/mmol; [^{3}H]-N-ethylmaleimide, various batches from 1158-2075GBq/mmol; [^{35}S]-ADPβS, 48TBq/mmol; [^{35}S]-ATPαS, 53TBq/mmol.

2.1.3 Enzymes and proteins.

Pyruvate kinase, EC 2.7.1.40 (150U/mg) and lactate dehydrogenase, EC 1.1.1.27 (360U/mg) were obtained from Boeringer Mannheim. Protein standards for polyacrylamide gel electrophoresis, carbonic Anhydrase, EC 4.2.1.1 and trypsin, EC 3.4.21.4 were supplied by Sigma Chemical Company. Polyclonal antibodies against the 39kDa subunit of the chromaffin granule H^+-ATPase were the generous gift of

Nathan Nelson, Roche Institute for Molecular Biology, Nutley, New Jersey. Polyclonal antibodies against 120kDa subunit of the chromaffin granule H^+-ATPase were prepared in the lab by previous postgraduate students, Mr Mark Warren and Mrs Judith Percy.

2.2 Methods.

2.2.1 Purification procedures.

2.2.1.1 Triton X-114 condensation.

16mg of butylated hydroxytoluene dissolved in 100µl ethanol and 20g of Triton X-114 were added to 980ml of 20mM Tris-Cl, pH7.4, 150mM NaCl (TBS) in a 1 litre separating funnel and kept on ice for about 8 hours or until the solution had gone clear. The mixture was then incubated at 30°C overnight to condense the Triton X-114 and the next morning the detergent-rich phase was collected and the aqueous phase discarded and replaced with the same volume of fresh TBS. The solution was mixed and again kept on ice for about 8 hours. The process of dissolution and condensation was repeated three times to yield around 100ml of approximately 10%w/v Triton X-114. Triton X-114 was assayed as described later.

2.2.1.2 Preparation of chromaffin granule membranes.

Chromaffin granule membranes were prepared as described previously (Apps and Schatz, 1979) and stored in a solution of 10mM HEPES-NaOH, pH 7.4, 1mM DTT and 2mM EDTA at -20°C. The protein content of the membranes was usually between 5 and 10mg/ml as measured by the Bradford assay (Bradford, 1976). Membranes were normally used within two to three weeks of preparation.

2.2.1.3 Purification and reconstitution of chromaffin granule vacuolar H^+-ATPase.

Purification of H^+-ATPase was based on that described previously (Pérez-Castiñeira and Apps, 1990) with slight modification. Chromaffin granule membranes were suspended in an initial volume of 10mM HEPES-KOH, pH 7.4, 150mM KCl, 1mM DTT, 0.1mM EDTA (buffer A), and 10% w/v Triton X-114 added to give a final concentration of 2%. The final protein concentration was 4mg/ml. The mixture was homogenised and then incubated for five minutes on ice before being centrifuged in a Beckman TL100 tabletop ultracentrifuge at $412000xg_{av}$, for ten minutes. The resulting supernatant was discarded and the pellet (P1) resuspended by homogenisation in the same initial volume of buffer A containing 2% Triton X-114. After a further incubation for five minutes on ice, the mixture was centrifuged at $412000xg_{av}$ for fifteen minutes. The supernatant was discarded and the washed

P1 resuspended in half the initial volume of 1.8% n-octyl-β-glucoside in buffer A containing 5mg/ml lipid. The solution containing lipid was prepared by dispensing the appropriate volumes of each solution of lipid from stocks of 20mg/ml into a conical tube. The lipid stocks were in chloroform:methanol, 2:1 with butylated hydroxytoluene at 0.01% . The lipid mixture was dried down under a stream of nitrogen and the residue resuspended by gentle mixing in buffer A with 1.8% n-octyl-β-glucoside. The lipid composition was 69% phosphatidyl ethanolamine, 11% phosphatidyl serine, and 20% cholesterol. The P1 and lipid/detergent mixture was homogenised and incubated at room temperature for ten minutes before being spun at 412000xg_{av} for ten minutes. All homogenisation steps were performed in glass-glass homogenisers (Jencons). The resulting supernatant was the solubilised H^+-ATPase and was reconstituted by gentle agitation for five minutes at room temperature with Calbiosorb adsorbent (200µl calbiosorb/300µl solubilised H^+-ATPase) which had previously been equilibrated with buffer A. The Calbiosorb resin was then separated from the reconstituted H^+-ATPase by removal of the supernatant after allowing the resin to sediment. Alternatively a procedure for the removal of n-octyl-β-glucoside involving gel filtration was used. Biogel P6-DG was equilibrated in buffer A and columns of 1ml unpacked volume were poured into Eppendorf tubes with a hole pierced in the bottom and a plug of glass wool. The columns were packed by centrifuging at 1400rpm for 2 minutes in an MSE bench centrifuge. 200µl of solubilised H^+-ATPase was loaded on to the top of the packed columns and the columns spun at 1400rpm for 2 minutes as before. The filtrate was cloudy and was the reconstituted H^+-ATPase. The Calbiosorb method was the method of choice since often large volumes of reconstituted H^+-ATPase were required. H^+-ATPase reconstituted by both procedures had the same activities of proton translocation and ATP hydrolysis and was usually 0.2-0.3mgprotein/ml as measured by Peterson's adaptation of the Lowry assay (Peterson *et al*, 1977).

2.2.1.4 Glycerol gradient centrifugation.

Glycerol gradients were poured using a two-chamber gradient mixer from the bottom to the top of Beckman Ultraclear centrifuge tubes. The more dense solution was pumped into the mixing chamber which contained the more dilute solution and was being stirred with a flat flea. Simultaneously the solution from the mixing chamber was pumped to the Ultraclear tube using a single-channel Gilson MinipulsII set to a flow rate of 0.64ml/min. The concentration of glycerol in the dense chamber was calculated according to the equation;

$$C_B=C_A+V_t/V_g(C_{bott}-C_{top})$$

where C_A and C_B are the concentrations of glycerol in the mixing and dense chambers respectively, V_g is the volume of the gradient (11.2 or 4.8ml), V_t is the total volume of solution initially in both chambers (usually $V_t = V_g + 1ml$) and C_{bott} and C_{top} are the concentrations of glycerol required at the bottom and top of the gradient respectively. Hence for a 5-20%w/v glycerol gradient $C_{bott} = 20\%$ and $C_{top} = C_A = 5\%$. Gradients were usually poured with 10mM HEPES-KOH, pH7.4, 150mM KCl, 10% methanol, 0.1mM EDTA and 1mM dithiothreitol in the pouring solutions. Detergents and lipids were included where indicated in the text of the following results chapters. Gradients were usually stored for 2-4 hours at 4°C before use. 12ml gradients were spun for 13-15 hours in a Beckman SW41 rotor at $150000xg_{av}$. 5ml gradients were spun for 8 hours in a Beckman SW50 rotor at $189000xg_{av}$. The gradients were fractionated from the bottom into fractions of either 1ml (12ml gradients) or 0.5ml (5ml gradients) using the same Gilson peristaltic pump set to 0.76ml/min. The convention throughout is to number fraction 1 as being from the bottom of the gradients.

2.2.1.5 Dibutyltin dibromide flavone complex formation.

Equimolar solutions in ethanol of dibutyl tin dibromide and flavones (usually 10mM) at 60°C were mixed in glass conical tubes in a water bath then incubated in the dark overnight to yield a 5mM solution of the resulting flavone dibutyltin bromide (Usta and Griffiths, 1993).

2.2.2 Analytical methods.

2.2.2.1 Assay of proton translocation.

H^+-translocation by reconstituted H^+-ATPase was assayed by recording the quenching of ACMA fluoresence (emission measured at 480nm on excitation at 420nm) at 30°C in a specially-modified Perkin-Elmer 3000 fluorimeter, the output of which was connected in parallel to a PCL-718 LabCard data acquisition card (Advantech) and a Servoscribe chart recorder. The assay mix (final volume 500µl) contained 0.3M sucrose, 10mM Hepes-NaOH pH7.4, 1.0mM MgSO4, 0.8µM ACMA and 0.45µM valinomycin. When required ADPMg (or other nucleoside diphosphates, as their magnesium complexes) was added to the required final concentration before the addition of proteoliposomes. About 30 seconds after the addition of proteoliposomes (10µl, approximately 2µg protein) to the continuously-stirred cuvette, the fluorescence had stabilized and enzymic reaction was initiated by the rapid injection of ATPMg (or other nucleoside triphosphates, as their magnesium complexes) to the required final concentration through a light-tight port, using a 25µl-Hamilton syringe fitted with a 7-cm needle.

The digitised signal from the fluorimeter was collected at 10Hz on an IBM286 computer, using software written by Dr M B Dutia, Department of Physiology, University of Edinburgh; it was also displayed on a monitor in graphical form. Optional three-point smoothing of noisy quench-curves could be applied if necessary; the range of points for initial-rate estimation was then selected, and a straight line fitted by linear regression using the Apple Macintosh version of Regression (Blackwell Scientific Publications). Individual data points were not weighted and regression was based on a least-squares routine with a Marquardt algorithm. This procedure produced the estimates of the initial rates of proton translocation that were fed into the model-fitting programme.

2.2.2.2 Coupled assay for ATP hydrolysis.

ATP hydrolysis was assayed in mix containing 0.3M sucrose, 50mM HEPES-KOH, pH7.4, 50mM KCl, 1mM phosphoenol pyruvate, 0.2mM NADH, 2mM ATP, 10mM MgSO4. The assay was carried out at 30°C in 1ml plastic cuvettes with 1cm path length. The enzymes lactate dehydrogenase and pyruvate kinase were added to final concentrations of 2.7U/ml and 2.2U/ml respectively and the absorbance at 340nm was allowed to stabilise. The ATPase sample was added to give a final volume of 1ml and the oxidation of NADH was followed by observing the decrease in absorbance at 340nm using a Pye-Unicam recording spectrophotometer. The addition of uncouplers such as FCCP or the potassium ion ionophore valinomycin had no effect on the initial rate of ATP hydrolysis by reconstituted ATPase or chromaffin granule membranes. ATPase activity is expressed as the rate of conversion of NADH in nmols/min/mg of protein, taking the molar absorbance of NADH as $\varepsilon = 6.22 \times 10^3 M^{-1}cm^{-1}$.

2.2.2.3 Assay of ATP hydrolysis by phosphate release.

ATPase assays were performed at 30°C in mix containing 10mM HEPES-NaOH, pH7.4, 0.3M sucrose, 0.5mM ATP, 1mM MgSO4, 0.5µg/ml valinomycin. $5x10^5$cpm [γ-32P] ATP was present in each assay. The assay was carried out in Eppendorf tubes and is based on that of Nelson (Nelson, 1980). ATPase was added to give a final assay volume of 200µl and the mix incubated for 10 minutes. The reaction was terminated by the addition of 20µl of 30% trichloroacetic acid and the tubes centrifuged for 10 minutes at 5000rpm in a Sanyo MSE Microcentaur microfuge. 100µl of the resulting supernatant was transferred to a glass conical tube and 800µl of 1.2% ammonium molybdate in 1.2N HCl added. The solution was vortexed before the addition of 1.4ml 5:5:1, isobutanol:benzene:acetone and was again vortexed for about 20 seconds. 500µl of organic phase and 20µl of aqueous

phase (controls without ATPase) were removed to a scintillation vial and 3ml of cocktail T or Ultima Gold was added before the samples were counted for radioactivity in a Packard scintillation counter.

2.2.2.4 Ultraviolet absorption data for 5'-ribonucleotides.

Molar absorptivity for adenosine and guanosine nucleosides was $15400M^{-1}cm^{-1}$ at 259nm and $13700M^{-1}cm^{-1}$ at 252nm respectively (Dawson *et al*, 1986) and for inosine nucleosides was $12250M^{-1}cm^{-1}$ at 248.5nm (PABST laboratories: Circular OR-10, 1967).

2.2.2.5 Protein estimation by dye binding.

The protein content of chromaffin granule membranes was estimated by the method of Bradford (Bradford, 1976) using 0-10μg bovine serum albumin as the standard except that the assay was performed in distilled water rather than NaCl. A typical standard curve is shown in figure 2.1a. The exact concentration of BSA was determined using $A^{1\%w/v} = 6.6$ at 280nm. Triplicate determinations were used to give an accurate estimate with A_{595} sample values around midway up the standard curve.

2.2.2.6 Protein estimation in reconstituted H^+-ATPase samples.

The protein content of solubilised and reconstituted H^+-ATPase was determined by the method of Lowry with Peterson's adaptations (Peterson *et al*, 1977) using 0-100μg bovine serum albumin as standard. A typical standard curve is shown in figure 2.1b. Exact BSA concentration was determined as above. Sample determinations covering different amounts of protein were used to check for chemical interference and the lowest value on the straight part of the standard curve used for estimation of protein.

2.2.2.7 Estimation of Triton X-114.

Triton X-114 was estimated as described previously (Garewal, 1973) with Triton X-100 (Pierce and Warner (UK) Ltd, Chester) used as the standard. 2mg/ml standard Triton X-100 in 50% ethanol was added to glass conical tubes to give 0-400μg final. The volume was made up to 300μl with 50% ethanol before the addition of 0.4ml cobaltothiocyanate reagent (17.8% NH_4SCN, 2.8% $Co(NO_3)_2$ in distilled H_2O). The samples were vortexed and left for 5 minutes at room temperature before the addition of 1.5ml dichloromethane. The samples were vortexed for 2 minutes to extract the colour into the solvent phase and then the phases separated by centrifugation at 3000rpm in an MSE bench centrifuge.

a

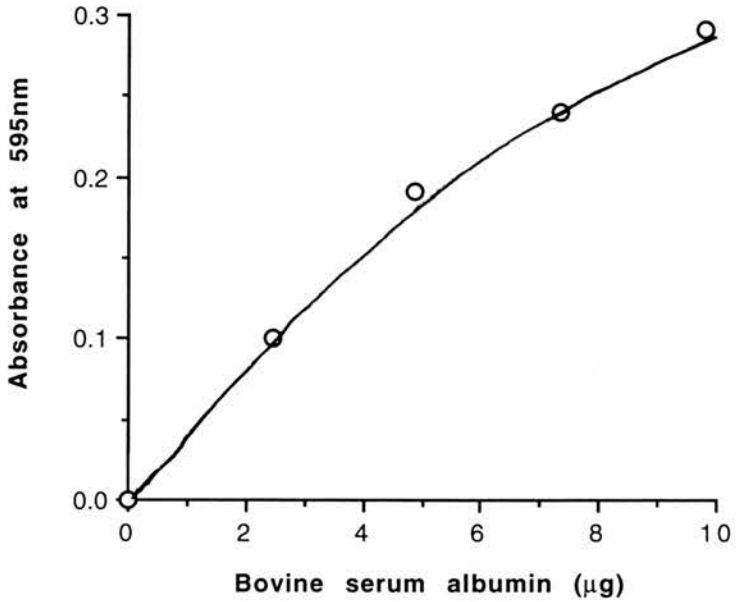

b

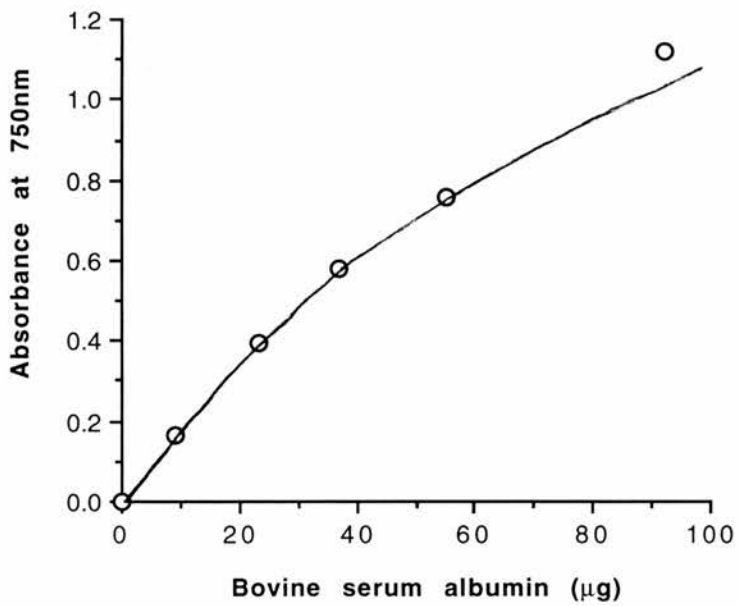

Figure 2.1 (a and b) Typical standard curves for the estimation of protein concentrations by the method of Bradford (a) or Peterson's adaptation of the Lowry Assay (b).

The lower solvent layer was scanned in a recording spectrophotometer between 570 and 700nm and the difference in absorbance between 622 and 688nm plotted against the amount of Triton X-100 (Figure 2.2). The baseline sample was that which did not contain any Triton. Samples were carried out in triplicate and an average taken for estimation of Triton X-114.

2.2.3 Polyacrylamide gel electrophoresis (PAGE).

2.2.3.1 SDS polyacrylamide gel electrophoresis (SDS-PAGE).

Polyacrylamide gel electrophoresis was usually performed using Hoefer Scientific Instruments' "Tall Mighty Small" mini-gel apparatus containing an exponential gradient of 6-15% acrylamide (30:0.8, acrylamide:bisacrylamide) unless otherwise indicated. The buffering system used was that of Laemmli (Laemmli, 1970) with 0.1% sodium dodecyl sulphate in the separation and stacking gel buffers and 10mM dithiothreitol, 0.05mg/ml bromophenol blue in the sample loading buffer containing 4% SDS, 2mM EDTA, and 10% glycerol in 0.05M tris-Cl, pH6.5. The gels were 0.75mm thick unless otherwise indicated and were run at a constant current of 15-20mA for 1.5-2 hours.

2.2.3.2 Native gel electrophoresis.

The native gel electrophoresis system used was based on that developed by Schägger (Schägger and von Jagow, 1987; Schägger *et al*, 1994) and is more properly named blue-native gel electophoresis (BN-PAGE). The acrylamide : bisacrylamide ratio was 48:1.5 and linear gradient gels of 5-12% acrylamide were run in Hoefer mini-gel apparatus with thick (1.5mm) spacers. The stacking gel was 4% acrylamide in the same buffers as the separating gel. The gel buffer was 50mM BisTris-Cl, pH7.0, 0.5M amino caproic acid (ACA). Samples were suspended in 0.75M ACA, 0.05M BisTris-Cl, pH 7.0 and 10% dodecyl maltoside added to a final concentration of 1.5%. The sample was homogenised in a glass-glass homogeniser and centrifuged for 5 minutes at 356000xg_{av} at 4°C before the supernatant was collected and 5% Serva blue G in 500mM ACA was added to a final concentration of 0.4%. The anode buffer was 50mM BisTris-Cl, pH7.0 and the cathode buffer was 50mM Tricine, 15mM BisTris, and 0.02% Serva blue G. The gel was run at 4°C on constant voltage at 100V until the sample had entered the stacking gel. The voltage was then increased to 250V for 1 hour. The voltage was further increased to around 350V for the remainder of the gel run which took 3.5-4 hours in total. Following the gel run the entire gel is blue and the bands visualised by fixing and destaining in 20% methanol, 10% acetic acid.

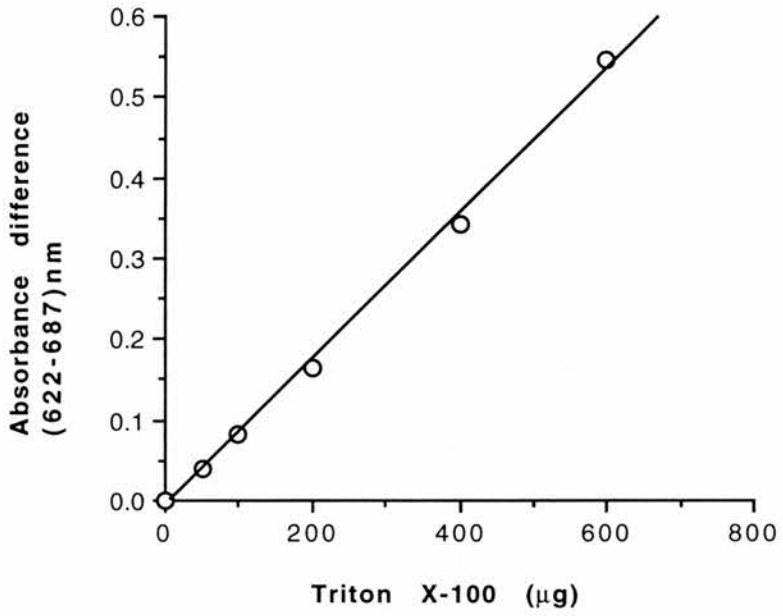

Figure 2.2 Typical standard curve for Triton X-114 estimation.

The complexes seen in the first dimension BN-PAGE can be separated further into their subunit components by performing electrophoresis in a second dimension gel with buffers containing SDS. The second dimension glass gel plates were around 24x18cm with spacers 24x2.5x0.13cm. The lanes in the first dimension were excised, placed onto one of the second dimension glass plates. The gel strips were soaked in a small volume (sufficient to cover the strips with a little underneath, about 250µl) of 1% SDS, 1% mercaptoethanol (or 10mM dithiothreitol) for 2 hours with turning of the strip after 1 hour. After incubation excess buffer was removed with tissue and two gel plates fixed together so that the strip was pressed between the two plates about 1cm from the top. The gel plates were sealed with 1.5% hot agar.

Three different gels stacked one on top of the other were used in the second dimension; the separating gel was 12% acrylamide in 1.0M Tris-Cl, pH8.45, 0.1% SDS; the stack was 4% acrylamide in the same buffer; the third gel was an overlay gel of the same composition as the first dimension separating gel (see above). These gels were poured in succession into the gel apparatus taking care not to create bubbles. Each type of gel was overlaid with distilled water and allowed to set before the water was poured off, the plates dried with tissue and the next layer poured on top. The strip from the first dimension was embedded in the overlay gel. Protein standards could be added in a lane formed through the overlay gel so that the standards touched the stack before the gel run was started. The second dimension was run overnight on a constant voltage of 100V. Gels were then fixed in the same way as for SDS-PAGE gels and then stained with 0.025% Serva blue G in 10% acetic acid for two hours with gentle agitation. The gels were destained in 10% acetic acid and stored as described below.

2.2.3.3 Silver staining of polyacrylamide gels.

Silver staining was performed as described previously (Wray *et al*, 1981). SDS-PAGE gels were fixed overnight in 50% methanol, 10% acetic acid and were then washed for 3 hours in three changes of 50% methanol with 5 minute washes in distilled water between the methanol washes. Silver stain solution was prepared by mixing 21ml of 0.36% NaOH with 1.4ml of 14.8M ammonia. As this solution was rapidly stirred, 0.4g of silver nitrate dissolved in 2ml of distilled water was added dropwise and the resultant colourless solution was made up to 100ml. The gel was rinsed for 5 minutes in distilled water before the silver stain solution was added for 15 minutes with gentle agitation. The gel was then rinsed in ditilled water for 5 minutes before developer (2.5ml of 1% citric acid and 0.25ml of 38-40% formaldehyde in 500ml total volume) was added. Stain development was stopped by pouring off the developer and rinsing the gel in 50% methanol, 10% acetic acid.

All washing, staining and rinsing steps were carried out at room temperature with the gel being agitaged gently on a Denley orbital mixer.

2.2.3.4 Coomassie staining of polyacrylamide gels.

SDS-PAGE gels were fixed for 30 minutes in a solution of 20% methanol, 10% acetic acid before 0.25% Coomassie blue-R in 50% methanol, 7.5% acetic acid was added for 5 minutes. The gels were destained to remove background in 10% methanol, 7% acetic acid. Again gels were agitated for all steps as for silver staining.

2.2.3.5 Polyacrylamide gel storage and drying.

Gels were usually stored in the dark in 30% methanol, 3% glycerol. It was often necessary to restain Coomassie stained gels before they were photographed or scanned. Gels were dried onto Whatman 3MM filter paper after being soaked in gel storage solution using a BioRad model 1125B slab gel drier set for 50-60 minutes at 80°C.

2.2.3.6 Autoradiography.

SDS-PAGE gels were fixed as above for 30 minutes and were then soaked in Amplify solution (Amersham) for 30 minutes before being dried on a BioRad model 1125B slab gel drier for 1 hour at 80°C. The dried gel was taped flat into an autoradiography cassette and exposed to Hyperfilm MP (Amersham) at -70°C for the length of times indicated in the text.

2.2.3.7 Western Blotting.

Western blotting was carried out as described previously (Towbin *et al*, 1979). The transfer buffer consisted of 20mM Na_2HPO_4, 0.02% SDS, and 20% methanol. A cassette was assembled submerged in a tray of transfer buffer to prevent air bubbles between layers with scouring pads on the outer faces then filter paper towards the inside then the gel next to a sheet of nitrocellulose in the centre of the sandwich. The side of the cassette with the nitrocellulose was placed next to the positive electrode and proteins transferred from the gel to the nitrocellulose for 2-3 hours with a current of 0.8A. The nitrocellulose blot was blocked overnight in TBS, 0.5% Tween 20, 2mg/ml BSA and 0.5mg/ml sodium azide. Primary antibodies were added in TBS, 0.05% Tween 20, 5mg/ml BSA, 0.5mg/ml sodium azide, and 5% heat-inactivated horse serum and incubated with the blot for two hours with gentle rocking (30rpm) on a platform shaker STR6, Stuart Scientific. The blot was then washed 5 times on an orbital shaker in TBS, 0.05% Tween 20 with 5 minutes for each wash. The last wash was poured off and the second-antibody/horseradish

peroxidase conjugate added in TBS, 5% heat inactivated horse serum and the blot incubated for 1 hour with gentle rocking. After incubation the second antibody was removed and the blot was washed as above and incubated with Amersham ECL solution for 2-3 minutes before being exposed to FUJI medical X-ray film.

Chapter 3. Analysis of initial rates of proton translocation.

3.1. Introduction.

In biological systems transmembrane proton gradients play a central role in energy transduction and consequently most cells contain enzymes and transporters which catalyse the transport of protons across membranes. Permeant weak bases can move freely across membranes in their unprotonated form and the uptake of monoamines and diamines is used to monitor intravesicular acidification. If a positive ΔpH (i.e. acidic inside) is established they will accumulate inside the membrane-bound compartment in the impermeant, protonated form. In the case of some acridines this protonation and accumulation results in quenching of the fluorescence which can be quantitatively related to the pH inside (Schuldiner *et al*, 1972), so ΔpH generation can be monitored continuously using a fluorimeter. Continuous assays are invaluable when studying the kinetics of proton-translocating ATPases since assays of ATP hydrolysis are generally discontinuous and as such do not provide accurate initial rate estimates. Also H^+-translocation is the primary function of V-ATPases, with ATP hydrolysis a necessary consequence, so in analyses of their physiological regulation it is desirable to measure H^+-translocation as well as ATP hydrolysis. The use of fluorescence quenching as a measure of H^+-translocation activity is widely reported (Flatmark *et al*, 1985; Grønberg and Flatmark, 1988; Gluck *et al*, 1982; Bennett and Spanswick, 1983; Thevenod *et al*, 1989).

Fluorescence quenching of the probe used must accurately report changes in the ΔpH to be useful for kinetic analysis of H^+-translocation and a theoretical justification of the use of fluorescent probes for rate measurements has been published (Bennett and Spanswick, 1983). The probe of choice for the measurement of relatively small ΔpH values (0.1-1.5 units) is 9-amino-6-chloro-2-methoxyacridine (ACMA) (Fregni and Casadio, 1993). It has been shown previously that the response of ACMA to pH changes in V-ATPase-containing proteoliposomes is very rapid and that the initial rate of fluorescence quenching is proportional to the H^+-translocation activity over a very wide range (Pérez-Castiñeira and Apps, 1990). In previous work with the chromaffin granule V-ATPase (Pérez-Castiñeira and Apps, 1990) and Kalanchoë tonoplast V-ATPase (Warren *et al*, 1992) initial rates of fluorescence quenching were estimated manually from chart recorder traces. This approach was difficult to apply to slow rates where the curvature of the quench curve was pronounced, and also to very rapid rates, which tended to be underestimated. An additional problem with the experimental set-up used in these experiments was the speed with which the recording could be initiated. The act of opening and closing

the lid of the fluorimeter to add substrate meant that for very fast rates the first part of the quench curve was lost, leading to underestimates of initial rates. Computer analysis of the quenching of fluorescent probes has been used previously (Jennings *et al*, 1988) to determine rapid H^+-translocation rates. This chapter reports how the basic H^+-translocation assay was developed using substrate injection systems and computer analysis to allow more accurate determination of initial rates for study of the kinetics of the V-ATPase reported in the next chapter.

3.2 Special Methods.

3.2.1 General Assay procedure.

Three different methods of determining initial rates were compared using the assay for proton translocation described in chapter 2. The assay mix remained the same throughout as did the volumes of components added: 10µl reconstituted ATPase (about 2µg protein); 10µl MgATP solution. The ATPase and substrate were added at the same time points as are indicated in chapter 2. When assaying stored proteoliposomes non-ATP dependent quenches were often observed due to the presence of valinomycin and the K^+-gradient hence it was sometimes necessary to add K_2SO_4 to a final concentration of 2mM to the assay mix to prevent this.

Variations in the procedure were in the method of addition of substrate and in the method of quench data collection. The most basic analysis of initial rates involves the addition of substrate by opening the lid of the fluorimeter, injecting 10µl of MgATP, stirring with a plastic rod and closing the lid. This procedure takes several seconds and fluorescence can be measured only after the lid of the fluorimeter is closed. Initial rates were then analysed by drawing tangents to the first part of the quench curves and determining the slopes of these lines. The first modification used was to inject the substrate into an electrically stirred cuvette. This meant that fluorescence could be continuously measured even during the addition of substrate. The initial rates were then determined from the chart record manually as above. The second modification of initial rate analysis was to use substrate injection and digital data collection and is described fully in chapter 2.

All additions of substrate were made using a 25µl Hamilton syringe fitted either with a standard needle for the addition with lid opening or with a 7cm needle for the injection through a port in the fluorimeter lid.

3.2.2 Error function analysis.

Five concentrations of MgATP were chosen to cover the entire experimental range and with each of these concentrations ten replicate determinations of initial rates were carried out. For each set of initial rates the mean initial velocity and its

standard deviation (SD) were calculated. An error function:

$$var = SD^2 = a + b.v^2$$

(where *var* is the variance and v is the mean initial velocity) was fitted to the data by linear regression, to give estimates for the two constants, a and b. Having determined a and b for each method of measuring initial rates the data for individual experiments could then be weighted as $1/var$ and the weights normalised. This was an inportant feature of the model fitting, since it was impossible to obtain replicates of all the points in a data set, during a single day's work.

3.2.3 Linear and non-linear regression analysis.

Data for linear and non-linear regression analysis were weighted as described in section 3.2.2 and fitted to the stated equations with a Marquardt algorithm using the Apple Macintosh version of Regression (Blackwell Scientific Publications). For linear regression the goodness of fit of the data can be statistically interpreted using the correlation coefficient value, r:

$$r = \frac{n\Sigma xy - \Sigma x\Sigma y}{([n\Sigma x^2 - (\Sigma x)^2][n\Sigma y^2 - (\Sigma y)^2])^{1/2}}$$

The determination coefficient, d for goodness of fit of non-linear analyses is defined as:

$$d = 1-[\Sigma(v - v_{calc})^2/\Sigma(v-\bar{v})^2]$$

where v, v_{calc} and $\bar{v}$ represent the observed, calculated form model fitting and the mean initial rate respectively. The closer r or d are to unity the better the fit of the data.

3.3 Results.

Figures 3.1-3.3 show chart recordings of quench curves. Addition of the substrate MgATP by opening and closing the lid of the fluorimeter cause the loss of recording for around 8 seconds (Figure 3.1). For very fast rates this is an unacceptable time lag and will lead to the underestimation of initial rates. The development of the injection system abolished this time lag allowing the initial rate to be recorded immediately after the substrate was injected (Figure 3.2). The small dilution/quench artefact is over in less than a second and does not interfere significantly with the initial rate measurement (Figure 3.2). The magnitude of this artefact was observed to depend not only on the dilution but also on the concentration of substrate added suggesting that there is some quenching of ACMA fluorescence caused by the Mg^{2+}-complexed nucleotide (results not shown). When manually estimating very fast rates the chart recorder was set to faster speeds since the fractional error on a slope is a minimum when the slope is at an angle of 45°.

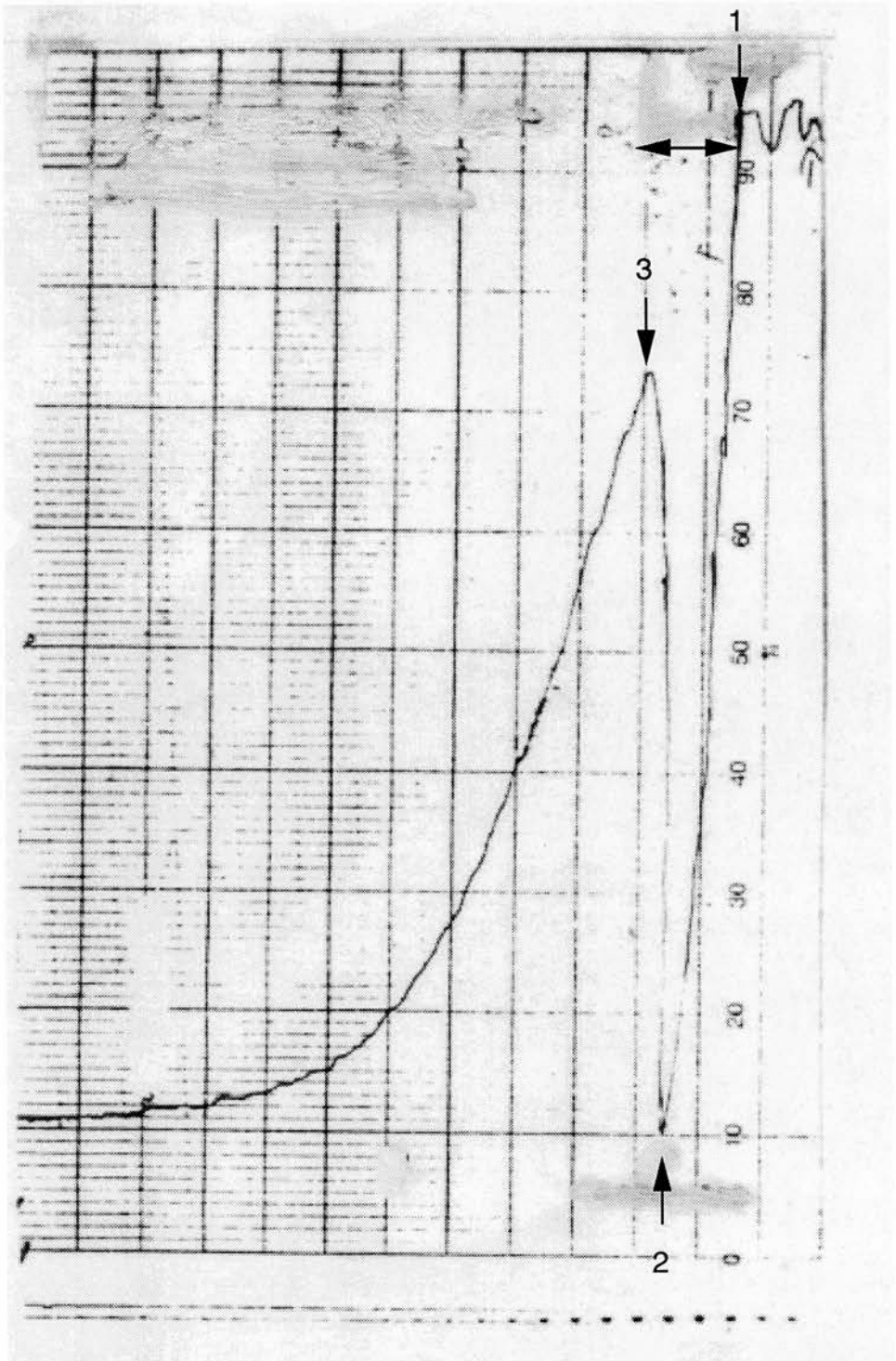

Figure 3.1. Chart recorder trace of a fast rate of proton translocation with the original set-up. Arrow 1 is point of lid opening for addition of MgATP to 1mM in the cuvette; arrow 2 is the point of lid closure; arrow 3 is when the quench rate starts to be recorded. The chart speed is 120mm/min and the horizontal arrow shows the 8 second time lapse between opening the fluorimeter lid and starting the recording.

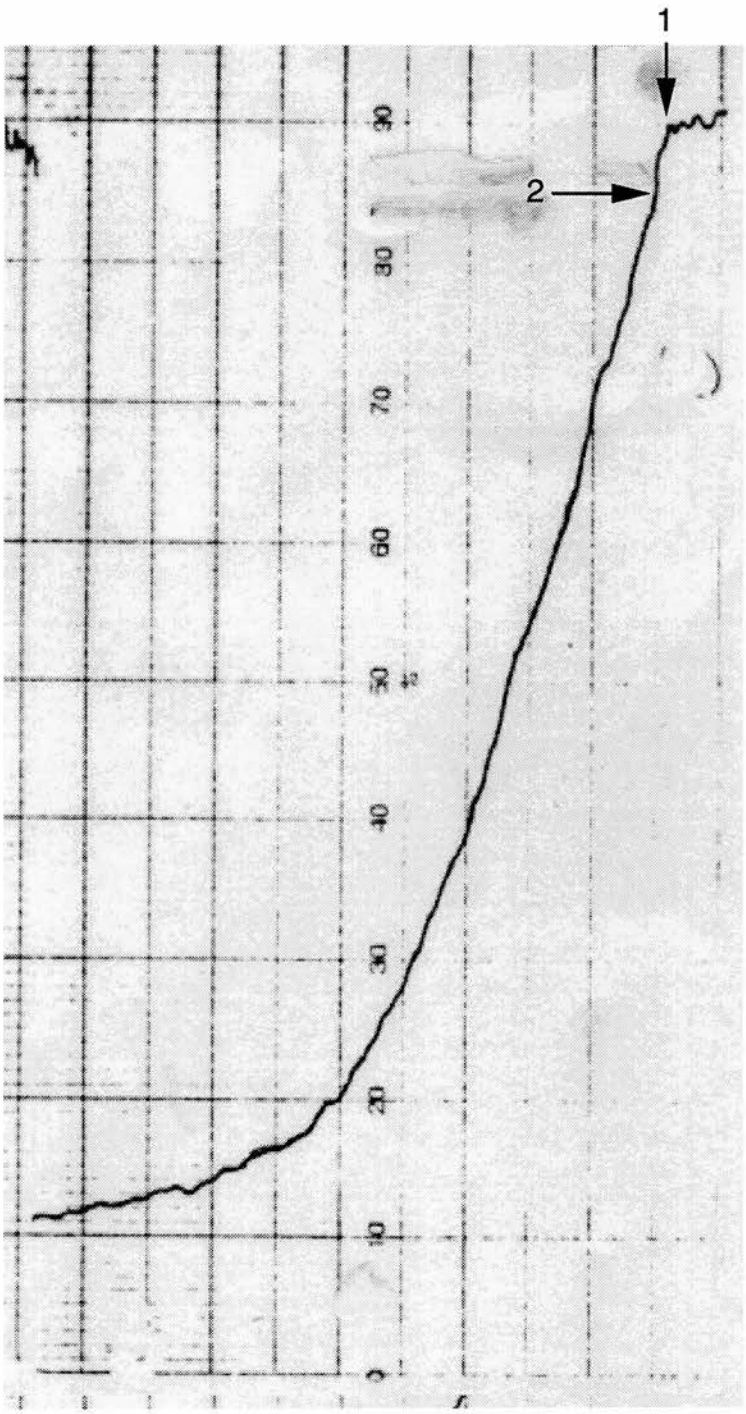

Figure 3.2. Chart record illustrating injection set-up: arrow 1 shows the point of injection of MgATP to 1mM in the cuvette; arrow 2 indicates the position where the injection artefact finishes and the initial rate begins. Chart speed is 120mm/min.

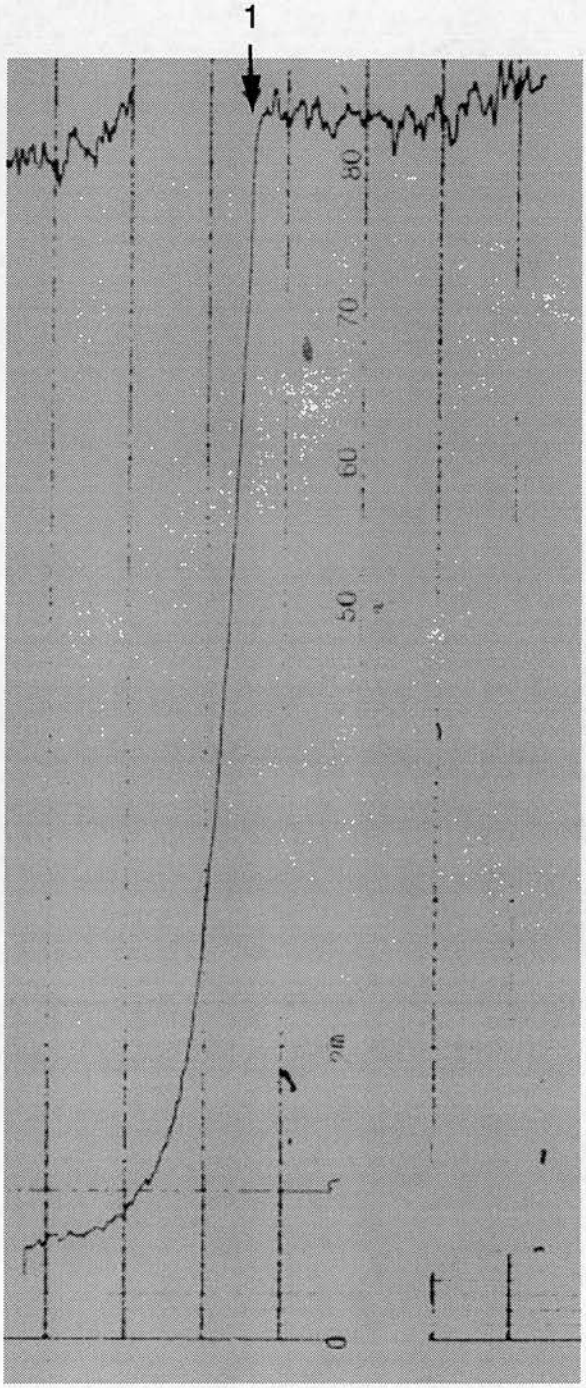

Figure 3.3 Chart record showing a fast quench curve with injection of MgATP to 1mM (arrow 1). The chart speed is 30mm/min.

Figure 3.3 shows a fast quench curve recorded at 30mm/min chart speed and it is easy to see the difficulty in manually determining the slope of such a steep line. For a range of MgATP concentrations the chart recorder was set to a speed of 120mm/min (Figures 3.1 and 3.2) for manual estimation of very fast rates and was slowed to 10mm/min for the slowest rates of H^+-translocation.

The development of the data collection system using software for data acquisition written by Dr.M. B. Dutia (Department of Physiology, Edinburgh University Medical School), allowed us to keep the data collection parameters constant by collecting data at 10Hz regardless of the initial rate. The quench curves were collected and stored on an IBM 286 computer and could be displayed on the screen as graphical representations (Figure 3.4a). Initial rate data could be collected from this curve and the range of individual points selected, then fitted by linear regression to obtain estimates of initial rates (Figure 3.4b). Good fits to linearity were observed with the correlation coefficient values being very close to 1 in all cases (for example see Figure 3.4b). The advantage of this technique is mainly with high initial rates, which can easily be extracted from the computer quench curve without the need to alter the data collection parameters. At lower rates this approach is still better than the manual estimation for the same reason i.e. data collection parameters remain constant throughout, although these rates are not so difficult to determine by the manual method.

Weighting and reproducibility analyses were carried out to compare the three methods of data collection (Figure 3.5a-c). The average fractional error was calculated for the entire set of ten replicates at the five concentrations of MgATP. It was found that the order of reproducubility of the methods was manual/non-injection > manual/injection > digital, with average errors of 6, 9 and 15% respectively. With a manual approach it is easy to see how replicates can be biased since the ten replicate determinations are carried out in sequence on the chart and the tendency would be to draw a set of near-parallel lines. However with digital data collection any tendency to bias the results is avoided: quench curves cannot be displayed on the screen simultaneously so one cannot compare the rates from individual replicates and hence each curve must be treated separatly. Although reproducibility is lower with the digital method this is more likely to be a reflection of the accuracy of the results than a disadvantage.

The weighting function used for the kinetic analysis can have a large influence on the interpretation of best fit and hence it is important to use a weighting function that accurately fits the replicate determinations. Comparison of the three methods of collection show that the weighting function fits all of the data quite well,

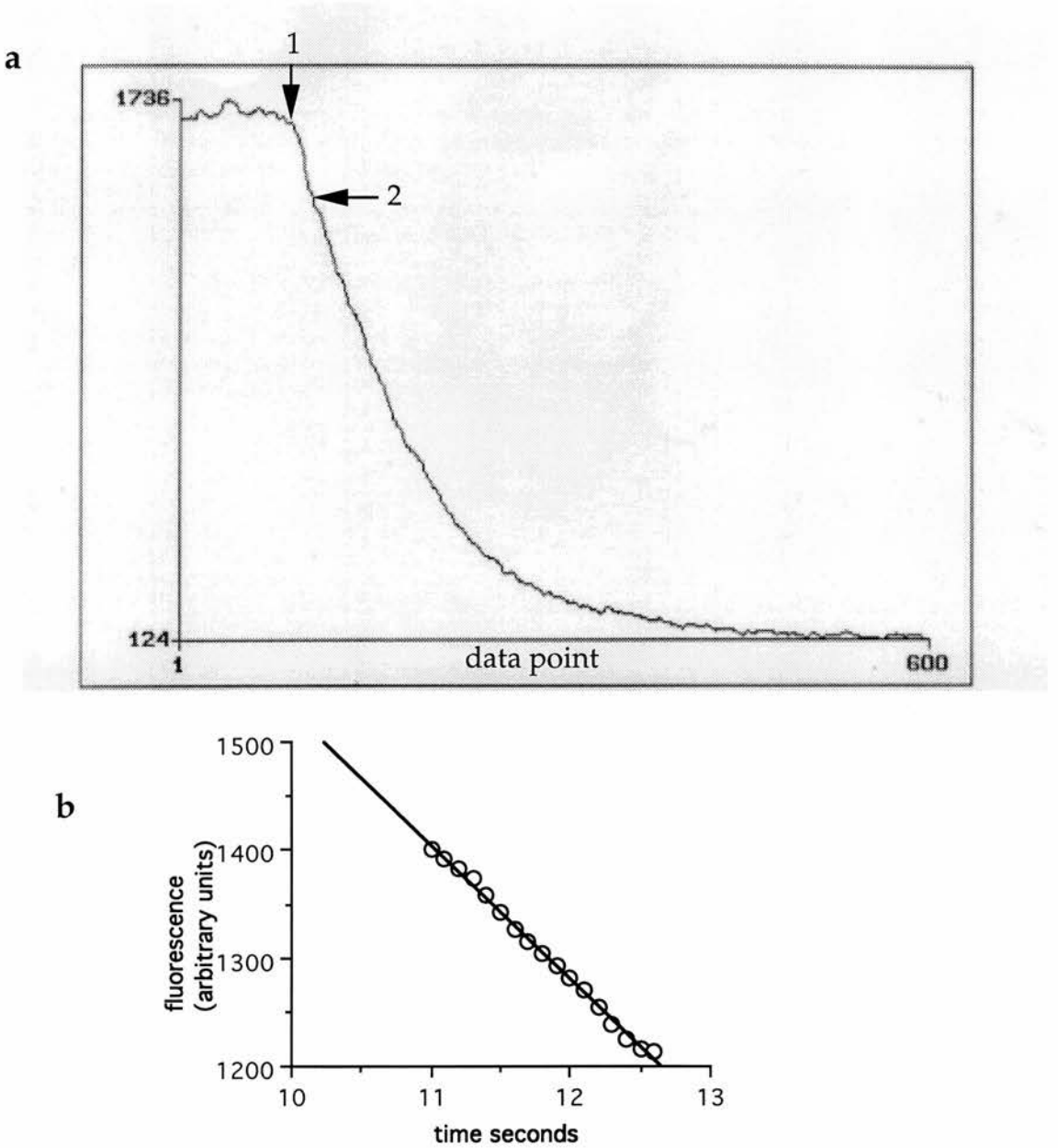

Figure 3.4(a andb). (a) Screen dump showing graphical representation of a digitally-collected quench curve; arrows 1 and 2 have the same meaning as in figure 3.2. The y axis values represent fluorescence in arbitrary units; the x axis values are data points collected at 1 per sec; the entire curve was collected over 1 minute. (b) linear regression of points selected from Figure 3.4a to determine the initial rate (r=0.996).

a

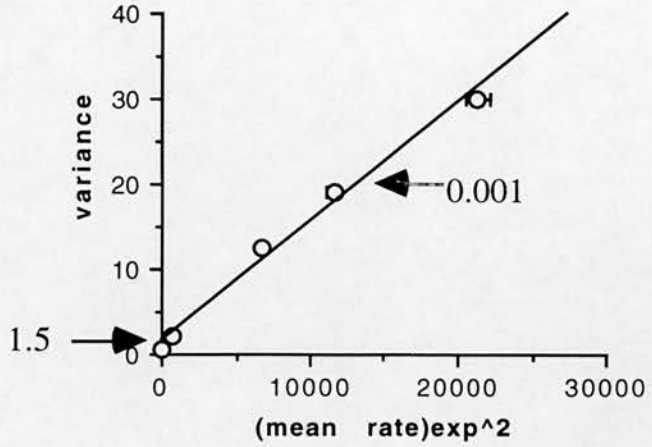

b

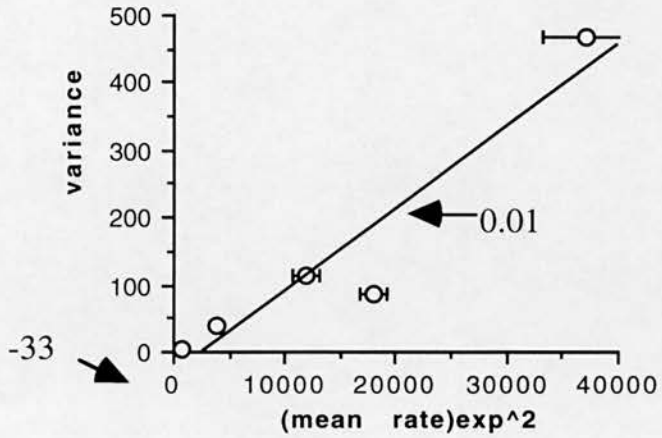

c

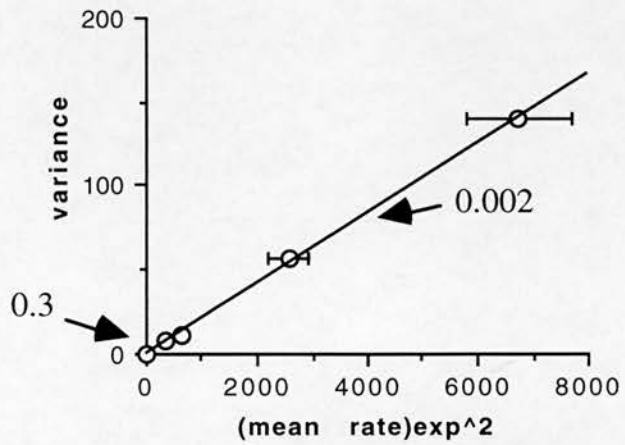

Figure 3.5(a-c) Determination of weighting functions for manual/non-injection (a), manual/injection (b) and digital (c) methods of data colection. The errors on the mean squared rates are shown as error bars: the average error overall is 6%(a), 9%(b) and 15%(c). The correlation coefficients, r are: 0.990(a); 0.906(b) and 0.999(c). Values for the slopes and intercepts on the y-axis are indicated by the arrows.

but is marginally better with the digitally collected data (r = 0.999, Figure 3.5c) and this method of collection is likely to provide accurately weighted data for entry into the complex model-fitting programs in chapter 4.

The methods of initial rate measurement were also compared by analysis of velocity against substrate concentration curves and study of the goodness of fit to the Michaelis-Menten equation using non-linear regression. The best fit to Michaelian kinetics was from the digital data collection method (Figure 3.6b and Table 3.1); this is shown by the value of the determination coefficient (Figure 3.6a and Table 3.1). In all cases the K_m value was 60-90μM, but the standard deviation on the K_m value for the three methods are 10%, 20% and 27% for digital,manual without injection and manual with injection respectively (Table 3.1). The fit for the method without injection is apparently slightly better than for the equivalent manual method with injection (Table 3.1). This is probably a consequence of attempting to fit the faster rates obtained with the injection system using a pen-and-ruler approach. It was already noted that manually estimating initial rates obtained with injection from a chart record is inherently difficult because of the steep slope of the quench curve (Figure 3.3).

3.4. Discussion.

Measurement of ΔpH in acidic vesicles can be accomplished by several approaches. Reliable methods for the quantitative estimation of ΔpH in acidic vesicles based on the distribution of radiolabelled amines are difficult to apply, require large quantities of vesicles and have poor time resolution so that only estimates of steady state values can be determined (Rottenberg, 1989). pH electrodes and external pH indicators are not sufficiently sensitive enough to measure the rates of proton disappearance from the medium and internally-trapped pH indicators have not yielded satisfactory results for most of the systems tested (Rottenberg, 1989).

Fluorescent amines were introduced as probes for ΔpH more than two decades ago (Schuldiner *et al*, 1972) and have yet to be replaced by a better form of assay for the generation of pH gradients. The extent of fluorescent quenching can be related to the magnitude of the ΔpH by a simple expression:

$$\Delta pH = \log\{Q/(1-Q)\}+\log(V_o/V_i) \qquad \textbf{(1)}$$

where Q is the fractional quenching and V_o and V_i are the medium and vesicle volume respectively (Schuldiner *et al*, 1972). Although most probes tested obey this relationship, at least over a certain range of ΔpH values, the value of V_i, in particular, may appear to be quite different from that measured by passive permeation methods, indicating departure from ideal behaviour. For a long time

a

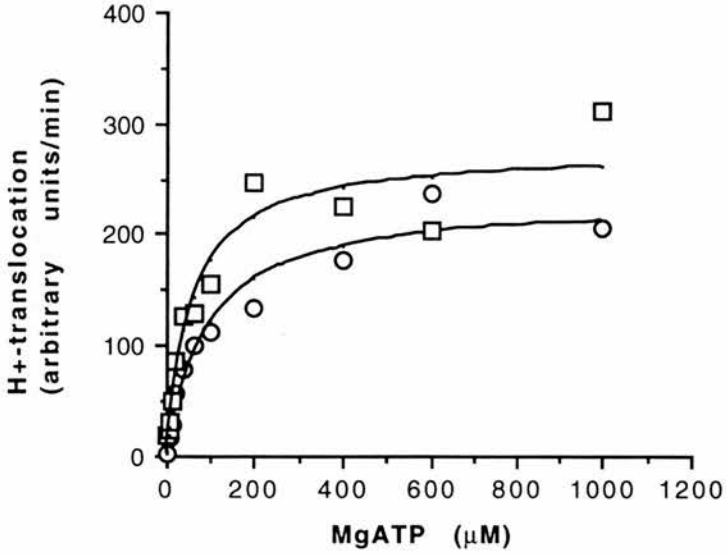

b

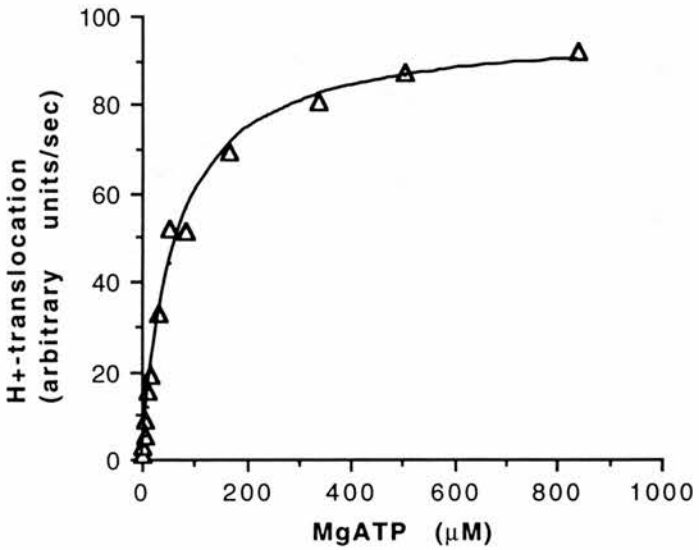

Figure 3.6(a and b) Comparison of the methods of initial rate analysis by fitting of the data to the Michaelis-Menten equation. The lines represent the best fit of the experimental points to the Michaelis-Menten equation. (a) manual estimations with (□) or without (○) injection of substrate. (b) digital estimation of initial rates with injection.

Method	Iterations	Determination coefficient	Vmax	Km (μM)
Manual/ non-injection	35	0.962	231±14	88±18
Manual/ injection	40	0.930	275±20	55±15
Digital/ injection	37	0.992	97±3	60±6

Table 3.1. Statistics of non-linear regression of the data shown in figures 3.6a and b. The method of initial rate analysis is shown as either manual i.e. from the chart record or digital from the computer stored results with or without injection. The number of iterations to reach the minima and the resulting goodness of fit parameters are illustrated. The parameters are shown ± their standard deviation. Vmax is comparable in the first two rows (chart units in mm/min) but has different units for the digital collection method.

9-aminoacridine was widely used for determining ΔpH and confirmed the validity of the Schuldiner equation (Casadio and Melandri, 1985; Reenstra *et al*, 1980). However, 9-aminoacridine is only suitable for measuring ΔpH values of 2 or more (Schuldiner *et al*, 1972) and in systems producing smaller ΔpH values this probe is not able to report the changes. For this reason sensitive probes of ACMA and acridine orange are now used. The quenching of acridine orange in response to ΔpH has been shown to be highly non-ideal possibly as a result of quench amplification caused by the accumulation of anions in response to the ΔpH or the effects of membrane-dye interaction (Palmgren, 1991). ACMA fluorescence is responsive to the magnitude of ΔpH at low values (<2.0) but is completely insensitive at higher ΔpH values (>3.0) (Rottenberg and Moreno-Sanchez, 1993) and an assay combining ACMA and 9-aminoacridine was recently developed to obtain a response over a very wide range of ΔpH values (Rottenberg and Moreno-Sanchez, 1993). This combined assay was tested with V-ATPase proteoliposomes but without success: more extensive work is required to determine the exact conditions required for the combined assay in this system. The use of ACMA alone as a probe for the generation of small pH gradients has been studied in bacterial chromatophores (Casadio, 1991) and it was found that the fluorescence of the probe is quenched according to Schuldiner's equation with modifications to account for the dye interacting with the membrane once it accumulates inside. The quenching of ACMA fluorescence was found to be accurately related to ΔpH in the range 0.1-1.5, so it is the probe of choice for the measurement of small ΔpH values (Fregni and Casadio, 1993). The interaction of ACMA with membranes only occurs at very low ionic strength (Casadio, 1991) and since the ionic strength inside the vesicles is reasonably high (150mM, KCl being the major ionic component) this interaction is unlikely to be a problem. Hence in our assay ACMA is likely to be acting in a near-ideal way with quench curves being described by the Schuldiner equation.

The rate of quenching is also related to the buffering capacity inside the vesicles which is dependent on phospholipid head group and amino acid side chain pKa values. With a single buffer inside the vesicles a plot of internal pH versus H^+-pumped would have an inflection point at the pKa of that particular buffer. The buffering situation inside the vesicles is different with many groups with differing pKa values and a similar plot would essentially be linear. However, only the initial part of the quench curve is used for initial rate measurement and hence any non-linear behaviour due to buffering should not be a problem.

With ACMA validated as a reporter of ΔpH it was necessary to modify the assay system to obtain the best possible estimates of initial rates. The development

of an injection system allowed the calculation of rates at high substrate concentration which had previously been underestimated because of the loss of up to 10 seconds of quench curve. The faster curves were more difficult to analyse by the pen-and-ruler approach. This is reflected in the lower values of correlation and determination coefficients for the manual/injection derived data sets (Figure 3.5b; Table 3.1). It is clearly preferable to keep all data collection parameters constant over the entire range of initial rates to prevent unnecessary errors. The introduction of the digital data collection method prevented this source of error since all data is collected at the same rate regardless of the reaction rate and hence this data collection parameter is controlled. The digital collection method also produced the most accurate initial rates with the best fit to Michaelian kinetics and calculated K_m values were consistent with the results seen later in chapter 4 and with results obtained by other research groups (Johnson *et al*, 1982; David and Baron, 1994)

Chapter 4. Kinetics of H^+-translocation and ATP hydrolysis.

4.1 Introduction.

Recent progress in establishing the number of different subunit types, their stoichiometry, arrangement and function in the V-ATPases (Forgac, 1989; Nelson, 1992) has resulted in the recognition of some structural similarities between V-ATPases and ATPases (more properly, ATP-synthases) of the F-type (Kibak *et al*, 1992). In comparison with the large amount of structural information available, there has been relatively little work published on the kinetics of the V-ATPases. Studies have been carried out on ATP hydrolysis by plant vacuolar membranes (Thom and Komor, 1994; Bennet *et al*, 1985), by the V-ATPase purified from brain clathrin-coated vesicles (Arai *et al*, 1989) and by the V-ATPase of bovine chromaffin granules, either in resealed chromaffin granule 'ghosts'(Johnson *et al*, 1982) or as a purified, reconstituted preparation (Hanada *et al*, 1990). These results are complicated in some cases by the use of unfractionated membranes - for example in chromaffin-granule membranes a second ATPase, of unknown function is present (Percy *et al*, 1985; Moriyama and Nelson, 1988a) - and in every case by the use of discontinuous assays for ATP hydrolysis, which makes it difficult to measure initial reaction rates accurately, especially at low substrate concentrations. Alternatively it is possible to measure rates of ATP-dependent proton-translocation into resealed membrane vesicles or proteoliposomes, using suitable probes to provide a continuous spectrophotometric or fluorimetric record of intravesicular acidification as discussed in the preceeding chapter. Results of this type have been published for the H^+-ATPases of plant vacuoles (Bennet and Spanswick, 1983) and for chromaffin-granule 'ghosts' (Flatmark *et al*, 1985). This approach has yielded interesting information about the properties of these enzymes in membranes of physiological lipid composition, although because of the complexity of the systems used, the results are difficult to interpret in terms of mechanistic or regulatory features of the H^+-ATPases.

Previously a rapid method for the purification and reconstitution of V-type H^+-ATPases was developed in this laboratory (Pérez-Castiñeira and Apps, 1990). This procedure was applied to the enzymes from bovine chromaffin granule membranes and from the tonoplast of the Crassulacean acid metabolism plant *Kalanchoë daigremontiana* (Pérez-Castiñeira and Apps, 1990; Warren *et al*, 1992) and ATP-dependent proton-translocation into ATPase-proteoliposomes measured by the quenching of the fluorescence of permeant weak bases derived from acridine. This provided a sensitive means of determining initial reaction rates without the

complications of impure samples and contaminating ATPase II activity. Preliminary studies using these preparations suggested that the V-ATPase was allosterically regulated by nucleotide diphosphates (Apps *et al*, 1992). The aim of this part of the project was to carry out more detailed kinetic studies on the H^+-ATPase from the bovine chromaffin granule membrane by producing data over a wide range of substrate and inhibitor concentrations. Subsequently this data was fitted to rate equations derived from theoretical models of allosteric regulation. It should be possible to correlate the features of these models (numbers of binding sites and binding affinities) with the results of parallel work on nucleotide binding by the ATPase (chapters 5 and 6), and on ligand-induced protein conformational changes.

4.2 Special Methods.

4.2.1 General kinetic analysis.

V-ATPase was purified and reconstituted from chromaffin granule membranes as described in chapter 2. H^+-translocation and ATP hydrolysis were assayed according to chapter 2 with digital data collection used as the method of choice for initial rate determination in H^+-translocation assays. Initial rates of H^+-translocation were entered into the model-fitting programs with normalised weights calculated from the weighting function described in chapter 3:

$$var = a + bv^2$$

where a=0.35 and b=0.002. The weighting factor is the reciprocal of the variance.

At the pH of the assays, and with the concentrations of free Mg^{2+} used, ATP is essentially present wholly as its magnesium complex, $ATPMg^{2-}$. This is not true of ADP, which is present as 20 - 24% ADP^{3-}, and up to 80% $ADPMg^-$. The actual concentration of ADPMg was calculated using a dissociation constant for the complex of 2.4×10^{-4} M (Phillips, 1966) and it is this concentration which is used in the model fitting programs and which is seen in all relevant figures.

Simple linear (Hanes and Hill plots) and non-linear regression (Michaelis Menten plots) were carried out using the Apple Macintosh version of Regression (Blackwell Scientific Publications) and goodness of fit statistics are interpreted from the correlation and determination coefficients respectively which have the same definitions as in chapter 3.

More complex kinetic models were fitted on a Sequent computer under UNIX at the Edinburgh University Computing Service using weighted non-linear regression with substrate concentration (S) and inhibitor concentration (I) as the independent variables and the rate, v as the dependent variable. All of the data points from one experiment were used in each model-fitting run enabling "global" fitting to be done. The program for model fitting is written in 'C' and the least-

squares routine for regression calls the NAG FORTRAN library routines EO4FCF, which uses a combined Gauss-Newton and modified Newton algorithm, and EO4CCF, which uses the Simplex method. Several lesser routines are also called from the NAG library. The number of parameters to be estimated was 6, 7, 8 and 9 respectively for the four models tested (see below). This was too many for the amount and quality of the available data to bear and early attempts to determine the complete set proved unreliable. However, by fixing four of the parameters beforehand, model fitting could be carried out successfully in most cases. This was done by giving n and m (the number of binding sites for ATPMg and ADPMg respectively) integer values (the combinations: n=3, m=1; n=2, m=1 and n=3, m=2 proved to be the most successful) and fitting the Michaelis-Menten equation to the first curve (nucleoside triphosphate concentration varied in the absence of inhibitor), thus obtaining the values of V_{max} and K_r (the equivalent of the Michaelis constant, K_m). The questions posed were (i) which of the four proposed models (see below) and (ii) which of the three combinations of n and m produced the best fit of the data. The two major statistical tests used for this purpose were (i) a Runs test, which analysed the distribution of residuals about a fitted curve and (ii) Akaike's Information Theoretic Criterion (AIC) (Akaike, 1974). The number of runs is the number of times that the sign of the residual changes, from one point to the next along a curve: its theoretical maximum is the number of data points in that particular data set. Obviously the number of positive and negative residuals should approach equality for the best fit. The AIC uses the residual sum of squares adjusted for the number of parameters estimated (Akaike, 1974), and is defined as:

$$AIC = (-2)\log[\text{residual}]^2 + 2(\text{no. of independently-adjusted parameters})$$

A third, subjective criterion was that each of the curves in one experiment should fit equally well.

4.2.2 Labelling with [^{35}S]-ADPβS and effect of ADPMg.

[^{35}S]-ADPβS was purchased from NEN-Dupont at a specific activity of 47.99TBq/mmol (185MBq/ml). 5µl ADP to the indicated final concentrations and 5µl $MgSO_4$ to 5mM final were added to 170µl ATPase solution in a microtitre well 2 minutes before addition of 20µl of 7.4MBq/ml [^{35}S]-ADPβS (of the above specific activity). The samples were illuminated with a 30 watt UV light source (Hanovia, Slough) placed 1cm away, for 30 minutes at room temperature with stirring every 5 minutes. Non-illuminated controls were maintained in normal room light. Samples were transferred to 15ml Corex tubes containing 1.6 ml acetone:ethanol (1:1 v/v) and the microtitre plate wells washed with 2x200µl of acetone:ethanol (1:1 v/v) with the

washes being transferred to the Corex tubes. The samples were incubated overnight at -20°C before being spun for 30minutes at 12K in a Beckman JA20 rotor. The supernatant was discarded and any remaining droplets dried under a stream of N_2 before the pellets were resuspended in 40µl of sample buffer for SDS-PAGE (see chapter 2). The samples were transferred to Eppendorf tubes using a Hamilton syringe with a blunt needle and 20µl of each was loaded onto a 6-15% exponential SDS-PAGE. The gel was treated as for autoradiography in chapter 2.

4.3 Theoretical models proposed for V-ATPase regulation by nucleotides.

We approached the problem of describing the allosteric regulation of the V-ATPase by nucleotides by using a model which describes such regulation with assumptions of enzyme symmetry (Monod *et al*, 1965). The basis for the model is that in the region of the sigmoidal substrate-binding curve below half-saturation where the degree of saturation increases more steeply than the substrate concentration the actual amount of active enzyme is increasing. The cooperative enzyme is envisaged as existing in two conformations, R and T, that differ in their affinity for substrate and/or their catalytic activity. The change between the two states affects all subunits simultaneously and symmetry is conserved in the R/T transition. The assumption of symmetry greatly simplifies the algebra involved in deriving the rate equations. The binding of activators or inhibitors can show cooperativity, providing the number of substrate binding sites is greater than one, by shifting the equilibrium between states of differing activity or affinity for substrate. In the absence of activators or inhibitors the degree of cooperativity observed will depend on the equilibrium position, for example with an equilibrium position very much in favour of the state which binds substrate tightly, very little of cooperativity will be seen in the absence of effectors. In attempting to obtain the best fit to the experimental data we considered four variations of this general two-state concerted-transition model of allosteric regulation. They have the following features in common:

(i) The ATPase exists as an equilibrium mixture of two conformational states, R and T. The equilibrium constant, L for the conformation change is :

$$L = [T]/[R]$$

The value of L is assumed to be independent of the number of nucleotide-binding sites filled.

(ii) The enzyme contains n catalytic sites and m regulatory, nucleotide-binding sites.

(iii) Free nucleotides are assumed to be in equilibrium with nucleotides bound at the catalytic and regulatory sites, i.e. ligand binding reactions and protein conformational changes are much faster than the catalytic step, which is rate-limiting.
(iv) The dissociation constants for binding of nucleotides to the catalytic and to the regulatory nucleotide-binding sites are altered by the protein conformational change, and are therefore different in the R- and T-states.
(v) In either conformational form, the affinities of all sites within a particular class (catalytic or regulatory) are assumed to be equal because the enzyme has the level of symmetry assumed by the model.
(vi) The R- and T-states of the ATPase differ in their catalytic activities; in three of the models the T-state is assumed to be inactive.

The derivation of the general rate equation for the model of Monod *et al* (1965) is illustrated in appendix 1. Four models, of increasing complexity, were considered:

Model 1.

The substrate (S) and inhibitor (I) bind exclusively to the R- and T-states of the enzyme, respectively. The R-state is catalytically active, but the T-state is inactive. There are just two binding reactions, plus the conformational equilibrium and the catalytic reaction. Solution of the algebraic equations describing them gives the rate equation:

$$v/V_{max} = \frac{([S]/K_r)\,(1 + [S]/K_r)^{n-1}}{L(1 + [I]/K_i)^m + (1 + [S]/K_r)^n}$$

where v is the initial rate of the reaction; V_{max} is the maximum velocity of the reaction; [S] the concentration of substrate, and K_r its dissociation constant from catalytic sites; [I] is the concentration of inhibitor and K_i its dissociation constant from regulatory sites.

Model 2.

The inhibitor binds only to the T-state of the enzyme; the substrate binds to both the R- and the T-states, although the latter is inactive. There are three binding reactions, the conformational equilibrium and the catalytic reaction. The rate equation is:

$$v/V_{max} = \frac{([S]/K_r)\,(1 + [S]/K_r)^{n-1}}{L(1+[I]/K_i)^m\,(1+[S]/K_t)^n + (1+[S]/K_r)^n}$$

where K_t is the dissociation constant of the substrate from catalytic sites in the T-state.

Model 3.

As for model 2, but both the R- and the T-states of the enzyme are catalytically active, with different Vmax values. There are three binding reactions, two catalytic reactions and the conformational equilibrium. The rate equation is:

$$v = \frac{V_r([S]/K_r)(1 + [S]/K_r)^{n-1} + V_t L'([S]/K_t)(1 + L'[S]/K_t)^{n-1}}{L'(1 + [S]/K_t)^n + (1 + [S]/K_r)^n}$$

where $L' = L(1 + [I]/K_i)^m$ and V_r and V_t are the maximum velocities of the reactions catalysed by the R- and T-states respectively.

Model 4.

The substrate binds to catalytic sites in both the R- and the T-states, with different affinities; and the inhibitor binds competitively at these sites. Binding of the inhibitor to distinct regulatory sites occurs only in the T-state. Only the R state is catalytically active. There are five ligand-binding reactions, the conformational equilibrium and the catalytic reaction, and the rate equation is:

$$\frac{v}{V_{max}} = \frac{[[S]/\{K_r(1 + [I]/K_a)\}] \cdot [1 + [S]/\{K_r(1 + [I]/K_a)\}]^{n-1}}{[1 + [S]/\{K_r(1 + [I]/K_a)\}]^n + L(1 + [I]/K_i)^m [1 + [S]/\{K_t(1 + [I]/K_b)\}]^n}$$

where K_a and K_b are the dissociation constants of the inhibitor from catalytic sites in the R- and T-state, respectively, and K_i is its dissociation constant from the regulatory site in the T-state.

4.4 Results.

4.4.1 General kinetics and regulation.

The kinetic data were collected as sets of measurements of initial rates; for each set the concentration of the substrate ATPMg was varied between 1μM and 1000μM (up to 15 points) at a number of concentrations of the inhibitor ADPMg. Usually 6 inhibitor concentrations were used, between 0 and 150μM. With the highest ADPMg concentrations, the rates were unmeasurably low with low [ATPMg], but were measured down to the lowest practicable substrate concentration, so that each data set contained some 60-70 rate measurements.

a

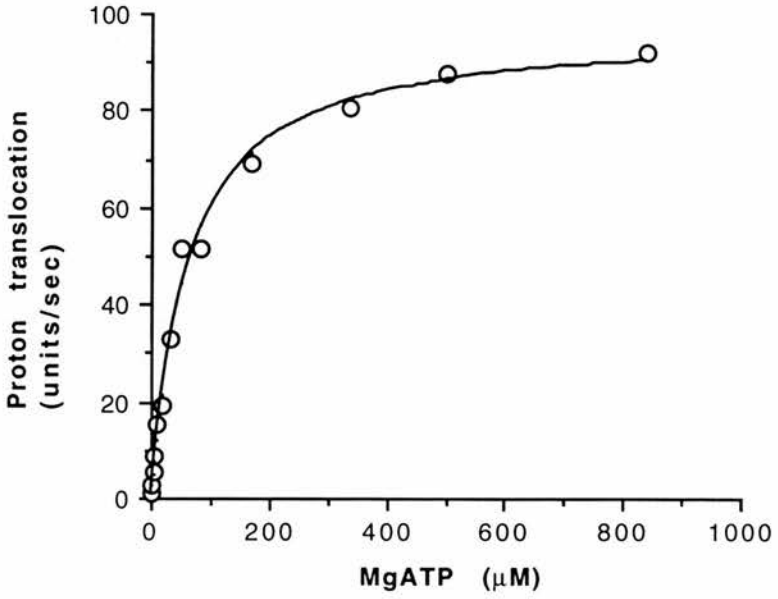

b

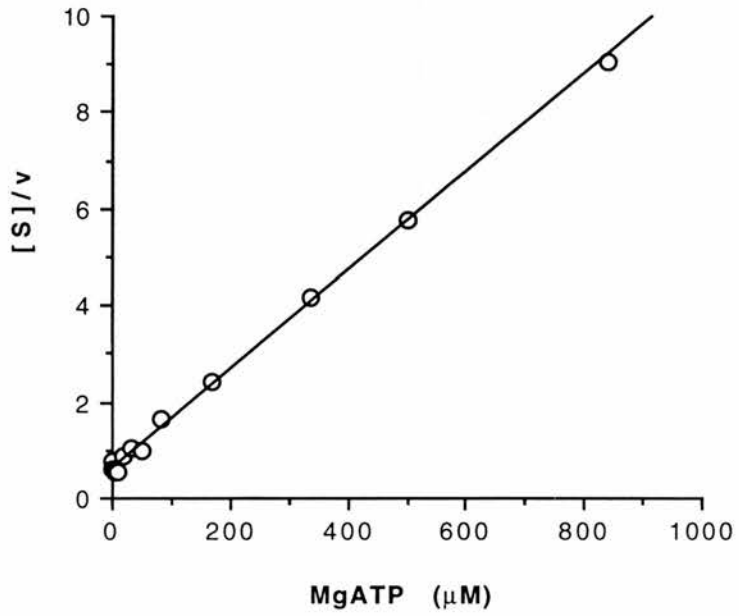

Figure 4.1 (a and b) Initial rates of fluorescence quenching as a function of ATPMg concentration. (a) Michaelis plot: the points are experimental; the line is that calculated by non-linear regression to the Michaelis-Menten equation. (b) Hanes transformation of the data in figure 4.1a: the line was fitted by linear regression. The calculated parameters from both graphs are given in table 4.1.

In the absence of inhibitors the H^+-ATPase exhibits Michaelis-Menten kinetics for proton translocation, i.e. initial-rate/substrate concentration curves are fitted well by the Michaelis equation (Figure 4.1a), and a Hanes plot of the same data is linear (Figure 4.1b). Values of the determination coefficient for the Michaelis-Menten plot and of the correlation coefficient for the Hanes plot are very close to unity with all three nucleoside triphosphates examined as substrates, confirming that the proton-pump exhibits Michaelian kinetics in the absence of inhibitors and suggesting therefore that the ATPase exists in an equilibrium very much favouring the active, high substrate affinity state, R with little T-state present. The order of apparent affinities is ATPMg > GTPMg > ITPMg; with MgGTP as substrate V_{max} is lower than with MgATP or MgITP (Table 4.1). When the same data are expressed as Hill plots (Figure 4.2) a Hill coefficient (n_H) of 1.07 is obtained in the absence of ADP, (Table 4.2), consistent with a good fit by the Michaelis-Menten equation and the absence of cooperativity in the absence of inhibitor. The ATP analogue BzBzATP was also tested as a substrate in the proton translocation assay and was found to act as a substrate at low concentrations but become inhibitory at higher concentrations (Figure 4.3; Table 4.3). The K_m value calculated from the Hanes plot (Figure 4.3) is 5±0.8μM but this value may be inaccurate due to the significant inhibitory effect of BzBzATPMg at concentrations as low as 40μM (Table 4.3).

The kinetics of phosphate release during ATP hydrolysis in the absence of inhibitors are also accurately fit by the Michaelis Menten equation (Figure 4.4) and give a K_m value of 80μM which is close to that observed for H^+-translocation (54μM; Figure 4.1; Table 4.1). The V_{max} values cannot be compared since rates of fluorescence quenching do not yield absolute rates of H^+-translocation. In the presence of 200μM ADPMg the velocity versus substrate curve becomes sigmoidal consistent with allosteric regulation of ATP hydrolysis by ADPMg (Figure 4.4).

All of the nucleoside diphosphates tested produced similar types of inhibition of proton translocation: with increasing inhibitor concentration, there was a change from hyperbolic to sigmoid dependence of the H^+-translocation rate on ATP concentration, with a decrease in V_{max}. The value of n_H rises progressively from 1.07 to 1.75 as the ADPMg concentration is raised to approximately 200μM (Table 4.2) and produces characteristic sigmoid Michaelis-Menten plots indicating that the inhibitor induces cooperative binding of ATPMg.

Inhibition was studied with various total Mg^{2+} concentrations. At the standard Mg^{2+} concentration of 1mM used in all the kinetic data sets, around 80% of the total ADP is present as ADPMg. Increasing the free [Mg^{2+}] to 5mM increases this value to 95% with corresponding reduction in the proportion of free ADP. The

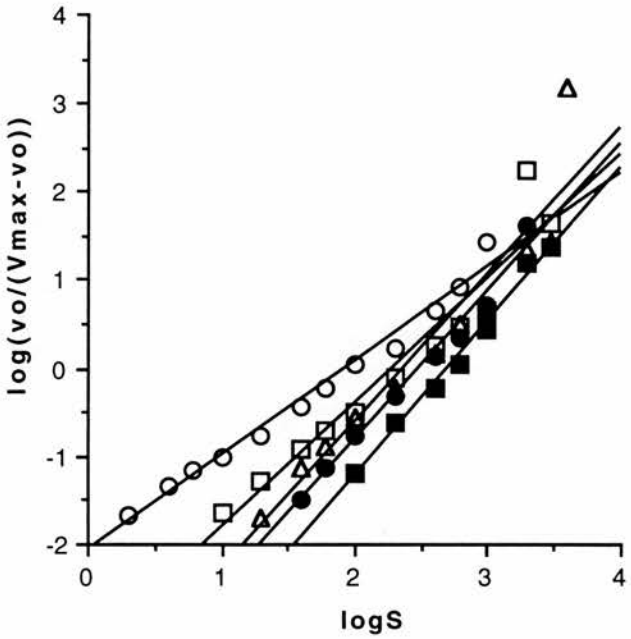

Figure 4.2 Hill plots for initial rates of proton translocation as a function of the substrate (ATPMg) concentration at various concentrations of ADPMg: 0μM, (○);25μM, (□) ; 50μM, (△); 100μM, (●); 200μM, (■).

	parameter	MgATP	MgITP	MgGTP
	n	13	10	8
Michaelis plot	V_{max} (units/sec)	94±5	82±11	16±1
	K_m (μM)	54±5	413±77	161±25
	d	0.991	0.981	0.968
Hanes plot	V_{max} (units/sec)	100±10	84±21	16±1
	K_m (μM)	65±3	441±18	168±10
	r	0.998	0.971	0.986

Table 4.1 Kinetic parameters for proton transloaction in the absence of inhibitors. Parameters were obtained either by using nonlinear regression to fit the Michaelis-Menten equation, or by linear regression in the Hanes plot. The goodness of fit statistics are the determination (d) and the correlation (r) coefficients respectively. In the latter case the criterion $1 > r > 2/\sqrt{(n-1)}$, where r is the correlation coefficient and n is the number of data points, is met in each case.

[MgADP] (μM)	$K_{0.5}$ (μM)	n_H	r
0	85±3.3	1.07±0.04	0.985
25	186±18	1.42±0.13	0.933
50	230±27	1.68±0.18	0.909
100	303±15	1.68±0.07	0.984
200	491±20	1.75±0.07	0.992

Table 4.2 Hill coefficients for ATPMg, with different concentrations of the inhibitor ADPMg. Parameters were obtained using linear regression to fit the Hill equation and the data are graphically represented in figure 4.2.

		[MgBzBzATP] (μM)			
		0	**40**	**200**	**1000**
H+-translocation	**no MgATP**	0	14.5	4.5	0
(U/min)	**+MgATP 1mM**	293	162	45.5	0

Table 4.3 Effect of BzBzATP on proton translocation ± MgATP.

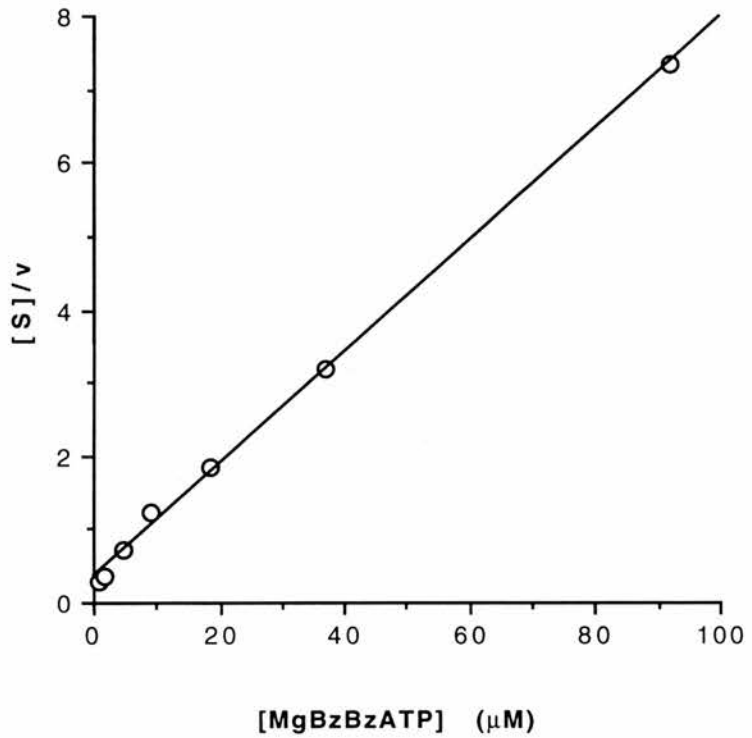

Figure 4.3 Hanes plot for determination of Km value for BzBzATP. Proton translocation was assayed as descibed in chapter 2 but rates were determined manually. The line drawn represents linear regression of the data with slope=0.077±0.001(U/min)$^{-1}$, intercept=0.351±0.056μM(U/min)$^{-1}$ and correlation coefficient=0.998.

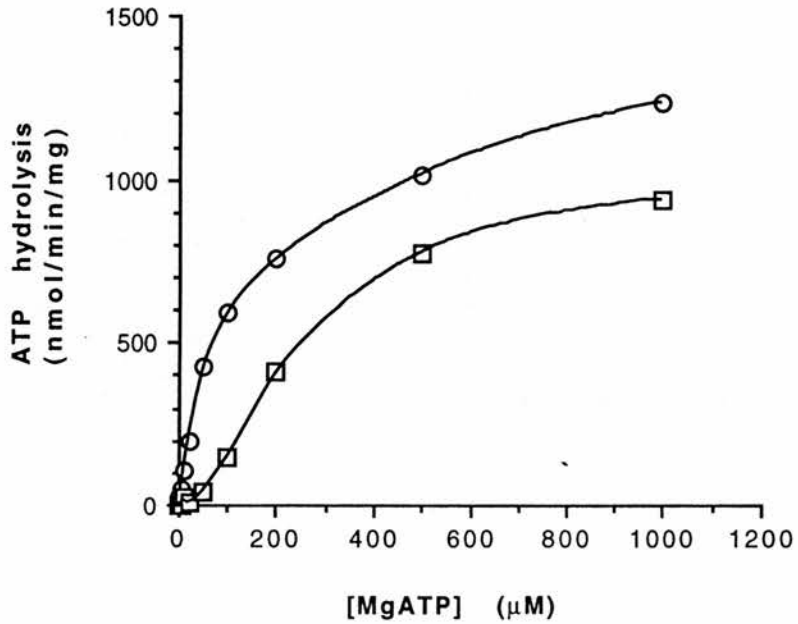

Figure 4.4 Kinetics of ATP hydrolysis in the absence (○) or presence (□)of 200μM MgADP. The data in the absence of inhibitor was fitted by non-linear regression to the Michaelis-Menten equation. ATP hydrolysis was assayed by measuring release of [^{32}P]-inorganic phosphate from [γ^{32}P]-ATP as described in chapter 2. 10μl of reconstituted ATPase was used in each assay.

overall changes in ADPMg concentrations are small compared to the changes in free ADP concentration so if free ADP is the main species interacting with the enzyme then we should see a significant difference in the kinetics of inhibition with these concentrations of Mg^{2+}. With 33μM ADP, 5mMMg^{2+} produces a lower V_{max} than 1mM Mg^{2+}, which may suggest that the increased ADPMg at 5mM has caused greater inhibition but this trend is not evident at 66μMADP (Figure 4.5). Overall then no real significant difference to the kinetics was seen indicating that the main species inhibiting the ATPase is ADPMg and not free ADP (Figure 4.5). Some experiments were also carried out in which the total concentration of ATP exceeded that of Mg^{2+}, so that the concentration of the substrate ATPMg was determined by the total magnesium concentration, and there was significant free ATP but only low levels of free Mg^{2+} (Figures 4.6a and b). With increasing free ATP the initial fluorescence of the assay mix was significantly reduced so to normalise data the rates of proton translocation were corrected by dividing by the average initial fluorescence for that particular concentration of free ATP. Using EDTA to chelate divalent cations shows that free ATP itself is not a substrate, yet there is a background rate of proton translocation in the Mg^{2+}-free mix before the addition of ATPMg, suggesting that a trace of divalent cation complexes with the ATP in the mix and supports proton translocation. These background rates were very small and were subtracted from initial rates obtained on addition of ATPMg. The K_m for ATPMg was increased from 92μM in the absence of free ATP to 187μM at 5mM free ATP while the V_{max} remained unchanged (Table 4.4) suggesting that inhibition by free ATP occurs by simple competition at the active site. The values of the correlation coefficients for the Hanes plots (Table 4.4) also suggest good fit to Michaelian kinetics consistent with competitive inhibition. At 10mM free ATP the K_m is increased further but the Vmax value also decreases (Table 4.4) suggesting that at this higher concentration another form of inhibition is occurring, possibly interaction of free ATP with the T-state catalytic sites. Under the conditions where free ATP is present inhibition by added ADP was very slight (results not shown) as is expected since all ADP will be present as free ADP and this is not the species responsible for allosteric regulation.

The pyrimidine nucleotides uridine- and cytidine triphosphate are poor substrates (Figure 4.7a) but can be shown to stimulate proton translocation supported by ATPMg (Figure 4.7b) consistent with the results of Moriyama and Nelson (1987b). This may suggest that pyrimidine nucleotides stimulate the activity by pulling the equilibrium further over to the R-state side thereby increasing the amount of active enzyme but in the presence of ADPMg, CTPMg exhibits no

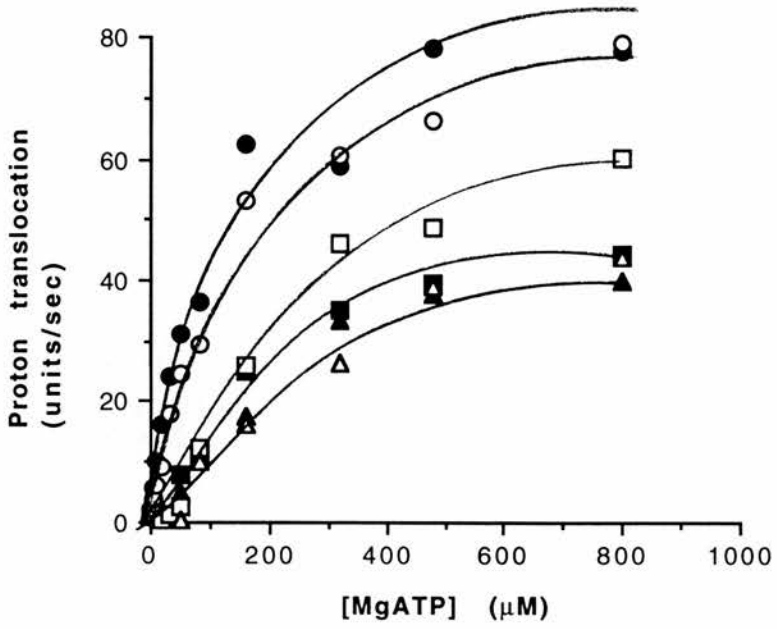

Figure 4.5 Effect of free Mg^{2+} on proton translocation in the absence (○ , ●) or presence of ADPMg at final concentrations of 33μM (□ ,■) and 66μM (△ ,▲). The open and closed symbols represent 1 and 5mM$MgSO_4$ respectively.

a

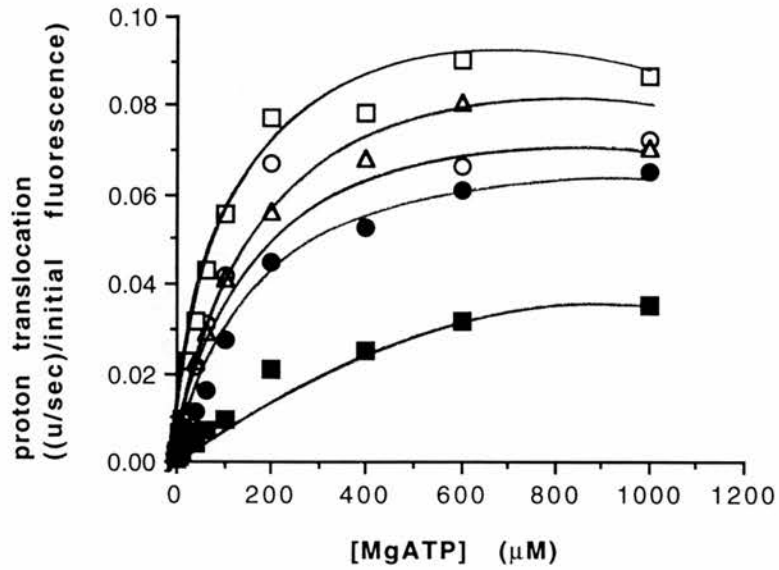

b

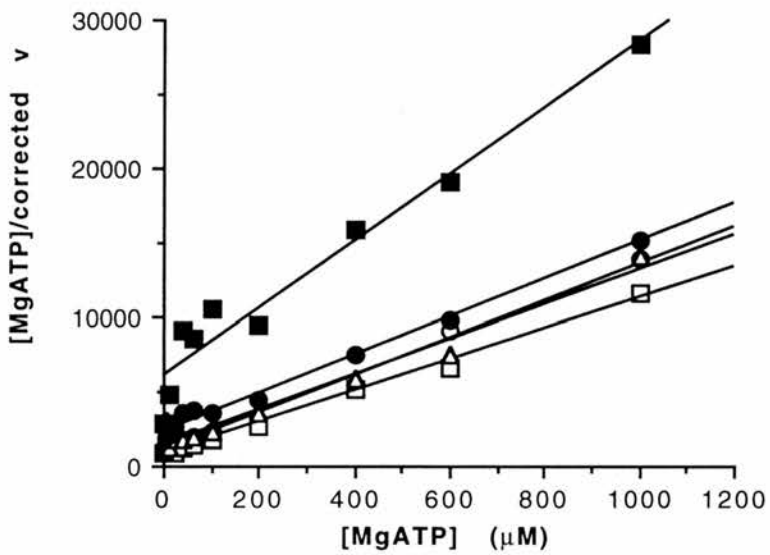

Figure 4.6 (a and b) Proton translocation as a function of ATPMg concentration in the presence of 0 (○), 1mM (□), 2mM (△), 5mM (●), and 10mM (■) free ATP. (a) Typical Michaelis plot. (b) Hanes transformation of the data in figure 4.6a. The rates of proton translocation shown are corrected for different initial fluorescence values at each concentration of free ATP by dividing by the initial fluorescence of the mix at the appropriate concentration.

[ATP] (mM)	K_m (μM)	corrected V_{max}	average initial fluorescence (units)	correlation coefficient
0	92	0.08	1828	0.982
1	79	0.10	1478	0.994
2	123	0.08	1368	0.967
5	187	0.08	1153	0.991
10	268	0.04	1019	0.950

Table 4.4 Statistical and kinetic parameters calculated from the linear regressions of the Hanes plot data in figure 4.6b. V_{max} is shown as the corrected value: multiplication by the initial fluorescence gives the actual value in units/sec. The average initial fluorescence is calculated by averaging the initial fluorescence values for the set of quench curves at each concentration of free ATP.

a

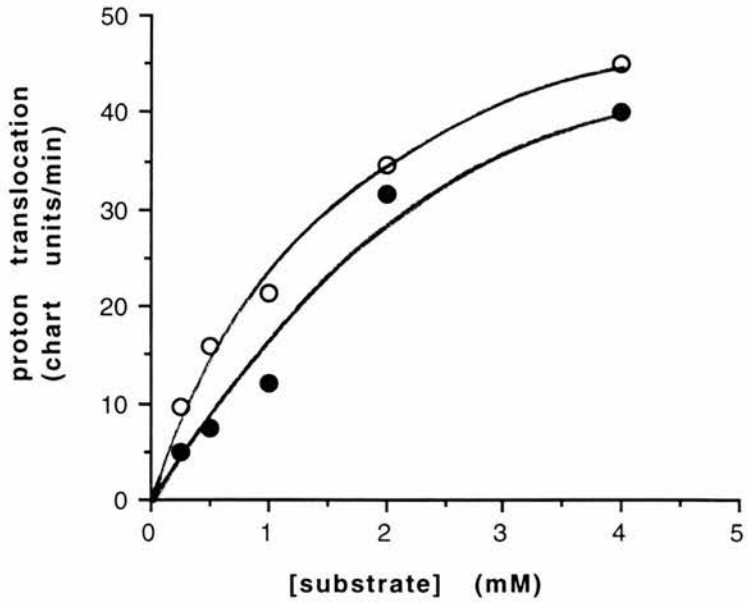

b

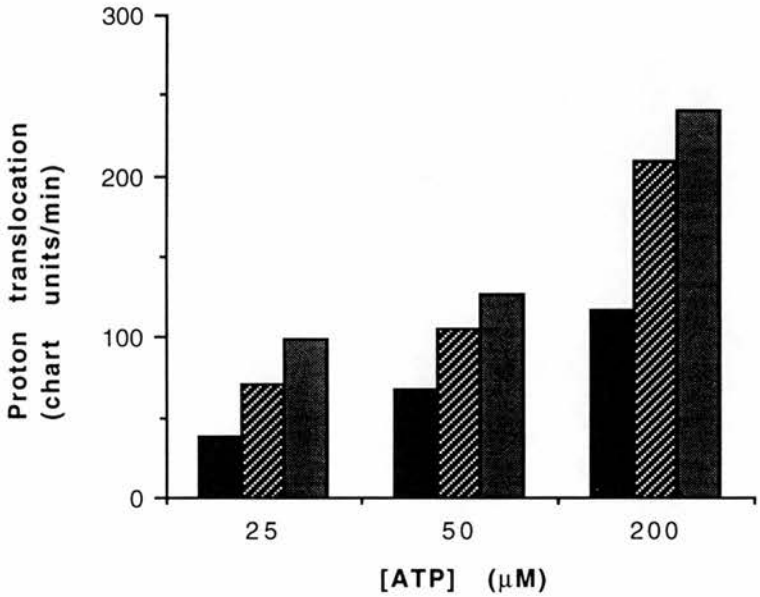

Figure 4.7 (a and b) (a) UTPMg (○) and CTPMg (●) as substrates of proton translocation. Solubility problems were encountered at higher concentrations of Mg^{2+}-complexed nucleotide stocks. (b) the effect of CTP and UTP on proton translocation catalysed by ATPMg at various concentrations: the first bar in each set of three is the control rate in the absence of pyrimidine nucleotide; the second is in 100μM UTPMg; and the third is in 100μM CTPMg. All proton translocation rates for this experiment were determined manually.

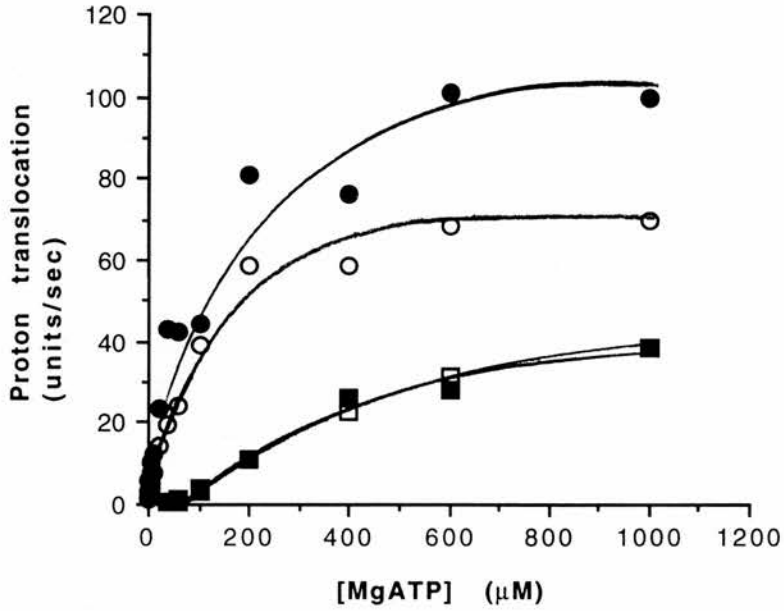

Figure 4.8 Effect of CTPMg on proton translocation catalysed by MgATP in the absence (○ ,●) or presence (□ ,■) of 100μM ADPMg. Open symbols are in the absence of CTPMg; closed symbols are in the presence of 100μM CTPMg.

enhancement of activity (Figure 4.8) indicating that stimulation is not simply a consequence of shifting the equilibrium to the R-state side but occurs by some other mechanism.

4.4.2 Model fitting and kinetic parameter determination.

The four models explored differed in the assumptions made about which of the two states of the enzyme are active, and which bind nucleotides at either the catalytic or the regulatory sites. A summary of the results of model-fitting attempts appears in tables 4.5 and 4.6. No data appear for model 1, because with this model no convergence of the fitting program was obtained even after several hundred iterations.

Convergence was obtained with each of the three other models tested. Comparisons of the fit achieved by the different models was made using the AIC value, which takes into account the number of independently adjusted parameters, and by comparison of the number of "runs", i.e. the distribution of the experimental points about the velocity/substrate curve calculated from the best fit of the model to the data as a whole. The sum of squares of residuals (SSQ) can only be used for evaluation of results obtained with different values of parameters within a particular model (i.e. with the fit obtained using different values of m and n), and should not be used for comparisons between models with different numbers of parameters.

Model 4 consistently produced the best fit to the experimental data points as indicated by the lowest AIC values and better run statistics. In most cases model 3 approaches the statistical performance of model 4; for example with ATPMg as substrate and IDPMg as inhibitor the AIC values for the best fit for models 3 and 4 are very close, at 87 and 85 respectively (Table 4.5). The runs are also very similar for this data set. Thus these data do not discriminate between models in which the T-state was active (model 3) and inactive (model 4). However on closer inspection of optimised parameters it is apparent that in the best fits of model 3 the catalytic activities of the T-state were very small or even negative. This suggests that model 3 is not applicable, and that the T-state of the enzyme is inactive.

Examples of the results of fitting of two data sets are illustrated graphically to show the difference in the fit obtained with models 2 and 4 (Figures 4.9 and 4.10). Although there is only a relatively small difference between the AIC values (Table 4.5) it is obvious that model 4 produces a far superior fit to the experimental data, particularly in predicting the significant decrease in V_{max} produced even by low concentrations of MgADP. This is an aspect of the enzyme's behaviour that model 2 does not predict.

The main data set with ATPMg as substrate and ADPMg as inhibitor was fitted to all three models, using various fixed values of n and m . In every case,

Substrate , inhibitor (Mg^{2+}-complexed)		ATP,ADP				ATP,GDP				ATP,IDP				ATP,ADPβS			
Model	**n,m**	**SSQ**	**runs**	**+/-**	**AIC**	**SSQ**	**runs**	**+/-**	**AIC**	**SSQ**	**runs**	**+/-**	**AIC**	**SSQ**	**runs**	**+/-**	**AIC**
	3,1	137	19	22/26	57	123	24	30/27	50	263	23	24/24	89	168	26	27/35	68
2	2,1	155	19	22/26	63												
	3,2	411	13	18/30	110												
	3,1	124	19	23/25	55	115	24	31/26	49	246	23	20/28	87	151	29	29/33	64
3	2,1	151	20	23/25	64												
	3,2	312	11	18/30	98												
	3,1	74	21	24/24	32	98	25	29/28	42	223	25	21/27	85	151	30	29/33	66
4	2,1	99	21	23/25	45	121	25	25/32	54	252	27	20/28	90	202	22	28/34	84
	3,2	160	17	19/29	66	196	18	27/30	80	341	16	18/30	103	236	25	22/40	93

Table 4.5 Statistical comparison of fitting the different models to data sets with MgATP as substrate, different nucleoside diphosphates as inhibitors and various values of m and n .

Substrate, inhibitor (Mg^{2+}-complexed)		**ITP,ADP**				**GTP,ADP**			
MODEL	**n,m**	**SSQ**	**runs**	**+/-**	**AIC**	**SSQ**	**runs**	**+/-**	**AIC**
	3,1	95	19	17/18	41	11	15	15/14	-20
2	2,1								
	3,2								
	3,1	44	21	18/17	17	11	15	15/14	-20
3	2,1								
	3,2								
	3,1	23	20	17/18	-3	10	18	14/15	-21
4	2,1	28	17	19/16	4	14	13	15/14	-10
	3,2	85	14	19/16	41	21	15	13/16	2

Table 4.6 Statistical comparison of fitting the different models to data sets with different nucleoside triphosphates as substrate, ADPMg as inhibitor and various values of m and n .

a

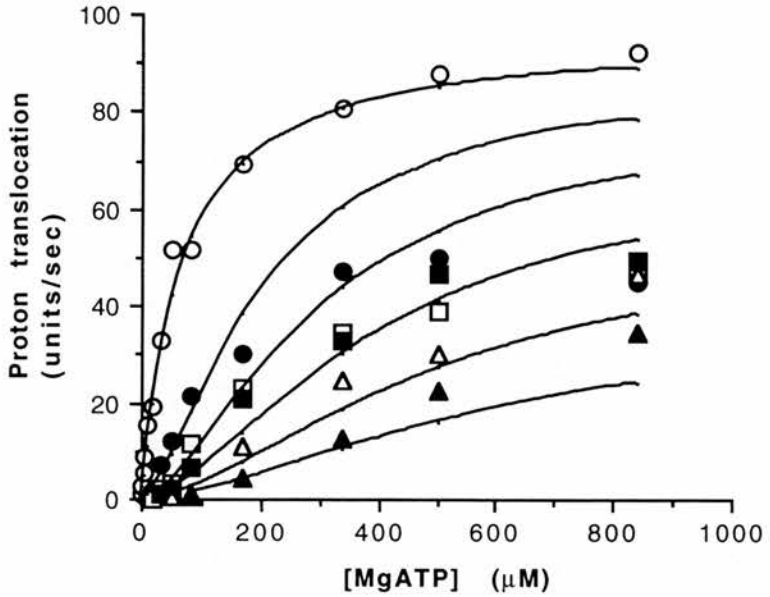

b

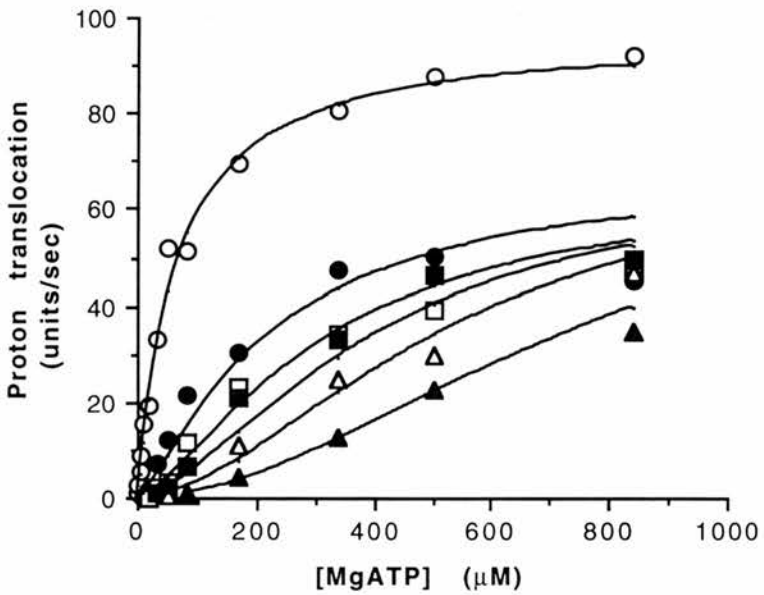

Figure 4.9 (a and b) Fitting of models 2 (a) and 4 (b) to a kinetic data set over a range of ATPMg concentrations with various concentrations of ADPMg: 0 (○); 6.6μM (●); 16.5μM (□); 33μM (■); 66μM (△); and 132μM (▲). The points are experimental; the lines are calculated from the best fit of the rate equation derived from models 2 and 4 with m=1, n=3 and V_{max} and K_r fixed as described in table 4.7.

a

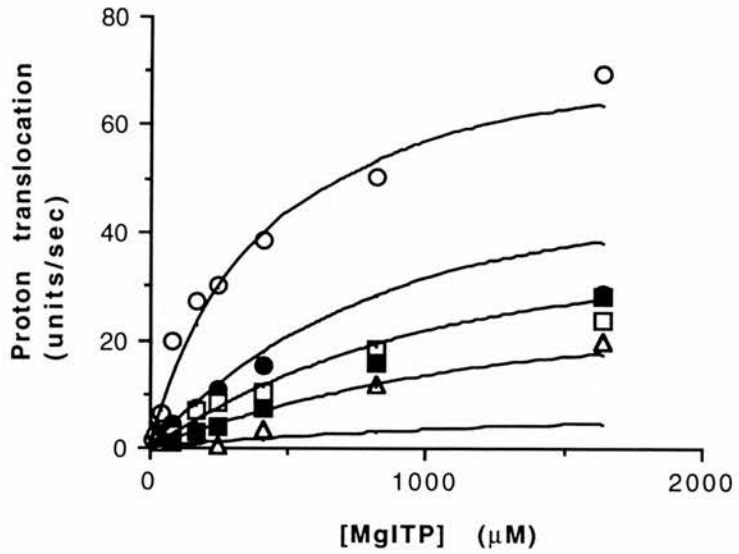

b

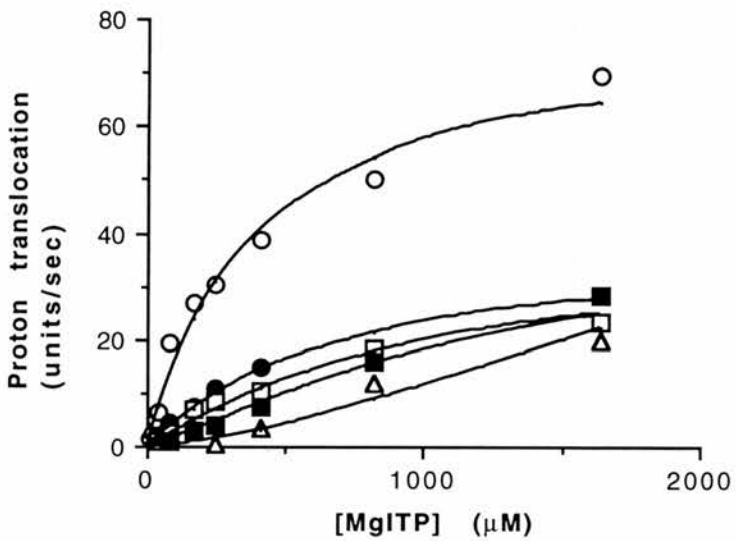

Figure 4.10 (a and b) Fitting of models 2 (a) and 4 (b) to a kinetic data set over a range of ITPMg concentrations with various concentrations of ADPMg: 0 (○); 0.33μM (●); 0.66μM (□); 1.32μM (■); and 6.6μM (△). The points are experimental; the lines are calculated from the best fit of the rate equation derived from models 2 and 4 with m=1, n=3 and V_{max} and K_r fixed as described in table 4.7.

including models that gave a generally less satisfactory fit than model 4, the best convergence was obtained with n and m set at 3 and 1 respectively as indicated by the lowest SSQ and AIC values and by the good run statistics (Tables 4.5 and 4.6). This was also the case for the fitting of model 4 to data sets obtained with various other combinations of substrate and inhibitor (Tables 4.5 and 4.6). If there are indeed 3 nucleoside-triphosphate binding sites as the stoichiometry of the ATPase suggests, the value of n_H is expected to approach 3 at high concentrations of ADPMg, which displace the conformational equilibrium so far that all of the enzyme is in the T state. The highest value of obtained in this work was 1.75 (Table 4.2); but the simple Hill analysis is complicated by the fact the ADPMg acts as a competitive, as well as an allosteric, inhibitor.

A major aim of this work was to determine the dissociation constants for the regulation of the H^+-ATPase by allosteric inhibitors. The value of K_r, the dissociation constant of the substrate from catalytic sites in the R-state, is around 60μM for ATPMg (Table 4.7); the affinity for other purine nucleoside triphosphates is lower in the order ATPMg > GTPMg >ITPMg (increasing K_r values (Table 4.7)). In all cases the substrate binds more tightly to the catalytic sites in the R-state than in the T-state ($K_r < K_t$) although for ATPMg the difference in affinity is less than two-fold. In contrast, nucleoside diphosphates bind to the catalytic site more tightly in the T-state than in the R-state (the exception to this being ADPβS, for which the very large value of K_b suggests that binding to the T-state catalytic site is insignificant). In all cases where ADPMg was used as inhibitor it was found that ADPMg bound with higher affinity to the T-state catalytic site than the substrate ($K_b<K_t$) (Table 4.7). In essence this means that at the concentrations of ADP used in the assays much of the enzyme will be in the T-state with ADPMg bound at both the regulatory sites and the catalytic sites, and this may further enhance the allosteric regulation by ADPMg since ATPMg must empty all of these sites to pull the equilibrium back to the active R-state form. All other nucleoside diphosphates bind to the T-state catalytic sites with lower affinity than ATPMg which may be the reason why these are so much less effective than ADPMg as inhibitors. It is noteworthy that the values of K_a and K_b, which should be characteristic of the inhibitor used but independent of the substrate, are different in the first three data sets reported in table 4.7, all of which are for ADPMg; probably this just reflects the difficulty of fitting such a complex rate-equation to a data-set containing a relatively low number of data points. In any case the values of K_a are larger than the concentrations of ADPMg actually used in the experiments, so they are not significant. We tried fitting the data with a rate-equation derived from a modified version of model 4, in which binding of ADPMg to the R-state was ignored (i.e. $K_a = \infty$), but the overall fit to this model was

Substrate,Inhibitor (Mg^{2+}-complexed)	K_r (μM)	K_t (μM)	L	K_i (μM)	K_a (μM)	K_b (μM)	V_{max} (units/sec)
ATP, ADP	63 ±2.1	147 ±8	5.7×10^{-7} $\pm 2.7 \times 10^{-6}$	3.4×10^{-7} $\pm 3.7 \times 10^{-8}$	232 ±1	17.1 ±1.1	97 ±2.5
ITP, ADP	384 ±27	395 ±12	0.015 ±0.009	0.002 ±0.001	44 ±5.4	0.8 ±0.06	81 ±3.7
GTP, ADP	142 ±0	778 ±79	0.047 ±0.036	0.002 ±0.002	7×10^5 $\pm 1.0 \times 10^9$	1.6 ±0.4	15 ±0
ATP, IDP	63 ±2.6	127 ±7.5	0.008 ±0.02	0.3 ±0.8	1.8×10^6 $\pm 8.5 \times 10^7$	425 ±64	128 ±3.3
ATP, GDP	63 ±2.0	176 ±5.7	0.019 ±0.014	0.6 ±0.4	7.4×10^5 $\pm 7.2 \times 10^6$	780 ±75	103 ±2.0
ATP, ADPβS	37 ±0.9	253 ±9.2	0.053 ±0.016	1.2 ±0.4	4.1×10^3 0.4×10^3	1.2×10^6 $\pm 8.2 \times 10^7$	121 ±1.7

Table 4.7 Kinetic parameters obtained by fitting the rate equation derived from model 4 to a number of data sets, with different substrates and inhibitors. In each case the values of m and n were set at 1 and 3, respectively, and the V_{max} and K_r values were also fixed after calculating their values from the Michaelis curve in the absence of inhibitor.

significantly inferior to that to model 4 (data not shown) illustrating that this parameter, although seemingly insignificant under our experimental conditions, still has an effect on the shapes of the allosteric curves.

Unfortunately the complexity of the rate equation means that although it has been possible to develop models that adequately describe the kinetic features of the ATPase, such as sigmoidal velocity/substrate curves in the presence of ADP, and the effect of ADP on the apparent V_{max} , it was not possible to determine the value of the dissociation constant of ADPMg from its regulatory site with any degree of confidence. This is illustrated by considering the values of L and K_i, constants which describe the allosteric regulation by nucleoside diphosphates, and which always appear in the same term in the rate equations. The value of L, the conformational equilibrium constant, is predicted to be small due to the observed lack of cooperativity in the absence of inhibitor: a good fit to the simple Michaelis-Menten equation (Figure 4.1) and a Hill coefficient close to 1 (Table 4.2), indicates that the enzyme is mostly in the R-state in the absence of ADPMg. As it is a property of the free enzyme, the value of L should be independent of the substrate or inhibitor studied. In most cases L takes a value of 0.01 - 0.05 (Table 4.7). A data set for ATPMg and ADPMg was fitted to the equation derived from model 4, with m and n fixed at 1 and 3 respectively, K_r and V_{max} fixed, and L fixed at 0.01, 0.02 or 0.05: the other constants were allowed to float. There was no significant change in the goodness of fit with the different values of L , nor were the values of K_t, K_a or K_b altered: only K_i was changed (Table 4.8). Since K_i is of the order of 10^{-8}M, under the experimental conditions employed ($[I] >> K_i$) the denominator term $L (1 + [I]/K_i)$ approximates to $[I].L /K_i$, and L/K_i remained approximately constant at $1.7\mu M^{-1}$ (Table 4.8).

4.4.3 Labelling with [^{35}S]-ADPβS and effect of ADPMg.

Labelling of the H^+-ATPase with ADPβS and the effect on this by ADPMg is consistent with the results of model fitting. Under UV irradiation ADPβS is crosslinked to subunits of molecular weights 116, 72, 57, around 40kDa and ones of smaller size (Figure 4.11) with labelling of the 72kDa and the subunits around 40kDa being the most intense. The non-illuminated control also shows labelling of these subunits suggesting some non-UV-dependent crosslinking activity or very tight binding. Labelling is more intense in the presence of Mg^{2+} (Figure 4.11, lanes 2 and 3) confirming that the Mg^{2+}-complexed species is the important one. In the presence of low concentrations of ADPMg the labelling is more intense than with ADPβSMg alone (Figure 4.11, lane 4) while at higher concentrations of ADPMg the sites seem to be protected and the labelling intensity is reduced to that of the non-illuminated

L	K_i (μM)	K_t (μM)	K_a (μM)	K_b (μM)
0.01	0.006	148	233	18
0.02	0.012	141	221	16
0.05	0.031	142	221	16

Table 4.8 Interdependence of the kinetic parameters L and Ki . The equation derived from model 4 was fitted to a data set with ATPMg and ADPMg, with m = 1 and n = 3. V_{max} and K_r were fixed at 97 units/sec and 63 μM respectively, L at one of the values shown in the table and the other parameters allowed to float.

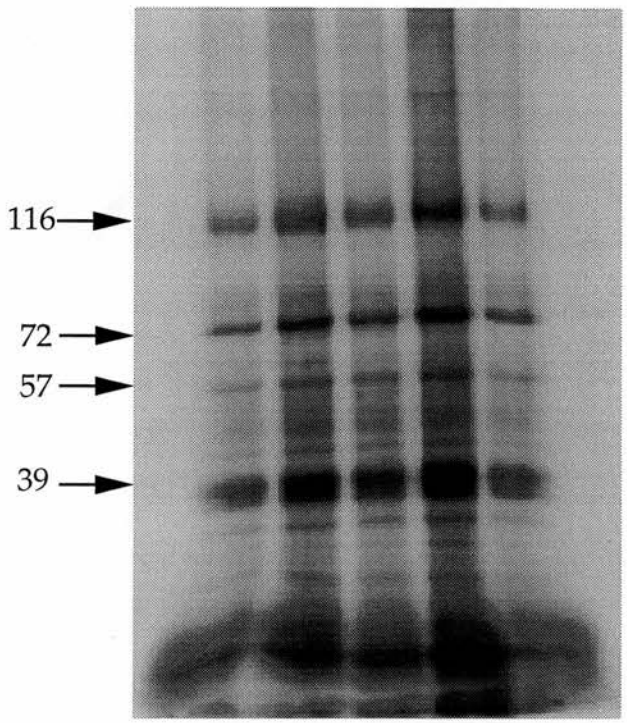

UV	-	+	+	+	+
Mg^{2+} 5mM	+	+	-	+	+
[^{35}S]-ADPβS	+	+	+	+	+
ADP 1μM	-	-	-	+	-
ADP 100μM	-	-	-	-	+

Figure 4.11 Autoradiograph showing labelling of the reconstituted ATPase with [^{35}S]-ADPβS and protection by ADPMg. The conditions for labelling are indicated. Where ADPMg was used it was added before [^{35}S]-ADPβS and before illumination.

control (Figure 4.11, lane 5). Changes in labelling do not appear to be specific for any in particular subunits but rather occur across the range of labelled subunits.

4.5 Discussion.

Although some studies of the kinetics of V-type ATPases have been reported, in most cases comparison with the present work is difficult either because rates of ATP hydrolysis, rather than of H^+-translocation, were measured, or because the ATPase preparations were different (for example, many workers have used unfractionated membranes or sealed membrane vesicles, rather than purified H^+-ATPase). Johnson *et al* (1982) studied ATP hydrolysis by chromaffin granule membranes, and reported simple kinetics with a K_m value of 69μM for ATPMg. Inhibition by ADPMg of proton-translocation into chromaffin-granule 'ghosts' , however, indicated complex binding of ATPMg in the presence of the inhibitor (Grønberg and Flatmark, 1987); in this study proton-translocation was measured from the change in the spectrum of acridine orange, so the presence in the membranes of a second ATPase which does not pump protons should not have affected the results. Recently the kinetics of proton translocation into impure kidney and osteoclast-derived vesicles was studied and again Michaelian kinetics in the absence of inhibitor were observed with K_m values of 62μM and 191μM for ATPMg in the kidney and osteoclast preparations respectively (David and Baron, 1994). No evidence of sigmoidicity was observed with ADPMg in these preparations and a uni-bi-ordered release mechanism was proposed to explain competitive binding of ADPMg and non-cooperative binding of inorganic phosphate. Model fitting was not carried out to explore this proposed mechanism. Studies on ATP hydrolysis by plant V-type ATPases (Kibak *et al*, 1992; Thom and Komor, 1994) have generally shown simple kinetics, although complex inhibition by ADPMg of the reconstituted H^+-ATPase from the tonoplast of *Kalanchoë daigremontiana* (Apps *et al*, 1992) has been reported. In a recent study on a fractionated form of F-ATPase (from the thermophilic bacterium, *Bacillus* PS3) containing only two subunits, α and β (the minimum catalytic unit), this unit of F_1 was found to exhibit non-cooperative, Michaelian ATP hydrolysis with a K_m of 70μM (Saika and Yoshida, 1995). This catalytic unit may represent a close homologue of the catalytic site of the V-ATPases although the hydrolysis catalysed by this F-ATPase unit was not affected by 7-chloro-4-nitrobenzofrazan (Nbf-Cl).

The data of Moriyama and Nelson (1987b) on ATP hydrolysis by purified, reconstituted chromaffin granule ATPase show simple kinetics (K_m = 83μM) in the absence of inhibitors, while 100μM ADPMg produced a complex ATP saturation curve, with a Hill coefficient approaching 2.2: these results are similar to those

reported here. However more complex kinetic behaviour of a similar preparation has also been reported (Hanada *et al*, 1990) with graphical analysis suggesting three different K_m values for ATP (5μM, 30μM and 300μM). Similar results were reported with the ATPase of bovine brain clathrin coated vesicles (Arai *et al*, 1989), which is presumably derived from neurosecretory vesicles and likely to be similar or identical to the chromaffin-granule enzyme; in this case two different K_m values were obtained (80 and 800μM). However when H^+-translocation was measured in this preparation it was found that high concentrations of ATPMg were inhibitory. Kinetic behaviour suggesting two or more types of catalytic site, with different affinities for ATPMg, might reflect inhomogeneity in the ATPase preparation, with two or more separate types of ATPase having different K_m values, or it could be the result of negative cooperativity between different classes of catalytic site within the same enzyme. Similar results were obtained when studying ATP hydrolysis by the reconstituted chromaffin granule ATPase (Pérez-Castiñeira and Apps, 1990), and in this case modelling gave a good fit to the data of a double Michaelis function, with K_m values 1.4μM and 128μM for ATPMg; however when studying proton translocation multiple K_m values, or Hill coefficients significantly less than 1.0, have never been observed. A possible explanation of this discrepancy is that the reconstituted preparation contains several types of ATPase molecule, of different subunit composition or in different environments, not all of which are capable of proton-translocation. The ATPase activity of the reconstituted preparation used in the present work is insensitive to vanadate, so contamination with ATPase II can be excluded; similarly the Triton X-114 fractionation procedure, used in the first stage of purification, removes F_1F_O-ATPase. In any case results such as those shown in table 4.2, with Hill coefficients greater than 1.0, cannot arise through enzyme inhomogeneity, and it can be concluded that the cooperativity induced by ADPMg is a real effect, occurring in the form of the ATPase 'seen' in the assay for proton-translocation. That such effects also occur when ATP hydrolysis is studied are confirmed by the results of Moriyama and Nelson (1987b), and those shown in figure 4.4.

Important assumptions are made in each of the models tested: that equilibrium binding of nucleotides applies; that the rate of the reaction is proportional to the fraction of catalytic sites occupied by nucleoside triphosphate; and that within a given state all catalytic sites are equivalent. Although k_{cat} has not been determined it can be assumed that nucleotide binding is likely to be diffusion-controlled with a k_{on} around $10^8 M^{-1}sec^{-1}$ (Gutfreund, 1972) and hence binding should be much faster than catalysis even at the lowest concentrations used here. The major assumption of symmetry in all the models tested is supported by evidence

in the following chapter although this property does not apply to the F-ATPases (Abrahams *et al*, 1994).

Analysis of the closely-similar V-ATPase isolated from bovine brain clathrin-coated vesicles has suggested that it contains 3 copies each of subunits A (72 kDa) and B (57 kDa) (Arai *et al*, 1988). It is established that the 72 kDa subunits contain the catalytic sites (Forgac, 1992), and the present kinetic results, suggesting three nucleoside-triphosphate binding sites, are therefore in agreement with the proposed subunit stoichiometry. The sequence similarity between the A and B subunits, and their evolutionary relationship to the α and β subunits of F-type ATPases (Kibak *et al*, 1992), suggest that the B subunits might contain the regulatory nucleotide-binding site, and the 57 kDa subunit of the V-ATPase from beet tonoplast has been shown to be labelled by the covalently-reacting ATP analogue, BzBzATP (Manolson *et al*, 1985). It is possible that the single high-affinity nucleoside-diphosphate binding site identified in the present work is located on one of these subunits, but it is noteworthy that subunit D (39 kDa), probably-present in a single copy (Arai *et al*, 1988), can also be labelled by ATP analogues (Moriyama and Nelson, 1987b).

The results of labelling the ATPase with ADPβS confirm the results of the model fitting. ADPβS appears to label the active site of the enzyme (the 72kDa subunit) as well as several other subunits including the 57kDa subunit identified as a nucleotide-binding subunit using BzBzATP (Manolson *et al*, 1985). At low concentrations of ADPMg permitting binding to the regulatory site in the T-state, the intensity of labelling with ADPβS is increased. ADPβS has greater affinity for the T-state regulatory site from the results of model fitting so the presence of low concentrations of ADPMg might be expected to cause this increase by pulling the equilibrium further over to the higher affinity T-state position. At high ADPMg concentrations the nucleotide will compete with ADPβS for binding to the catalytic sites on the T-state and hence we would expect to see protection occurring which is illustrated by the reduction in labelling intensity. Labelling of the subunits around 40kDa implicates a role for these subunits in nucleotide binding and regulation of the ATPase. In chapter 5 it is shown that the 39kDa subunit is labelled by [^{3}H]-NEM and protected by nucleotides. Only one 39kDa subunit is thought to be present in each holoenzyme complex (Supek *et al*, 1994) and this together with labelling and protection of this subunit with nucleotides may suggest that it is this subunit which contains the single ADP regulatory binding site. It is significant also that this subunit has been shown to be dissociable under particular conditions (see chapter 5) which may allow for another level of regulation of the enzyme. It is possible that the lack of allosteric regulation by ADPMg in the kidney and osteoclast V-ATPase

(David and Baron, 1994) may be due to lack of a homologue of this subunit but this is purely speculative and remains to be tested.

The observations of activation by CTP and UTP (Figure 4.7; Moriyama and Nelson, 1987b), and of tight and loose binding sites for TNP-ATP (Adachi *et al*, 1990a) may be relevant here, but the subunit locations of the binding-sites for these nucleotides have not been determined. Evidence showing for the first time that V-ATPases have nucleotide-binding sites which exchange at different rates has recently been published (Zhang *et al*, 1995). Using the photoaffinity probe, 2-azidoATP it was shown that both the A and B subunits were labelled under conditions designed to favour the modification of rapidly exchangeable sites (<2min) while only the A subunit was labelled under conditions revealing slow nucleotide exchange (>2min). These results will have important implications when the final mechanism of the V-ATPases is being discussed but are difficult to relate to the results presented here since proton translocation was usually measured after the ATPase had been in contact with nucleotide for longer than two minutes.

Very recently we have studied the effect of 2-azido- and 8-azido ADP as inhibitors of H^+-ATPase activity. Although 8-azido ADPMg was only slighlty inhibitory it was found that the affinity for 2-azido ADPMg was only around three times lower than that for ADPMg. The availability of [^{32}P]-2-azido ADP will be invaluable in probing the location of the regulatory site.

The physiological significance of the inhibition by ADPMg is at present unclear. The value of K_i deduced from model fitting is very small (< 0.1μM) but since the value of L is also small ADPMg only becomes an effective inhibitor at much higher concentrations (> 1μM) which are in the physiological range.

Chapter 5. Kinetics of N-ethylmaleimide inactivation of V-ATPases.

5.1 Introduction.

The use of covalently-reacting, residue-specific reagents has facilitated the study of many enzymes. N-ethylmaleimide (NEM) is a specific sulphydryl group alkylating reagent and reacts with exposed cysteines often altering enzymatic activity. NEM has been shown to inhibit H^+-translocation and amine uptake in chromaffin granule "ghosts" (Apps *et al*, 1980) and also to inhibit H^+-ATPase activity in purified chromaffin granule membranes (Percy and Apps, 1986) and purified ATPase (Moriyama and Nelson, 1987b; Percy *et al*, 1985). V-ATPases from other sources including plasma membrane (Gluck *et al*, 1992), coated vesicle (Arai *et al*, 1989) and plant tonoplast (Griffith *et al*, 1986; Mandala and Taiz, 1986) are also inhibited by NEM. Inactivation by 10-20μM NEM is a specific characteristic which helps distinguish V-ATPases from the NEM-resistant F-ATPases. V-ATPases can be distinguished from those of the P-type which are also inhibited by NEM but have a much lower sensitivity being inhibited in the 100μM-1mM range (Forgac, 1989). The sensitivity to low concentrations of NEM has been exploited in purifications of the V-ATPase from chromaffin granules to distinguish between ATPase II, a P-type ATPase and the V-ATPase itself (Cidon and Nelson, 1986; Moriyama and Nelson, 1988a).

NEM was the major probe used to determine that the 72kDa subunit is the site of substrate binding and hydrolysis in the V-ATPases (Percy and Apps, 1985; 1986). It was shown that NEM labels the 72kDa subunit of the chromaffin granule ATPase (Percy and Apps, 1986; Moriyama and Nelson, 1987b) and the coated vesicle ATPase (Arai *et al*, 1987b) and that this labelling is blocked in the presence of MgATP. NEM was also shown to label subunits of molecular weights 115 and 39kDa (Moriyama and Nelson, 1987b) but those subunits had lower reactivity and the presence of MgATP had little effect on the labelling intensity. The cysteine residue responsible for the NEM sensitivity of the coated vesicle ATPase has recently been identified as cysteine 254 of the 72kDa subunit (Feng and Forgac, 1992a). It was demonstrated that both NEM and Nbf-Cl inactivate the enzyme by reaction with this same cysteine (Forgac, 1992), which is located in the Walker consensus "A" sequence, GXXGXGKTV (Walker *et al*, 1985), an established nucleotide-binding motif. All vacuolar ATPases sequenced to date have a cysteine at this location in the Walker consensus: these include V-ATPases from bovine coated vesicles (Puopolo *et al*, 1991), *Neurospora* (Bowman *et al*, 1988b), carrot tonoplast (Zimniak *et al*, 1988), and yeast vacuole(Hirata *et al*, 1990) whereas it is a valine residue in the F-ATPases and a

serine in the archaebacterial (H^+)-ATPases (Penefsky and Cross, 1991), accounting for the resistance of the latter two classes to sulphydryl reagents. It has even been suggested (Nelson, 1992b) that the elimination of this residue is an evolutionary adaptation to an oxidising environment.

NEM has proved to be a useful tool in investigations of the regulation of the V-ATPases by the formation of intramolecular disulphide bonds. Feng and Forgac (1992, b) recently demonstrated that the coated vesicle ATPase could be inactivated by the formation of an intramolecular disulphide bond between cysteines 254 and 532 during autooxidation on removal of reducing conditions. The inactivating disulphide bond could be distinguished from others because its formation could be selectively blocked by the presence of MgATP. This is consistent with the importance of cysteine 254 in the nucleotide-binding domain and inactivation of the ATPase by removal of its sulphydryl group by disulphide bond formation. In the folded enzyme these residues are likely to be in close proximity and the results were taken to suggest a possible role for reversible sulphydryl group oxidation and reduction in regulating intracellular acidification.

The kinetics of NEM inactivation of the vacuolar ATPases have never been studied in detail. Timecourses of inhibition of ATP hydrolysis activity by NEM have suggested that the ATPase is inactivated in a pseudo-first order process with a second order rate constant of $10.8 \times 10^3 min^{-1}M^{-1}$ (Percy and Apps, 1986). This rate constant of inactivation was reduced to $180 min^{-1}M^{-1}$ in the presence of 2mM ATP. We have exploited this property of NEM inactivation and protection by nucleotides to investigate the dissociation constants for these nucleotides from their binding sites.

5.2 Special Methods

5.2.1 Materials.

[^{3}H]-NEM (specific activity of 2075GBq/mmol) was purchased from NEN/Dupont. The radiolabelled NEM was supplied as a solution in pentane and was extracted into an equal volume of ethanol with the pentane then being removed under a vacuum. The recovery of NEM during this procedure was about 65% as measured by scintillation counting. [^{3}H]-NEM was used at 1μM final concentration in all labelling experiments with the addition of various concentrations of non-radioactive NEM as indicated in the figure legends. Soluene-350 and Ultima Gold were purchased from Packard.

5.2.2 Kinetics of NEM inactivation of proton translocation.

V-ATPase was purified and reconstituted as described in chapter 2 one day before the NEM experiment. On the day of the experiment 200µl aliquots of ATPase were passed through 1ml packed Biogel P6-DG columns equilibrated with 150mM KCl, 10mM HEPES-KOH, pH7.4, 5mM $MgSO_4$ (1mM for nucleoside triphosphate experiments) to remove DTT and to equilibrate the ATPase with Mg^{2+}. The ATPase samples from individual Biogel columns were pooled to avoid any variation in samples. The pooled ATPase was added to nucleotide or distilled water in controls and incubated for 3-5minutes before NEM as an ethanolic solution was added (the ethanol was kept constant throughout at 1%v/v and the reaction mix kept on ice). Immediately after the addition of NEM, 10µl of the reaction mix was taken and added to 10µl of assay mix (proton translocation ACMA mix with the addition of 1mM DTT) to stop the alkylation reaction. This was the zero-time sample and represented 100% activity. Each 20µl sample was left on ice until assay. Proton translocation was assayed by adding 470µl of assay mix to the 20µl stopped reaction mix and then transferring to the glass fluorimeter cuvette. The fluorescence was allowed to stabilise and proton translocation initiated by injection of 10µl of 50mM MgATP. Initial rates were estimated manually since rates were slow enough to allow accurate measurement without the need of the digital data collection which would have take considerably more time than was available in view of the large numbers of data points required. The exact concentration of NEM used in each experiment was calculated according to its molar absorbance of $620M^{-1}cm^{-1}$ at 300nm (Alexander, 1958).

5.2.3 Autoradiography and labelling of the V-ATPase with [^{3}H]-NEM.

Reconstituted ATPase was prepared as usual but with the omission of dithiothreitol from the purification buffers. 100µl reconstituted ATPase was incubated with various concentrations of NEM as indicated in the figure legends after incubation with or without nucleotide. After the specified time on ice the reaction was stopped by the addition of 10µl dithiothreitol. The solution was vortexed before the addition of 10 volumes of ice-cold acetone:ethanol (1:1 v/v) and the samples incubated overnight at -20°C. Following precipitation with acetone:ethanol the tubes were centrifuged for 10 minutes at 13000rpm in an MSE microcentaur microfuge the supernatant was removed and any remaining droplets dried under a stream of Nitrogen. 20µl of sample buffer for SDS-PAGE (see chapter 2 for composition) was added to solubilise the pellets and 15µl of the resuspended pellets were loaded onto 6-15% exponential acrylamide gels. The gels were then treated for autoradiography as in chapter 2 and exposed to Hyperfilm for as long as was necessary to record a significant signal.

For labelling experiments in which solubilised ATPase was used the ATPase was purified as usual with the omission of DTT and lipids. The purification was stopped with the ATPase either left solubilised in 1.8% octylglucoside or passed through 1ml columns of P6-DG equilibrated in 1% $C_{12}E_9$, 150mM KCl, 10mM HEPES-KOH, pH7.4. The labelled samples were precipitated and prepared for SDS-PAGE in exactly the same way as the reconstituted samples.

5.2.4 Gradient separation of [^{3}H]-NEM labelled ATPase.

Unwashed P1 was prepared as described in chapter 2 and solubilised in 1.8% octyl glucoside as usual but with the omission of DTT and lipids from the purification buffers. The solubilised sample was centrifuged (g_{av}=412000xg) for ten minutes and the supernatant was the partially purified ATPase which was then incubated with 5μM [^{3}H]-NEM (2.1MBq/ml) for 30minutes on ice. The reaction was stopped by the addition of one tenth volume of 10mM DTT and was then loaded onto a 5-20% glycerol gradient (see chapter 2) with the addition of 1% octyl glucoside to the gradient buffers. The gradients were treated as in chapter 2. Any pellet present was resuspended in 1ml 10mM HEPES-NaOH, pH7.4. 10 volumes of ice cold acetone:ethanol (1:1v/v) was added to each fraction which were then treated for autoradiography as above but with the concentration factor being 10 .

An antiserum against the 39kDa subunit was obtained from N.Nelson and was used at a 1:1000 dilution.

5.2.5 Trypsin digest of reconstituted and solubilised ATPase.

Reconstituted ATPase with or without the addition of one tenth volume of 10% w/v $C_{12}E_9$ was used in a trypsin digestion experiment. The soluble or reconstituted ATPase was added to trypsin to give the final concentrations indicated in the figure legends and proteolysis allowed to proceed for 30minutes at room temperature. The reaction was stopped by the addition of PMSF, TLCK and TPCK to 50μM final concentrations and then one third volume of hot (95°C) 4X stock phthalate sample buffer (200mM KHPhthalate, 40%w/v glycerol, 20% SDS) containing the same concentrations of DTT and Bromophenol blue as the normal sample buffer (see chapter 2, SDS-PAGE) was added and the samples left at 95°C for 5 minutes before loading equivalent volumes onto SDS-PAGE.

5.2.6 Subunit specificity of NEM labelling and stoichiometry.

Reconstituted ATPase was prepared in the absence of DTT and incubated with 10μM [^{3}H]-NEM (2.1MBq/ml) in the presence of 5mM $MgSO_4$ on ice. At the specified times 100μl of the reaction mix was added to 10μl of DTT in an Eppendorf

tube and the samples then treated with acetone:ethanol and prepared for SDS-PAGE as in section 5.2.3. The gel was fixed, stained with Coomassie blue R and destained as usual. A corresponding gel loaded with carbonic anhydrase standards was run and was fixed, stained and destained in the same box for determination of the amount of protein in each subunit band. Following destaining the amount of protein in each band was determined using two-dimensional raster scans of the standard protein and the ATPase samples on a Joyce-Loebl chromoscan 3. Following raster scanning the subunit bands were excised, solubilised in 500µl Soluene-350 overnight at room temperature and then counted in 10ml Ultima Gold scintillant.

5.3 Results.

5.3.1 Inactivation of ATP-dependent proton translocation by NEM.

We investigated the kinetics of interaction of N-ethylmaleimide with the purified reconstituted H^+-ATPase by studying the timecourse of inactivation in the presence of different concentrations of inhibitor. The interaction between NEM and the enzyme can be described:

$$E + NEM = E^*$$

and $$dE/dT = -k_{(real)}[E][NEM] \qquad \textbf{(Equation 1)}$$

Where $k_{(real)}$ is the second-order rate constant of the reaction.
Equation 1 describes a second order reaction but since [NEM]>>[E] in all experiments, [NEM] effectively becomes a constant and we can write:

$$dE/dT = -k_o[E] \qquad (2)$$

Where $k_o=k_{(real)}[NEM]$ and equation 2 describes a first order reaction. k_o therefore is a pseudo-first order rate constant for a given NEM concentration. We observed that the decay of proton translocation with time is indeed exponential (Figure 5.1a) as would be expected from pseudo-first order kinetics. By integrating, rearranging and taking logarithms of equation 2 we can derive a linear relationship between activity and time:

$$\log E = \log E_o - k_o t/2.3 \qquad (3)$$

We can equate E to activity and hence a plot of log activity versus time will give a straight line of slope $k_o/2.3$ if the reaction is indeed pseudo-first order. Figure 5.1b shows semilog plots at various NEM concentrations with straight lines fitted through the experimental points by unweighted linear regression. The correlation coefficients for these fitted lines are very close to unity indicating a good fit to

a

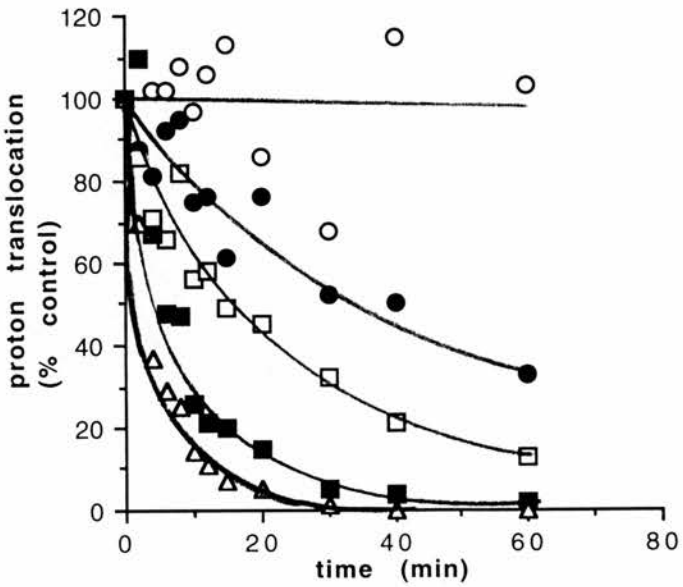

b

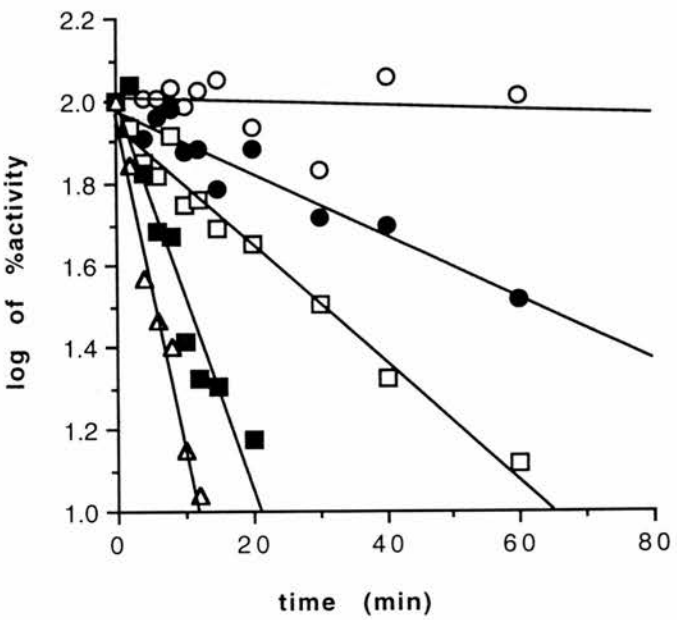

Figure 5.1 (a) Timecourses of inactivation of proton translocation by NEM. (b) semilog plot transformation of the data in Fig 5.1(a).

Proton translocation was assayed as described in chapter 5 "special methods" in different NEM concentrations: 0μM NEM (○); 10.1μM NEM (●); 20.2μM NEM (□); 50.5μM NEM (■); 101μM NEM (△).

[NEM] (μM)	correlation coefficient	$k_o \times 10^3 (min^{-1})$
0	0.019	1.1±2.5
10.1	0.914	17.5±1.7
20.2	0.973	33.4±1.8
50.5	0.923	108±11.9
101	0.978	182±12.1

Table 5.1 Dependence of k_o on the concentration of NEM and correlation to pseudo-first order kinetics. k_o values were determined from the slopes of the regression lines shown in figure 5.1.

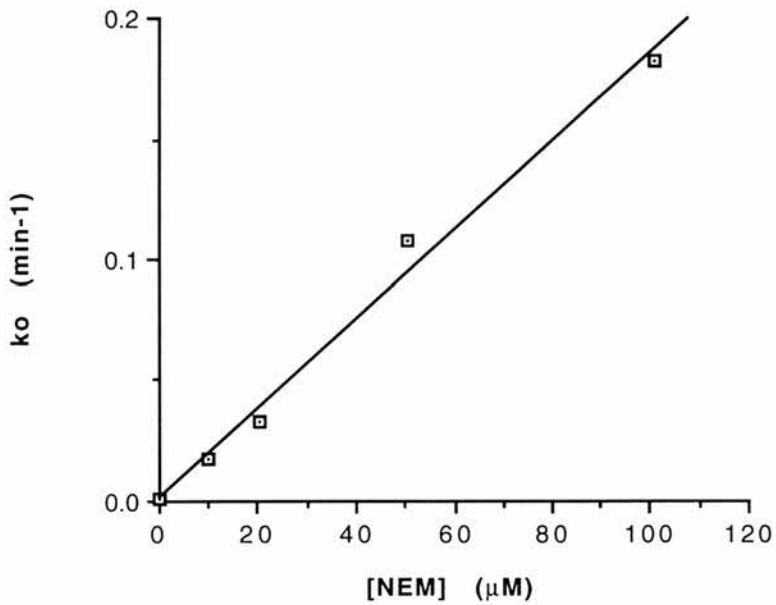

Figure 5.2 Determination of the true second order rate constant for inactivation by NEM. The line represents linear regression of the data points to give a correlation coefficient value of r=0.989 and a real second order rate constant value of $k=1.8 \times 10^{-3} min^{-1} \mu M^{-1}$.

equation 3 (Table 5.1) and the k_o values increase from $1.1x10^{-3}min^{-1}$ in the absence of NEM to $181.7x10^{-3}min^{-1}$ at 101μM NEM. A plot of the calculated k_o values versus the concentration of NEM shows the expected linear relationship with correlation coefficient, r = 0.989 (Figure 5.2) and allows the calculation of the real rate constant, k of $1.8x10^{3}min^{-1}M^{-1}$. The linearity of the semilog plots (Figure 5.1b) and the plot of k_o versus the [NEM] (Figure 5.2) indicate a good fit to pseudo-first order kinetics and also suggest that NEM inactivates the H^+-ATPase by binding to one class of site.

5.3.2 Protection from NEM inactivation by nucleotides.

NEM and nucleotides have been used together by several laboratories as competitors for the same binding sites in the V-ATPases and these interactions have led to many insights into the location of the catalytic site. The presence of bound nucleotide has been shown to inhibit binding of NEM at this same site and hence the enzyme is protected from inactivation (Moriyama and Nelson, 1987b; Percy and Apps, 1986). If the enzyme, E is inactivated at a rate k_o and the nucleotide-enzyme complex, EI is fully protected we can write:

$$k_{app} = k_o(E/e_t)$$

where e_t is the total enzyme concentration.

But $$e_t = E(1+[I]/K_D)$$

Substituting gives:

$$k_{app} = k_o/(1+[I]/K_D)$$

and hence:

$$1/k_{app} = 1/k_o + [i]/K_D.k_o \qquad \textbf{(4)}$$

where [i] is the concentration of protecting nucleotide, k_{app} is the measured rate constant derived from semilog plot linear regression slopes such as figure 5.1a, k_o is the pseudo-first order rate constant in the absence of nucleotide at a particular NEM concentration that remains fixed throughout the experiment and K_D is the dissociation constant of that nucleotide from the protecting site. It is therefore possible to design a protocol whereby dissociation constants can be determined by plotting $1/k_{app}$ versus the concentration of protecting nucleotide at a fixed NEM concentration.

Due to difficulties in determining dissociation constants of nucleoside diphosphates in allosteric regulation of proton translocation and kinetic model fitting (see chapter 4) we decided to exploit the pseudo-first order kinetics exhibited in inactivation of the chromaffin granule ATPase by NEM to determine dissociation constant values for the nucleotides that exhibit allosteric regulation of proton translocation.

Reconstituted ATPase was incubated with various concentrations of nucleotide before NEM was added to a constant value of 50μM to start the inactivation reaction. For competitive binding at a single site a plot of $1/k_{app}$ versus [nucleotide] would be linear according to equation 4 but this was not the case for most nucleotides tested. The ATPase was protected from NEM inactivation by submicromolar concentrations of MgADP (Figure 5.3a). It should be noted that controls were performed in the absence of NEM but in the presence of nucleotide to check for control rates of inactivation. For nucleoside diphosphates there was no significant inactivation in the absence of NEM but MgATP produced some inactivation in control experiments and a possible reason for this is explained later. When the data from figure 5.3a is transformed into a semilog plot for determination of k_{app} values linearity was observed (Figure 5.3b) indicating that inactivation is pseudo-first order in the presence of nucleotides. The apparent rate constant value was reduced from $48.3x10^{-3}\pm5.3x10^{-3}min^{-1}$ in the absence of nucleotide to $6.4x10^{-3}\pm2.9x10^{-3}min^{-1}$ in 4.9μM MgADP (Table 5.2) but when the data was plotted for determination of dissociation constants as in figure 5.4 the protection profile was a complex biphasic curve indicating that protection from NEM by nucleotides is not a simple process but involves more than one type of binding site. Similar results were obtained for free ADP and MgIDP as protecting nucleotides. k_{app} decreases between 0 and 195μM free ADP (Table 5.4) and between 0 and 495μM MgIDP (Table 5.6). This decrease in the apparent rate constant is again nonlinear (Figures 5.6 and 5.6) indicating that these nucleotides also protect the ATPase by binding to different types of binding site. In all cases there is partial protection at low nucleotide concentrations followed by full protection at higher concentrations of nucleotide. The efficacy with which the nucleotides protect is in the order MgADP>MgIDP>ADP. This is consistent with regulation of proton translocation seen in chapter 4 and with results which suggest that it is MgADP and not free ADP which is the species responsible for regulation of the enzyme. These biphasic curves of $1/k_{app}$ versus [nucleotide] are consistent with the predictions of the kinetic models (chapter 4) that MgADP does not bind only to a single regulatory site but also to the catalytic sites on the enzyme with lower affinity (Webster *et al*, 1995). A model was developed to describe the inactivation of the enzyme by NEM incorporating these features of nucleotide binding in an effort to fit the biphasic NEM inactivation data to this equation and obtain dissociation constants using an optimisation program. We assumed that the R and the T states of the enzyme are inactivated by NEM at different rates, k_1 and k_2 respectively and that there is no interaction between NEM-reactive sites as is indicated from the pseudo-first order kinetics.

a

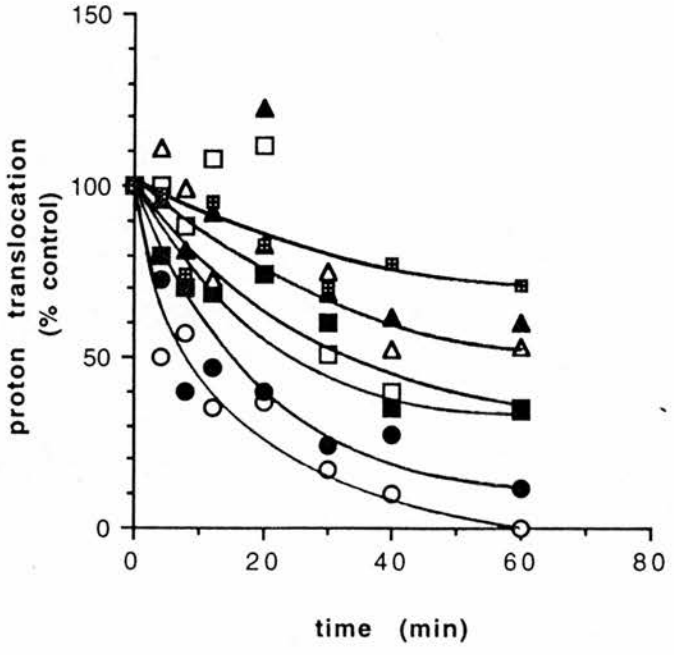

b

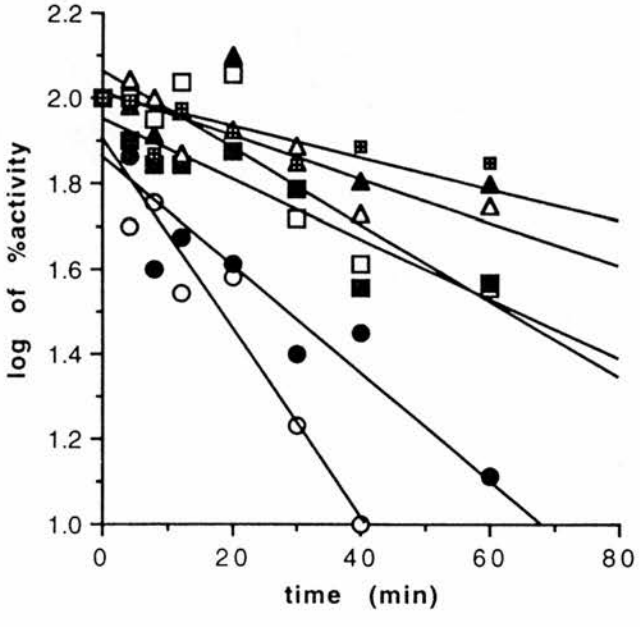

Figure 5.3 (a) Effect of MgADP on timecourse of inactivation of proton translocation by 50.5μM NEM. (b) semilog plot transformation of the data in Fig 5.2(a). Proton translocation was assayed as described in chapter 5 "special methods". MgADP concentrations in the protection mix were 0μM (○); 0.2μM (●); 0.5μM (□); 1.0μM (■); 2.0μM (△); 4.9μM (▲); 9.8μM (▣).

[MgADP] (μM)	correlation coefficient	k_{app} x 10^3(min^{-1})
0	0.904	48.3±5.3
0.2	0.871	27.6±3.4
0.5	0.794	19.3±3.1
1.0	0.816	15.4±2.3
2.0	0.781	11.0±1.8
4.9	0.335	6.4±2.9
9.8	0.535	5.1±1.9

Table 5.2 Dependence of k_{app} on the concentration of MgADP at constant NEM of 50.5μM. k_{app} values were determined from the slopes of the regression lines of a plot of log%activity versus time (fig.5.3b).

Iterations	r	k1	k2	K_a	K_b	K_i	L
		(min^{-1})		(μM)			
318	0.999	0.05	0.011	133	5.5	0.003	0.018

Table 5.3. Fitted values obtained from fitting the NEM inactivation model to the data of table 5.2 and figure 5.4.

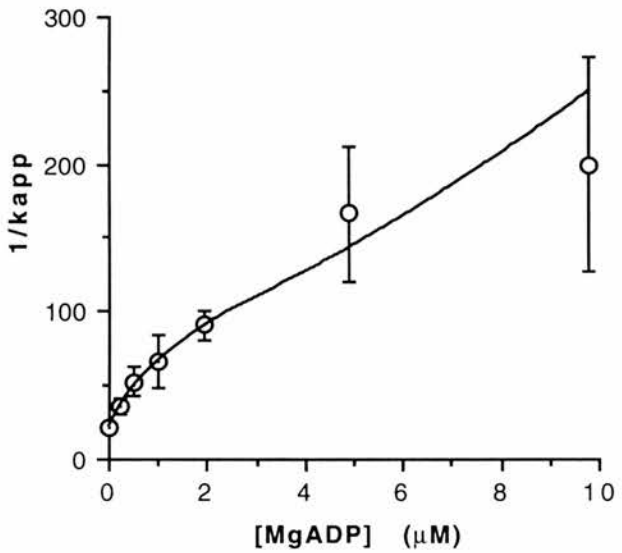

Figure 5.4 Dependence of apparent pseudo-first order rate constant at 50.5μM NEM on MgADP concentration. The points are experimental the line is that fittedto the inactivation model equation.

[ADP] (μM)	correlation coefficient	k_{app} x 10^3(min^{-1})
0	0.940	78.2±9.0
9.8	0.996	35.6±0.9
19.5	0.943	30.8±3
48.8	0.981	21.8±1.2
97.5	0.969	16.3±1.2
195	0.922	14.3±1.7

Table 5.4 Dependence of k_{app} on the concentration of free ADP at constant NEM of 50.5μM. k_{app} values were determined from the slopes of the regression lines of a plot of log%activity versus time. Reconstituted ATPase was stripped of Mg^{2+} by passage through P-6DG equilibrated in 150mM KCl, 10mM HEPES/KOH, pH7.4, 0.1mM EDTA before the reaction was initiated.

Iterations	r	k1	k2	K_a	K_b	K_i	L
		(min^{-1})		(μM)			
686	0.998	0.09	0.023	13000	218	0.45	0.1

Table 5.5. Optimised parameter values obtained from fitting the NEM inactivation model to the data of table 5.4 and figure 5.5.

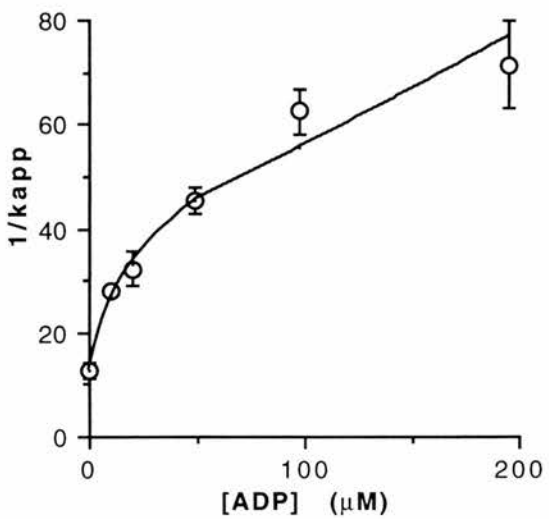

Figure 5.5 Dependence of pseudo-first order apparent rate constant at 50.5μM NEM on free ADP concentration. The line is that calculated from the inactivation model equation.

[MgIDP] (μM)	correlation coefficient	k_{app}x 10^3(min^{-1})
0	0.951	55.7±5.2
19.8	0.835	23±4.2
49.5	0.954	15.9±1.4
99	0.801	12.7±2.6
495	0.367	5.9±3.2

Table 5.6 Dependence of k_{app} on the concentration of MgIDP at constant NEM of 50.5μM. k_{app} values were determined from the slopes of the regression lines of a plot of log%activity versus time.

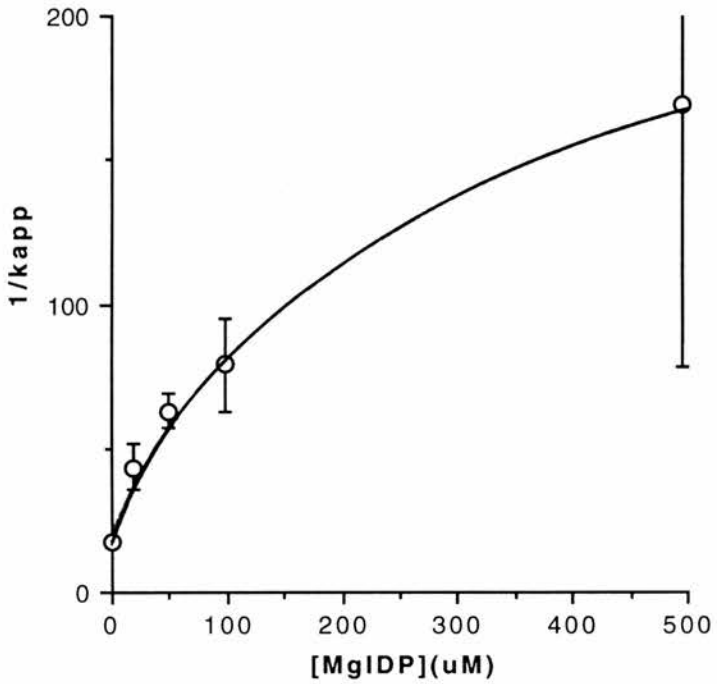

Figure 5.6 Dependence of pseudo-first order apparent rate constant at 50.5μM NEM on MgIDP concentration. The plot represents transformation of the data in table 5.4.

The reactions involved are:

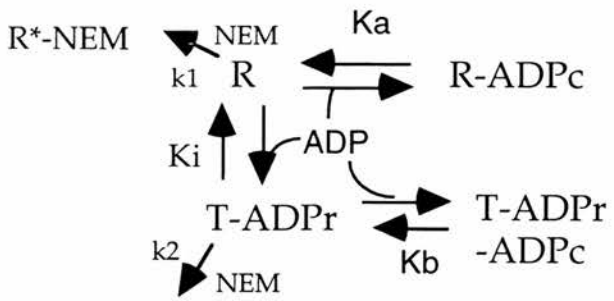

where the dissociation and equilibrium constants have the same notation as for chapter 4. T.ADPr represents ADP bound at the regulatory site of the T state; R.ADPc represents ADP bound at the catalytic site in the R state; T.ADPr.ADPc represents ADP bound at the regulatory and catalytic sites in the T state.
$L' = L(1+ADP/K_i)$. Since all indications suggest that L is very small essentially all T-state molecules present have ADP bound at the regulatory site. Hence T-ADPr is written as T.
From the above equilibria we have:

$$[T]/[R] = L(1+[ADP]/K_i) \quad \textbf{(5)}$$

$$K_a = ([R].[ADP])/[R\text{-}ADP] \quad \textbf{(6)}$$

$$K_b = ([T].[ADP])/[T\text{-}ADP] \quad \textbf{(7)}$$

We can write:

$$\text{total enzyme, } E_t = R + T + R\text{-}ADP + T\text{-}ADP \quad \textbf{(8)}$$

and by incorporating rearrangements of equations 5-7 into equation 8 we have:

$$\frac{R}{E_t} = \frac{1}{1+L(1+[ADP]/K_i)(1+[ADP]/K_b) + [ADP]/K_a} \quad \textbf{(9)}$$

and:

$$\frac{T}{E_t} = \frac{1}{1+[K_a+[ADP]]/K_a.L(1+[ADP]/K_i) + [ADP]/K_b} \quad \textbf{(10)}$$

The apparent rate constant is the sum of the inactivation rates of the two states multiplied by the fraction in that state i.e.:

$$k_{app} = k_1(R/E_t) + k_2(T/E_t) \quad \textbf{(11)}$$

Substituting equations 9 and 10 into 11 we have:

$$k_{app} = \frac{k_1}{1+[ADP]/K_a+L'(1+[ADP]/K_b)} + \frac{k_2}{1+[ADP]/K_b+[K_a+[ADP]]/K_a.L'} \quad \textbf{(12)}$$

Equation 12 describes the inactivation by NEM with protection by nucleotides with the indicated dissociation constants and was fitted to the data obtained for MgADP and free ADP (Figures 5.4 and 5.5). Estimates of the initial parameters were made

from the results of kinetic model fitting to proton translocation (chapter 4) and the data were fitted using an optimisation program with a simplex algorithm. The data for protection by MgIDP could not be fitted because the program would not run with the smaller number of data points. Fittings of both MgADP and free ADP data sets took considerable time because of the complexity of the model and the small number of data points and hence the number of iterations to reach the minima is very large in each case: 318 for MgADP data (Table 5.3); 686 for free ADP data (Table 5.5). The correlation coefficient values, r are very close to unity in each case indicating that the model fits the data very well. In both cases the rate of inactivation by NEM is greater in the R- than the T-state ($k_1>k_2$) as would be expected if the cysteine residue is more accessible in the active R-state (Tables 5.3 and 5.5) and nucleotide binding to the T-state catalytic site is tighter than to the R-state ($K_a>K_b$) This result is consistent with the results of chapter 4. The predicted values of K_a are 133μM and 13mM for MgADP and ADP respectively (Table 5.5). In effect then the binding of MgADP and free ADP to the catalytic sites in the R-state is negligible at the concentrations used in the protection experiments. The value of K_i, the dissociation constant for binding to the regulatory site, is 0.003 and 0.45μM for MgADP and free ADP respectively. These values are again consistent with previous results indicating very tight binding of nucleotides at this regulatory site and also illustrate the need for Mg^{2+}-complexed nucleotides for high affinity binding since the K_i for free ADP is 150 times greater than that for MgADP. The value for the equilibrium constant, L for the R-T transition should in theory be the same regardless of which nucleotide is present but we observed a 10 fold difference (L=0.01, MgADP (Table 5.3); L=0.1, free ADP (Table 5.5)). This may merely reflect the complexity of the model and the small numbers of data points.

Other nucleotides tested produced results consistent with protection at a single binding site. MgADPβS is different from other nucleotides in its regulation of proton translocation in that it binds more tightly to the R-state catalytic site than to the T-state (Webster *et al*, 1995) and these properties are consistent with the data shown in table 5.7 and linear plot in figure 5.7. The k_{app} values are reduced in proportion to the concentration of MgADPβS and a dissociation constant, K_D of 6±0.5μM can be determined (Figure 5.7). MgBzBzATP exhibited a similar relationship between k_{app} and its concentration (Table 5.8 and Figure 5.8) to give a final K_D value of 0.6±0.04μM. This nucleotide acts as a substrate at low concentrations but becomes inhibitory at higher concentrations (chapter 4). The kinetics of MgBzBzATP as a substrate of proton translocation were analysed and plotted according to Hanes and give a K_m value of 5±0.8μM (chapter 4). This value

[MgADPβS] (μM)	correlation coefficient	k_{app}x 10^3(min^{-1})
0	0.953	35.0±4.4
1.1	0.983	28.5±1.3
2.2	0.934	23.9±2.3
5.4	0.968	16.8±1.1
10.8	0.950	14.6±1.2
21.6	0.865	7.2±1.3

Table 5.7 Dependence of k_{app} on the concentration of MgADPβS at constant NEM of 50.5μM. k_{app} values were determined from the slopes of the regression lines of a plot of log%activity versus time.

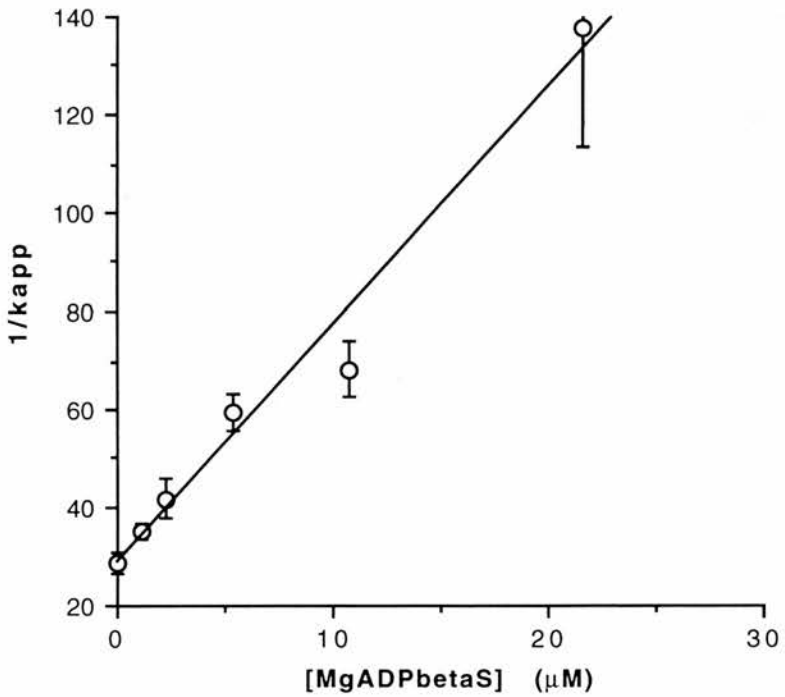

Figure 5.7 Dependence of apparent pseudo-first order rate constant at 50.5μM NEM on MgADPβS concentration. The plot represents transformation of the data in table 5.5 with linear regression: slope=4.8±0.4minμM^{-1}; intercept=28.8±4.0min; correlation coefficient=0.974.

[MgBzBzATP] (μM)	correlation coefficient	k_{app}x 10^3(min^{-1})
0	0.984	45.3±2.2
0.2	0.969	27.8±1.8
0.5	0.985	25.3±1.1
0.9	0.946	14.3±1.2
1.8	0.848	7.5±1.1
4.6	0.327	4.2±2.1

Table 5.8 Dependence of k_{app} on the concentration of MgBzBzATP at constant NEM of 50.5μM. k_{app} values were determined from the slopes of the regression lines of a plot of log%activity versus time.

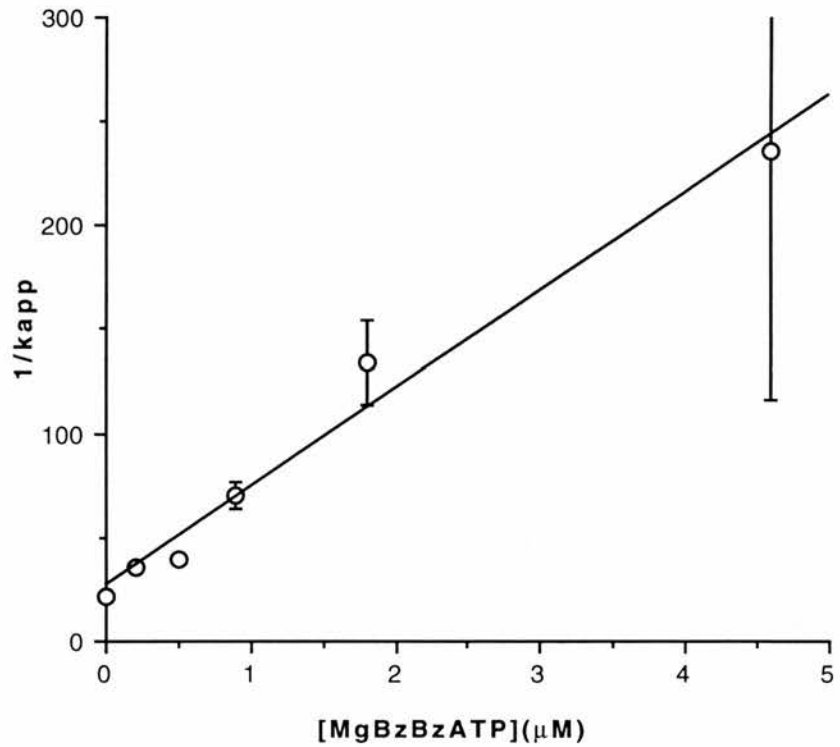

Figure 5.8 Dependence of apparent pseudo-first order rate constant at 50.5μMNEM on MgBzBzATP concentration. The plot represents transformation of the data in Table5.6 with linear regression: slope=447.3±3.4minμM^{-1}; intercept=26.7±7.1min; correlation coefficient=0.979.

for the Michaelis constant is 10 times greater than the K_D determined using NEM inactivation and protection profiles (Figure 5.8) and may reflect the problems associated with using a simple Hanes plot when we have the additional complication of the inhibitory effect of MgBzBzATP seen at concentrations as low as 40μM (chapter 4).

The interaction of the substrate MgATP and free ATP in protection from NEM inactivation were analysed and complete protection of the enzyme did not occur even at concentrations of MgATP up to 100μM (Figures 5.9a-c). Higher concentrations of substrate could not be used because in the absence of NEM but in the presence of MgATP a substantial background rate of inactivation took place that may be related to the cold inactivation seen by Moriyama and Nelson (1989a). Surprisingly free ATP protected the ATPase from inactivation in a similar way to MgADP, MgIDP and free ADP with biphasic relationships of $1/k_{app}$ versus the concentration of free ATP (Figure 5.10 a and b).

5.3.3 Subunit labelling with [^{3}H]-NEM and protection by MgADP.

The interaction of MgADP with different ATPase subunits was studied by looking at protection from [^{3}H]-NEM labelling. 5μM NEM labelled the 116 and the 72kDa subunits but also a subunit around 40kDa and two smaller proteins around 15-20kDa (Figure 5.11), with the 40kDa subunit having the greatest incorporation. Since the vacuolar ATPase has several subunits around 40kDa we performed glycerol gradient analysis of labelled ATPase in an attempt to assign the site of NEM labelling to the correct subunit. The ATPase (as a P1 fraction) was labelled with NEM and then solubilised and fractionated with glycerol gradient centrifugation. It had previously been observed that the 39kDa subunit could dissociate from the holoenzyme complex under these conditions so that NEM labelling would be expected at the top of the gradients if this was indeed the NEM binding subunit. An autoradiograph (Figure 5.12a) and blot with anti-39kDa antibody (Figure 5.12b) of the same fractions showed labelling near the top of the gradient and there was also strong labelling of fraction 5, where the holoenzyme appears (Figure 5.12c), in undissociated 39kDa subunit. This correlation confirms that the 39kDa subunit is the NEM-reactive subunit as opposed to the 40kDa or the 45kDa glycosylated subunits recently identified (Supek *et al*, 1994). The small proteins that were labelled remain unidentified but it would be interesting to determine whether one of the smaller bands is the M16 subunit recently identified (Supek *et al*, 1995).

MgADP added before reaction with NEM reduced the intensity of labelling in all of the susceptible bands (Figure 5.11, lanes 5-10). This is in contrast to the results of Nelson (1987b) who observed protection preferentially at the 72kDa subunit with

a

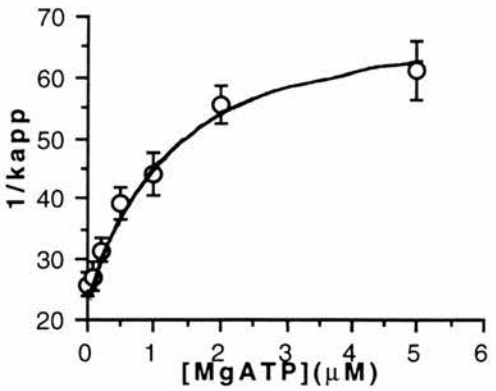

b

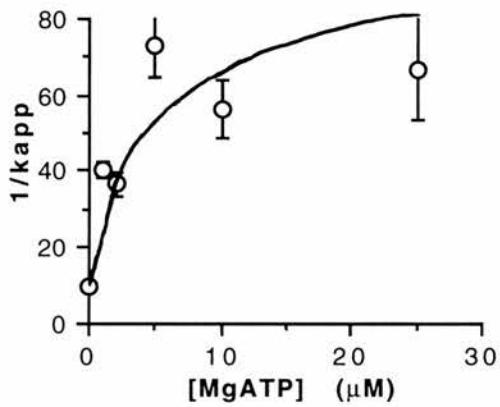

c

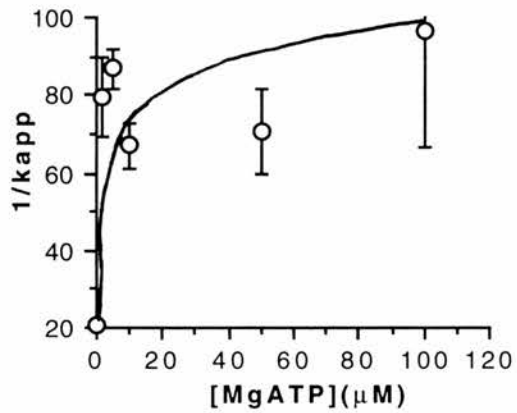

Figure 5.9(a-c) Dependence of apparent rate constants on the concentration of MgATP. Figures a-c represent results of three separate experiments at constant NEM of 51.1μM. Reconstituted ATPase was equilibrated in 1mM $MgSO_4$.

a

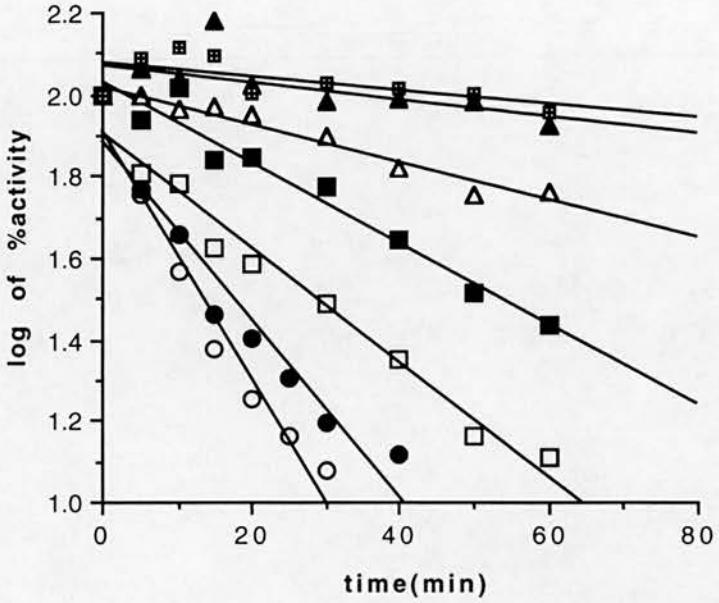

b

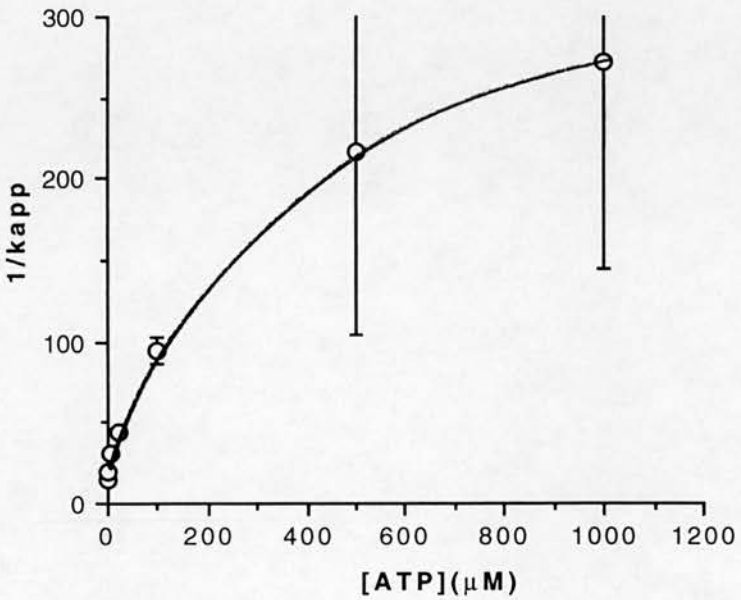

Figure 5.10(a and b) (a) Semilog plot showing effect of free ATP on timecourse of inactivation of proton translocation by 51.5μM NEM. Proton translocation was assayed as described in chapter 5 in different free ATP concentrations: 0μM (○); 1μM (●); 5μM (□); 20μM (■); 100μM (△); 500μM (▲); 1000μM (⊞).(b) Dependence of apparent rate constant of inactivation on free ATP concentration. ATPase was prepared as described in figure 5.4 to remove any Mg^{2+} ions from the preparation.

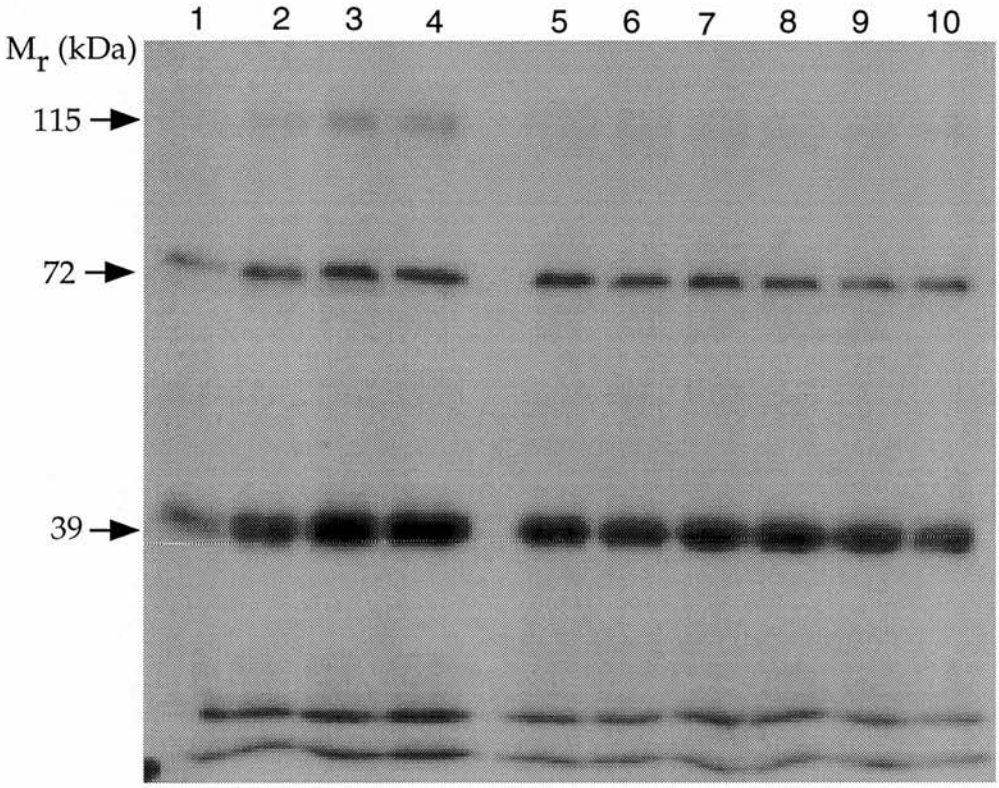

Figure 5.11. [^{3}H]-NEM labelling of the reconstituted ATPase. ATPase was incubated with 5μM [^{3}H]-NEM (2.1MBq/ml) for 15, 30, 45, and 60 minutes (lanes1-4 respectively) or for 30minutes (lanes5-10) on ice with (lanes5-10) or without (lanes1-4) the prior addition of MgADP. The concentrations of MgADP are 0, 0.2, 0.5, 1, 2 and 5μM in lanes 5-10 respectively. The positions of the labelled subunits are indicated.

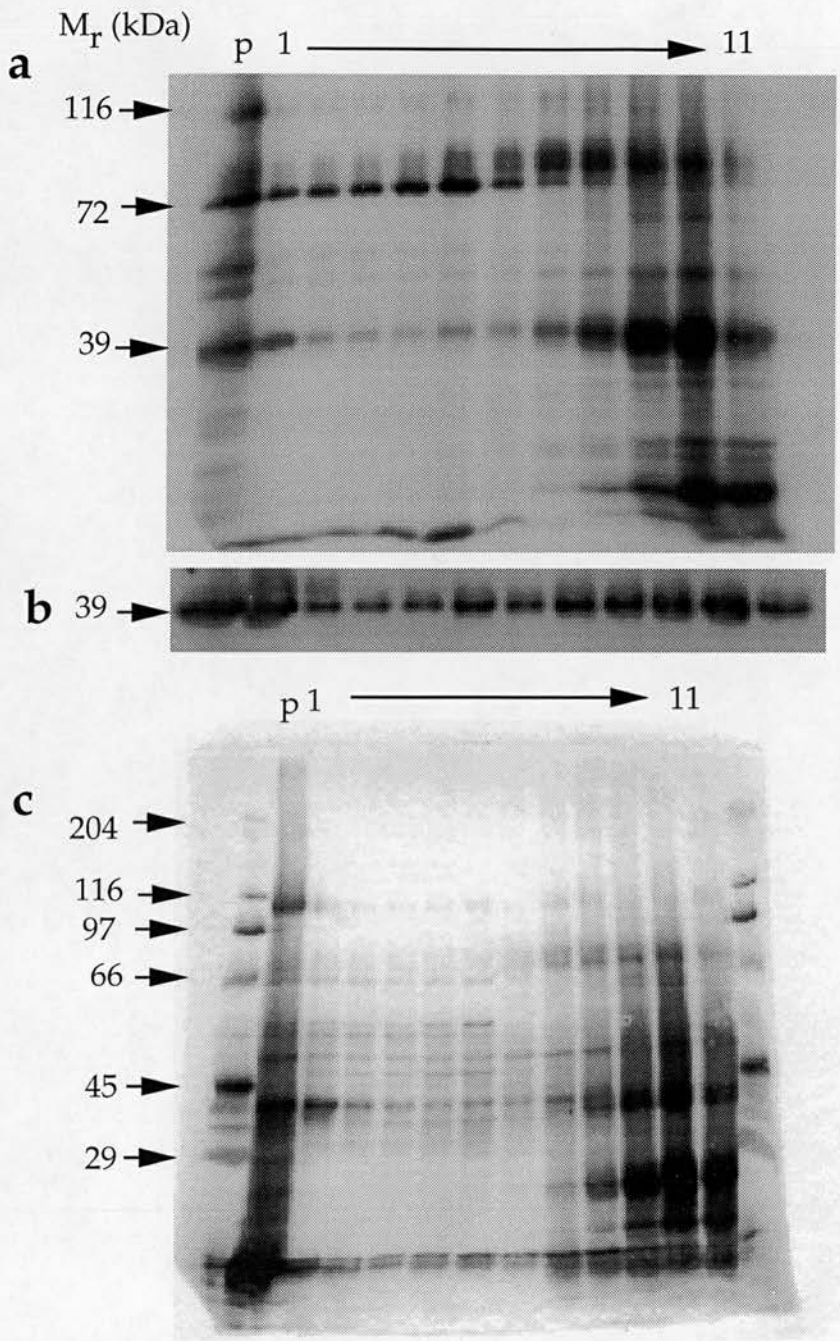

Figure 5.12 a-c. Identification of 39kDa NEM binding subunit.
Partially purified ATPase was labelled with 5μM [^{3}H]-NEM (2.1MBq/ml) for 30min at 0°C and was then further purified by glycerol gradient centrifugation (0.9% octyl-glucoside). lane p represents the pellet at the bottom of the gradient, lanes 1-11 represent fractions 1-11 respectively with fraction 1 being the bottom of the gradient. Equlivalent loadings of all fractions are shown.
(a) autoradiograph. (b) blot with anti 39kDa subunit antibodies. (c) silver stained gel of the same fractions.

little effect on labelling of the other subunits. Since the 72kDa subunit is known to be the site of ATP hydrolysis and is therefore probably the nucleotide-protectable site in NEM-inactivation experiments we carried out two-dimensional raster scans to quantify labelling of this subunit and to study the effect of MgADP. Labelling of the 72kDa subunit by 5μM NEM increases linearly with time to reach a maximum at about 60 minutes (Figure 5.11, lanes 1-4; Figure 5.13a) and a time point on the linear part of the curve (30minutes) was used in MgADP protection experiments. The reduction in labelling of the 72kDa subunit band by MgADP was quantified using raster scans of the autoradiograph in figure 5.11 (lanes 5-10) and it was observed that the maximum reduction in labelling was only 40-45% in the reconstituted ATPase with 5μM MgADP (Figure 5.13b). This is in contrast to the results of protection from NEM in proton translocation assays where 5μM MgADP almost completely protects the enzyme (Figure 5.3b; Figure 5.4; Table 5.2). This inconsistency suggested that there is a large pool of ATPase in the reconstituted preparation which is labelled by NEM but is not protectable by MgADP, possibly present on the proteoliposomes in an inverted configuration. NEM is a hydrophobic molecule which is able to partition into and traverse across lipid bilayers and hence will be able to label both populations of ATPase but MgADP is impermeant and will only be able to protect the ATPase in the correct orientation; this explains the complete protection in proton translocation where only right side-up enzyme is "seen" and the 50% protection in labelling experiments where total enzyme is "seen".

Trypsin digestion was used to compare the topology of the ATPase in its reconstituted and soluble forms (Figure 5.14a, b). The 116kDa subunit was used as a marker for the enzyme because of its transmembrane location and the trypsin digest samples were blotted with an anti-116kDa polyclonal antibody (Figure 5.14a). Although this antibody is not particularly clean it reveals that in the reconstituted preparation much of this subunit is not accessible to trypsin since a significant band is still present even at 100μg/ml trypsin whereas in the $C_{12}E_9$-solubilised ATPase a large amount of this subunit has been degraded at 1μg/ml with almost complete proteolysis at 10μg/ml trypsin. This result is more clearly seen in the silver stained gel (Figure 5.14b) and indicates that a large proportion of the ATPase in the reconstituted preparation is not accessible to trypsin digestion and hence the reason for the lack of protection in [^{3}H]-NEM labelling experiments may be due to the NEM accessibility of a large non-ADP protectable pool of inverted enzyme.

The problem of the inaccessibility of a significant pool of ATPase to MgADP was addressed by carrying out NEM labelling experiments using the $C_{12}E_9$-solubilised enzyme. A timecourse of incorporation of NEM into the 72kDa subunit again showed linearity (Figure 5.15a)and again a timepoint on this linear part of the

a

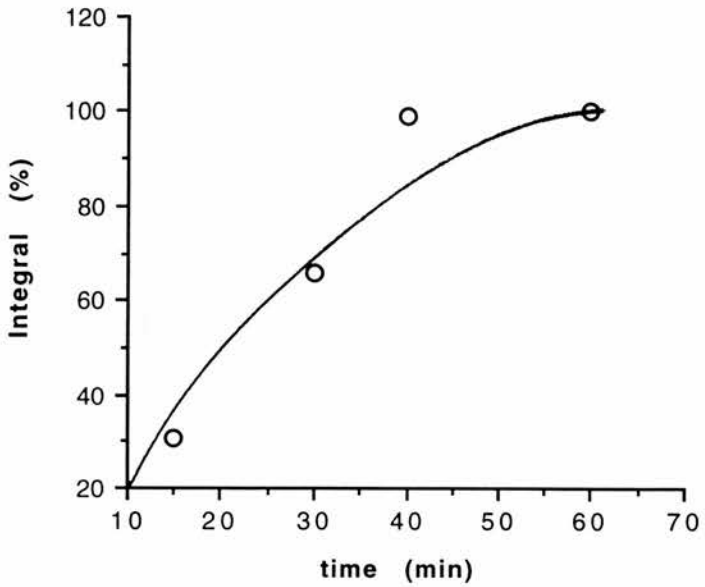

b

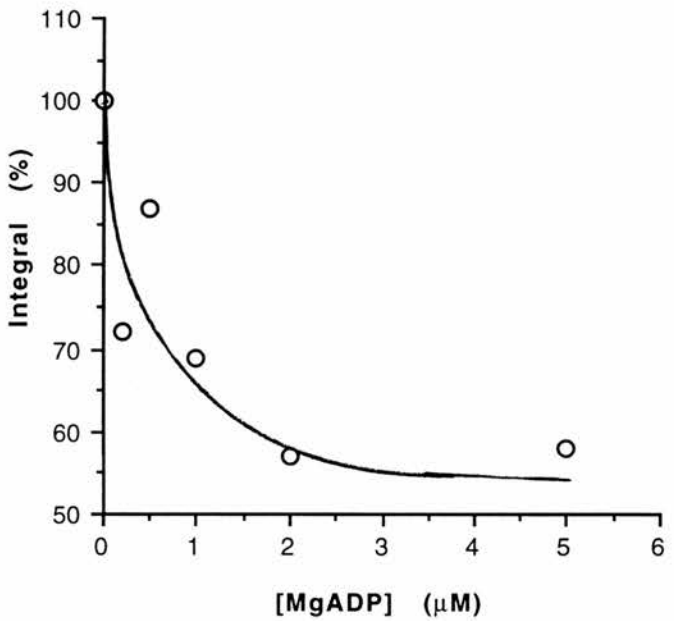

Figure 5.13(a+b) Results of two-dimensional densitometric scans of the 72kDa subunit band in figure 5.11. (a) - timecourse of labelling (lanes 1-4 fig.5.11). 100% represents the labelling at the longest time point taken (60minutes). (b) - Effect of MgADP on labelling by NEM. 100% represent maximal labelling (in the absence of MgADP).

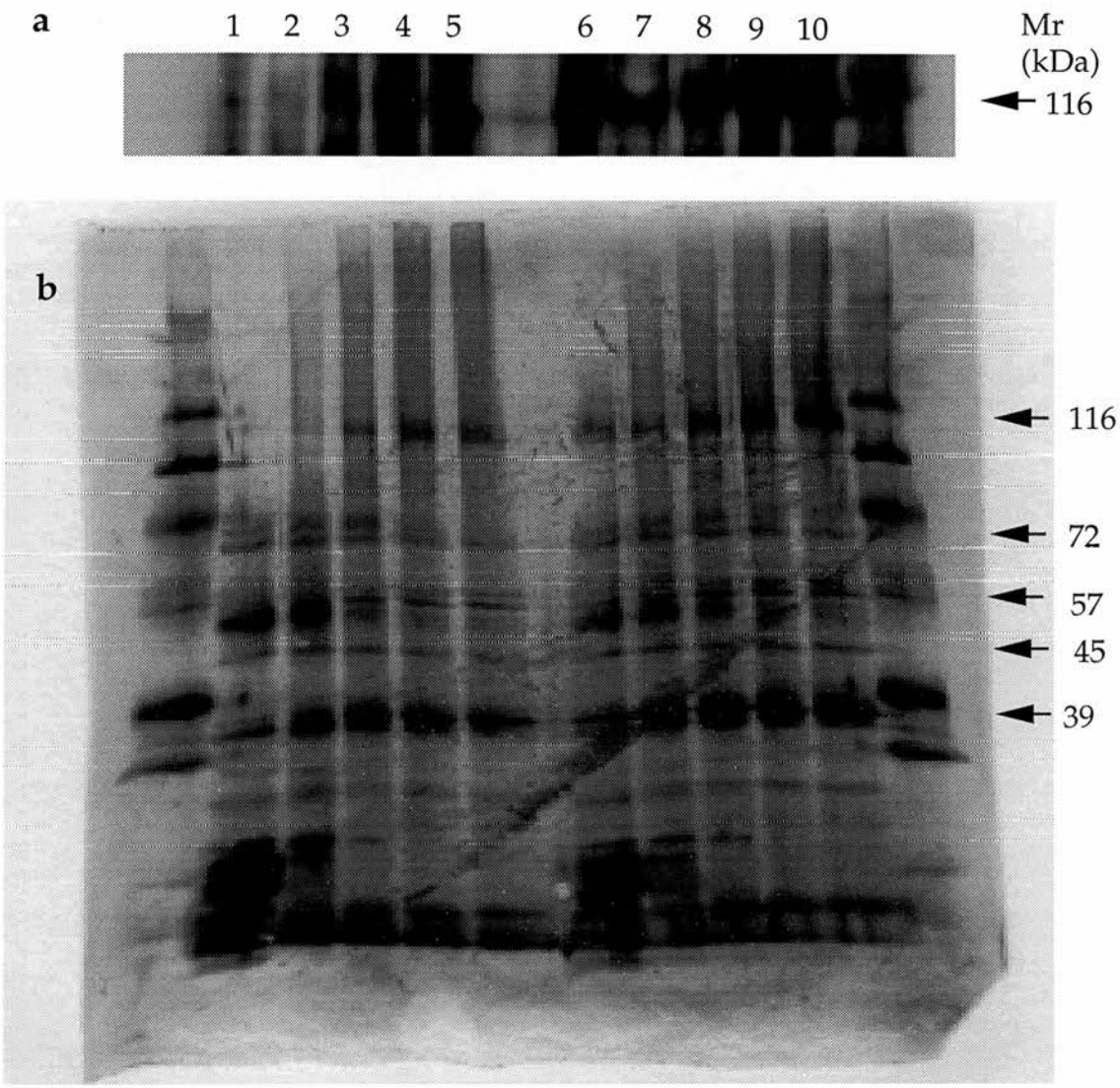

Figure 5.14 (a and b) (a) Blot with anti-116kDa subunit antibody (1:1000) and (b) silver stained SDS-PAGE showing trypsin digest of solubilised (lanes 1-5) and reconstituted (lanes 6-10) ATPase. The concentrations of trypsin are 100, 10, 1, 0.1 and 0 in lanes 1-5 and lanes 6-10 respectively. The position of the ATPase subunits are indicated by the arrow.

a

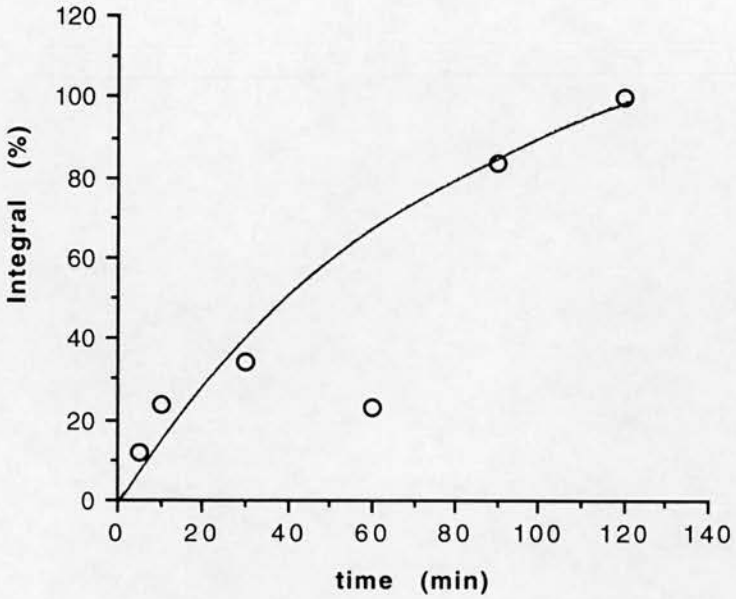

b

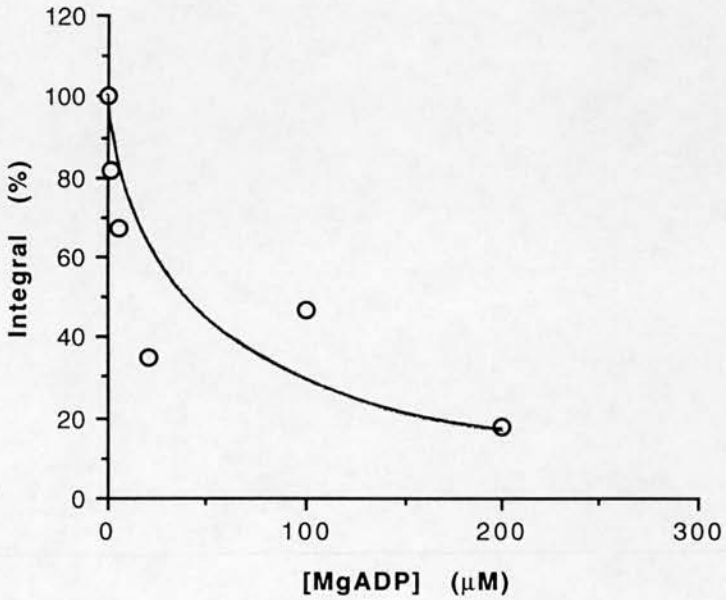

Figure 5.15(a+b) Results of two dimensional densitometric scans of the 72kDa subunit bands labelled with [^{3}H]-NEM in $C_{12}E_9$-solubilised ATPase (a) - timecourse of labelling with 5μM [^{3}H]-NEM (2.1MBq/ml) on ice. 100% represents the labelling at the longest time point taken (120minutes). (b) - Effect of MgADP on labelling by NEM in the solubilised ATPase. 100% represent maximal labelling (in the absence of MgADP).

incorporation curve was used to study the effects of MgADP in the soluble enzyme (Figure 5.15b). Although again there is little protection at 5μM MgADP (about 40%) the maximum level of protection reaches about 80% at 200μM MgADP (Figure 5.15b), a value significantly above the 45% maximum protection level seen in the reconstituted enzyme (Figure 5.13b). This still indicates the presence of some non-protectable pool of ATPase, amounting to 10-20% of the total ATPase present.

Subunit incorporation of NEM was quantified using a direct approach of radioactive counting of polyacrylamide gel slices to try and assign some level of stoichiometry to the incorporation. Carbonic anhydrase was used as the standard for determination of protein due to the formation of tight bands on SDS-PAGE and the raster scan integrals varied linearly with the amount of protein (Figure 5.16a). Timecourses of incorporation were consistent with the pseudo-first order kinetics of NEM inactivation (Figure 5.16b).

For a first order process where the substrate, A becomes the product, p we can write:

$$p = A_o (1-e^{-k_{app}t}) \quad \textbf{(13)}$$

where A_o is the concentration of A when t = 0 and k_{app} is the apparent rate constant at the incubating concentration of NEM. By taking logarithms and rearranging equation 13 becomes:

$$\log(A_o-p) = (-k_{app}/2.3)t \quad \textbf{(14)}$$

Equation 14 describes a linear relationship of $\log(A_o-p)$ versus time with y-axis intercept = $\log A_o$ and slope = $-k_{app}/2.3$. We can equate A_o to the maximum incorporation reached for each subunit (Figure 5.16b) and p to the incorporation at time t. Knowing p at each time point we can plot the data according to equation 14 (Figure 5.17) to obtain apparent rate constants and stoichiometry of incorporation of NEM for the different subunits labelled (Table 5.9). For each of the subunits the correlation coefficients for the semilog plots (Figure 5.17) are close to unity (Table 5.9) indicating good fit to first order kinetics. NEM is incorporated much faster into the 72kDa subunit ($k = 460 min^{-1}M^{-1}$) than the 39kDa ($k = 149 min^{-1}M^{-1}$) and 116kDa ($k = 192 min^{-1}M^{-1}$) subunits (Table 5.9). The 39kDa subunit exhibits the highest level of incorporation with 5 moles of NEM per mole of subunit (Table 5.9). This is the calculated A_o value from the semilog plot (Figure 5.17) but it is evident from figure 5.16b that this is an underestimate and that labelling of this subunit is still increasing even after an overnight incubation. The 116kDa subunit has 4 NEM equivalents bound per mole subunit and again this is likely to be an underestimate (Table 5.9; Figure 5.16b) whereas the fast rate constant for incorporation into the 72kDa subunit has allowed NEM incorporation to reach a *bona fide* maximum of 2 moles NEM per mole of subunit (Table 5.9; Figure 5.16b).

a

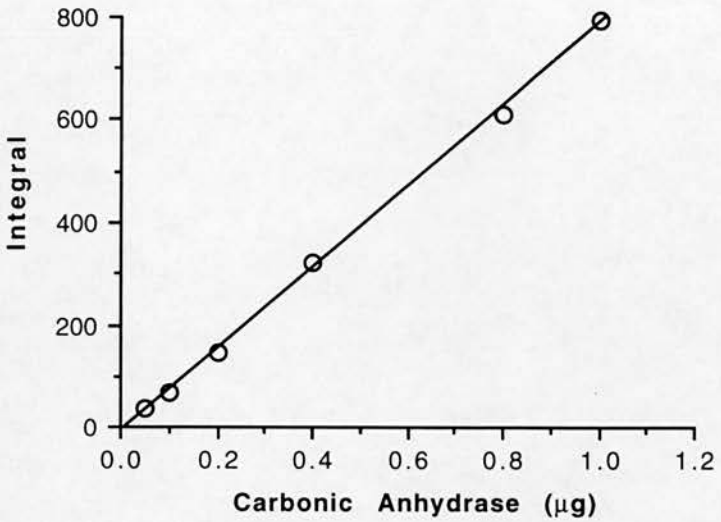

b

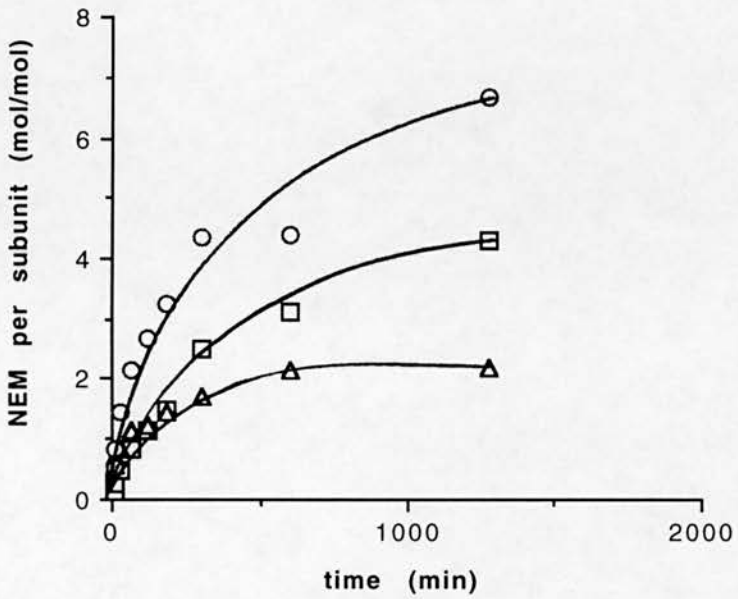

Figure 5.16(a+b) Subunit incorporation of [^{3}H]-NEM into reconstituted ATPase. ATPase was incubated with 11.4µM [^{3}H]-NEM (2.1MBq/ml) on ice for the indicated times. (a) - carbonic anhydrase standard curve used for the determination of protein in each subunit band. (b) - incorporation of NEM into subunits of molecular weight 39 (○), 116 (□) and 72kDa (△) calculated from the exact concentration of NEM in the reaction mix and the number of moles of each subunit present.

subunit (Mr)	A_o(mol/mol)	k($min^{-1}M^{-1}$)	correlation coefficient
72	1.7±0.3	460±32	0.973
116	4.1±0.1	192±13	0.974
39	5.2±0.3	149±30	0.814

Table 5.9 Kinetics of subunit incorporation of NEM calculated from figure 5.17.

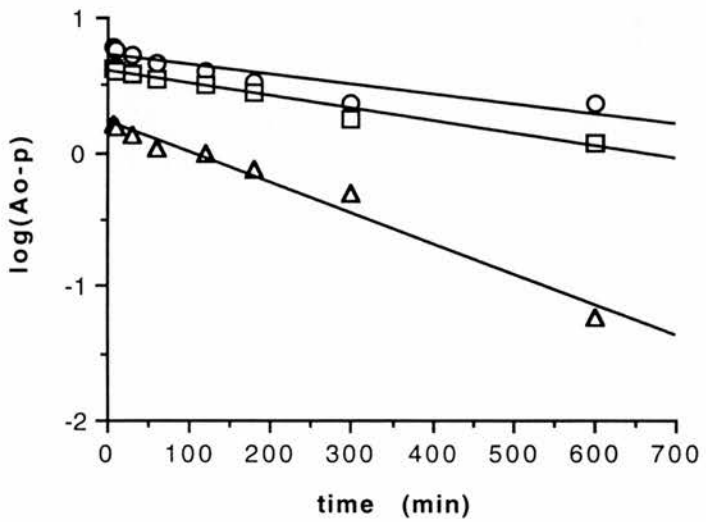

Figure 5.17 Determination of second order rate constants for incorporation of NEM into the various subunits. The data is transformed from that in figure 5.16b. The lines represents linear regression of the data points. Key to symbols is as figure 5.16b.

5.4 Discussion.

5.4.1 Protection by nucleotides from NEM inactivation .

The results of chapter 4 provide a model for the regulation of the vacuolar ATPase by the binding of MgADP at two distinct sites: a single regulatory site in the inactive T-state only and by competition with the substrate at the catalytic sites in both conformational states of the enzyme. As the model fitting progressed it became apparent that it would be difficult to obtain values for the dissociation constants for MgADP binding due to the complexity of the models needed to fit the data. For this reason alternative approaches were explored.

Inactivation of proton translocation by NEM has been shown to be described very well by pseudo-first order equations with the pseudo-first order rate constant for NEM inhibition being directly proportional to the NEM concentration. The second order rate constant, k is calculated to be $1.8x10^3 min^{-1}M^{-1}$. Inactivation of ATP hydrolysis by NEM has been measured previously (Percy and Apps, 1986) and a value for the rate constant, $k = 10.8x10^3 min^{-1}M^{-1}$ was obtained. Aside from the fact that this study was of ATP hydrolysis not proton translocation and that the ATPase was only partially purified and used in a soluble form, the value was obtained at 20°C which would explain why it is greater than was obtained at 0°C.

The presence of nucleotides has been shown to protect the enzyme from inactivation by NEM in the order MgADP>MgIDP>ADP. The biphasicity of plots relating apparent rate constants to the nucleotide concentration indicates that protection is by a complex mechanism involving more than one type of binding site rather than by simple competition at a single type of binding site. The complexity of this interaction was unfortunate in that dissociation constants could not be measured directly but the protection profiles confirmed some of the results of the kinetic model fitting of chapter 4. The results of chapter 4 were used to develop a model describing inactivation of the two states of the ATPase by NEM and this model was fitted to the experimental data obtained in the form of $1/k_{app}$ versus [nucleotide]. The model for inactivation by NEM fitted the MgADP and free ADP data very well as indicated by the correlation coefficient values. In line with the results of chapter 4 nucleotides were shown to bind very tightly to a regulatory site on the T-state as indicated by submicromolar K_i values. MgADP is by far the most potent regulator and protector of the ATPase and a K_i value of 3nM was obtained from fitting of the NEM inactivation model to the data. Free ADP bound to this same site with a K_i 150 times greater than for MgADP indicating the importance of Mg^{2+}-complexed nucleotides in the regulation of V-ATPases. Dissociation constant values for MgIDP could not be determined because of the smaller number of data points. The study of NEM inactivation has also shown that MgADP and free ADP bind with higher

affinity to the T- than to the R-state catalytic site and once again that the magnesium complexed form of ADP is by far the more potent. Experiments with MgADPβS and BzBzATP and their effect on protection by NEM provided some interesting results. MgADPβS has been shown to differ from the other nucleotides tested in binding with higher affinity to the R-state catalytic site than to the T-state but still binding more tightly to the regulatory site. BzBzATP is both an inhibitor and a substrate of the ATPase which distinguishes this nucleotide from the others. Both MgADPβS and BzBzATP produced linear $1/k_{app}$ versus [nucleotide] plots indicating protection by a simpler mechanism than applies to MgADP, MgIDP and free ADP.

Analysis of the data as a whole provides insights into the mechanism of nucleotide protection. Those nucleotide diphosphates that have complex biphasic protection profiles are thought to bind first to the regulatory site in the T-state and hence pull the ATPase over into a conformation that is inactivated slower by NEM. This would represent the first part of the $1/k_{app}$ plots. The next stage in protection is when the nucleotides begin to fill the catalytic sites on the T-state thereby excluding NEM and leading to complete protection - the second part of the $1/k_{app}$ plot. At the concentrations used in the experiment MgADPβS binds to the regulatory site and displaces the equilibrium toward the T-state. Binding to the catalytic sites by MgADPβS is negligible under our conditions and hence the slope of the $1/k_{app}$ versus [nucleotide] plot will not alter which explains the straight line profile for MgADPβS. BzBzATP is acting in substrate mode under the conditions of the protection experiments (the concentrations are below those required for inhibition) and hence is likely to protect the enzyme by simply binding competitively to the R-state catalytic site thereby excluding NEM. It is difficult to interpret the results of protection from NEM by the physiological substrate MgATP because of the phenomenon of cold inactivation (Moriyama and Nelson, 1989a). The experimental methodology does not yield results for MgATP without subtracting large background rates of inactivation from the NEM rates of inactivation and this is statistically difficult to validate. The protection profile for free ATP is biphasic suggesting that it does not protect by simply binding to the catalytic site but also has other effects at higher concentration although results in chapter 4 suggest that inhibition is competitive up to concentrations as high as 5mM. In conclusion the results of protection from NEM by nucleotides are almost entirely consistent with their properties in the regulation of proton translocation.

5.4.2 Subunit labelling with [^{3}H]-NEM and protection by nucleotides.

NEM has been used to identify the 72kDa subunit of the V-ATPase as the location of the site of ATP hydrolysis in the chromaffin granule (Moriyama and

Nelson, 1987b) and the coated vesicle ATPase (Arai *et al*, 1987b) by virtue of nucleotide protection from NEM inactivation. NEM has also been shown to label the subunits of molecular weights 116 and 39kDa but these are less reactive than the 72kDa subunit (Moriyama and Nelson, 1987b) and the presence of MgATP or MgADP had little effect on their labelling compared to the 72kDa subunit. The results presented here are consistent with the previous results: the 72kDa subunit and also subunits of Mr, 116, 39 and 15-20kDa were shown to be labelled by [^{3}H]-NEM but the presence of MgADP reduced the labelling in all subunits in contrast to the results mentioned above. In the reconstituted preparation MgADP only caused a reduction of 45% in the labelling of the 72kDa subunit by NEM at concentrations which gave almost complete protection in the proton translocation assays . This is similar to previous results where 80% protection was seen in proton translocation but at the same concentration of nucleotide only 50% protection of labelling was observed (Moriyama and Nelson, 1987b). It was originally thought that the lack of complete protection in labelling experiments was due to the presence of two cysteine residues which can bind NEM only one of which is protectable by nucleotides. This now seems unlikely and the lack of complete protection is probably a consequence of the preparation. Trypsin digestion suggests that a large proportion of the ATPase molecules are inverted in the proteoliposomes and because NEM is freely permeant there is effectively a large NEM-accessible pool that is not protectable by ADP. The proton translocation assay only "sees" those ATPase molecules that are active and in the correct orientation and hence complete protection by MgADP by the assay method is inferred. The effects of nucleotide on NEM labelling of solubilised ATPase show that 200μM MgADP reduces the label in the 72kDa subunit by 80%. Hence there is still a non-nucleotide protectable pool of enzyme even in the soluble preparation which may represent ATPase which has lost its ability to be regulated by nucleotide for example through the loss of subunits or proteolysis during purification.

Investigation of the stoichiometry of NEM labelling of the individual subunits of the enzyme showed that NEM reacts faster with the 72kDa subunit than with those of 116 and 39kDa. The 72kDa subunit has been shown to react with only two NEM molecules per molecule of subunit which is consistent with previous results (Moriyama and Nelson, 1987b) whereas the 116 and 39kDa molecules incorporate as many as 5-6 molesNEM/mole subunit. The number of cysteines present in the published sequences of V-ATPase are: 13 (in bovine brain coated vesicle, 116kDa; Peng *et al*, 1994a); 8 (in bovine brain coated vesicle, 72kDa; Puopolo *et al*, 1988); 7 (bovine chromaffin granule, 39kDa; Nelson, personal communication). The total

numbers of cysteine residues present in the published sequences of these subunits does not exceed the maximum NEM incorporated in these experiments.

The importance of cysteines at the active site of the 72kDa subunit has prompted the search for conserved cysteine residues within this subunit. Only three cysteine residues are conserved in all of the 72kDa V-ATPase subunits sequenced to date: C254, C277 and C532 (coated vesicle numbering, Feng and Forgac, 1992b) with C254 being identified as the site of alkylation by NEM. C254 of the 72kDa subunit is the most reactive cysteine in the V-ATPase complex (Feng and Forgac, 1994) and is found in the glycine-rich motif, $G(X)_4GKT$ more often known as the Walker consensus "A" sequence (Walker *et al*, 1985). This consensus sequence is conserved in many nucleotide-binding proteins (Saraste *et al*, 1990). The crystal structures of the Ha-*ras* oncogene product p21 (Pai *et al*, 1989) and adenylate kinase (Kim *et al*, 1990) implicate this sequence in the binding of the phosphate moiety of nucleotides. Also a 50-amino acid peptide containing the Walker consensus sequence has been shown to bind nucleotides (Garboczi *et al*, 1988). In the archaebacterial ATPase the V-ATPase 72kDa homologue has a serine at the corresponding position (Inatomi *et al*, 1989) while the β subunit of the mitochondrial F-ATPase has a lysine in the same position (Runswick and Walker, 1983). Site directed mutagenesis shows that the conserved cysteine in V-ATPases can be mutated to a serine without loss of ATP hydrolytic activity and the V-ATPase becomes archaebacterial-like with the loss of sensitivity to NEM (Cutler *et al*, 1992). In the F-ATPase catalytic β subunit Val153 in the consensus sequence can be mutated to a cysteine and confers NEM sensitivity protectable by ATP (Iwamoto *et al*, 1994). Hence it appears that the cysteine residue itself is not essential for ATP hydrolysis. C277 is also part of a conserved nucleotide binding motif, GXGER found in the crystal structure of adenylate kinase to be in close proximity to the site of nucleotide binding (Kim *et al*, 1990). It was only recently that the significance of the conservation of C532 in all V-ATPases sequenced to date was determined. Formation of an intramolecular disulphide bond between C532 and C254 (Feng and Forgac, 1994) causes inactivation of the V-ATPase implicating C532 in possible regulation of the enzyme. 2 moles of NEM were found to be incorporated into each 72kDa subunit of the chromaffin granule ATPase. C254, the cysteine residue in the Walker consensus sequence, is likely to represent one of these residues since it is the cysteine responsible for inactivation by NEM (Feng and Forgac, 1992a). The remaining cysteine could be equally C277 or C532 (coated vesicle numbering) since both have been shown to play important roles in the catalytic site.

The data presented here further indicate the importance of cysteine residues at the active site of the V-ATPase and confirms the results of studies on regulation of

proton translocation through the enzyme by nucleotides (chapter 4). NEM inactivation studies show that the V-ATPases possess regulatory sites which bind nucleotides with very high affinity (dissociation constants in the submicromolar range) and that they also bind nucleotides competitively at the catalytic sites in the T and R-conformational states. Autoradiography indicated that NEM alkylates several subunits in the V-ATPase complex and that the labelling intensity of these subunits can be reduced by nucleotides in a way that may indicate gross conformational changes since all labelled subunits are affected. The direct labelling experiments with [^{3}H]-NEM confirm pseudo-first order kinetics with respect to the 72kDa subunit and the incorporation timecourse (Figure 5.16b) suggests that the three copies of this subunit behave identically indicating that the R-state of the V-ATPase is symmetrical. For direct labelling, 11.4μM NEM gave 2mol NEM/mol subunit after 5 hours while in assays at 50μM NEM the ATPase was completely inactivated after 1 hour. The equivalent conditions for complete inactivation in the assay method suggest that there are 6 identical NEM-reactive sites in the holoenzyme. This is confirmation of the major assumption of the model of Monod *et al* (1965) and is in contrast to the recent results with F-ATPases indicating that these are asymmetrical enzymes (Walker *et al*, 1994). It appears from this evidence that the V- and F-ATPases may not be as similar as at once thought.

Chapter 6. Direct determination of the dissociation constants for ADPMg from the regulatory binding site.

6.1 Introduction.

Although vacuolar ATPases have previously been shown to be inhibited by nucleoside diphosphates (Moriyama and Nelson, 1987b; Apps *et al*, 1992) no detailed study of this inhibition has been attempted until now. In the preceding chapters it has been shown that the V-ATPase shows Michaelian kinetics in the absence of nucleoside diphosphates and that ADPMg allosterically regulates the V-ATPase from chromaffin granules by binding to a very high affinity regulatory binding site. The enzyme is thought to exist in two conformations, only the R-state being active, and the high-affinity regulatory site being present only on the inactive T-state conformation of the enzyme. The high-affinity binding of ADPMg to this site should be amenable to study using direct binding analysis with radiolabelled nucleotide.

The binding sites for ATPMg in the V-ATPases have been studied by several laboratories but as is discussed in chapter 4 there is still controversy as to the number of these sites and whether there are sites of differing affinity for ATPMg. From the present work there is only one type of binding site for ATPMg, the catalytic site with a K_m of around 60μM, in agreement with results from other laboratories working on the chromaffin granule ATPase (Johnson *et al*, 1982; Moriyama and Nelson, 1987b) or on the vacuolar ATPase from kidney microsomes (David and Baron, 1994).

It is evident from the work presented in the preceding chapters that V-ATPases are regulated differently from the extensively-studied ATP synthases (Boyer, 1993). Although the mechanism of ATP hydrolysis by ATP synthases is now well understood at the molecular level (Abrahams *et al*, 1994) these results are unlikely to be applicable to the V-ATPases which although fundamentally similar in their catalytic abilities, have very different functions in the cell. The fact that these enzymes appear to be regulated by different mechanisms and therefore independently may be important to the cell in controlling the proton-linked processes that they catalyse.

The aim of the work reported in this chapter was to explore the high-affinity regulatory binding site for ADPMg on the inactive T-state of the chromaffin granule ATPase by direct measurement of equilibrium binding of radiolabelled ADP, with separation of bound from free nucleotide by gel filtration, either in a long column under equilibrium conditions or using spin centrifugation. Both of these methods have been successfully employed during the determination of the various

dissociation and rate constants for nucleotide binding to the ATP synthases (Grubmeyer *et al*, 1982).

6.2 Special Methods.

[^{3}H]-ADP was purchased from NEN Dupont at a specific activity of 0.99TBq/mmol in a 50% v/v ethanol solution; in binding experiments the ethanol concentration did not exceed 1% v/v. All samples for liquid scintillation counting were suspended in 3ml Ultima Gold (Packard).

Spin centrifugation columns consisted of an Eppendorf tube with small holes in the bottom and in the cap and plugged with glass wool into which was poured 1.3-1.5ml Biogel P6-DG which had been swollen and equilibrated in the appropriate buffer. The small columns were spun for 2-3 minutes at 1400rpm in a MSE bench centrifuge to give approximately 1ml packed bed volume. The sample to be separated was pipetted on top of the packed columns before another centrifugation to separate bound from free ligand. The sample volume and composition is indicated in the figure legends. Controls for non-specific binding were of two types: controls for non-vesicular-associated material which consisted of samples with no reconstituted ATPase but with the same volume of 150mM KCl, 10mM HEPES-KOH, pH7.4, 1mM DTT and 0.1mM EDTA; and controls for vesicular-associated material which consisted of no ATPase but the same volume of non-protein liposomes at 2mg/ml lipid with the same lipid composition as in the reconstituted ATPase. These liposomes were prepared using the same method as for reconstitution of the ATPase (chapter 2). The controls were performed over a range of ADP concentrations and showed no difference in non-specific background over the ranges tested. There was also no significant difference between non-vesicular and vesicular background. In a typical spin centrifugation experiment control only 0.4-0.5% of the loaded counts come through the column so the columns have the capacity to separate the free from the bound nucleotide with 99.5% efficiency. It should be noted that samples in large binding experiments were staggered so only four P6-DG columns were used at any one time to prevent the dissociation of bound label while the sample was on top of the column immediately before centrifugation. This was achieved by starting each set of four binding reactions at 10 or 15 minute intervals. The spin centrifuge method was tested initially as the method of choice due to the ease with which large numbers of data points can be obtained. All spin columns, centrifugation steps and sample incubations were at room temperature.

Equilibrium separation of bound from free nucleotide was performed using a Sephadex G-50 column of 3ml bed volume. The column used was 15cm in length and 0.5cm in diameter with a reservoir that could hold about 5ml of liquid. The

column was equilibrated with the appropriate buffer by passing 2 bed volumes through using a peristaltic pump to give a constant flow rate of approximately 0.1ml/min. The sample to be separated did not exceed 200µl (exact sample composition and volume is given in the figure legends) and was eluted with 2 bed volumes of equilibration buffer. Fractions of the volumes indicated in the figure legends were collected in glass test-tubes and left on ice until an appropriate time for assay or for processing for counts (addition of 3ml Ultima Gold to 100µl fractions). Each column run represents only one concentration of ADP for the binding curve so it is more difficult to obtain large numbers of data points using this method. All column runs and loading sample incubations were performed at room temperature.

For experiments investigating the presence of endogenously-bound nucleotide the ATPase was purified as usual up to solubilisation in 1.8% octyl glucoside. At this point activated charcoal was added to 0.9%w/v, the solution gently stirred and then incubated at room temperature for 10 minutes. The purification and reconstitution were then continued as usual.

Blue native polyacrylamide gel electrophoresis (PAGE) was performed as described in chapter 2.

6.3 Results.

6.3.1 Direct binding of [^{3}H]-ADP.

Initially the method of choice for obtaining data for binding curves was to use non-equilibrium spin centrifugation, since such data can be obtained and the results of the preceding chapters indicate that the binding of ADPMg is of very high affinity. This high-affinity binding should be amenable to testing by fast separation of bound nucleotide from free. The binding of ADP at 0.1-300µM in the presence or absence of Mg^{2+} ions was studied this way (Figure 6.1). In the absence of Mg^{2+} there was no significant binding of ADP, confirming the results of the preceding chapters. In the presence of 5mM Mg^{2+} binding of ADPMg was observed but the binding appeared to be non-saturable even at very high concentrations of nucleotide. This may be a result of non-specific binding of nucleotide to the vesicles since the background of nucleotide coming through the columns was very low and did not vary with the loaded concentration. The lack of saturable binding observed suggested that the technique was unlikely to yield estimates of dissociation constants and as a consequence of this a long column was tried to achieve equilibrium separation of bound nucleotide from free.

Initially Sephadex G-25 was used for gel filtration but gave inadequate resolution of the peak of vesicular material from the control phenol red peak (results not shown) and Sephadex G-50 was used for subsequent experiments. The column

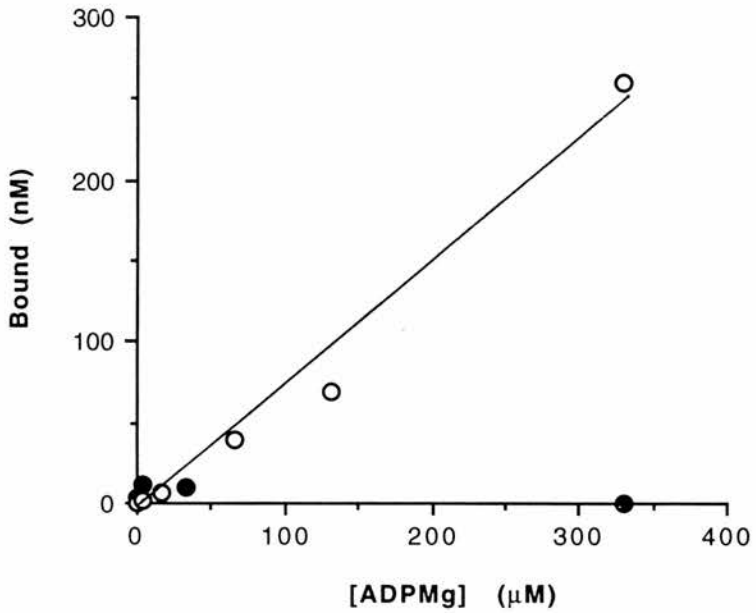

Figure 6.1 Binding of [^{3}H]-ADP to reconstituted ATPase using spin centrifugation through 1ml packed P6-DG columns equilibrated in 150mM KCl, 10mM HEPES-KOH, pH 7.4, 1mM DTT with (○) or without (●) 5mM $MgSO_4$. Samples consisted of 50μl reconstituted ATPase at 5mM $MgSO_4$, 0.1MBq/ml [^{3}H]-ADP in a total volume of 100μl. 80μl of this sample was passed through the columns after incubation for 3-5 minutes: 10μl of remaining sample was counted for total counts; 40μl of effluent was counted for bound nucleotide. Controls for non-specific background were phospholipid vesicles at 2mg/ml or P6-DG equilibration buffer with or without $MgSO_4$. There was no difference between these controls and the concentration of MgADP also had no effect on the level of non-specific binding under these conditions.

was calibrated with blue dextran for the void volume, and phenol red and [^{3}H]-ADP for the position of elution of free nucleotide (Figure 6.2a). The blue dextran eluted in fractions 7-11 with a peak in fraction 8 while the phenol red eluted in fractions 16-24 with a peak in fraction 21. [^{3}H]-ADP eluted between fractions 14-24 with a peak at 18 slightly ahead of phenol red (Figure 6.2a). The 3ml Sephadex G-50 column therefore allows separation of high molecular weight material from the loading buffer without any overlap of elution peaks. When proton translocation was assayed in the fractions from binding experiments in different equilibration buffers it was found that the activity of the ATPase was higher in KCl-HEPES buffers (Figure 6.2c) than in sucrose-HEPES buffers (Figure 6.2b) suggesting that the ATPase is stabilised in higher ionic strength. The ionic strength may be important for maintaining intersubunit interaction and therefore the integrity of the ATPase by preventing dissociation of subunits as the ATPase passes through the column. The peak of proton translocation activity (Figures 6.2b and c) corresponds with elution of blue dextran in the calibration column (Figure 6.2a): this is expected as vesicular material is eluted in the void volume. However there is no peak of counts associated with the peak of proton translocation at 1μM ADPMg. At this concentration of nucleotide the ATPase regulatory site should be saturated according to kinetic and NEM inactivation analysis which suggest that the dissociation constant for ADPMg from the regulatory site is submicromolar. The concentration of ATPase in the loading sample is 200nM assuming holoenzyme purity and a molecular weight of the holoenzyme complex of 800kDa. At saturating ADPMg then a peak of 20% above background might be expected. This would increase the counts by around 2400dpm, an increase which should be easily resolved. The absence of such a peak of ADPMg binding suggests either a lower concentration of holoenzyme than thought or that the enzyme present is unable to bind nucleotide: this is consistent with later results (Figures 6.12 and 6.13).

A trough between fractions 11-17 with a peak at 14 (Figure 6.2b) or 15 (Figure 6.2c) suggests some binding of ADPMg but the absence of a corresponding binding peak and the differing position of this trough from the free [^{3}H]-ADP peak in the calibration column (Figure 6.2a) argue against this.

In an attempt to reduce the background relative to the peak of bound ADP, equilibrium columns were run at 10nM (Figure 6.3a), 20nM (Figure 6.3b) and 50nm ADPMg (Figure 6.3c). The peak positions of H^+-translocation activity and phenol red were in similar fractions (Figure 6.3c) to those found previously (Figure 6.2). There is no peak of [^{3}H]-ADP associated with the ATPase-containing fractions (Figures 6.3 a-c) and no trough in the position of phenol red. In each case there is a

a

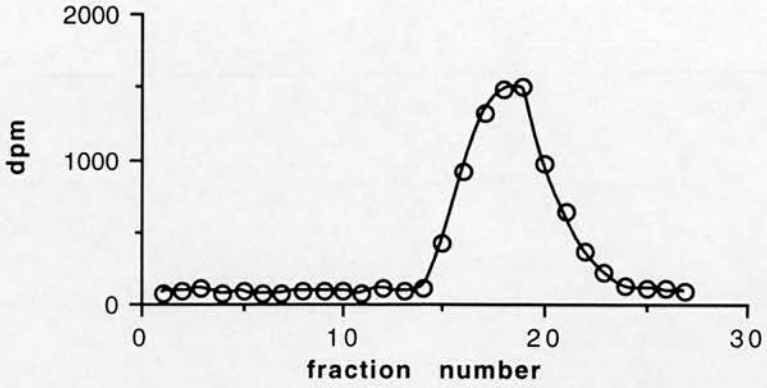

b

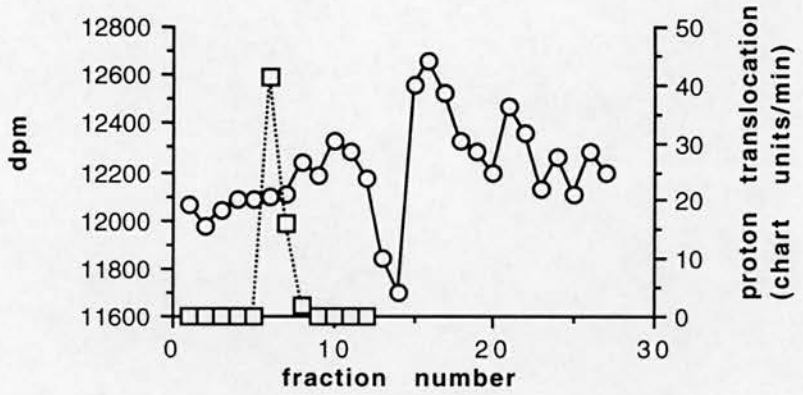

c

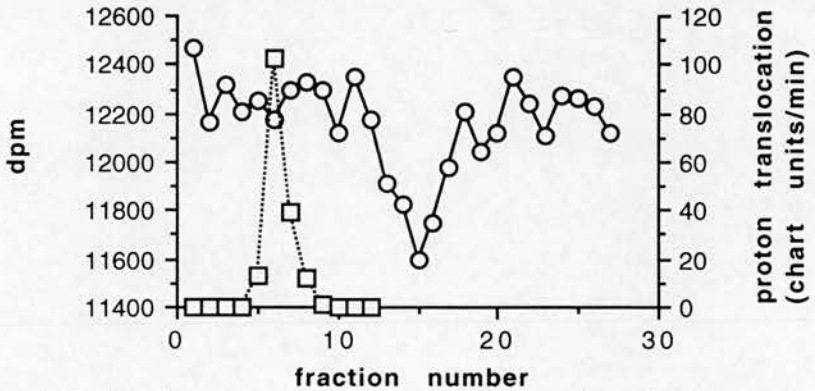

Figure 6.2(a-c) Sephadex G-50 separation of bound and free nucleotide. Columns were equilibrated in 150mM KCl (a and c) or 0.3M sucrose (b) and 10mM HEPES-KOH, pH7.4, 5mM $MgSO_4$, 1mM DTT with 1µM [^{3}H]-ADP, specific radioactivity 1.7GBq/mmol (b and c) or without ADP (a). Fractions of 200µl were collected: 100µl was counted (o) and 50µl assayed for proton translocation (□ , dotted lines). (a) calibration of column: 100µl sample of [^{3}H]-ADP at 1.7GBq/mmol, 1µM, 2mg/ml blue dextran, 0.1mg/ml phenol red in column equilibration buffer loaded. Fractions 7-11 (peak 8 (a)) and 16-24 (peak 21, (a); 18, (b and c)) contained blue dextran and phenol red respectively. (b and c) 50µl of reconstituted ATPase loaded in a final volume of 100µl of appropriate equilibration buffer.

a

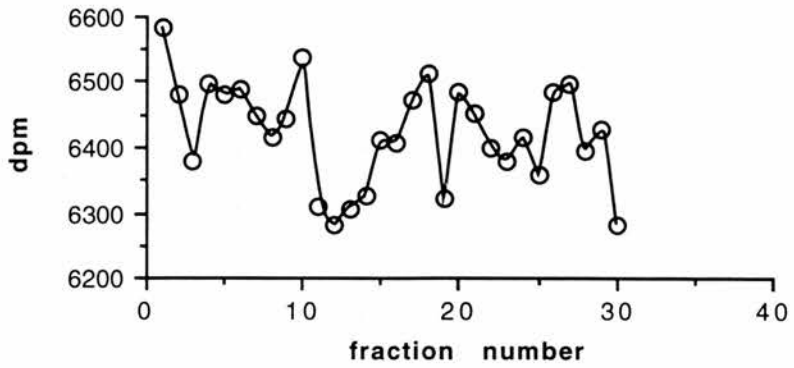

b

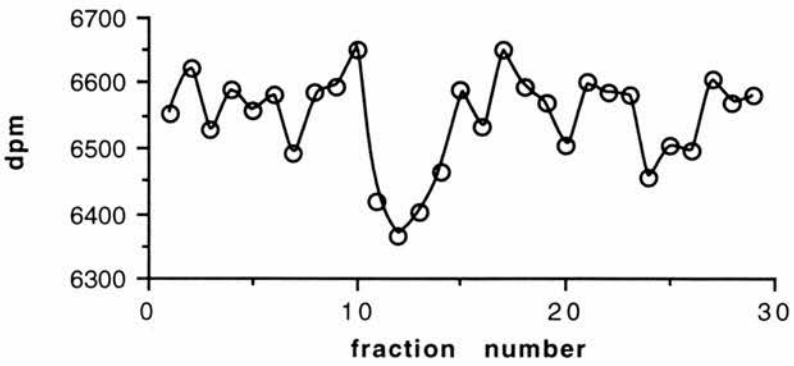

c

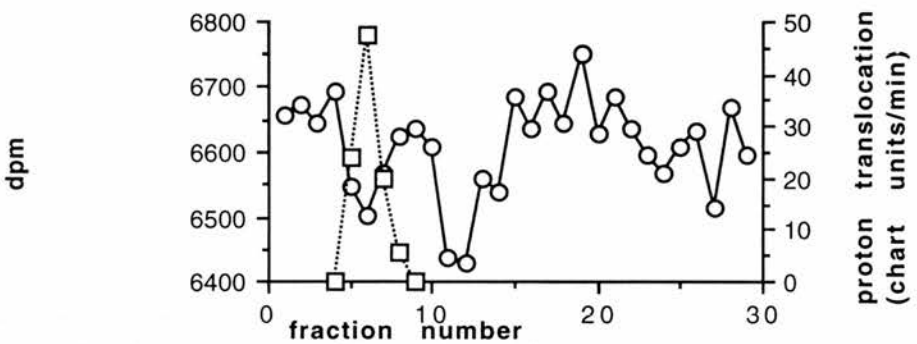

Figure 6.3(a-c) Separation of bound and free nucleotide on Sephadex G-50. Columns (3ml) were equilibrated in 150mM KCl, 10mM HEPES-KOH, pH7.4, 5mM MgSO4, 1mM DTT with [^{3}H]-ADP (1.7kBq/ml) at 10nM (a), 20nM (b) and 50nM (c). The specific radioactivities were 0.17TBq/mmol (a), 0.08TBq/mmol (b) and 0.03TBq/mmol (c). Fractions of 200µl were collected: 50µl was counted for tritium (○). 50µl of fractions from the 50nM column (c) were assayed for proton translocation (□ , dotted lines). The loaded sample was 100µl reconstituted ATPase in a total volume of 160µl column equilibration buffer, 0.1mg/ml phenol red. Fractions 15-23 contained phenol red with a peak around 18-19.

trough around fractions 11-15. The size of this trough does not vary with the concentration of ADPMg confirming that it does not represent the binding of ADP to the ATPase.

Concentration of the reconstituted ATPase by centrifugation of the vesicles and resuspension in a smaller volume was attempted but the ATPase concentrated in this way was not active in proton-translocation and again no binding of nucleotide was seen. Columns were also ran in the presence of 0.5% v/v $C_{12}E_9$ and in the absence of phenol red but no binding was seen in any of these columns.

The absence of saturable binding led to experiments to investigate the presence of slowly-exchangeable sites and endogenously bound nucleotide. The possibility that the holo-ATPase was present at a much lower concentration than expected prompted the investigation of the effect of detergents to gain access to any holoenzyme which is inverted in the phospholipid bilayer. A timecourse of binding of ADPMg was carried out with liposomes either untreated or solubilised with $C_{12}E_9$ (Figure 6.4). The solubilised ATPase exhibited significantly greater ADPMg binding than the reconstituted enzyme with maximum binding being four times greater (Figure 6.4). The timecourse of binding of ADPMg is very similar regardless of the concentration of nucleotide or the type of preparation which may suggest that it depends on the slow exchange of nucleotide at the binding site . The results illustrated in figure 6.4 indicated that once maximal binding had occurred at around 60 minutes (Figure 6.4) the binding was directly proportional to the incubating ADPMg concentration: 20nM bound at 86nM total ADPMg and 5nM bound for 19nM total ADPMg. It was apparent that problems with the initial spin centrifugation experiments (Figure 6.1) were two-fold: the reconstituted preparation did not have a high enough concentration of available binding sites as is indicated by the four times increased binding capacity in the presence of detergent; and the incubation times used initially were too short to obtain maximal binding of nucleotide.

These factors were taken into account and experiments performed using detergent-solubilised ATPase and the samples incubated for 60 minutes at room temperature to obtain maximal binding. The binding curves were biphasic, with tight binding at low ADPMg concentrations followed by a non-saturable component (Figure 6.5b). This prompted investigation of binding at concentrations of ADPMg between 20nM and 20μM (Figure 6.6a). Very tight binding was observed up to about 3μM ADPMg followed by the linear non-satureable component of the curve (Figure 6.6a). The slope of the non-saturable component ([ADPMg] 5-20μM) is many more times less than the slope where *bona fide* binding occurs ([ADPMg] 20nM-

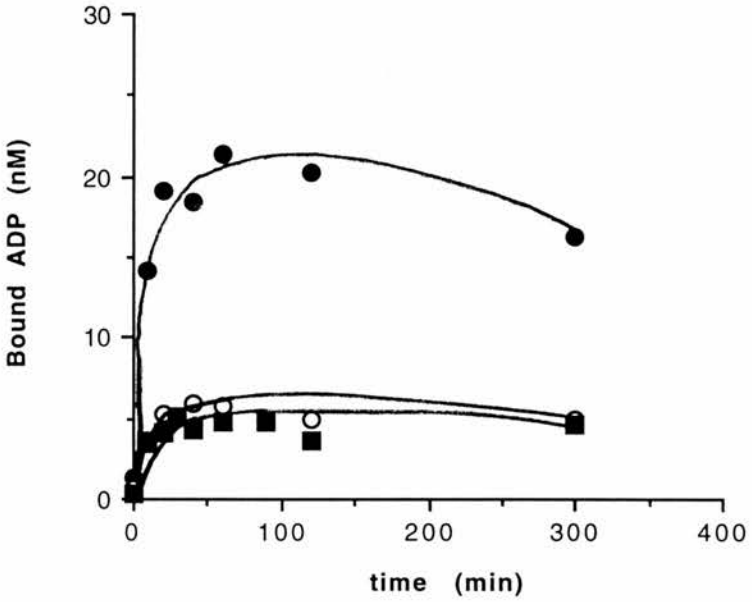

Figure 6.4 Binding of [^{3}H]-ADP to reconstituted ATPase using spin centrifugation through 1ml packed P6-DG columns equilibrated in 150mM KCl, 10mM HEPES-KOH, pH 7.4, 1mM DTT, 5mM $MgSO_4$. $C_{12}E_9$ to 1% w/v: (closed symbols) was added to reconstituted ATPase before the addition of $MgSO_4$ (to 5mM final) and [^{3}H]-ADP (to 86nM, 86kBq/ml (circles) and 19nM, 19kBq/ml (squares) final) to start the timecourse. Points with open symbols contained no $C_{12}E_9$. The samples were kept at room temperature throughout the timecourse. 100µl of sample was passed through the columns at the indicated time points. At the end of the timecourse 10µl of remaining sample was counted ; 50µl of effluent was counted for bound nucleotide. Controls for non-specific background were phospholipid vesicles at 2mg/ml or vesicle media buffer plus 5mM $MgSO_4$ and there was no difference between these as in figure 6.1.

a

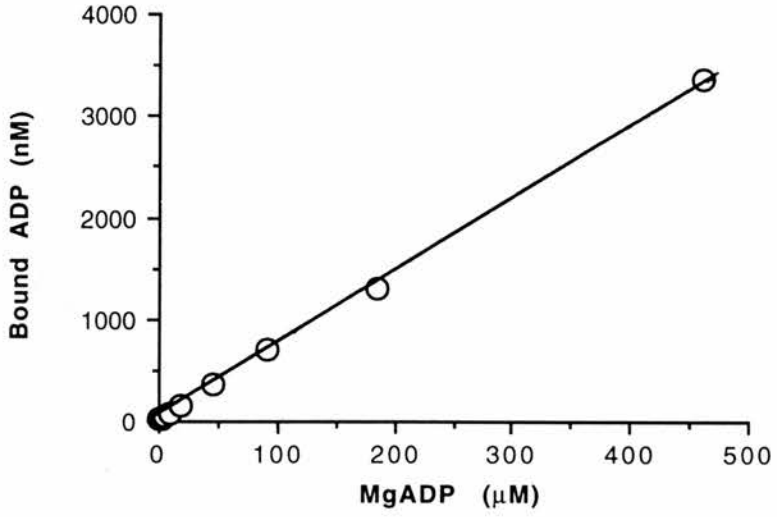

b

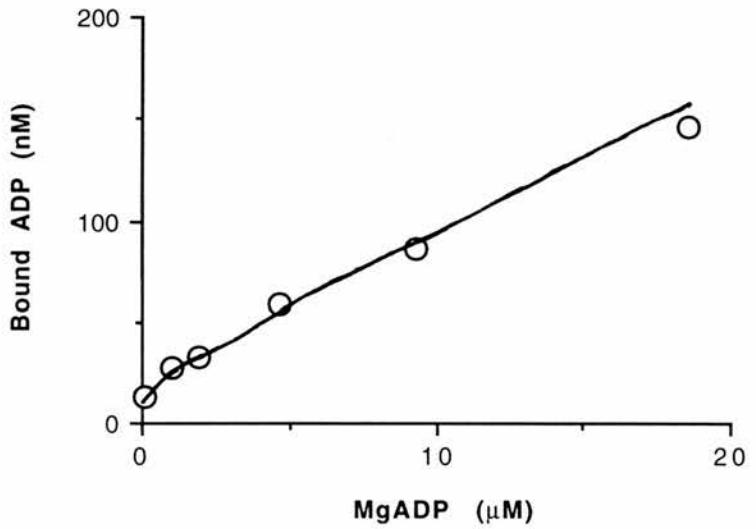

Figure 6.5(a+b) Direct binding analysis of [^{3}H]-ADP to solubilised ATPase (1%v/v $C_{12}E_9$) by passage through 1ml packed colums of P6-DG equilibrated in buffer as in figure 6.4. 91μl solubilised ATPase was made to a total volume of 100μl with $MgSO_4$ (to 5mM final) and [^{3}H]-ADP (0.09MBq/ml). The specific activity of [^{3}H]-ADP is different at each concentration. The sample was incubated for 60minutes at room temperature before 80μl was passed through the column samples. 40μl of effluent was counted for bound nucleotide; 10μl of remaining sample was counted for total radioactivity. Non-specific controls were as in figure 6.4. (a) complete binding curve; (b) the same curve as fig 6.5a but scaled to 20μMADP.

a

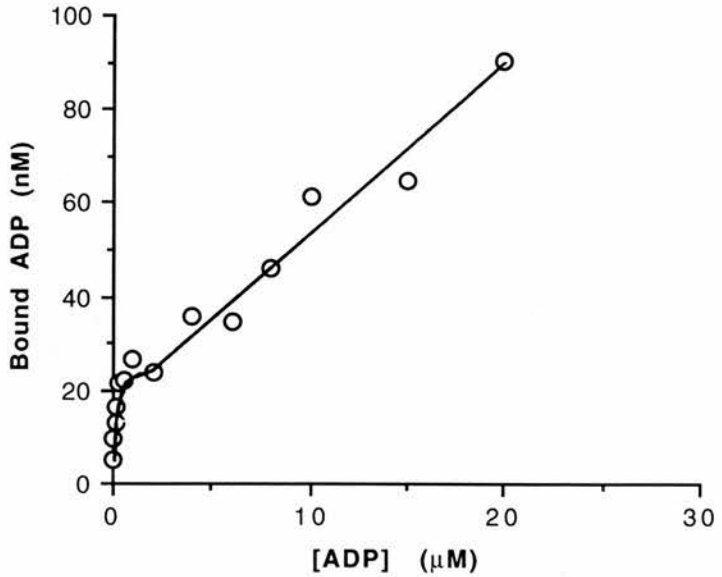

b

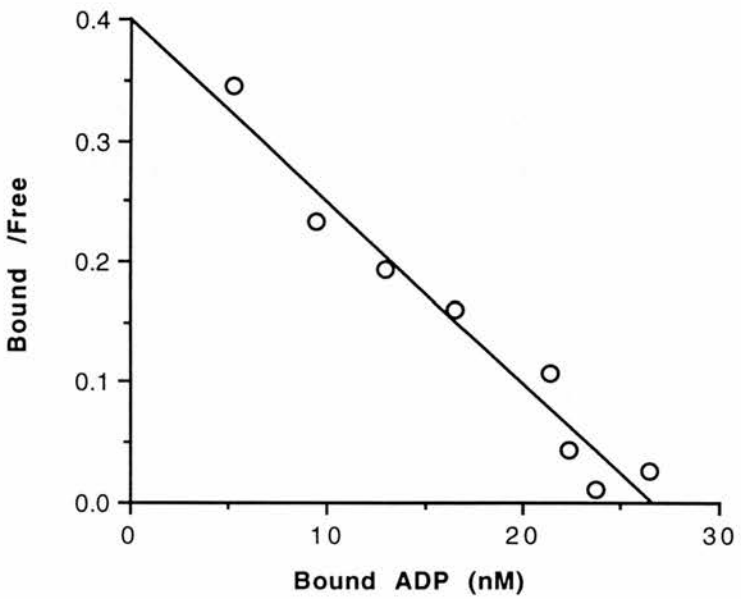

Figure 6.6(a+b) Direct binding analysis of [^{3}H]-ADP to reconstituted ATPase using the same protocol as in figure 6.5 except that the concentration of [^{3}H]-ADP is 0.02MBq/ml. (a) binding curve up to 20μM total ADP; (b) data plotted according to Scatchard up to 30nM bound. The line in figure 6.6b is calculated by linear regression and gives K_D=66±6nM and B_{max}=27nM±1.7nM with correlation coefficient, r=0.955.

3μM), so the background in the saturable binding range is insignificant. The binding data up to 3μM ADPMg were plotted according to Scatchard to give an apparent dissociation constant for binding of ADPMg to the regulatory site of 66±6nM (Figure 6.6b). The Scatchard plot is linear in this range of nucleotide concentrations since competitive binding of ADPMg to the catalytic sites in the T-state is apparently insignificant (K_b=17μM, chapter 4). Maximum binding of 27±2nM was also calculated from the Scatchard plot (Figure 6.6b). This value is very low when one considers that if all protein in the vesicle preparation is native holoenzyme then the concentration will be approximately 400nM for a typical preparation assuming Mr for the holoenzyme of 800kDa.

ATP hydrolysis catalysed by the $C_{12}E_9$-solubilised ATPase was analysed according to Hanes (Figure 6.7) to give calculated values of K_m and V_{max} of 50μM and 90nmol/min/mg respectively. The specific activity is around ten times lower than that for the reconstituted ATPase suggesting that the enzyme functions better in a lipid bilayer. The K_m value is close to that obtained with the reconstituted ATPase in either proton translocation (54μM) or ATP hydrolysis (80μM) assays (chapter 4) suggesting that binding reactions in the detergent-solubilised enzyme are similar to the reconstituted form.

The analysis of endogenously bound nucleotide was performed using activated charcoal to strip the ATPase of any bound nucleotide and then comparing the binding properties of the stripped and untreated preparations. The rate of ADPMg binding and the maximum reached are not significantly different in the charcoal-treated preparation compared to the unstripped ATPase (Figure 6.8a), using 22nM ADPMg. Over a range of ADP concentrations the two preparations are also not significantly different (Figure 6.8b). It thus appears that the lengthy period of time taken to reach maximum binding of ADPMg (30-60 minutes) is not due to slow exchange of bound nucleotide.

6.3.2 Determination of the stoichiometry of ADPMg binding.

To estimate the stoichiometry of ADPMg binding it was necessary to determine the concentration of enzyme which could bind ADPMg. The technique of blue native PAGE (Schägger and von Jagow, 1994) was found to be useful in separating the holo-ATPase (V_1V_O)from the membrane sector (V_O) and was used to obtain an estimate of the ratio of the two components. Chromaffin granule membranes and mitochondria were run on the same blue native gel (Figure 6.9). The mitochondrial complexes: I, NADH-coenzyme Q reductase, (800kDa); II, succinate-coenzyme Q reductase, (130kDa); III, coenzyme Q-cytochrome c reductase,

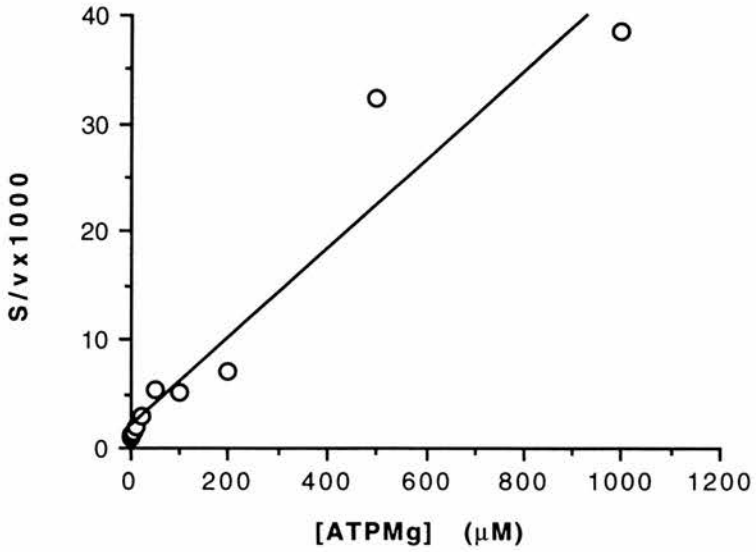

Figure 6.7 ATP hydrolysis catalysed by reconstituted ATPase solubilised by the addition of 1/10th volume of 10%v/v $C_{12}E_9$ and assayed by liberation of [$^{32}P_i$] from [$\gamma^{32}P$]-ATP. The data are plotted according to Hanes and the fitted line gives K_m=50μM and V_{max}=24nmoles/min/ml solubilised ATPase (specific activity=90nmoles /min/mg. The correlation coefficient, r for the fitted line is 0.922.

a

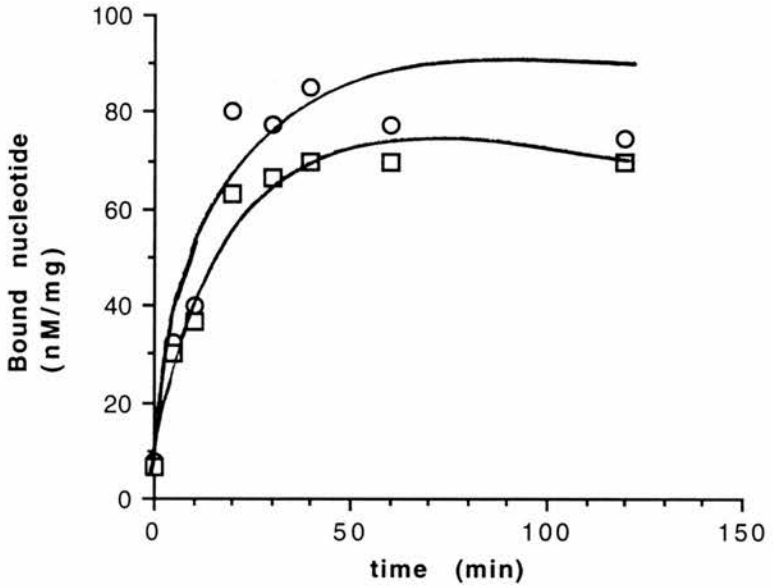

b

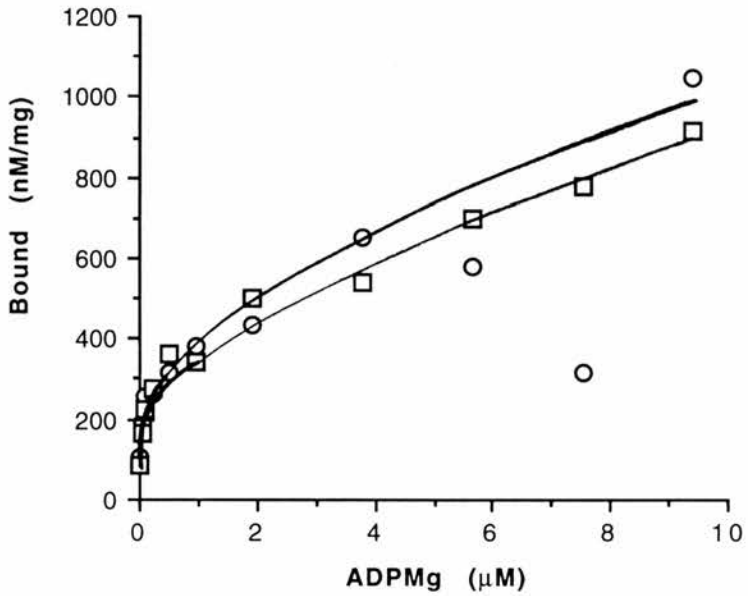

Figure 6.8 Binding of [^{3}H]-ADP to ATPase reconstituted after treatment with (O) or without (□) the addition of activated charcoal to 0.9% w/v at the octyl glucoside-solubilised stage in the ATPase purification (chapter 2). The timecourse was performed as in figure 6.4 with the reconstituted ATPase being solubilised with the addition of 1/10th volume of 10% w/v $C_{12}E_9$. The concentration of [^{3}H]-ADP in the timecourse samples was 22nM. Binding is represented as bound nucleotide /mg protein since the ATPase preparations plus or minus charcoal were slightly different in terms of protein concentration.

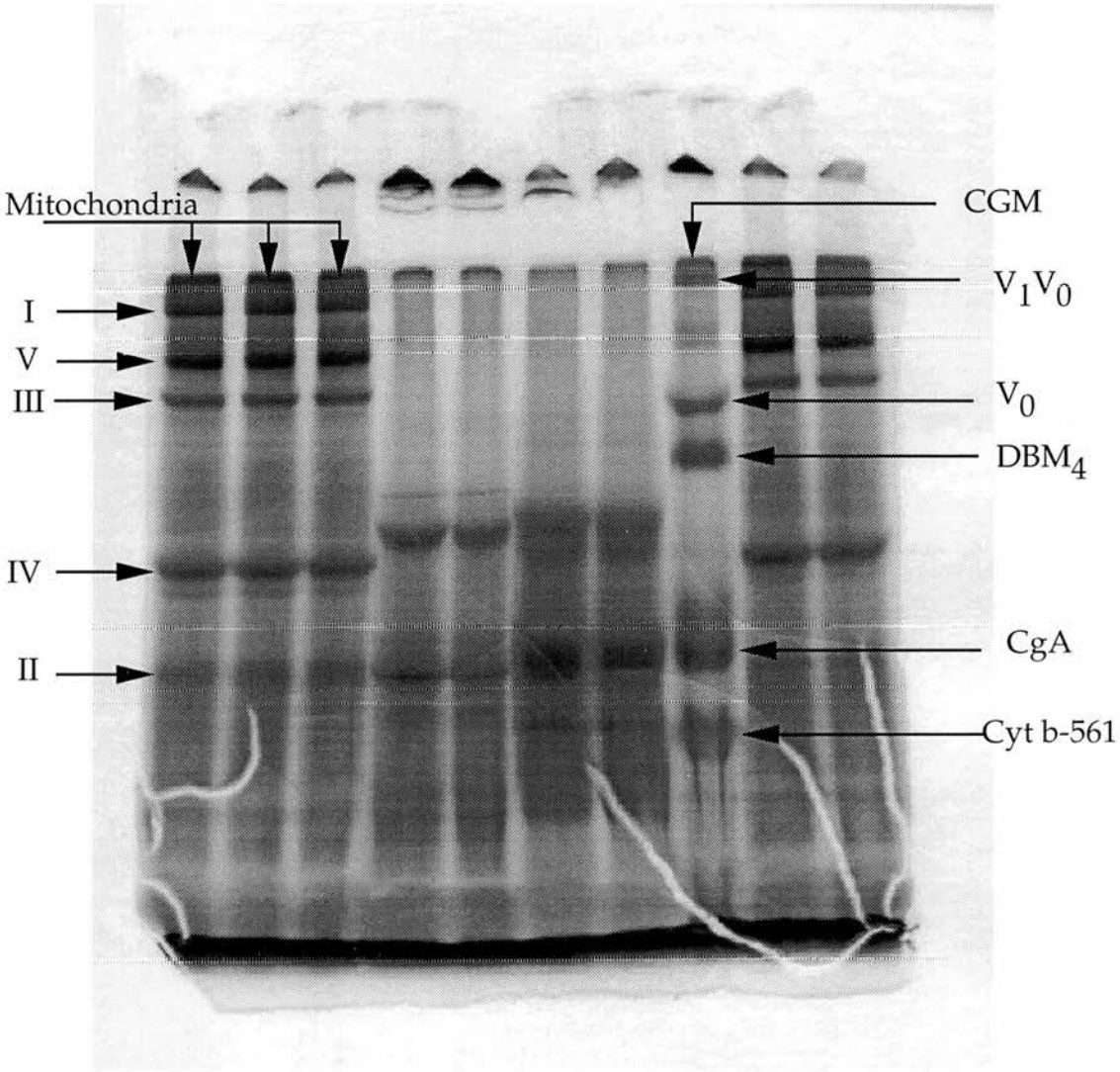

Figure 6.9 Blue native gel electrophoresis of mitochondria and chromaffin granule membranes (CGM) showing positions of the mitochondrialrespiratory complexes (I - V) and the major complexes present in CGM: holo(V)-ATPase (V_1V_0); membrane sector (V_0); tetrameric (DBM_4) dopamine β-monooxygenase ; chromogranin A (CgA) and cytochrome b-561.

(485kDa); IV, cytochrome c oxidase, (200kDa); and V, ATP synthase, (600kDa) were used as molecular mass markers. The relationship between Mr and relative mobility, Rf is logarithmic (Figure 6.10). When run in the second dimension under SDS-denaturing conditions (Figure 6.11) the individual subunits of the bands in the first dimension are resolved allowing identification of the complexes as V-ATPase, V_1V_O and V_O; Dopamine β monooxygenase (DBM); Chromogranin A (CgA); and cytochrome b-561 monomers. The molecular masses of the holoenzyme and the membrane sector can be calculated from the respiratory complexes standard curve (Figure 6.9b) as 851±12kDa and 457±6kDa respectively. Raster scans of the subunits in the 2-D gel were carried out but the results were difficult to interpret since the staining with Coomassie Blue G depended on properties of the individual subunits: for example the 45 and 16kDa subunits did not stain as well with Coomassie Blue G as they did with silver, making an accurate estimation of stoichiometry from stained second dimension blue gels difficult. A better approach may be to excise the bands and perform amino acid analysis since the sequence of most of the subunits have now been cloned. Suggested stoichiometries of the V_1 subunit are 3:3:1:1 (72:57:40:33kDa) while for V_O the ratio is thought to be 6:1:1:1:1 (16:19:116:45:39kDa) (Forgac, 1989, Supek *et al*, 1994). These figures give V_1V_O=775kDa and V_O=315kDa suggesting that glycosylation of the 116 and 45kDa subunits may affect the mobility of the complex. However these estimates of the stoichiometry may be wrong or there may be other subunits present which do not stain well with Coomassie Blue or silver (Supek *et al*, 1995). The molecular weight of the DBM tetramer is calculated to be 363±5kDa (Figure 6.9; 6.10b) which is greater than four times the 75kDa subunit size but the discrepancy may be due to heavy glycosylation of DBM. When purified ATPase is subjected to blue native PAGE only two major complexes are seen: V_1V_O and V_O (Figure 6.12) consistent with the removal of DBM and cytochrome in the Triton X-114 fractionation steps. When run in the denaturing second dimension some contamination with DBM tetramers is evident but comparison of figure 6.13 and 6.11 show that most of the DBM has been removed and that the V-ATPase is fairly pure.

It has become evident that in both chromaffin granule membranes (Figure 6.11) and P1 (Figure 6.13) there is a large proportion of V_O compared to holoenzyme. Two-dimensional raster scans of the separated complexes were carried out on blue native gels such as those illustrated in figure 6.12. The integrals for the bands were divided by the calculated molecular weights of the complexes to give an average ratio of V_1V_O:V_O of 1:11±1.1. Raster scans of the 116kDa subunit in V_1V_O and V_O in second dimension gels gave a similar ratio of V_1V_O:V_O = 1:10.5±3.5. The presence of significant amounts of membrane sector is also a feature of chromaffin granule

a

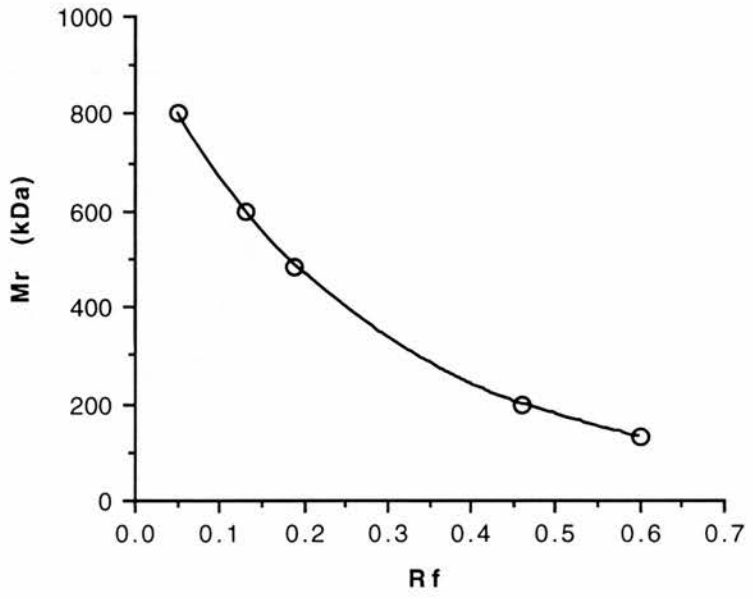

b

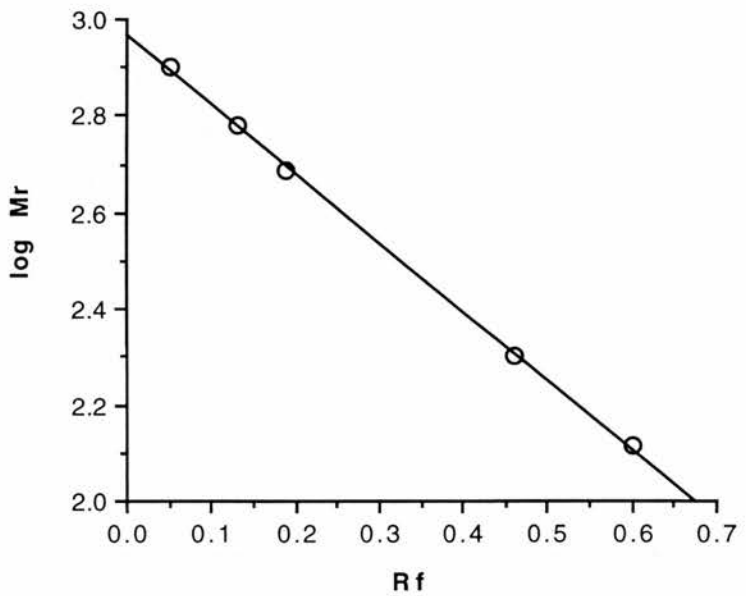

Figure 6.10(a+b) Plots showing the relationship between M_r (a) and log M_r (b) and the relative distance migrated in the blue native polyacrylamide gel electrophoretogram shown in figure 6.8. The mitochondrial respiratory complexes are used as standards. Linear regression was performed using the data in figure 6.9b to give slope=-1.43±0.02 and y-axis intercept=2.97±0.007 with a correlation coefficient, r=0.999.

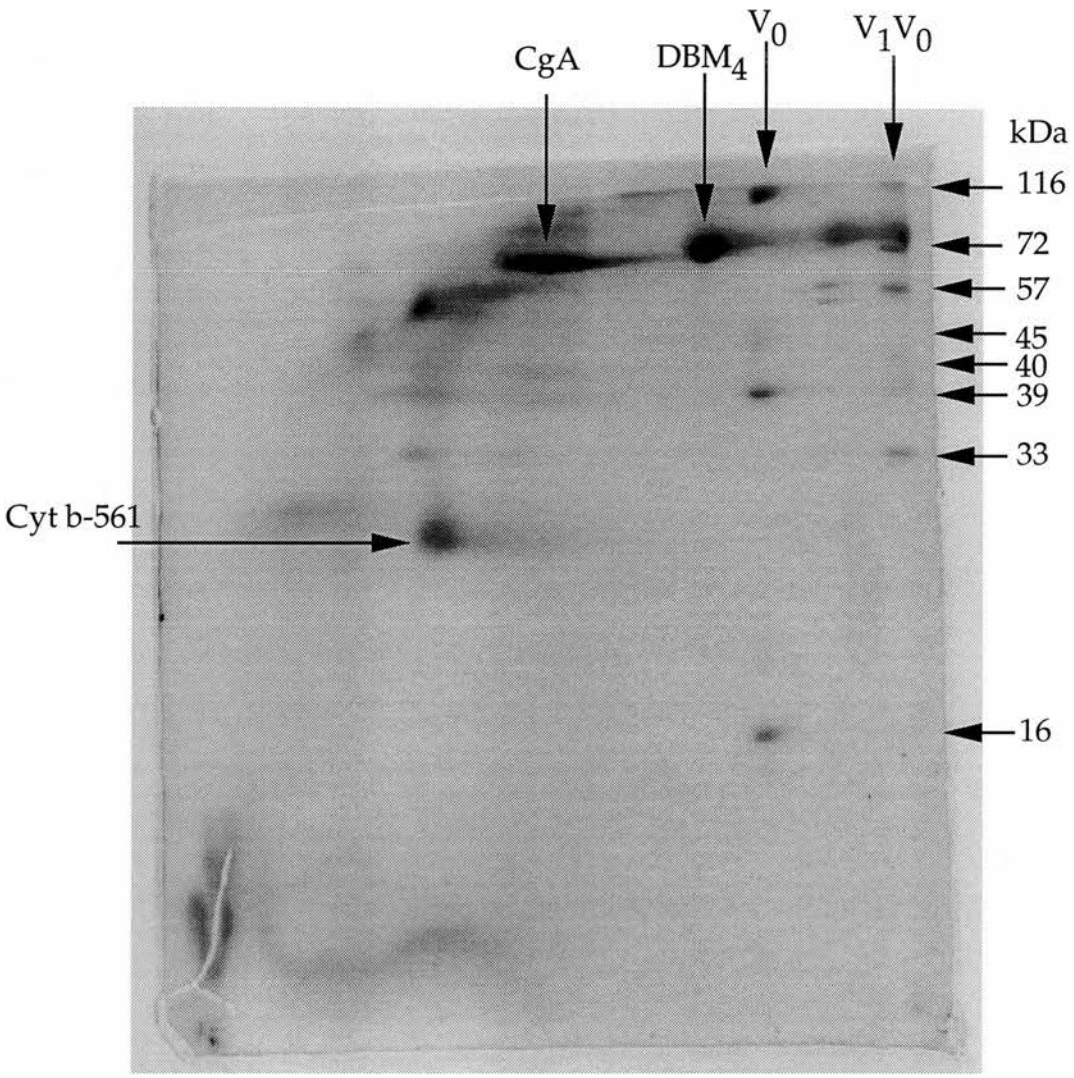

Figure 6.11 Second dimension SDS-PAGE of chromaffin granule membranes ran in the first dimension on blue native PAGE. The M_r values for the V-ATPase subunits are indicated on the left with other chromaffin granule proteins indicated using the same notation as in figure 6.8.

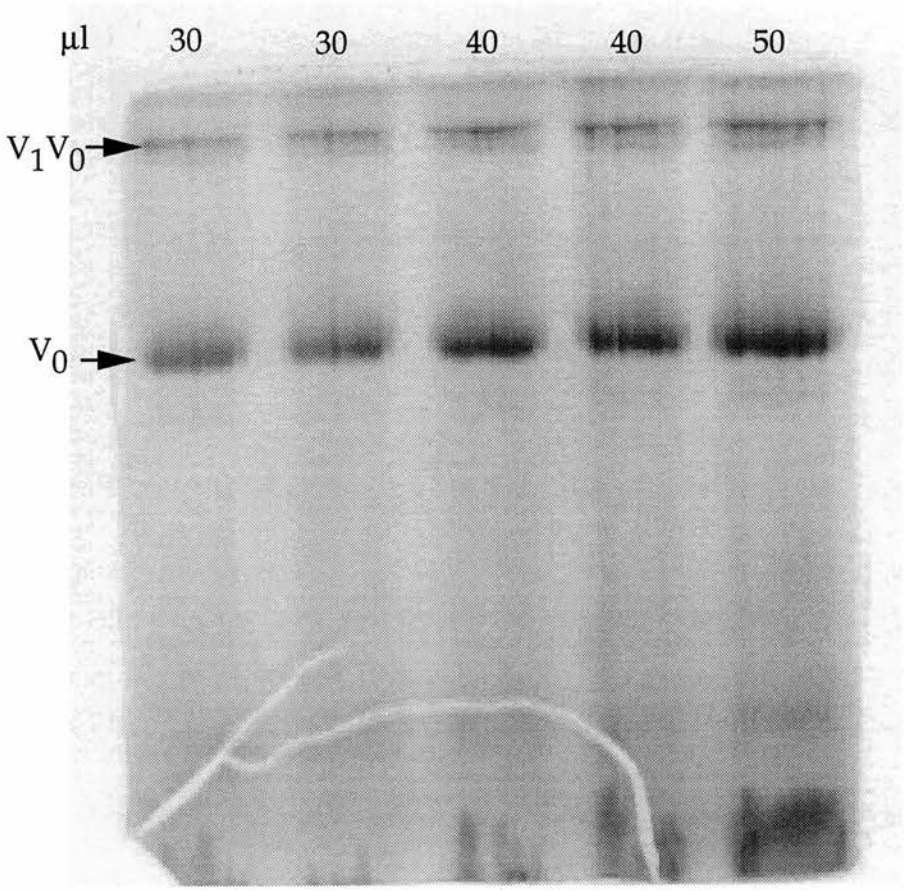

Figure 6.12 Blue native PAGE of P1 samples. The sample volumes loaded and the positions of the different forms of the ATPase are indicated as in figure 6.8.

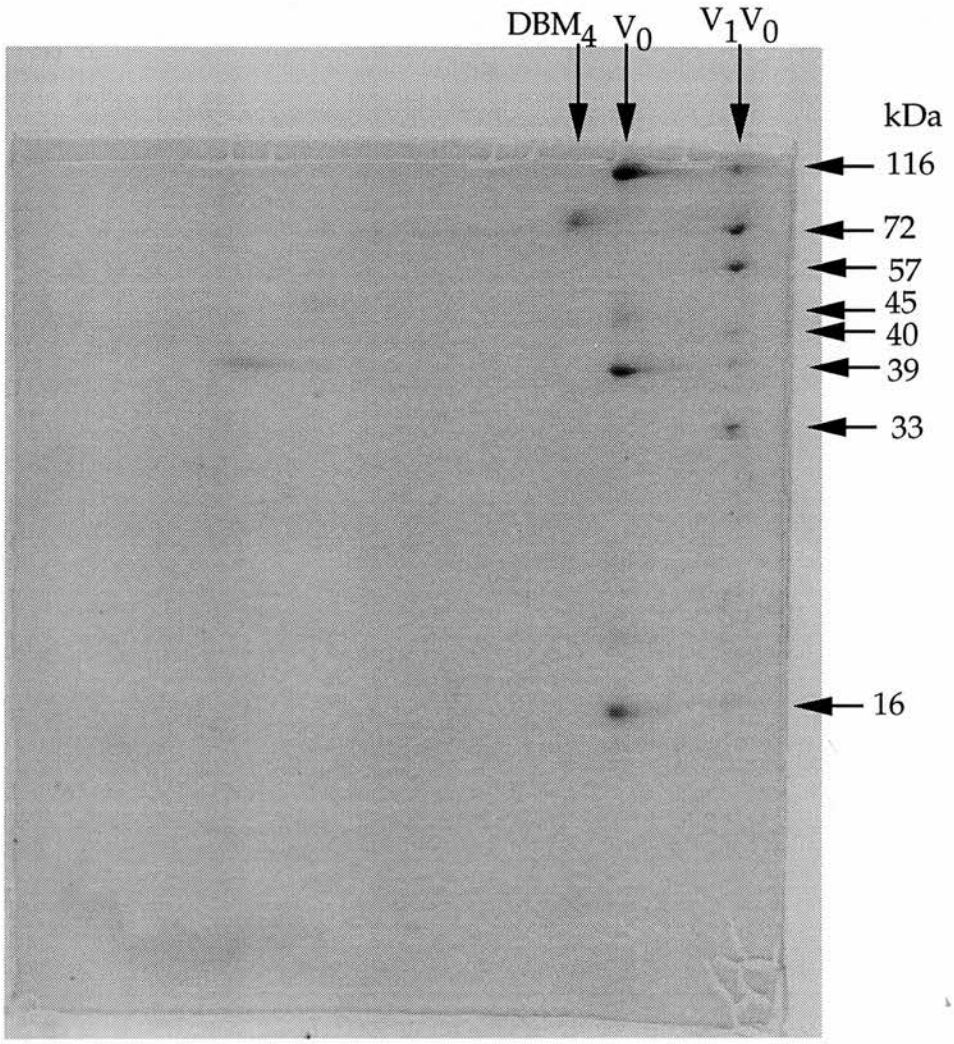

Figure 6.13 Second dimension SDS-PAGE of P1 ran in the first dimension on blue native PAGE. The M_r values for the V-ATPase complex are indicated and the other protein complexes are indicated by the same notation as in figure 6.8. The position of contaminating dopamine β-monooxygenase is shown (DBM_4).

membranes (Figure 6.9 and 6.11) and it may be that this represents a method for regulating V-ATPase activity. The concentration of holo-ATPase in each sample in figure 6.6b can be calculated to be 43nM taking into account the protein content (0.5mg/ml), the dilution of the enzyme and the ratio of holoenzyme to membrane sector (1:11) calculated above. The maximum binding of ADPMg was calculated to be 27±2nM (Figure 6.6b) and hence there are 0.6moles ADPMg bound per mole of holoenzyme. This is consistent with the results of kinetic model fitting which suggested that there is a single regulatory site. Again binding to the catalytic site is not evident because the affinity for binding to the catalytic site, K_b=17μM means that under the conditions employed here only the high-affinity regulatory site will be filled.

An independent method for determination of the stoichiometry of holoenzyme:membrane sector was carried out using a very high affinity analogue of Bafilomycin A_1 (compound 2) obtained from Rhône-Poulenc Rorer. These results were not passed for publication by this company. Bafilomycin has been shown to bind to the V_O sector of the ATPase (Crider *et al*, 1994; Zhang *et al*, 1994). The tight binding by the analogue allowed the use of substoichiometric amounts in proton translocation assays and titration of the analogue with reconstituted ATPase (Figure 6.14a). The rates of proton translocation are linearly proportional to the amount of ATPase present and the data in the presence of compound 2 are displaced to the right of the graph. Extrapolation to proton translocation rate = zero will give the volume of ATPase equivalent to that particular concentration of compound 2. The set of lines at various concentrations are not parallel with more inhibition than expected at higher concentrations of compound 2. This may be due to for example, an uncoupling effect in the assay. In any case the ATPase equivalents can be plotted against the respective concentration of compound 2 and extrapolation to zero compound 2 gives the concentration of V_1V_O+V_O = 338±39nM (Figure 6.14b) assuming 1 binding site per ATPase for compound 2. The ratio from blue native gel electrophoresis is 1:11 (V_1V_O:V_O) giving a concentration of V_1V_O= 28±3nM. The protein concentration of the preparation was 0.4mg/ml and hence taking the molecular mass of the holoenzyme as 815kDa (from blue native PAGE) the ratio using this method is 1:17 (V_1V_O:V_O). Such a ratio gives 1 ADP binding site per holoenzyme present.

6.4 Discussion.

Until now nothing has been published on the properties of the ADP binding site in the V-ATPases although it has long been known that these enzymes are allosterically regulated by ADPMg. The major problem faced in experiments to

a

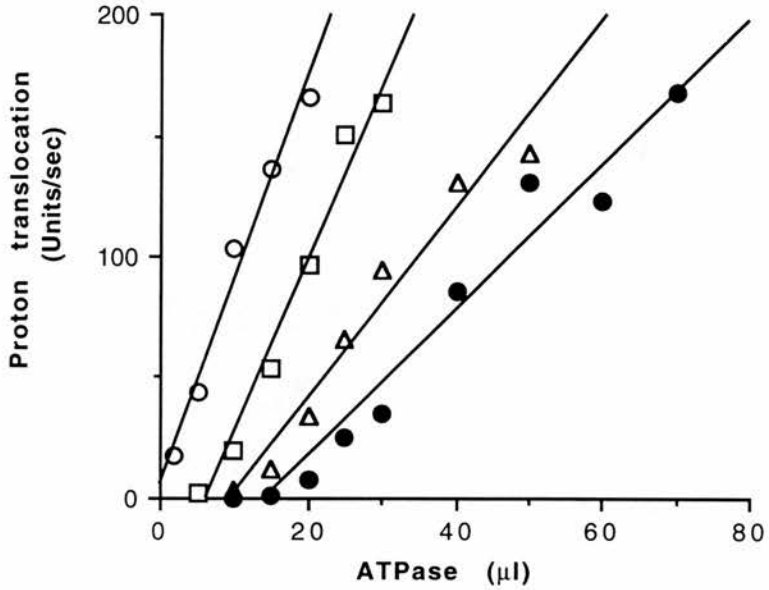

b

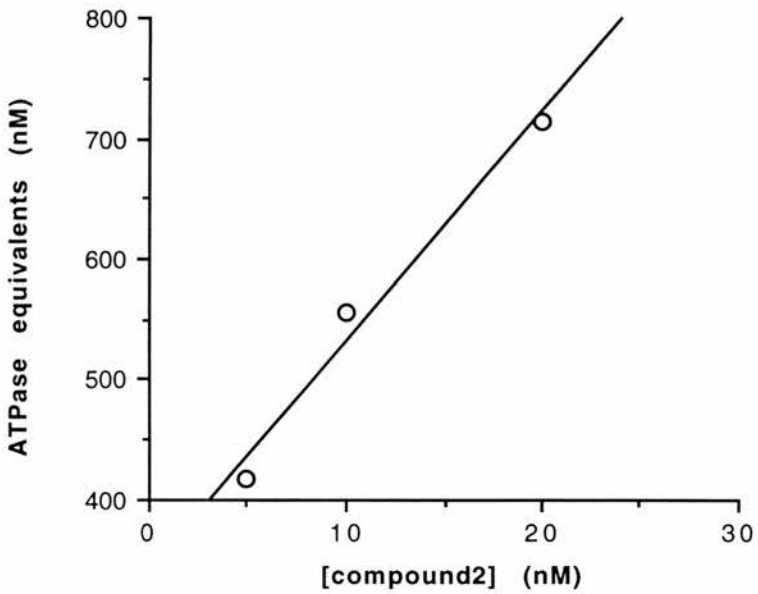

Figure 6.14(a+b) (a) Titration of compound 2 : 0, (○); 5nM, (□); 10nM (△); and 20nM, (●) with reconstituted ATPase. (b) Transformation of the x-axis intercept (Figure 6.14a) into ATPase equivalents. All lines are drawn by linear regression Proton translocation was assayed as described in chapter 2 with the rates being determined using the digital method of data collection.

determine the dissociation constant for ADP from the high affinity regulatory site is the low concentration of ATPase in the preparation which can bind ADP. Different values for the ratio of V_1V_O:V_O were observed with two methods. Bafilomycin-like Compound 2 is likely to be impermeable and hence will only be able to bind to enzyme complexes inserted in the correct orientation in the liposome. Therefore an underestimate of the amount of holoenzyme is likely in view of the fact that it has been shown in chapter 5 that a significant proportion of the holoenzyme is inverted. The ratio from blue native PAGE is also likely to be more valid because the lack of spectroscopic data means that the exact concentrations of compound 2 used could not be calculated and also the number of binding sites is not known.

In calculating the number of ADP binding sites it is assumed that all holoenzyme present is able to bind ADPMg but this may not be the case and the value of 0.6 for rather than 1 for the number of regulatory ADP binding sites (using blue native PAGE ratios of V_1V_O:V_O) may be due to an overestimate of the amount of native enzyme present. It will be interesting to excise the holoenzyme band from blue native PAGE gels and test for ATPase activity and nucleotide binding.

It should also be noted that the calculated dissociation constant is an apparent value since according to the model for regulation (chapter 4) the binding of ADP to the regulatory site is dependent on the equilibrium constant, L for the conformational transition E_R to E_T. If ADP binds only to E_T with a dissociation constant, Ki:

$$Ki = E_T .I/E_TI$$

$$L = E_T /E_R$$

and hence $E_R = (Ki/L.I).E_TI$

total enzyme, $e = E_R + E_T + E_TI$

by rearranging the above equations and substituting we get:

$$E_TI /e = 1/[1+(Ki/I)(1+1/L)]$$

So $Ki_{apparent} = Ki_{real}(1+1/L)$.

Because L is very small this approximates to:

$$Ki_{apparent} = Ki_{real}/L.$$

It follows that with the estimated value for L of around 0.01 (chapter 4) that the real Ki is about 0.66nM.

It has also become apparent that the binding of ADP to the ATPase takes a considerable amount of time although this feature is not observed in the kinetics of proton translocation. The dissociation constant for ADP, Ki is related to the rate of binding, k_{on} and release of nucleotide, k_{off}:

$$Ki = k_{off}/k_{on}$$

Binding is likely to be diffusion controlled with $k_{on} = 10^7$-$10^8 M^{-1}s^{-1}$ (Gutfreund, 1972). The half-time for dissociation of nucleotide , $t_{1/2} = \ln 2/k_{off}$. Hence with Ki = 66nM, $t_{1/2}$=0.1-1s and even with the real Ki of 0.66nM, $t_{1/2}$ = 10-100s. These values are too fast to explain the slow binding component of nucleotide binding. It may be that the slow binding in direct labelling experiments is due to slow conformation change from the R- to the T-state and that this is possibly not observed in the kinetic studies because the enzyme changes conformation much faster in the presence of ATPMg.

Due to the lack of published data on the binding of ADPMg to V-ATPases it is difficult to compare these results with other binding studies. Recently the group of M. Forgac investigated labelling of the coated vesicle V-ATPase by 2-azido-[^{32}P]ATP, and this may be relevant (Zhang *et al*, 1995). It was found that the enzyme had both rapidly ($t_{1/2}$<2 min) and slowly exchangeable ($t_{1/2}$>2 min) nucleotide binding sites and that the timecourse of inactivation by this azido analogue best coincided with labelling of the catalytic, 73kDa subunit. The level of endogenously-bound nucleotide was not determined. Proteolysis and sequencing of the azido-ATP-labelled subunits showed that the A (73kDa) subunit contains both rapidly and slowly exchangeable sites while the B (58kDa) subunit is only labelled under rapidly exchanging conditions. It was also shown that the rapidly exchanging sites on the 73kDa subunit appear to correlate with the Walker consensus nucleotide binding motif (Walker *et al*, 1985) and with the catalytic region of the β subunit of the F-ATPase (Abrahams *et al*, 1994) suggesting that the rapidly exchangeable sites are the site of ATP hydrolysis and that the molecular mechanism of ATP hydrolysis in the two enzymes may be very similar. The rapidly-exchangeable site in the 58kDa subunit labels a fragment which is slightly upstream of the corresponding nucleotide-binding region in the F-ATPase α subunit. This region in the F-ATPase comprises part of a noncatalytic site and may explain why labelling of the B subunit of V-ATPases by ATP analogues is seen when this is not the catalytic subunit (Manolson *et al*, 1985). The slowly-exchangeable sites in the V-ATPase were found to be distinct from the rapidly-exchangeable sites but are also very close to the Walker consensus sequence. This is in contrast to the F-ATPases where the noncatalytic site is located distally from the catalytic site (Cross and Nalin, 1982) and suggests that a different region contributes to the noncatalytic sites in the V-ATPases. This is not surprising when it is considered that the noncatalytic sites represent the regulatory sites and are likely to be different in the F- and V-ATPases.

Although no data for the binding of ADPMg was presented the evidence of slowly exchangeable sites is consistent with the results presented in this chapter. We

found that it took considerable time for the binding of ADPMg to the ATPase to reach a maximum but that this did not appear to be due to the presence of endogenously bound nucleotide. It is unlikely that the slowly exchangeable sites identified here are the same as those identified with 2-azido-ATP since the stoichiometry of the ATPase would suggest three binding sites while here the results suggest the presence of only one high affinity binding site. The recent findings that 2-azido-ADP inhibits the V-ATPase with about three-fold lower affinity than ADPMg and the availability of [^{32}P]-2-azido-ADP will allow investigation of the actual location of the regulatory, high-affinity binding site.

Chapter 7. Interaction of V-ATPases with fluorescent organotin-flavone complexes.

7.1 Introduction.

Trialkyltins have long been known to be potent inhibitors of mitochondrial ATP synthesis (Stockdale *et al*, 1971; Dawson and Selwyn, 1975). The mechanism of inhibition is two fold: firstly through direct inhibition of the ATP synthase; secondly through uncoupling by exchange of hydroxyl ions for other anions, such as chloride, mediated by trialkyltins (Selwyn *et al*, 1970).

Although regarded as a distinct class of proton pumps, V-type ATPases have extensive biochemical and morphological homology with F-type ATPases (ATP synthases) (Nelson, 1992a) and are inhibited by a number of agents in common, including dicyclohexylcarbodiimide (DCCD) and trialkyltins (Apps *et al*, 1980). DCCD has been shown to react covalently with the 16kDa subunit of the proton pore of the V-ATPases (Sutton and Apps, 1981), and with the F-ATPase homologue, the 8kDa subunit of the proton pore (Linnet and Beechey, 1979). The location of the trialkyltin binding site is thought to reside in the proton conducting segment (F_O) of the F-ATPases (Cain and Griffiths, 1977) although the actual subunit location has not yet been established. The location of the trialkyltin binding site in the V-ATPases has not been studied until now.

Recently, the synthesis of a series of novel pentacoordinate organotin-flavone complexes was described (Usta and Griffiths, 1992). These complexes interact with F-type ATPases, inhibit ATP hydrolysis and in some cases the fluorescence of the tin complex is strongly enhanced on binding to the ATPase. They appear to interact with the transmembrane (F_O) segment of the enzyme, and can be used to titrate this component in mitochondrial membranes and in preparations of F_1F_O- ATPases, or of F_O itself (Usta and Griffiths, 1993; Griffiths *et al*, 1993). The structure of the main trialkyltin derivative used, dibutyltin-3-hydroxyflavone bromide (Bu_2SnHOF)is shown below:

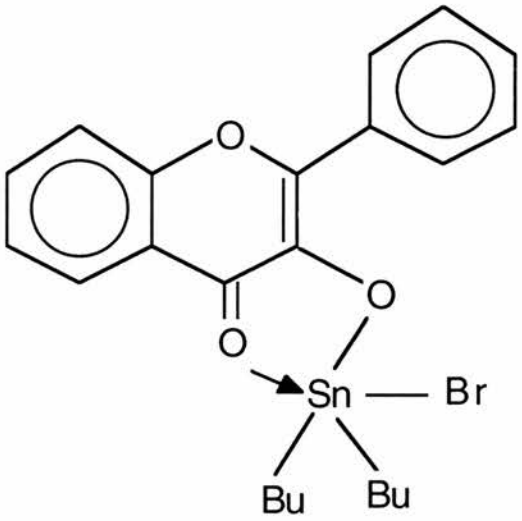

Initial interest in these compounds was as potential reporters of conformational changes in the V-ATPases. In this chapter the properties of these compounds have been exploited in efforts to determine the subunit location of the trialkyltin binding site.

7.2 Special methods.

7.2.1 Organotinflavone synthesis and fluorescent titrations.

Fluorescent alkyltin complexes were synthesised by mixing 10mM ethanolic solutions of the dialkyltin dibromide and the appropriate flavone at 60°C in a water bath. The reaction goes to completion almost simultaneously as measured by the disappearance of the absorbance peak for the flavone and the appearance of that of the complex. Flavones used were 3-hydroxyflavone, galangin (3,5,7-hydroxyflavone), apigenin (4',5,7-hydroxyflavone) and morin (2',3,4',5,7-hydroxyflavone). Alkyl groups tested were dibutyl- and diphenyltin dibromides. All of the flavones tested formed complexes with both dialkyltins with the exception of apigenin which did not form a complex with either of the dialkyltins. The morin complex had a very high intrinsic fluorescence, about 10 times greater than the 3-hydroxyflavone and galangin complexes; the latter two complexes were therefore more useful for titration and fluorescence enhancement studies.

Fluorescence titrations were performed with dibutyltin-3-hydroxyflavone bromide in a Perkin-Elmer 3000 fluorescence spectrophotometer at 30°C with the excitation and emission wavelengths set at 395nm and 450nm respectively. The

ethanol concentration in the cuvette did not exceed 3% for any one titration. Phospholipid vesicle controls were performed using a solution of 2mg/ml total lipid of the same composition as in the reconstituted ATPase preparation and were made in the same way.

7.2.2 Cold-inactivation of chromaffin granule membranes and reconstitution of proton translocation activity.

Chromaffin granule membranes (16mg) at a protein concentration of 2mg/ml were cold inactivated by incubation on ice for 2 hours in 50mM HEPES-NaOH, pH7.4, 1M NaBr, 5mM ATP, 5mM $MgSO_4$ and 1mM dithiothreitol (Moriyama and Nelson, 1989a). The solution was then diluted by addition of one volume of distilled water and centrifuged for 15 minutes, 412,000xg_{av} at 4°C. The cold-inactivated membrane pellet was resuspended by homogenisation to 4mg/ml in 10mM HEPES-NaOH, pH7.4 and washed by centrifugation as above. The supernatant was discarded and the washing step repeated before final resuspension after two washes to 4mg/ml in 10mM HEPES-NaOH, pH7.4. This suspension of cold-inactivated chromaffin granule membranes was used to prepare purified, reconstituted ATPase using purification buffers which have no DTT. The supernatant containing the V_1 sector of the V-ATPase was removed and spin-concentrated in Centricon-10 spin concentrators (Amicon) to about 200µl then diluted to 1ml with 10mM HEPES-NaOH, pH7.4, 1mM EDTA, 1mM DTT. This process of concentration and dilution was repeated twice more and the 1ml of supernatant stored at 4°C.

Reconstituted ATPase made from cold-inactivated membranes was incubated with 100µM N-ethylmaleimide for 30 minutes at room temperature to completely abolish proton-translocation activity. DTT to a final concentration of 1mM was added and 200µl aliquots of vesicles passed through 1ml packed columns of Biogel P6-DG equilibrated in 150mM KCl, 10mM HEPES-NaOH, pH7.4, 1mM DTT to remove any excess NEM. The cold-inactivated supernatant was also passed through these columns in 200µl aliquots to equilibrate in the same buffer. For alkyltin experiments the vesicles and heads were treated by P6-DG as above but with the omission of DTT from the buffers. Treatment of heads and vesicles was with either bafilomycin (1µM) or alkyltin compounds (5µM) for 10 minutes at room temperature. The treated samples were then passed through Biogel P6-DG as above to remove excess inhibitor. Reconstitution was performed by adding equal volumes of heads and vesicles and incubating at room temperature for the times indicated in the figure legends.

7.2.3 Purification of recombinant 39kDa subunit by affinity chromatography.

The 39kDa subunit clone was the generous gift of Nathan Nelson,and was

used to make a construct with an N-terminal decahistidine tag, by Leonora Ciufo in this laboratory. This was expressed in *E. coli* and purified by affinity chromatography using Ni^{2+}-agarose (Qiagen). 2L cultures of *E. coli* containing the cloned subunit plasmid were grown at 25°C to A_{600}=0.7-0.9 and induced by addition of IPTG to 0.3mM before being incubated for a further 2.5-3 hours. The cells were harvested by centrifugation for 10 minutes at 14,000xg_{av} and the pellet resuspended in 16ml 300mM NaCl, 50mM sodium phosphate-NaOH, pH8.0 (buffer w). The cells were sonicated at 0°C five times for 20 seconds at 1 minute intervals and then centrifuged for 5 minutes at 3,000g_{av}, 4°C. The supernatant, S_2 was kept and the pellet was resuspended in 16ml buffer w (150µl was kept for gel samples). The pellet was split into two, 1ml 50% suspension of NTA-agarose (Qiagen) added to each portion in glass conical tubes and rolled for 2 hours at 4°C. The tubes were centrifuged at top speed in an MSE bench centrifuge for 30-60 seconds and the supernatant removed (W_1). The resin was washed with 10ml aliquots of buffer w until the absorbance at 280nm was about 0.01 (solutions W_2-W_n). The resin was then washed with 10ml aliquots of buffer x (300mM NaCl, 50mM Na phosphate, pH6.0, 10% w/v glycerol) again to reach absorbance 0.01 (X_1-X_n) and then 10ml aliquots of buffer y (buffer x with 50mM imidazole) (Y_1-Y_n). Finally the recombinant subunit was eluted with three 6ml washes of buffer x with 250mM imidazole (buffer z) to give 18ml of recombinant subunit (Z_1-Z_3). Solid ammonium sulphate was added to this solution to 70% saturation with slow stirring at 0°C and the solution centrifuged for 20 minutes at 125,000xgav at 4°C and the pellet resuspended by homogenisation in 2ml 10mM HEPES-NaOH, pH7.4 before 200µl aliquots were passed through 1ml packed Biogel P6-DG columns equilibrated in the same HEPES buffer. The effluent from these columns was pooled and the protein concentration was measured by the Bradford assay.

The recombinant subunit was reconstituted into phospholipid vesicles by adding 1/4 volume of the 2mg/ml desalted solution to 2% octyl glucoside in 150mM KCl, 10mM HEPES-NaOH, pH7.4 containing lipid at 2mg/ml with the composition used in the reconstitution of ATPase. The sample was reconstituted in the same way as the ATPase. For estimation of incorporation of the recombinant subunit a 100µl sample of proteoliposomes was centrifuged for 10 minutes, 412,000xgav at 4°C. The supernatant and pellet were analysed separately.

7.3 Results.

7.3.1 Interaction of V-ATPases and organotinflavones.

When dibutyltin-3-hydroxyflavone bromide is titrated with aliquots of membranes of varying origins enhancement of fluorescence is observed with plots of fluorescence versus membrane protein being linear after correction for light scattering (Figure 7.1). The inhibitor concentration greatly exceeds the protein concentration so a linear response would be expected. Erythrocyte membranes were used as a control for incorporation of the tin complex into phospholipid bilayers and it can be seen that the specific enhancement is very low compared to the values for V-ATPase-containing membranes such as tonoplast and chromaffin granule membranes (Table 7.1). The specific enhancements calculated for the various membranes tested appears to correlate with the estimated V-ATPase content of these membranes (Table 7.1) suggesting that interaction is due to the V-ATPase component. The specific enhancement of the purified, reconstituted ATPase is over 6 times greater than that for chromaffin granule membranes (Figure 7.2) consistent with the expected degree of purification using this procedure (Pérez-Castiñeira and Apps, 1990).

Titration of 2μg of V-ATPase-containing proteoliposomes shows that the fluorescence of the dibutyltin-3-hydroxyflavone is enhanced 10 fold compared to the interaction with a phospholipid vesicle control containing no ATPase (Figure 7.3a). The enzyme appears to be half-saturated at 0.7μM dibutyltin-3-hydroxy flavone bromide. Neither DCCD nor bafilomycin at concentrations well in excess of those required to completely inhibit proton translocation and ATP hydrolysis had much effect on the fluorescence enhancement curve although the slight decrease in the maximum fluorescence reached in the presence of DCCD was reproducible. Nucleotides (ATPMg and ADPMg) added either before or after interaction with 5μM dibutyltin-3-hydroxyflavone bromide also had no effect on the fluorescence of the organotinflavone-V-ATPase complex. 10μM tributyltin chloride was the only V-ATPase inhibitor to exhibit a significant effect on the enhancement profile suggesting that there is competition by tributyltin chloride at the organotinflavone site. This is confirmed by the ability of tributyltin chloride to reduce the fluorescence of the organotin-ATPase complex after saturation (Figure 7.3b) although complete abolition of the fluorescence increase was not acheived even at high concentrations of trialkyltin which suggests a more complex interaction than simple competition.

In order to determine dissociation constants for the interaction of trialkyltins and dibutyltin-3-hydroxyflavone bromide, titrations of reconstituted V-ATPase were performed in the presence or absence of various concentrations

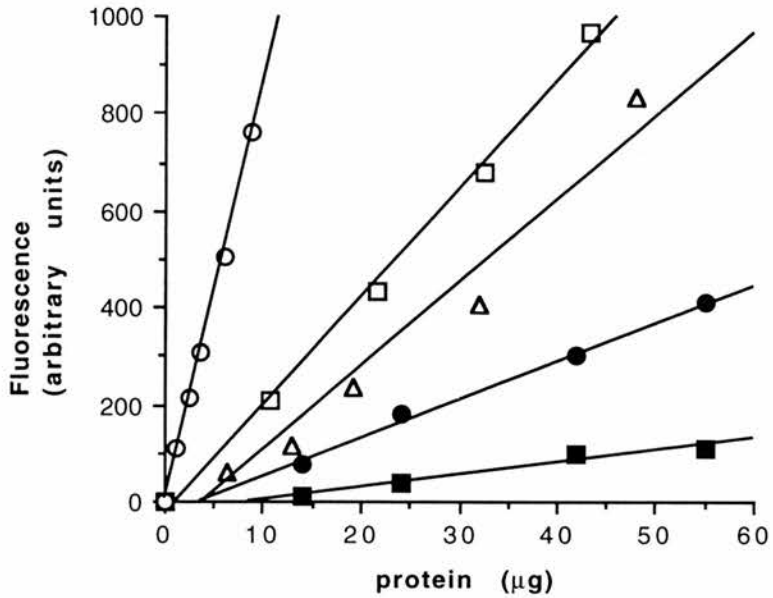

Figure 7.1 Titration of dibutyltin-3-hydroxyflavone bromide with purified membranes: *Kalanchoë daigremontiana* tonoplast, (○); bovine chromaffin granule membranes, (□); bovine kidney microsomes, (△); rat liver microsomes, (●); and bovine erythrocyte membranes, (■). Purified membranes were titrated into a solution of 10μM dibutyltin-3-hydroxyflavone bromide in 10mM HEPES-NaOH, pH 7.4 at 30°C. The lines are drawn by linear regression of the data to give slopes for specific enhancement indicated in table 7.1. The data have been corrected for light scattering. Protein content was determined using Peterson's adaptation of the Lowry assay (chapter 2).

Membrane source	**Specific enhancement (ΔF/μg)**
Kalanchoë daigremontiana tonoplast	86
bovine chromaffin granule membranes	22
bovine kidney microsomes	17
rat liver insulinoma granule membranes	10
rat liver microsomes	8
bovine pituitary dense-core granules	5.5
bovine erythrocyte membranes	2.6

Table 7.1 Specific enhancement data for titration of 10μM dibutyltin-3-hydroxyflavone bromide as above with membranes of different origin.

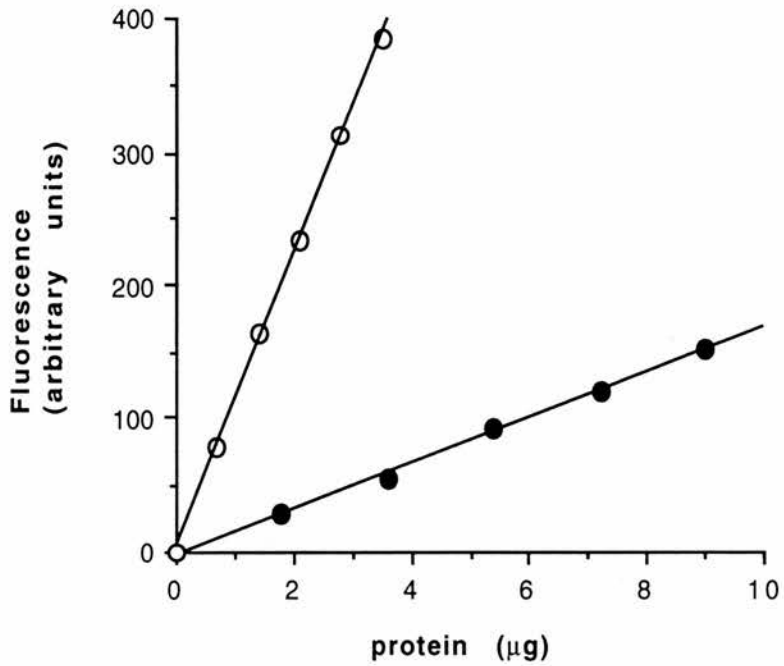

Figure 7.2 Titration of dibutyltin-3-hydroxyflavone bromide with chromaffin granule membranes (closed symbols) and purified, reconstituted ATPase (open symbols) as in Figure 7.1. The lines are drawn from linear regression of the data to give slopes for specific enhancement of 17 and 110ΔF/μg for chromaffin granule membranes and purified ATPase respectively. The data have been corrected for light scattering.

a

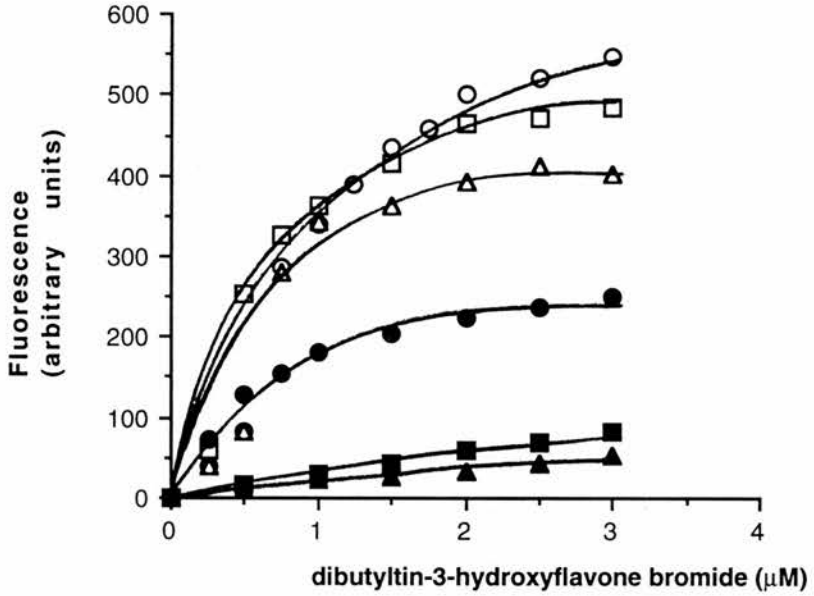

b

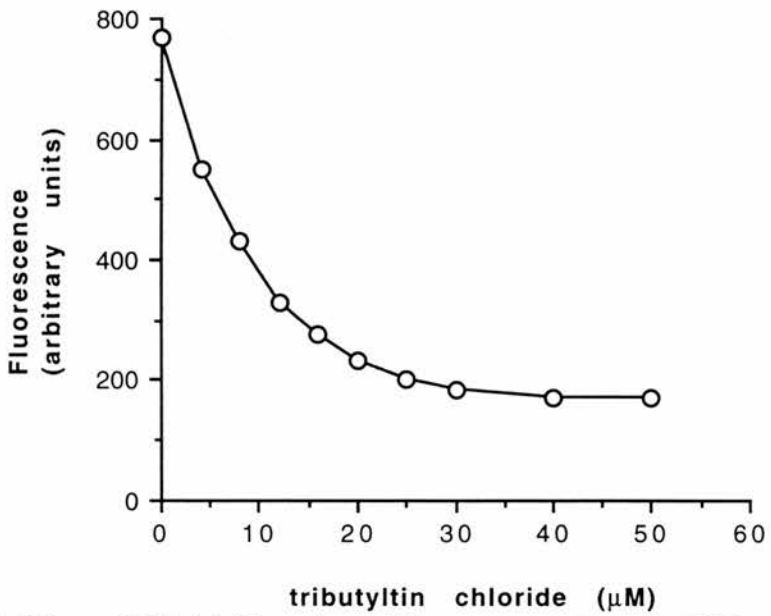

Figure 7.3(a and b) (a) Titration of 2μg reconstituted ATPase in 10mM HEPES-NaOH, pH 7.4, 0.3M Sucrose with dibutyltin-3-hydroxyflavone bromide: untreated ATPase control, (○); 1μM bafilomycin, (□); 50μM DCCD, (△); 10μM tributyltin chloride, (●); phospholipid control, (■); vesicle media control, (▲). For DCCD, preincubation at 4°C overnight was performed, for other inhibitors incubation was in the cuvette at 30°c for 2-3minutes. (b) Competition of tributyltin chloride with Bu_2Sn3OH. The fluorescence with 2μg ATPase and 5μM Bu_2SnHOF in buffered sucrose at 30°C was allowed to reach a maximum before tributyltin chloride was titrated into the cuvette.

of tributyltin chloride (Figure 7.4a). The enhancement curve corresponds to a Michaelian rectangular hyperbola:

$$f=F_{max}/[1+(K_D/[S])(1+[i]/K_i)]$$

Multiplying by S and rearranging gives:

$$[S]/f=K_D/F_{max}(1+[i]/K_i)+S/F_{max}$$

Where f is the observed fluorescence, F_{max} is the maximal fluorescence, [S] is the concentration of fluorescent tin and [i] is the concentration of tributyltin chloride, K_D is the dissociation constant for the fluorescent tin and K_i the dissociation constant for the tributyltin competing at that site. A plot of [S]/f versus [S] at different concentrations of tributyltin should be linear and allow calculation of the dissociation constants (Figure 7.4b). The dissociation constant for dibutyltin-3-hydroxyflavone bromide from the site exhibiting fluorescence enhancement is 0.3μM; however for tributyltin chloride the calculated dissociation constant is somewhat dependent on the concentration used (Figure 7.4b) which may also indicate complex binding.

Inhibition of ATP hydrolysis was studied using the coupled assay described in chapter 2. 3-hydroxyflavone-, galangin and morin complexes of dibutyltin showed similar inhibition kinetics (Figure 7.5a). The individual flavones did not show any inhibition at concentrations up to 10μM suggesting that it is the alkyltin part of the molecule which is interacting with the ATPase. Interestingly complexes of these flavones with diphenyltin also showed very little inhibition at concentrations up to 10μM suggesting that the butyltin compounds are more potent inhibitors. The data are plotted according to Dixon: with non-competitive inhibition:

$$1/v = (1/V_{max})(1+K_m/[S])+(1/V_{max})(1+K_m/[S])([i]/K_i)$$

so a plot of 1/v versus the inhibitor concentration, [i] gives a straight line with y-axis intercept, c:

$$c=(1/V_{max})(1+K_m/[S])$$

and slope, m:

$$m=(1/V_{max})(1+K_m/[S])(1/K_i)$$

hence the dissociation constant for the inhibitor, K_i is c/m. The data plotted as Dixon plots (Figure 7.5b) give dissociation constants which are very similar in all three flavone complexes tested suggesting that the inhibition is due to the alkyltin part of the flavone complex. Tributyltin chloride however was found to be a more potent inhibitor (Figure 7.6a) with a calculated K_i of 13nM (Figure 7.6b) suggesting that possibly the flavone moiety in the dibutyltin complexes causes some steric hindrance when interacting with the trialkyltin binding site. The fact that in fluorescence back titrations a much higher concentration of tributyltin is

a

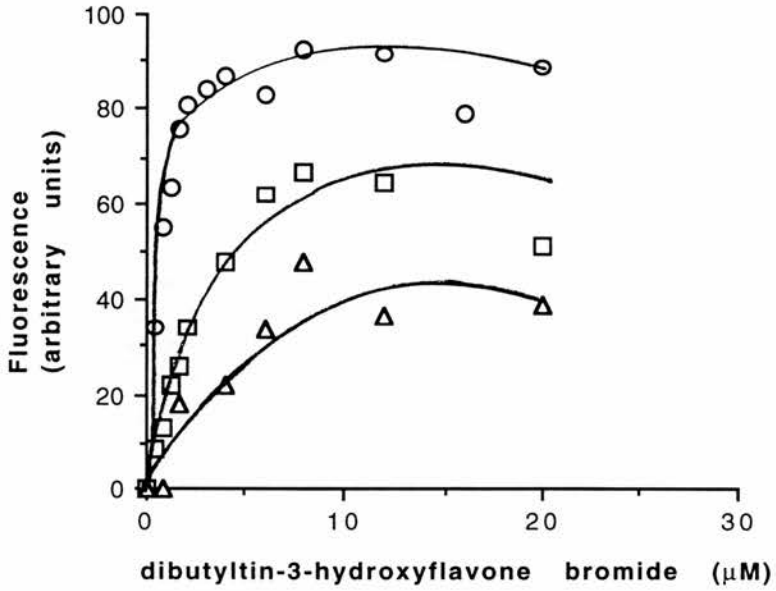

b

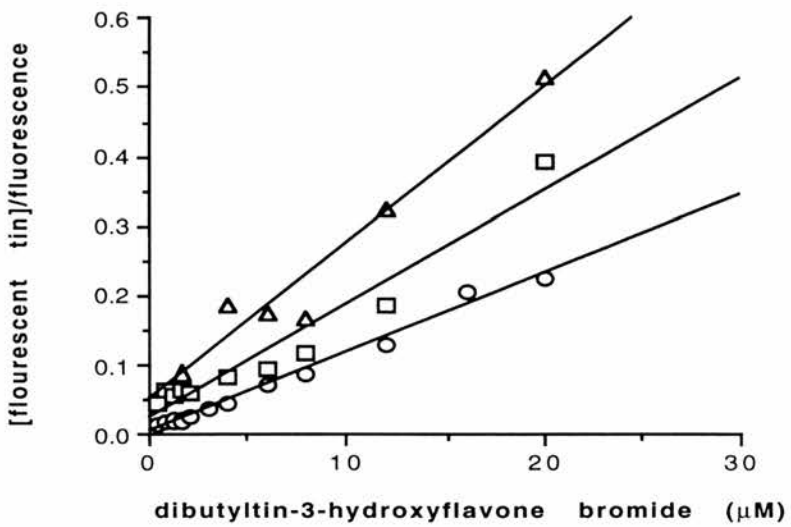

Figure 7.4(a and b) (a) Titration of 2μg reconstituted ATPase in 10mM HEPES-NaOH, pH 7.4, 0.3M Sucrose with dibutyltin-3-hydroxyflavone bromide: untreated ATPase control, (○); 2μM Tributyltin chloride, (□); 5μM Tributyltin chloride, (△) at 30°C. The ATPase was incubated with the tributyltin chloride or ethanol in the control for 2-3minutes before the titration was started. Enhancement in the presence of the same volume of phospholipid vesicles at 2mg/ml was subtracted as background. (b) Transformation of the data of Figure 7.5 with linear regression to give K_i=0.3μM for Bu_2Sn3OH and K_i=0.5μM and 0.9μM for tributyltin chloride with the competition data for 2μM and 5μM respectively.

a

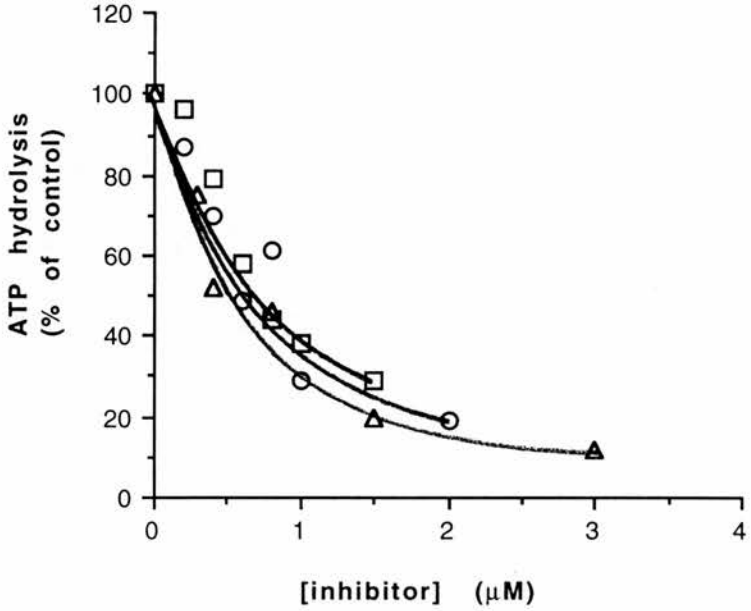

b

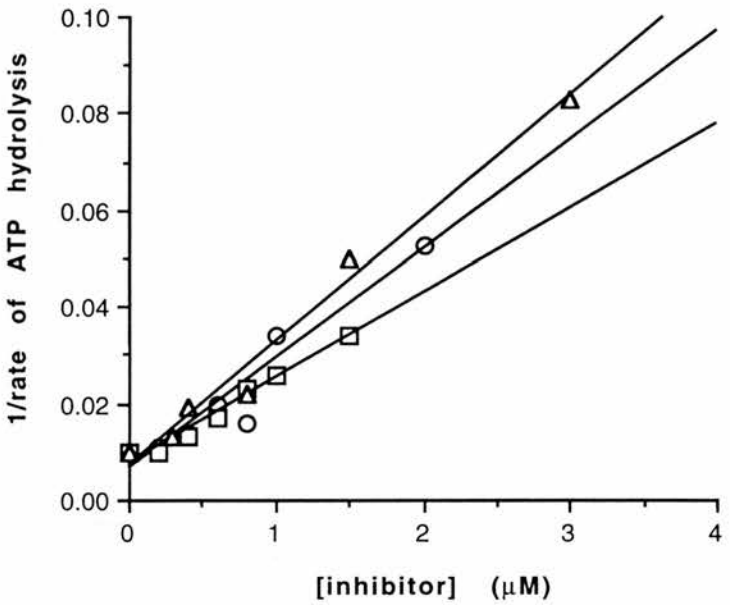

Figure 7.5(a and b) (a) Inhibition of ATP hydrolysis by dibutyltin-flavone bromide complexes: 3-hydroxyflavone complex, (○); Galangin complex, (□); Morin complex, (△). ATP hydrolysis was measured by the coupled ATPase assay described in chapter 2 at 37°C. The control rate is 1260±185nmol/min/mg. (b) Dixon plot transformations of the data in figure7.6a with lines drawn by linear regression to give non-competitive K_i values of 0.3μM, 0.4μM, and 0.3μM for 3-hydroxyflavone, galangin and morin complexes respectively.

a

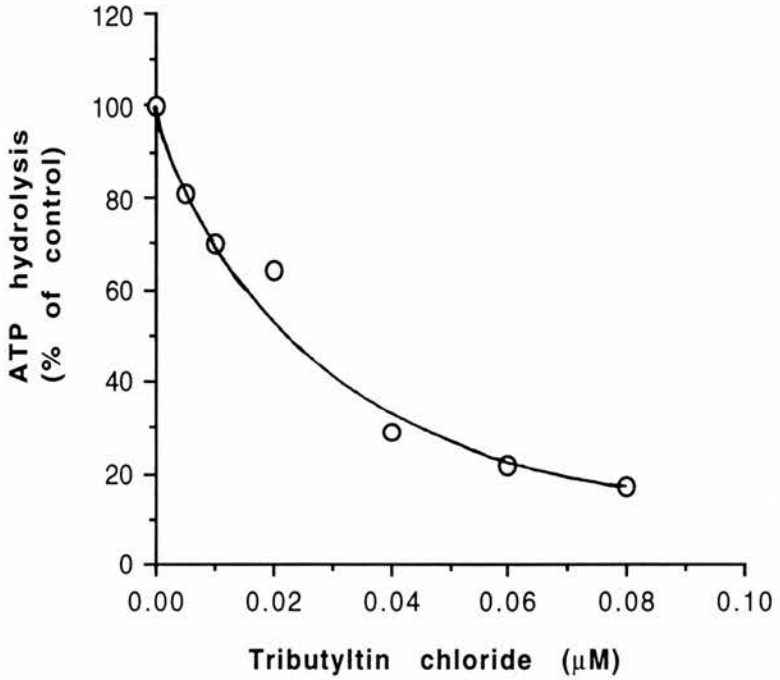

b

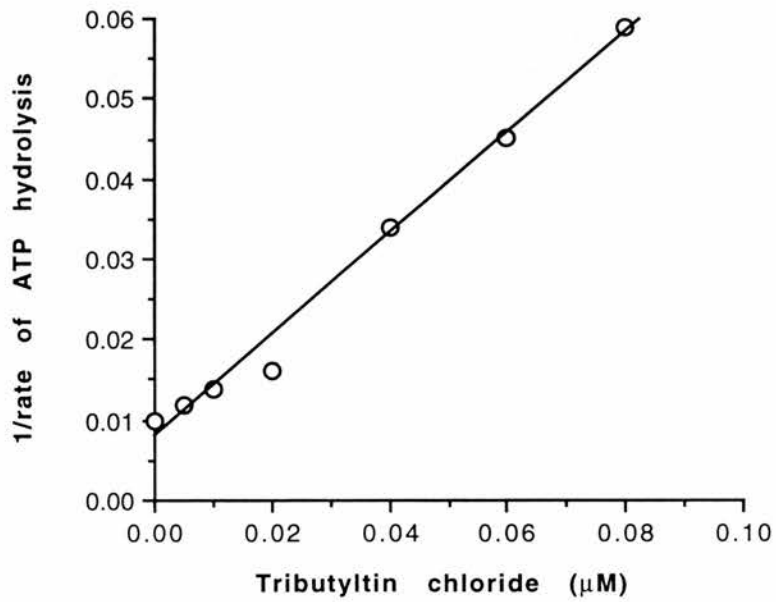

Figure 7.6(a and b) (a) Inhibition of ATP hydrolysis by tributyltin chloride. ATP hydrolysis was measured by the coupled ATPase assay described in chapter 2 at 37°C. The control rate is 1260±185nmol/min/mg. (b) Dixon plot transformation of the data in Figure 7.7a. The line is drawn by linear regression to give a non-competitive K_i value of 13nM.

needed to remove the flavone complex (Figure 7.3b) may suggest that the flavone is preventing the tributyltin from binding by making it sterically difficult for the tributyltin to gain access to the site.

7.3.2 Location of the trialkyltin binding site.

Initial attempts to assign a subunit as the site of trialkyltin binding involved distinguishing whether binding occurred on the membrane sector, V_O or the catalytic sector, V_1 (the heads of the ATPase). A method was developed whereby the ATPase was split by cold-inactivation into vesicular material containing V_O and soluble V_1 heads and then reconstitution of the two fractions after treatment with inhibitor. It was found that reconstitution of proton translocation was indeed possible using this procedure with maximal activity reached after about 60 minutes at room temperature (Figure 7.7a). Inhibition by bafilomycin, tributyltin chloride and dibutyltin-3-hydroxyflavone bromide was studied using this technique. Bafilomycin when reacted with the membrane sector of the ATPase caused a large reduction in proton translocation on reconstitution with untreated heads whereas when reacted with the heads of the ATPase, activity on reconstitution with untreated V_O was 88% of the control (Figure 7.7b). This strongly suggests that bafilomycin inhibits V-ATPases by interacting with the membrane sector consistent with recent results from other groups (Crider *et al*, 1994; Zhang *et al*, 1994). It was not possible to obtain any results with this protocol for the alkyltin compounds due to chloride-hydroxide exchange mediated by these compounds. Even after two passes through P6-DG to remove any unreacted tin compound, uncoupling of the vesicles was observed suggesting that even trace amounts interfere significantly with the assay. This is in contrast to results which suggest that this exchange phenomenon occurs at relatively high concentrations (Selwyn *et al*, 1970).

Interaction of fluorescent tins with ATPase separated on glycerol gradients was analysed in a second attempt to assign binding to V_1 or V_O but enhancement of fluorescence was consistently seen at the top of the gradient (Figures 7.8a and b) suggesting binding to an ATPase subunit that is dissociable under these conditions. The availability of an antibody to the 39kDa subunit has shown that this subunit dissociates under the gradient conditions (chapter 5) and hence the 39kDa subunit may be the site of trialkyltin binding and inhibition.

Recombinant 39kDa was purified using Ni^{2+}-Histidine affinity chromatography (Figure 7.9). The bacterial cultures were grown at 25°C to reduce the formation of inclusion bodies from which purification of recombinant proteins is more difficult. The P_3 contained the greatest proportion of recombinant 39kDa subunit and was incubated with Ni^{2+}-agarose. After several

a

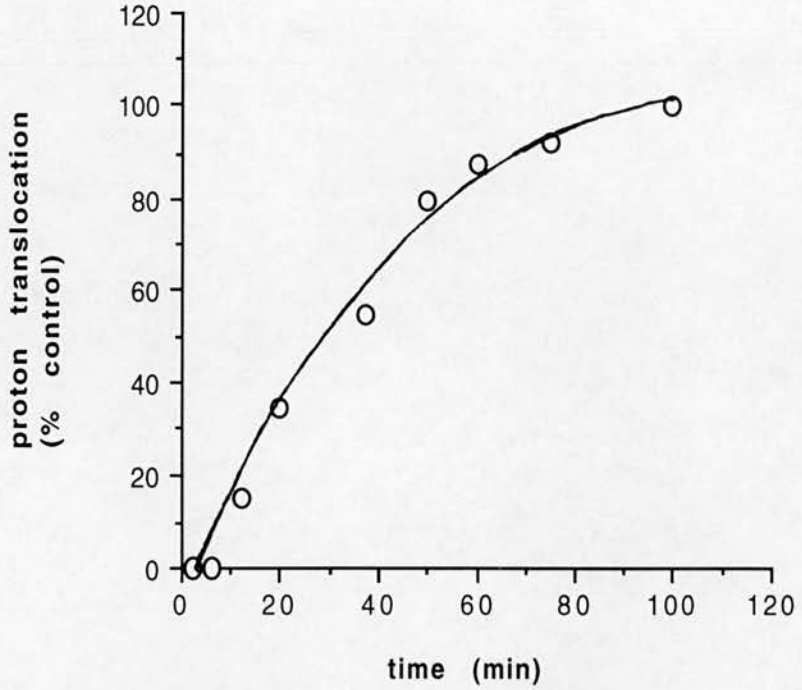

b

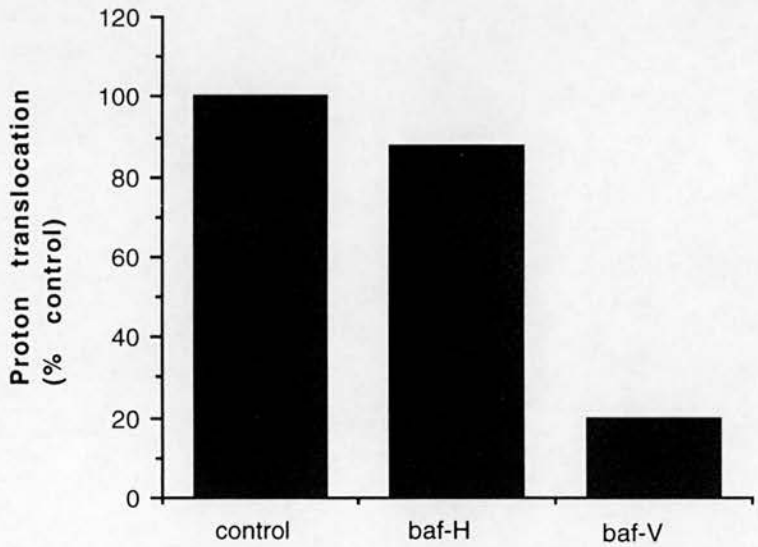

Figure 7.7(a and b) Reconstitution of ATPase "heads' with V_O. (a) timecourse of reconstitution. Equal volumes of "heads" and membrane sectors were incubated at room temperature and 20µl samples were assayed for proton translocation at the indicated times with 1mM ATPMg as substrate. 100% represents 20chart units/min with the rates being estimated manually. (b) Reconstitution of bafilomycin treated (1µM for 10 minutes at room temperature) heads (baf-H) or vesicles (baf-V) with untreated membrane sector or untreated heads respectively. The reconstitution samples were assayed after incubation for 60 minutes at room temperature.

a

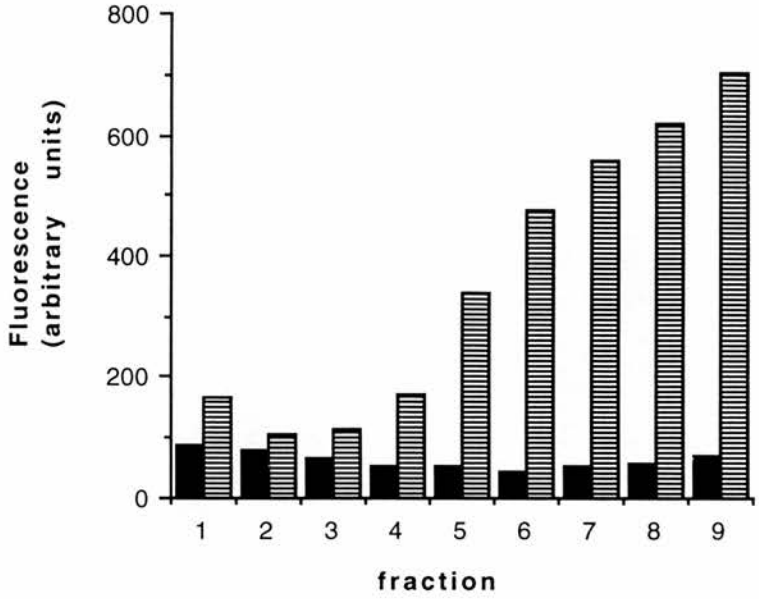

b

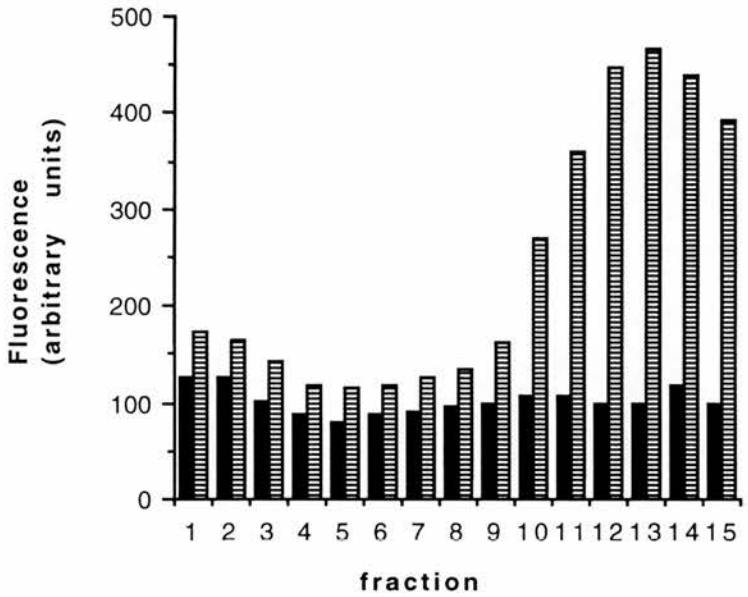

Figure 7.8(a and b) Fluorescent enhancement profile for a 5ml (a) and a 12ml (b) 5-20% glycerol gradient separation of P1 (stripped bars). The gradient separation was performed as described in chapter 2 with 0.9% octyl glucoside in the gradient solutions. Octyl glucoside purification buffer without P1 was loaded onto the control gradient (black bars). 100µl of each fraction was added to 400µl 10mM HEPES-NaOH, pH 7.4 before Bu_2SnHOF was added to 5µM final. The fraction size was about 0.5ml (a) and 0.8ml (b) with fraction 1 is the bottom of the gradient.

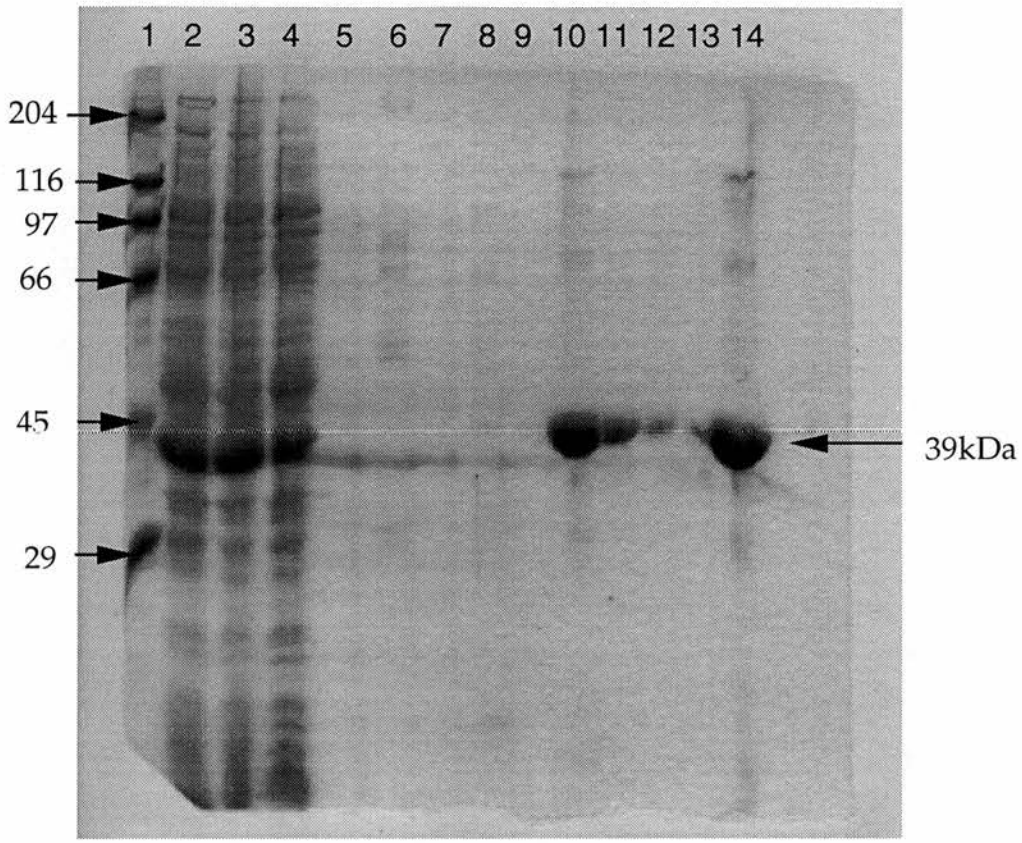

Figure 7.9 purification of recombinant 39kDa subunit. Lanes 1-14: 1, standards; 2, 10µl S3; 3, 5µl P3; 4, W1; 5, W10; 6, X1; 7, X10; 8, Y1; 9, Y10; 10-12, Z1-Z3; 14, 10µl purified, desalted 39kDa subunit. Lanes 3-12 all have 15µl loaded. Molecular weights of the standards are indicated.

washes the bound subunit was removed by competition with 250mM imidazole (Figure 7.9, lane 10). Although there is still some contamination with other proteins the recombinant 39kDa subunit is by far the major component. After desalting the 39kDa subunit was tested for interaction with phospholipids. Reconstitution of the subunit was attempted and equal amounts of 39kDa subunit were seen in equivalent loadings of the soluble and vesicular components of the reconstituted preparation (Figure 7.10a, lanes c and d). Since the vesicular material was effectively diluted on resuspension but equivalent volumes were loaded onto the gel this suggests that the 39kDa subunit does partition preferentially into the lipid bilayer. The subunit in three different environments was analysed for interaction with dibutyltin-3-hydroxyflavone bromide (Figure 7.10b). In the soluble form enhancement is approximately two fold less than when the subunit is present in phospholipid vesicles or phospholipid-detergent micelles but in any case the degree of enhancement is low compared to that seen with the reconstituted holoATPase (Figure 7.3a) and it also appears that the affinity for the fluorescent tin complex is lower in the purified subunit than in the holoenzyme.

7.4 Discussion.

5-coordinate organotin-flavone complexes of 3-hydroxyflavone and morin have been shown previously to inhibit F-ATPases and to exhibit fluorescence enhancement on binding to these enzymes (Usta and Griffiths, 1992). The titration of 5-coordinate organotin-flavone complexes of 3-hydroxyflavone with membranes of different origin suggests interaction with the V-ATPase component of these membranes. This is further supported by the increase in specific enhancement with purified V-ATPase compared to that present in the chromaffin granule membrane consistent with the degree of purification of the V-ATPase by Triton X-114 fractionation. Enhancement of fluorescence on binding to the purified V-ATPase is some 10-fold greater than in phospholipid controls and hence these compounds may be useful in quantifying V-ATPases in membrane preparations or during purification but care should be take since the organotin compounds are not specific to V-ATPases. V-ATPase inhibitors, DCCD (Sutton and Apps, 1981) and bafilomycin (Bowman *et al*, 1988a; Hanada *et al*, 1990) have little effect on the binding of the flavone-tin complexes. The only inhibitor found to affect fluorescence enhancement was the corresponding trialkytin compound, tributyltin chloride suggesting a common binding site for the fluorescent tins and their trialkyltin counterparts. DCCD has been shown to bind to the 16kDa subunit of the membrane sector of the chromaffin granule

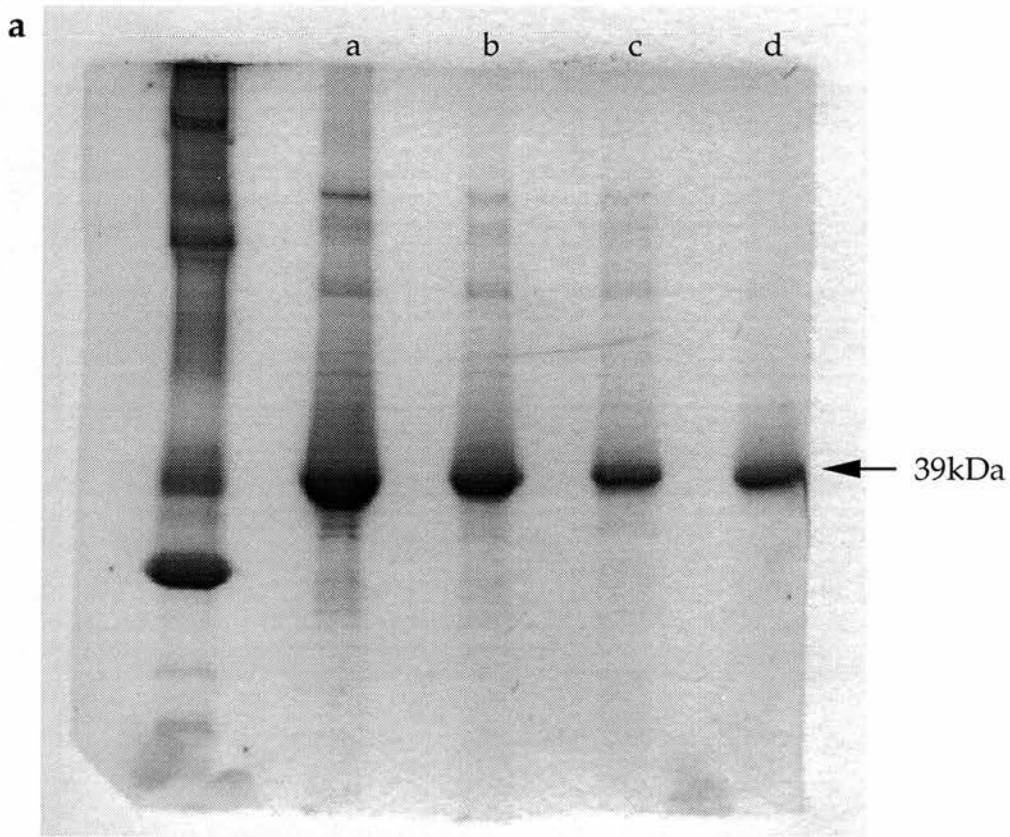

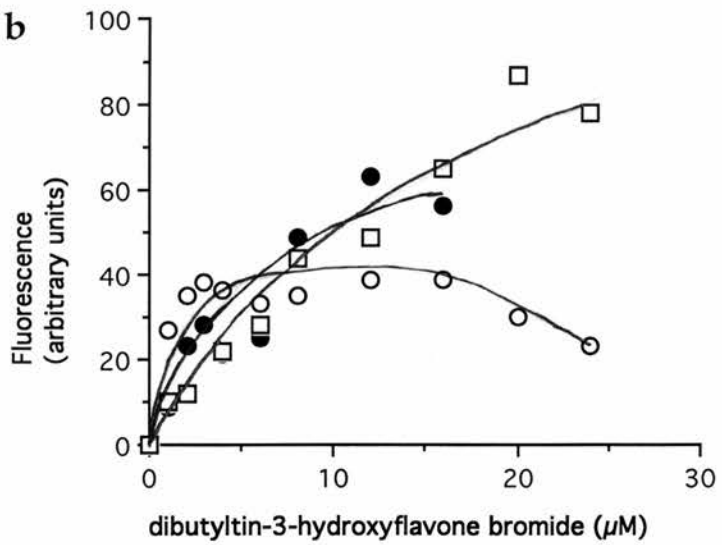

Figure 7.10 (a and b) (a) SDS-PAGE of reconstituted, recombinant 39kDa subunit: lane a, 2μg purified, desalted subunit; b, 1μg reconstituted subunit; c and d, 20μl vesicular and soluble fractions of reconstituted subunit preparation after pelleting the vesicular material and resuspending in the same volume of 10mM HEPES-NaOH, pH7.4. (b) titration of 5μg purified,desalted subunit (□), 2.5μg reconstituted subunit (○) and 2.5μg reconstituted subunit with 0.05%v/v $C_{12}E_9$ (●). All data have been corrected for background.

(Sutton and Apps, 1981) and the coated vesicle V-ATPase (Arai *et al*, 1987a). Recent evidence suggests that bafilomycin also interacts with the membrane sector (Crider *et al*, 1994; Zhang *et al*, 1994) probably by binding to the 100kDa subunit (Zhang *et al*, 1994) consistent with the reconstitution results presented here. The lack of any effect on flavone-tin binding with these inhibitors suggests that the binding of trialkyltin compounds is on the catalytic sector or at a site distal to the sites of interaction of bafilomycin and DCCD on the membrane sector. The putative site of interaction of organotin flavone complexes on the F-ATPases is the membrane sector F_O, although the site of interaction is likely to be distal to the site of oligomycin binding since incubation with oligomycin does not effect enhancement (Usta and Griffiths, 1993).

The calculation of dissociation constants for the fluorescent tins in enhancement assays and in ATP hydrolysis experiments are in the submicromolar range consistent with results for interaction with the F-ATPases (Usta and Griffiths, 1993). The dissociation constants calculated by inhibition of ATP hydrolysis for different flavone-tin complexes tested were very similar regardless of which flavone was attached suggesting that the alkyltin part of the molecule is important for interaction with the ATPase. However, the relationship between fluorescence enhancement and tributyltin competition suggests a dissociation constant for tributyltin which is much greater than that calculated from inhibition of ATP hydrolysis. This suggests that simple competition with tributyltin does not apply.

The profiles of the interaction of dibutyltin-3-hydroxyflavone bromide with V-ATPase purified on glycerol gradients suggest that binding of this compound is to a dissociable subunit later identified as the 39kDa subunit. This subunit is part of the membrane sector of the yeast V-ATPase but can be removed using chaotropic reagents which leave the other integral membrane proteins unaffected (Bauerle *et al*, 1993). Binding of the 39kDa subunit to the membrane sector also requires the presence of an already part-assembled V_O sector containing the 115kDa and 16kDa subunits. The cDNAs for the chromaffin granule and yeast V-ATPase 39kDa subunit have been cloned and sequenced (Wang *et al*, 1988; Bauerle *et al*, 1993) and the predicted polypeptide is hydrophilic overall with hydropathy analysis suggesting that there are no putative transmembrane helices present although in the chromaffin granule sequence there is a stretch of 25 amino acids which could function as a membrane anchor or a binding site for another protein (Wang *et al*, 1988). Recently the 39kDa subunit was also identified as being the synaptophysin-binding protein, physophilin (Siebert *et al*, 1994) once thought to be involved in the docking of

vesicles before formation of the fusion pore. Taken together these results suggest that this subunit binds to the membrane sector through protein-protein interaction and hence its removal by low concentrations of detergent present in the glycerol gradients seems feasible.

Purification of recombinant 39kDa subunit allowed the study of interaction of dibutyltin-3-hydroxyflavone bromide with the individual subunit. Enhancement of fluorescence with the individual subunit was much less than expected from the results of interaction of the holoenzyme and glycerol gradient enhancement profiles. The 39kDa subunit associates with phospholipid vesicles on reconstitution, possibly via the putative membrane anchor mentioned above. The interaction between dibutyltin-3-hydroxyflavone bromide and membrane- or detergent-lipid micelle-associated 39kDa subunit was greater than that in soluble form so enhancement may require the presence of a more hydrophobic environment. The high degree of enhancement with the individual subunit at the top of detergent-containing glycerol gradients may be as a result of the presence of lipid in the P1 fraction which is likely to "float" on the top of the gradient. It is possible therefore that there is interaction between dibutyltin-3-hydroxyflavone bromide and the recombinant subunit but that optimal conditions for fluorescence enhancement were not found. Preliminary studies using [^{125}I]-iodinated flavone-tin complexes have indicated that binding to the 39kDa subunit occurs in the holoenzyme but that interaction with the 72kDa subunit also occurs: the future study of binding to the purified recombinant subunits will be important.

These fluorescent probes although not useful in the initial experiments as conformational change reporters have none the less proved useful tools in probing the trialkytin binding site on V-ATPases and the development of iodination protocols for the synthesis of radiolabelled compounds should allow direct examination of the precise subunit location of the binding site.

Chapter 8. Conclusions and future work.

8.1 Conclusions.

Investigation of the regulation of the vacuolar ATPase from chromaffin granule membranes with particular reference to nucleotide binding sites was the major aim of this project. Three methods were employed to study these features: extensive kinetic analysis of proton translocation (and some less detailed analysis of ATP hydrolysis) and model fitting to the experimental data obtained with various substrates and inhibitors; analysis of the effects of the nucleotides tested in kinetic model fitting on inactivation of the ATPase by the alkylating reagent N-ethylmaleimide; and study of the binding of ADP to the ATPase to determine directly its dissociation constant. A secondary project was to study the interaction of fluorescent alkyltin compounds with the V-ATPase, since these were potential reporters of protein conformational changes.

A method for the rapid purification and reconstitution for the ATPase from chromaffin granules had already been developed, and some features of kinetic regulation had already been proposed. This facilitated an almost immediate start to the work with only a little time taken to optimise the procedure to obtain reconstituted ATPase optimised for proton translocation.

8.1.1 Kinetic analysis and model fitting.

Proton translocation was assayed as the catalytic feature of choice in extensive kinetic studies for two reasons: firstly proton translocation is the physiologically relevant function of the vacuolar ATPase whether it is functioning to create a low pH in organelles such as lysosomes, acting in urinary acidification in kidney epithelial cells or generating an electrochemical gradient for secondary transport systems such as in the chromaffin granule and other secretory organelles; secondly proton translocation can be assayed continuously using permeant fluorescent weak bases such as ACMA and it is established that the initial rate of fluorescence quenching accurately reflects the rate of proton translocation. Continuous ATP hydrolysis assays are coupled to the generation of ADP and therefore cannot be used to study the kinetic regulation of the ATPase by ADP. More accurate and sensitive assays for ATP hydrolysis, for example using [γ^{32}P]-ATP, are discontinuous and hence less suited to accurate initial rate analysis.

The optimisation of the reconstitution procedure for proton translocation prompted the development of substrate-injection and digital data collection systems

which allowed accurate estimates of even very fast initial rates. This data collection system is likely to be applicable to other fast reactions.

All purine nucleoside triphosphates (as their magnesium complexes) were shown to be substrates for the enzyme, with apparent affinity in the order ATP>GTP>ITP although GTP was unable to support such a high maximum rate as the other nucleotides. The adenine nucleotide analogue BzBzATP is also a substrate for the ATPase but causes inhibition at higher concentrations. Interestingly free ATP is a simple competitive inhibitor of the ATPase and hence, although not a substrate, must be able to bind to the catalytic site. The pyrimidine nucleotides, UTP and CTP are poor substrates but are able to stimulate the rate of proton translocation catalysed by ATP. The mechanism of this stimulation is unknown at present. In contrast to the situation in F-type ATP synthases, in the absence of any nucleoside diphosphate the V-ATPase exhibits simple Michaelian kinetics with a single K_m value. This is consistent with several previous reports; some conflicting results indicate the presence of several K_m values but this is likely to be due to heterogeneity in the preparations used.

In the presence of nucleoside diphosphates (ADP, GDP, IDP, ADPβS) the ATPase exhibited cooperative effects. ADPMg caused both K_m and V_{max} effects whereas GDPMg, IDPMg and ADPβS affected mainly the K_m. About 60 experimental points were collected covering a wide range of substrate and inhibitor concentrations and combinations and comprised one data set. This was fitted to various rate equations by an optimisation program. The concerted model of Monod *et al* (1965), which assumes symmetry in the enzyme tested, was used as the basis for the rate equations developed. Sequential models for regulation of the ATPase, which is proposed to have three catalytic sites, would produce rate equations too complex for the available data to bear in optimisation programs. The results of model fitting suggest that the enzyme exists in two conformational states and that in each state the catalytic binding sites are identical, so that symmetry is conserved in the conformational transition. Several variants of the basic rate equation were derived to describe different features of the two conformational states such as their ability to bind nucleotide. It was apparent from the Michaelian kinetics in the absence of inhibitors that the equilibrium for the conformational transition is shifted almost fully toward the active state. With all combinations of substrate and inhibitor tested it was found that both states have three binding sites for substrate which also bind nucleoside diphosphates in a competitive manner. Only the R-state is catalytically active and also has a higher affinity for substrate. The inactive T-state appears to have a single high-affinity binding site for nucleoside diphosphates in the approximate order ADP>>IDP>GDP>ADPβS.

Unfortunately values for the dissociation constants could not be determined unambiguously by kinetic methods alone but the high affinity binding of ADP and resultant cooperative behaviour is physiologically relevant. Although accurate data is not available for the adrenal medulla, ADP concentrations in the adrenal cortex (Williamson and Corkey, 1979) and heart (Opie and Owen, 1976) are around 0.6mM and 1mM respectively. At these concentrations the V-ATPase is likely to exist in an equilibrium with significant amounts of T-state present, with ADP bound at both the regulatory and the catalytic sites, so the availability of ATP will serve to "fine-tune" the activity.

8.1.2 NEM inactivation and the effect of nucleotides.

The kinetics of NEM inactivation and the fact that NEM reacts with an essential cysteine in the catalytic site of V-ATPases allowed analysis of dissociation constants for nucleotide binding to the ATPase by an independent method.

NEM was found to inactivate the ATPase in a pseudo-first order fashion and the rate of inactivation was reduced by the presence of nucleotides in the order ADPMg>>IDPMg≥ADP. Profiles of protection by nucleotides were entirely consistent with the results of kinetic model fitting reported in chapter 4, binding to a high-affinity site (at submicromolar concentrations for ADPMg) and incomplete protection representing a shift of the equilibrium to the more slowly NEM-reacting T-state. This was then followed at higher ADPMg concentrations by complete protection due to direct competition of nucleotide with NEM at the catalytic sites in the T-state. A model was developed which could describe these features of NEM inactivation and protection but it was too complex to allow unambiguous dissociation constant estimation. BzBzATP and ADPβS had differed from the other nucleoside diphosphates tested in their effects on NEM inactivation but this was also consistent with the kinetic model proposed in chapter 4.

Study of alkylation by NEM of the catalytic subunit of the ATPase showed that two cysteine residues were modified, consistent with previous results, but more importantly confirming the major assumptions used in the best fitting kinetic model: each conformational state of the enzyme is symmetrical, with identical substrate binding sites. This again is unlike ATP synthase.

8.1.3 Direct determination of ADP binding constants.

Although initially several problems were encountered in the direct analysis of ADP binding, finally a value likely to represent the binding of ADP to the single regulatory site in the T-state was obtained. The results confirmed that the binding site is of very high affinity with a real dissociation constant in the subnanomolar

range. Estimation of the stoichiometry of holoATPase:membrane sector gave a value of 0.6 for the number of regulatory binding sites although this value does not take into account any holoenzyme present which may be unable to bind ADP and may therefore be an underestimate.

The kinetics of ADP binding were unaccountably slow. On the basis of the experimental evidence this could not be explained by the presence of bound nucleotide in the isolated enzyme. The slow binding may represent the conformation change between the R- and the T-state but this is not seen in the kinetic studies. One possible explanation for this may be that the enzyme can undergo conformational changes much faster in the presence of the substrate, ATPMg.

8.1.4 Interaction with trialkyltins and their fluorescent derivatives.

The 5-coordinate organotin-flavone complexes dibutyltin-3-hydroxyflavone bromide was shown to exhibit fluorescence enhancement on binding to the vacuolar ATPase and to inhibit ATP hydrolysis with dissociation constants in the submicromolar range. The ability of corresponding trialkyltin compounds to reduce the fluorescence enhancement exhibited on binding to flavone complexes suggested a common binding site but the calculated dissociation constants for trialkyltins were different in ATP hydrolysis inhibition or competition in fluorescence enhancement experiments, suggesting a more complex interaction than simple competition. Other known V-ATPase inhibitors had little or no effect on the enhancement profiles.

Gradient separation of the ATPase and dissociation of the 39kDa subunit suggested that this subunit could be the binding site for the fluorescent complexes but a purified, recombinant 39kDa subunit did not exhibit significant fluorescent enhancement either in a soluble form or after reconstitution into liposomes. This may suggest that the binding of the tin compounds may require subunit interaction: initial experiments with radiolabelled fluorescent tin complexes suggest binding to several subunits of the enzyme. However, further experiments are required to determine optimum binding conditions to the recombinant subunit.

8.2 Future work.

Although some features of the regulation of the ATPase in proton translocation have been determined, more extensive ATP hydrolysis studies should be carried out to justify the model with respect to this aspect of the enzyme's behaviour. The subunit location of the single regulatory binding site is still unknown and inhibition of the ATPase by azido-ADP analogues and their availability in radiolabelled form should help answer this question. BzBzATP can also be synthesised in radiolabelled form and since it has also been shown to inhibit

the ATPase it may also be useful in these experiments. So far there is no direct evidence of conformational changes in the V-ATPases and this is an important aspect of the kinetic model. Circular dichroism spectroscopy did not produce any evidence of conformational changes and it may be that techniques such as tryptophan fluorescence, which has been used in the study of F-type ATPases, should be adopted. The presence of a reactive cysteine in the active site of the V-ATPase may be useful in attachment of conformational change reporter groups as was the original idea with the fluorescent tin complexes.

It has become apparent that the purified V-ATPase of chromaffin granules exists mainly as membrane sector with only a relatively small proportion of holoenzyme present. The function of this feature in the chromaffin granule has not been investigated and may be important for up-regulation of secondary transport through recruitment by V_O sectors of cytoplasmic V_1 sectors. It will be interesting to determine whether this is a general feature of V-ATPases in secretory granules or whether it applies to all V-ATPase-containing membranes. The assembly of V-ATPases is increasingly becoming an area of interest and will surely provide insight into this aspect of V-ATPase regulation.

Another line of experiment could be to ask whether the V-ATPases are covalently modified, for example by phosphorylation. The clathrin-coated vesicle ATPase has been shown to be phosphorylated *in vitro* by a subunit of the clathrin assembly protein AP2 called AP50 (Myers and Forgac, 1993) but this is so far the only evidence available and the function of the phosphorylation was not determined. Whether this occurs *in vivo* has yet to be determined. The blue native gel electrophoresis technique used here should be useful in studying covalent modification of the ATPase. The potential to develop this native gel system as a preparative technique may allow comparison of the activities of covalently modified forms of the enzyme. This technique will also be invaluable in studying subunit composition of V-ATPases from different membranes.

In conclusion there are many questions still unanswered regarding regulation of the V-ATPases in the cell. These questions encompass features such as how V-ATPases are targeted to different locations in the same cell and whether these enzymes are distinct in subunit composition and regulation but also more specific questions such as the location of the ADP binding subunit and whether ligand-induced conformation changes occur. It has become clear that the similarities between F- and V-ATPases exist mainly in morphology and in sequence similarity only in specific regions so care should be taken when drawing parallels between these two different classes of ATPase. In the future crystal structures will

presumably become available and may allow molecular analysis of catalysis as has happened with the F-ATPases.

Appendix 1

Derivation of the rate equation describing the basic model of Monod, Wyman and Changeux (1965).

A dimer is used as an example to simplify the algebra involved. The basic equilibria involved are represented diagrammatically:

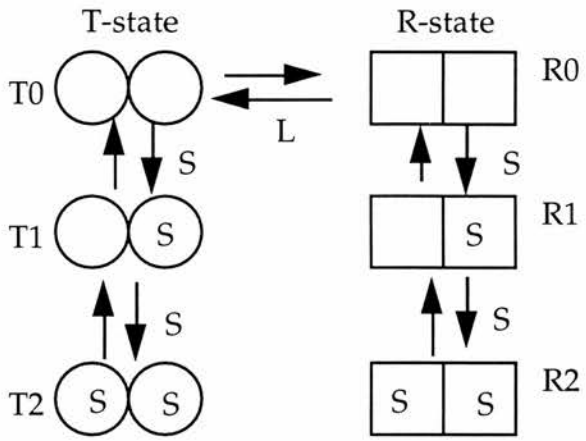

A heterodimer comprising of one of each of the R- and T-state subunits is never present - overall symmetry is conserved.

The subunits in each of the two states are identical and symmetrical so that the two subunits on the R-state will have the same affinity for substrate, S. The first substrate molecule "sees" two identical sites but once bound can only dissociate from one and hence the apparent dissociation constant, K_{r1} is related to the intrinsic dissociation constant, K_R by a factor of 0.5:

$$K_{r1}=1/2(K_R) \qquad \textbf{(equation 1)}$$

and similarly for the T-state:

$$K_{t1}=1/2(K_T) \qquad \textbf{(2)}$$

The second substrate molecule sees only 1 available site but can dissociate from two:

$$K_{r2}=2K_R \qquad \textbf{(3)}$$

$$K_{t2}=2K_T \qquad \textbf{(4)}$$

The equilibrium constant, L for the R to T transition is:

$$L=[T_0]/[R_0] \qquad \textbf{(5)}$$

$$[R_1]=\{[R_0][S]\}/K_{r1} \qquad \textbf{(6)}$$

$$=\{2[R_0][S]\}/K_R \qquad \textbf{(7)}$$

$$[R_2]=\{[R_1][S]\}/K_{r2} \qquad \textbf{(8)}$$

Substituting equation 6 into 8:

$$[R_2]=\{[R_0][S]^2\}/(K_{r1}.K_{r2}) \qquad \textbf{(9)}$$

Substituting equations 1 and 3 into 9:

$$[R_2]=\{[R_0][S]^2\}/K_R^2 \qquad \textbf{(10)}$$

Similarly for the T-state:

$$[T_1]=\{2[T_0][S]\}/K_T \quad \textbf{(11)}$$

and

$$[T_2]=\{[T_0][S]^2\}/K_T^2 \quad \textbf{(12)}$$

We can derive an expression for the degree of saturation at any given substrate concentration by calculating the fractional saturation (Y_S) where Y_S is the concentration of substrate bound to the enzyme divided by the total concentration of binding sites:

$$Ys = \frac{[R_1]+2[R_2]+[T_1]+2[T_2]}{2([R_0]+[R_1]+[R_2]+[T_0]+[T_1]+[T_2])} \quad \textbf{(13)}$$

By substituting equations 7, 10, 11, and12 into 13, we can obtain:

$$Y_S = \frac{([S]/K_R)(1+[S]/K_R) + (L[S]/K_T)(1+[S]/K_T)}{(1+[S]/K_R)^2 + L(1+[S]/K_T)^2} \quad \textbf{(14)}$$

To simplify this expression, we substitute:

$\alpha = [S]/K_R$, $c = K_R/K_T$ and n=number of binding sites

Assuming that the activity is proportional to the fractional saturation:

$$Y_S = v/V_{max} = \frac{\alpha(1+\alpha)^{n-1} + Lc\alpha(1+c\alpha)^{n-1}}{(1+\alpha)^n + L(1+c\alpha)^n} \quad \textbf{(15)}$$

Equation 15 describes a sigmoidal curve of v versus [S], and the degree of sigmoidicity depends on the values of the constants.

In the absence of ADP the V-ATPase obeys Michaelian kinetics suggesting that L tends to zero:

$$v/Vmax = \alpha/(1+\alpha) = [S]/(K_R+[S]$$

but in the presence of ADP sigmoidal behaviour is seen and we can write a real equilibrium constant, L':

$$L' = L(1+[ADP]/K_i)$$

Effectively L' is substituted for L in equation 15.

The four models tested are derived from the basic rate equation, 15 above:

Model 1:

Only R binds substrate. $K_T = \infty$ and $c = 0$:

$$v/Vmax = \frac{\alpha(1+\alpha)^{n-1}}{L' + (1+\alpha)^n}$$

Model 2:

The T-state is inactive therefore we lose the fractional activity for the T-state from equation 15:

$$v/Vmax = \frac{\alpha(1+\alpha)^{n-1}}{(1+\alpha)^n + L'(1+c\alpha)^n}$$

Model 3:

We assume that the rate attributable to each state is attributable to the fraction of enzyme in that state:

$$v_r = \frac{V_R[\alpha(1+\alpha)^{n-1}]}{(1+\alpha)^n + L'(1+c\alpha)^n}$$

and

$$v_t = \frac{V_T[L'c\alpha(1+c\alpha)^{n-1}]}{(1+\alpha)^n + L'(1+c\alpha)^n}$$

Summing these expressions:

$$v_r+v_t = v_o = \frac{V_R[\alpha(1+\alpha)^{n-1}] + VT[L'c\alpha(1+c\alpha)^{n-1}]}{(1+\alpha)^n + L'(1+c\alpha)^n}$$

Model 4.

The T-state is assumed to be inactive so the general equation for model 2 applies with modification for competitive binding at sites in the T and R-states. Hence K_R becomes $K_R(1+[ADP]/Ka)$ and similarly K_T becomes $K_T(1+[ADP]/K_b)$, where K_a and K_b are the dissociation constants of ADP from the catalytic sites in the R- and T -states respectively

Bibliography.

Abrahams, J. P., A. G. W. Leslie, R. Lutter, and J. E. Walker. 1994. Structure at 2.8Å resolution of F_1-ATPase from bovine heart mitochondria. *Nature* 370:621-628.

Adachi, I., H. Arai, R. Pimental, and M. Forgac. 1990a. Proteolysis and orientation on reconstitution of the coated vesicle proton pump. *J. Biol. Chem.* 265:960-966.

Adachi, I., K. Puopolo, N. Marquez-Sterling, H. Arai, and M. Forgac. 1990b. Dissociation, cross-linking and glycosylation of the coated vesicle proton pump. *J. Biol. Chem.* 265:967-973.

Akaike, H. 1974. A new look at the statistical model identification. *IEEE Trans. Auto. Cont.* 19:716-723.

Al-Awqati, Q., J. Barasch, and D. Landry. 1992. Chloride channels of intracellular organelles and their potential role in cystic fibrosis. *J. Exp. Biol.* 172:245-266.

Alexander, N. M. 1958. Spectrophotometric assay for sulphydryl groups using N-Ethylmaleimide. *Anal. Chem.* 30:1292-1294.

Allison, A. C. and M. R. Young. 1969. Vital staining and fluorescence microscopy of lysosomes. In Lysosomes in biology and pathology. J-T. Dingle and H. B. Fell, editors. North-Holland Publishing, Amsterdam. 600-628.

Anderson, R. G. W., J. R. Falck, J. L. Goldstein, and M. S. Brown. 1984. Visualisation of acidic organelles in intact cells by electron microscopy. *Proc. Nat. Acad. Sci. USA* 81:4838-4842.

Anderson, R. G. W. and L. Orci. 1988. A view of acidic intracellular compartments. *J. Cell Biol.* 106:539-543.

Anderson, R. G. W. and R. K. Pathak. 1985. Vesicles and cisternae in the *trans* golgi apparatus of human fibroblasts are acidic compartments. *Cell* 40:635-643.

Apps, D. K., J. M. Percy, and J. R. Pérez-Castiñeira. 1989. Topography of a vacuolar-type H^+-translocating ATPase: chromaffin-granule ATPase I. *Biochem. J.* 263:81-88.

Apps, D. K., J. G. Pryde, and R. Sutton. 1983. Characterization of detergent-solubilized adenosine triphosphatase of chromaffin granule membranes. *Neurosci.* 9:687-700.

Apps, D. K., J. G. Pryde, R. Sutton, and J. H. Phillips. 1980. Inhibition of adenosine triphosphatase, 5-hydroxytryptamine transport and proton-translocation activities of resealed chromaffin granule 'ghosts'. *Biochem. J.* 190:273-282.

Apps, D. K., J. R. Pérez-Castiñeira, M. Warren, and G. L. Atkins. 1992. Reconstitution and kinetics of vacuolar H^+-translocating ATPases from plants and animals. *Biochem. Soc. Trans.* 20:245S.

Apps, D. K. and G. Schatz. 1979. An adenosine triphosphatase isolated from chromaffin granule membranes is closely similar to F_1-adenosine triphosphatase of mitochondria. *Eur. J. Biochem.* 100:411-419.

Arai, H., M. Berne, and M. Forgac. 1987a. Inhibition of the coated vesicle proton pump and labelling of a 17,000 dalton polypeptide by N,N'-dicyclohexylcarbodiimide. *J Biol. Chem.* 262:11006-11011.

Arai, H., M. Berne, G. Terres, H. Terres, K. Puopolo, and M. Forgac. 1987b. Subunit composition and ATP site labeling of the coated vesicle proton-translocating adenosinetriphosphatase. *Biochemistry* 26:6632-6638.

Arai, H., S. Pink, and M. Forgac. 1989. Interaction of anions and ATP with the coated vesicle proton pump. *Biochemistry* 28:3075-3082.

Arai, H., G. Terres, S. Pink, and M. Forgac. 1988. Topography and subunit stoichiometry of the coated vesicle proton pump. *J. Biol. Chem.* 263:8796-8802.

Arai, K., A. Shimaya, N. Hiratani, and S. Ohkuma. 1993. Purification and characterization of lysosomal H^+-ATPase. *J Biol. Chem.* 268:5469-5660.

Bauerle, C., M. N. Ho, M. A. Lindorfer, and T. H. Stevens. 1993. The *Saccharomyces cerevisiae* VMA6 gene encodes the 36-kDa subunit of the vacuolar H^+-ATPase membrane sector. *J. Biol. Chem.* 268:12749-12757.

Benaim, G., A. Clark, and E. Carafoli. 1986. ATPase activity and Ca^{2+} transport by reconstituted tryptic fragments of the Ca^{2+} pump of the erythrocyte plasma membrane. *Cell Calcium* 7:175-186.

Bennet, A. P., S. A. O'Neill, M. Eilman, and R. M. Spanswick. 1985. H^+-ATPase activity from storage tissue of *Beta vulgaris*. *Plant Physiol.* 78:495-499.

Bennett, A. B. and R. M. Spanswick. 1983. Optical measurement of ΔpH and $\Delta\psi$ in corn root membrane vesicles: kinetic analysis of Cl^- effects on a proton-translocating ATPase. *J. Membr. Biol.* 71:95-107.

Berkelman, T., K. A. Houtchens, and F. M. Dupont. 1994. Two cDNA clones encoding isoforms of the B subunit of the vacuolar ATPase from barley roots. *Plant Physiol.* 104:287-288.

Bernasconi, P., T. Rausch, I. Struve, L. Morgan, and L. Taiz. 1990. An mRNA from human brain encodes an isoform of the B subunit of the vacuolar H^+-ATPase. *J Biol. Chem.* 265:17428-17431.

Betz, H. 1990. Homology and analogy in transmembrane channel design: lessons from synaptic membrane proteins. *Biochemistry* 29:3591-3599.

Blasi, J., E. R. Chapman, S. Yamasaki, T. Binz, H. Niemann, and R. Jahn. 1993. Botulinum neurotoxin C1 blocks neurotransmitter release by means of cleaving HPC-1/syntaxin. *EMBO J.* 12:4821-4828.

Boller, T. and A. Wiemken. 1986. Dynamics of vacuolar compartmentation. *Annu. Rev. Plant. Physiol.* 37:137-164.

Bowman, B. J., R. Allen, M. A. Wechser, and E. J. Bowman. 1988c. Isolation of genes encoding the *Neurospora* vacuolar ATPase. Analysis of *vma-2* encoding the 57-kDa polypeptide and comparison to *vma-1. J Biol. Chem.* 263:14002-14007.

Bowman, B. J., W. J. Dschida, and E. J. Bowman. 1992. Vacuolar ATPase of *Neurospora crassa* : electron microscopy, gene characterization and gene inactivation/mutation. *J. Exp. Biol.* 172:57-66.

Bowman, B. J., W. J. Dschida, T. Harris, and E. J. Bowman. 1989. The vacuolar ATPase of *Neurospora crassa* contains and F_1-like structure. *J Biol. Chem.* 264:15606-15612.

Bowman, E. J. 1983. Comparison of the vacuolar membrane ATPases of *Neurospora crassa* with the mitochondrial and plasma membrane ATPases. . *J Biol. Chem.* 258:15238-15244.

Bowman, E. J. and B. J. Bowman. 1982. Identification and properties of an ATPase in vacuolar membranes of *Neurospora crassa. J. Bacteriol.* 151:1326-1337.

Bowman, E. J., S. Mandala, L. Taiz, and B. J. Bowman. 1986. Structural studies of the vacuolar membrane ATPase from *Neurospora crassa* and comparison with the tonoplast membrane ATPase from *Zea mays. Proc. Nat. Acad. Sci. USA* 83:48-52.

Bowman, E. J., A. Siebers, and K. Altendorf. 1988a. Bafilomycins: A class of inhibitors of membrane ATPases from microorganisms, animal cells and plant cells. *Proc. Nat. Acad. Sci. USA* 85:7872-7896.

Bowman, E. J., K. Tenney, and B. J. Bowman. 1988b. Isolation of genes encoding the *Neurospora* vacuolar ATPase. Analysis of *vma-1* encoding the 67-kDa subunit reveals homology to other ATPases. *J Biol. Chem.* 263:13994-14001.

Boyer, P. D. 1993. The binding change mechanism for ATP synthase-some probabilities and possibilities. *Biochim. Biophys. Acta* 1140:215-250.

Bradford, M. M. 1976. A rapid and sensitive method for the quantitation of microgram quantities of protein utilizing the principle of protein-dye binding. *Anal. Biochem.* 72:248-254.

Brose, N., A. G. Petrenko, T. C. Südhof, and R. Jahn. 1992. Synaptotagmin: a calcium sensor on the synaptic vesicle surface. *Science* 256:1021-1025.

Brown, M. S., R. G. W. Anderson, and J. L. Goldstein. 1983. Recycling receptors: the round trip intinerary of migrant membrane proteins. *Cell* 32:663-667.

Burgoyne, R. D. 1991. Control of exoytosis in adrenal chromaffin cells. *Biochim. Biophys. Acta* 1071:174-202.

Cain, K. and D. E. Griffiths. 1977. Studies of energy-linked reactions. Localization of the site of action of trialkyltin in yeast mitochondria. *Biochem. J.* 162:578-580.

Capaldi, R. A. 1994. F_1-ATPase in a spin. *Nature Struct. Biol.* 1:660-663.

Capaldi, R. A., R. Aggeler, P. Turina, and S. Wilkens. 1994. Coupling between catalytic sites and the proton channel in F_1F_O-type ATPases. *Trends Biochem. Sci.* 19:284-289.

Carmichael, S. W. and H. Winkler. 1985. The adrenal chromaffin cell. *Sci. Am.* 253:40-49.

Caroni, P., M. Zurini, A. Clark, and E. Carafoli. 1983. Further characterisation of the purified Ca^{2+}-pumping ATPase of heart sarcolemma. *J Biol. Chem.* 258:7305-7310.

Casadio, R. 1991. Measurements of transmembrane pH differences of low extents in bacterial chromatophores. A study with the fluorescent probe 9-amino-6-chloro-2-methoxyacridine . *Eur. Biophys. J.* 19:189-201.

Casadio, R. and B. A. Melandri. 1985. Calibration of the response of 9-amino acridine fluorescence to transmembrane differences in bacterial chromatophores. *Arch. Biochem. Biophys.* 238:219-228.

Chatterjee, D., M. Chakraborty, M. Leit, L. Neff, S. Jamsa-Kellokumpu, R. Fuchs, M. Bartkiewicz, N. Hernando, and R. Baron. 1992. The osteoclast proton pump differs in its pharmacology and catalytic subunits from other vacuolar H^+-ATPases. *J. Exp. Biol.* 172:193-204.

Cidon, S. and N. Nelson. 1983. A novel ATPase in the chromaffin granule membrane. *J Biol. Chem.* 258:2892-2898.

Cidon, S. and N. Nelson. 1986. Purification of N-ethylmaleimide-sensitive ATPase from chromaffin granule membranes. *J. Biol. Chem.* 261:9222-9227.

Cidon, S. and T. S. Sihra. 1989. Characterisation of a H^+-ATPase in rat brain synaptic vesicles. *J Biol. Chem.* 264:8281-8288.

Cooper, A. A., Y-J. Chen, M. A. Lindorfer, and T. H. Stevens. 1993. Protein splicing of the yeast TFP1 intervening protein sequence: a model for self-excision. *EMBO J.* 12:2575-2583.

Crider, B. P., X-S. Xie, and D. K. Stone. 1994. Bafilomycin inhibits proton flow through the H^+ channel of vacuolar proton pumps. *J Biol. Chem.* 269:17379-17381.

Cross, R. L. and C. M. Nalin. 1982. Adenine nucleotide binding sites on beef heart F_1-ATPase. Evidence for three exchangeable sites that are distinct from three non-catalytic sites. *J Biol. Chem.* 257:2874-2881.

Cutler, T., K. Maggert, B. Yatabe, S. L. Taiz, and L. Taiz. 1992. Molecular analysis of the A-subunit of the yeast vacuolar ATPase: the role of cysteine and the non-homologous region. In Conference abstracts, 9^{th} international workshop on plant membrane biology. 210.

David, P. and R. Baron. 1994. The catalytic cycle of the vacuolar H^+-ATPase. Comparison of proton transport in kidney- and osteoclast-derived vesicles. *J Biol. Chem.* 269:30158-30163.

Dawson, A. P. and M. J. Selwyn. 1975. The action of tributyltin on energy-coupling in coupling-factor deficient submitochondrial particles. *Biochem. J.* 152:333-339.

Dawson, R. M. C., D. C. Elliot, W. H. Elliot, and K. M. Jones. 1986. Spectral data and pka values for purines, pyrimidines, nucleosides, and nucleotides. In Data for biochemical research. . Clarendon Press, Oxford. 103-114.

Diliberto, E. J. Jr, F. S. Menniti, J. Knoth, A. J. Daniels, J. S. Kizer, and O. H. Viveros. 1987. Adrenomedullary chromaffin cells as a model to study the neurobiology of ascorbic acid: from monooxygenation to neuromodulation. *Ann. N. Y. Acad. Sci.* 498:28-54.

Dröse, S., K. U. Bindseil, E. J. Bowman, A. Siebers, A. Zeek, and K. Altendorf. 1993. Inhibitory effect of modified bafilomycins and concanamycins on P-type and V-type Adenosinetriphosphatases. *Biochemistry* 32:3902-3906.

Feng, Y. and M. Forgac. 1992b. Novel mechanism for the regulation of the coated vesicle H^+-ATPase upon modification by sulphydryl reagents. *J Biol. Chem.* 267:19769-19772.

Feng, Y. and M. Forgac. 1992a. Cysteine 254 of the 73-kDa A subunit is responsible for the inhibition of the coated vesicle (H^+)-ATPase upon modification by sulphydryl reagents. *J. Biol. Chem.* 267:5817-5822.

Feng, Y. and M. Forgac. 1994. Inhibition of vacuolar H^+-ATPase by disulphide bond formation between cysteine 254 and cysteine 532 in subunit A. . *J Biol. Chem.* 269:13224-13230.

Finbow, M. E., T. E. J. Buultiens, N. J. Lane, J. Shuttleworth, and J. D. Pitts. 1984. Isolation and characterisation of arthropod gap junctions. *EMBO J.* 3:2271-2278.

Finbow, M. E., S. F. Goodwin, L. Meagher, N. J. Lane, J. Keen, J. B. C. Findlay, and K. Kaiser. 1994. Evidence that the 16kDa proteolipid (subunit c) of the vacuolar H^+-ATPase and ductin from gap junctions are the same polypeptide in *Drosophila* and *Manduca*: molecular cloning of the *vha 16k* gene from *Drosophila*. *J. Cell Sci.* 107:1817-1824.

Flatmark, T., M. Grqnberg, E. Jr. Husebye, and S. V. Berge. 1985. The assignment of the Ca^{2+}-ATPase activity of the chromaffin granule to the proton pump. *FEBS Lett.* 182:25-30.

Flatmark, T., O. Terland, and K. B. Hille. 1971. Electron carriers of the bovine adrenal chromaffin granules. *Biochim. Biophys. Acta* 226:9-19.

Forgac, M. 1989. Structure and function of vacuolar class of ATP-driven proton pumps. *Physiol. Rev.* 69:765-796.

Forgac, M. 1992. Structure and properties of the coated vesicle (H^+)-ATPase. *J. Bioenerg. Biomembr.* 24:341-350.

Forgac, M., L. Cantley, B. Wiedenmann, L. Altstiel, and D. Branton. 1983. Clathrin-coated vesicles contain an ATP-dependent proton pump. *Proc. Nat. Acad. Sci. USA* 80:1300-1303.

Forgac, M. and G. Chin. 1985. Structure of the (Na^+,K^+) and (Ca^{2+})-ATPases. In Topics in molecular and strucural biology: metalloproteins. P. Harrison, editor. Macmillan, New York. 123-148.

Foster, D. L. and R. H. Fillingame. 1982. Stoichiometry of subunits in the H^+-ATPase of *Escherichia coli*. *J Biol. Chem.* 257:2009-2015.

Fregni, V. and R. Casadio. 1993. Kinetic characterization of the ATP-dependent proton pump in bacterial photosynthetic membranes: a study with the probe 9-amino-6-chloro-2-methoxyacridine. *Biochim. Biophys. Acta* 1143:215-222.

Fuchs, R., A. Ellinger, M. Pavelka, I. Mellman, and H. Klapper. 1994. Rat liver endocytic coated vesicles do not exhibit ATP-dependent acidification *in vitro*. *Proc. Nat. Acad. Sci. USA* 91:4811-4815.

Fuchs, R., S. Schmid, and I. Mellman. 1989. A possible role for Na^+,K^+-ATPase in regulating ATP-dependent endosome acidification. *Proc. Nat. Acad. Sci. USA* 86:539-543.

Fuchs, R. P. and I. Mellman. 1989. Acidification and ion permeabilities of highly purified rat liver endosomes. *J. Biol. Chem.* 264:2212-2220.

Garboczi, D. N., P. Shenbagamurthi, W. Kirk, J. Hullihen, and P. L. Pedersen. 1988. Mitochondrial ATP synthase. Interaction of a synthetic 50-amino acid, β-subunit peptide with ATP. *J Biol. Chem.* 263:812-816.

Garewal, H. S. 1973. A procedure for the estimation of microgram quantities of triton X-100. *Anal. Biochem.* 54:319-324.

Gavine, F. S., J. G. Pryde, D. L. Deane, and D. K. Apps. 1984. Glycoproteins of the chromaffin granule membrane: separation by two-dimensional electrophoresis and by lectin binding. *J. Neurochem.* 43:1243-1252.

Gillespie, J., S. Ozanne, B. Tugal, J. Percy, M. Warren, J. Haywood, and D. K. Apps. 1991. The vacuolar H^+-transloacting ATPase of renal tubules contains a 115-kDa glycosylated subunit. *FEBS Lett.* 282:69-72.

Gluck, S. and J. Caldwell. 1987. Immunoaffinity purification and characterization of vacuolar H^+-ATPase from bovine kidney. *J. Biol. Chem.* 262:15780-15789.

Gluck, S., S. Kelly, and Q. Al-Awqati. 1982. The proton translocating ATPase responsible for urinary acidification. *J Biol. Chem.* 257:9230-9233.

Gluck, S. L., R. D. Nelson, B. S. Lee, Z-Q. Wang, X-L. Gou, J-Y. Fu, and K. Zhang. 1992. Biochemistry of the renal V-ATPase. *J. Exp. Biol.* 172:219-229.

Gogol, R. A., R. Aggeler, M. Sagermann, and R. A. Capaldi. 1989. Cryoelectron microscopy of *Escherichia coli* F_1 adenosinetriphosphatase decorated with monoclonal antibodies to individual subunits of the complex. *Biochemistry* 28:4717-4724.

Grqnberg, M. and T. Flatmark. 1987. Study on Mg^{2+}-dependent ATPase in bovine adrenal chromaffin granules. *Eur. J. Biochem.* 164:1-8.

Grqnberg, M. and T. Flatmark. 1988. Inhibition of the H^+-ATPase in bovine adrenal chromaffin granule ghosts by diethylstilbestrol. *FEBS Lett.* 229:40-44.

Graber, P., B. Bottcher, and E. J. Boekema. 1990. *In* Bioelectrochemistry III. G. Millazzo and M. Blank, editors. Plenum Press, New York. 247-276.

Griffith, C. J., P. A. Rea, E. Blumwald, and R. J. Poole. 1986. Mechanism of stimulation and inhibition of tonoplast H^+-ATPase of *Beta vulgaris* by chloride and nitrate. *Plant Physiol.* 81:120-125.

Griffiths, D. E,, J. Usta, and Y. M. Tian. 1993. The F_1F_O-ATPase binding site of dibutyltin-3-hydroxyflavone: interactions with venturicidin, oligomycin and DCCD. *J. App. Organometall. Chem.* 7:401-406.

Griffiths, G. and K. Simons. 1986. The *trans* golgi network: sorting at the exit site of the golgi complex. *Science* 234:438-443.

Grubmeyer, C., R. L. Cross, and H. S. Penefsky. 1982. Mechanism of ATP hydrolysis by beef heart mitochondrial ATPase. Rate constants for elementary steps in catalysis at a single site. *J Biol. Chem.* 257:12092-12100.

Gräf, R., A. Lepier, W. R. Harvey, and H. Wieczorek. 1994. A novel 14kDa V-ATPase subunit in the Tobacco hornworm midgut. *J Biol. Chem.* 269:3767-3774.

Gutfreund, H. 1972. The rates of diffusion controlled reactions. In Enzymes: physical principles. Wiley, London. 159-160.

Hanada, H., M. Hasebe, Y. Moriyama, M. Maeda, and M. Futai. 1991. Molecular cloning of cDNA encoding the 16-kDa subunit of vacuolar H^+-ATPase from mouse cerebellum. *Biochem. Biophys. Res. Comm.* 176:1062-1067.

Hanada, H., Y. Moriyama, M. Maeda, and M. Futai. 1990. Kinetic studies of chromaffin granules. H^+-ATPase and effects of bafilomycinA_1. *Biochem. Biophys. Res. Comm.* 170:873-878.

Harvey, W. R. 1992. Physiology of V-ATPases. *J. Exp. Biol.* 172:1-17.

Hirata, R., Y. Ohsumi, A. Nakano, H. Kawasaki, K. Suzuki, and Y. Anraku. 1990. The molecular structure of a gene *vma-1* encoding the catalytic subunit of the H^+-translocating ATPase from the vacuolar membrane of *Saccharomyces cerevisiae. J Biol. Chem.* 265:6726-6733.

Hirsch, S., A. Strauss, K. Masood, S. Lee, V. Sukhatme, and S. Gluck. 1988. Isolation and sequence of a cDNA clone encoding the 31-kDa subunit of bovine kidney vacuolar H^+-ATPase. *Proc. Nat. Acad. Sci. USA* 85:3004-3008.

Hook, V. Y. M., E. Mezey, L. D. Fricker, R. M. Pruss, R. Z. Siegel, and M. J. Brownstein. 1985. Immunocytochemical characterization of carboxypeptidase B-like peptide hormone-processing enzyme. *Proc. Nat. Acad. Sci. USA* 82:4745-4749.

Hudson, R. L. 1993. Bafilomycin-sensitive acid secretion by mantle epithelium of the freshwater clam, *Unio complantatus. Am. J. Physiol.* 264:R946-R951.

Hymel, L., A. Maurer, C. Berenski, C. X. Jung, and S. Fleischer. 1984. Target size of calcium pump protein from skeletal muscle sarcoplasmic reticulum. *J Biol. Chem.* 259:4890-4895.

Iacangelo, A., H-U. Affolter, L. E. Eiden, E. Herbert, and M. Grimes. 1986. Bovine chromogranin A sequence and distribution of its mRNA in endocrine tissues. *Nature* 323:82-86.

Ihara, K., T. Abe, K-I. Sugimura, and Y. Mukohata. 1992. Halobacterial A-ATP synthase in relation to V-ATPase. *J. Exp. Biol.* 172:475-485.

Ihara, K. and Y. Mukohata. 1991. The ATP synthase of *Halobacterium salinarium* (*halobium*) is an archaebacterial type as revealed from the amino acid sequence of its two major subunits. *Arch. Biochem. Biophys,* 286:111-116.

Inatomi, K. 1986. Characterisation and purification of the membrane-bound ATPase of the archaebacterium *Methanosarcina barkeri. J. Bacteriol.* 167:837-841.

Inatomi, K., S. Eya, M. Maeda, and M. Futai. 1989. Amino acid sequence of the α and β subunits of *Methanosarcina barkeri* ATPasr deduced from cloned genes.

Similarity to subunits of eukaryotic vacuolar and F_1F_O-ATPase. *J Biol. Chem.* 264:10954-10959.

Ingebretsen, O. C., O. Terland, and T. Flatmark. 1980. Subcellular distribution of ascorbate in bovine adrenal medulla. *Biochim. Biophys. Acta* 628:182-189.

Iwamoto, A., Y. Orita-Saita, M. Maeda, and M. Futai. 1994. N-Ethylmaleimide-sensitive mutant (βval-153-cys) *Escherichia coli* F_1-ATPase: cross-linking of the mutant β subunit with the α subunit. *FEBS Lett.* 352:243-246.

Jahn, R. and T. C. Südhof. 1994. Synaptic vesicles and exocytosis. *Annu. Rev. Neurosci.* 17:219-246.

Jennings, I. R., P. A. Rea, R. A. Leigh, and D. Sanders. 1988. Quantitative and rapid estimation of H^+ fluxes in membrane vesicles: software for analysis of fluorescence quenching and relaxation. *Plant Physiol.* 86:1257-1263.

Johnson, R. G., M. F. Beers, and A. Scarpa. 1982. H^+-ATPase of chromaffin granules. Kinetics, regulation and stoichiometry. *J Biol. Chem.* 257:10701-10707.

Johnson, R. G. and A. Scarpa. 1976. Internal pH of isolated chromaffin vesicles. *J Biol. Chem.* 251:2189-2191.

Johnson, R. G. and A. Scarpa. 1984. Chemiosmotic coupling and its applications to the accumulation of biological amines in secretory granules . In Electrogenic transport: fundamental principles and physiological implications. M. P. Blaustein and M. Lieberman, editors. Raven Press, New York. 71-91.

Joshi, S. and J. B. Hughes. 1981. Inhibition of coupling factor B activity by cadmium ion, arsenite-2,3-dimercaptopropanol and phenylarsine oxide, and preferential reactivation by dithiols. *J Biol. Chem.* 256:11112-11116.

Kane, P. M., C. T. Yamashiro, and T. H. Stevens. 1989. Biochemical characterisation of the yeast vacuolar H^+-ATPase. *J Biol. Chem.* 264:19236-19244.

Kent, U. M. and P. J. Fleming. 1990. Cytochrome b_{561} is fatty acylated and oriented in the chromaffin granule membrane with its carboxy terminus cytoplasmically exposed. *J Biol. Chem.* 265:16422-16427.

Kiang, W-L., T. Krusius, J. Finne, R. U. Margolis, and R. K. Margolis. 1982. Glycoproteins and proteoglycans of the chromaffin granule matrix. *J Biol. Chem.* 257:1651-1659.

Kibak, H., L. Taiz, T. Starke, P. Bernasconi, and J. P. Gogarten. 1992. Evolution of structure and function of V-ATPases. *J. Bioenerg. Biomembr.* 24:415-424.

Kim, H. J., S. Nishikawa, Y. Tokutomi, H. Takenaka, M. Hamada, S. A. Kuby, and S. Uesugi. 1990. *In vitro* mutagenesis studies at the argenine residues of adenylate kinase. A revised binding site for AMP in the X-ray-deduced model. *Biochemistry* 29:1107-1111.

Konishi, J., T. Wakagi, T. Oshima, and M. Yoshida. 1987. Purification and properties of the ATPase solubilised from membranes of an acidothermophilic archaebacterium *Sulfolobus acidocaldarius*. *J. Biochem.* 102:1379-1387.

Kornfield, S. and I. Mellman. 1989. The biogenesis of lysosomes. *Annu. Rev. Cell Biol.* 5:483-525.

Laemmli, U. K. 1970. Cleavage of structural proteins during the assembly of the head of bacteriophage T4. *Nature* 227:680-685.

Lai, S., J. C. Watson, J. N. Hansen, and H. Sze. 1991. Molecular cloning and sequencing of the cDNA's encoding the proteolipid subunit of the vacuolar H^+-ATPase from higher plants. *J Biol. Chem.* 266:16078-16084.

Laimins, L. A., D. B. Rhoads, K. Altendorf, and W. Epstein. 1978. Identification of the structural protein of an ATP-driven K^+ transport system in E. *coli. Proc. Nat. Acad. Sci. USA* 75:3216-3219.

Laubinger, W. and P. Dimroth. 1989. The sodium ion translocating adenosinetriphosphatase of *Propiogenium modestum* pumps protons at low sodium ion concentration. *Biochemistry* 28:7194-7198.

Linnet, P. E. and R. E. Beechey. 1979. Inhibitors of the ATP synthetase system. *Met. Enzymol.* 162:578-580.

Maclennan, D. H., C. J. Brandl, B. Korezak, and N. M. Green. 1985. Amino acid sequence of a Ca^{2+}- and Mg^{2+}-dependent ATPase from rabbit muscle sarcoplasmic reticulum, deduced from its complementary DNA sequence. *Nature* 316:696-700.

Malpartida, F. and R. Serrano. 1981. Reconstitution of the (H^+)-ATPase of yeast plasma membranes. *J Biol. Chem.* 256:4175-4177.

Mandala, S. and L. Taiz. 1986. Characterisation of the subunit structure of the maize tonoplast ATPase. *J Biol. Chem.* 261:12850-12855.

Mandel, M., Y. Moriyama, J. D. Hulmes, Y-C. E. Pan, H. Nelson, and N. Nelson. 1988. cDNA sequence encoding the 16-kDa proteolipid of chromaffin granules implies gene duplication in the evolution of H^+-ATPases. *Proc. Nat. Acad. Sci. USA* 85:5521-5524.

Manolson, M. F., B. F. F. Ouellette, M. Filion, and R. J Poole. 1988. cDNA sequence and homologies of the 57kDa nucleotide-binding subunit of the vacuolar ATPase from *Arabidopsis*. *J Biol. Chem.* 263:17987-17994.

Manolson, M. F., J. M. Percy, D. K. Apps, X. -S. Xie, D. K. Stone, M. Harrison, D. J. Clarke, and R. J. Poole. 1989. Evolution of vacuolar H^+-ATPases: immunological relationships of the nucleotide-binding subunits. *Biochem. Cell Biol.* 67:306-310.

Manolson, M. F., P. A. Rea, and R. J. Poole. 1985. Identification of 3-O-(4-benzoyl)benzoyladenosine 5'-triphosphate- and N,N'-dicyclohexylcarbodiimide-binding subunits of a higher plant H^+-translocating tonoplast ATPase. *J. Biol. Chem.* 260:12273-12279.

Matsuura-Endo, C., M. Maeshima, and S. Yoshida. 1990. Subunit composition of vacuolar membrane H(+)-ATPase from mung bean. *Eur. J. Biochem.* 187:745-751.

McEnery, M. W. and P. L. Pedersen. 1986. Diethylstilbestrol. A novel F_O-directed probe of the mitochondrial proton ATPase. *J Biol. Chem.* 261:1745-1752.

Mellman, I. 1992. The importance of being acid: The role of acidification in intracellular membrane traffic. *J. Exp. Biol.* 172:39-45.

Mellman, I., R. Fuchs, and A. Helenius. 1986. Acidification of endocytic and exocytic pathways. *Ann. Rev. Biochem.* 55:663-700.

Merion, M., P. Schlesinger, R. M. Brooks, J. M. Moehring, T. J. Moehring, and W. S. Sly. 1983. Defective acidification of endososmes in chinese hamster ovary cell mutants "cross resistant" to toxins and viruses. *Proc. Nat. Acad. Sci. USA* 80:5315-5319.

Mitchell, P. 1968. Chemiosmotic coupling and energy transduction. Glynn Research Ltd., Bodmin.

Monod, J., J. Wyman, and J-P. Changeux. 1965. On the nature of allosteric transitions: a plausible model. *J. Membr. Biol.* 12:88-118.

Moriyama, Y. and M. Futai. 1990. H^+-ATPase, a primary pump for accumulation of neurotransmitters, is a major constituent of brain synaptic vesicles. *Biochem. Biophys. Res. Comm.* 173:443-448.

Moriyama, Y. and N. Nelson. 1987a. The purified ATPase from chromaffin granule membranes is an anion-dependent proton pump. *J. Biol. Chem.* 262:9175-9180.

Moriyama, Y. and N. Nelson. 1987b. Nucleotide binding sites and chemical modification of the chromaffin granule proton ATPase. *J. Biol. Chem.* 262:14723-14729.

Moriyama, Y. and N. Nelson. 1988a. Purification and properties of a vanadate- and N-Ethylmaleimide-sensitive ATPase from chromaffin granule membranes. *J Biol. Chem.* 263:8521-8527.

Moriyama, Y. and N. Nelson. 1988b. Inhibition of vacuolar H^+-ATPase by fusidic acid and suramin. *FEBS Lett.* 234:383-386.

Moriyama, Y. and N. Nelson. 1989b. Lysosomal H^+-translocating ATPase has a similar subunit structure to chromaffin granule H^+-ATPase complex. *Biochim. Biophys. Acta* 980:241-247.

Moriyama, Y. and N. Nelson. 1989a. Cold inactivation of vacuolar proton-ATPases. *J Biol. Chem.* 264:3577-3582.

Moriyama, Y. and N. Nelson. 1989c. H^+-translocating ATPase in golgi apparatus: characterization as vacuolar H^+-ATPase and its subunit structures. *J. Biol. Chem.* 264:18445-18450.

Moriyama, Y., V. Patel, I. Ueda, and M. Futai. 1993. Evidence for a common binding site for omeprazole and N-ethylmaleimide in subunit A of chromaffin granule vacuolar-type H^+-ATPase. *Biochem. Biophys. Res. Comm.* 196:699-706.

Moriyama, Y., A. Yamamoto, Y. Tashiro, and M. Futai. 1991. Chromaffin granule H^+-ATPase has F1-like structure. *FEBS Lett.* 291:92-96.

Myers, M. and M. Forgac. 1993. The coated vesicle vacuolar (H^+)-ATPase associates with and is phosphorylated by the 50-kDa polypeptide of the clathrin assembly protein AP-2. *J. Biol. Chem.* 268:9184-9186.

Nelson, H., S. Mandiyan, T. Noumi, Y. Moriyama, M. C. Miedel, and N. Nelson. 1990. Molecular cloning of cDNA encoding the C subunit of H^+-ATPase from bovine chromaffin granules. *J Biol. Chem.* 265:20390-20393.

Nelson, H. and N. Nelson. 1989. The progenitor of ATP synthases was closely related to the current vacuolar H^+-ATPase. *FEBS Lett.* 247:147-153.

Nelson, N. 1980. Coupling factors from higher plants. *Methods. Enzymol.* 69:301-313.

Nelson, N. 1991. Structure and pharmacology of the proton-ATPases. *Trends Pharmacol. Sci.* 12:71-75.

Nelson, N. 1992b. Evolution of organellar proton-ATPases. *Biochim. Biophys. Acta* 1100:109-124.

Nelson, N. 1992a. Organellar proton ATPases. *Curr. Op. Cell Biol.* 4:654-660.

Njus, D., P. M. Kelley, G. J. Harnadeck, and Y. V. Pacquing. 1986. Mechanism of ascorbic acid regeneration mediated by cytochrome b561. *Ann. N. Y. Acad. Sci.* 493:108-119.

Njus, D., J. Knoth, and M. Zallakian. 1981. Proton-linked transport in chromaffin granules. *Curr. Top. Bioenerg.* 11:107-147.

Ohkuma, S. and B. Poole. 1978. Fluorescence probe measurement of the intralysosomal pH in living cells and the perturbation of pH by various agents. *Proc. Nat. Acad. Sci. USA* 75:3327-3331.

Opie, L. H. and P. Owen. 1976. Effect of glucose-insulin-potassium infusions on arteriovenous differences of glucose and of free fatty acids and on tissue metabolic changes in dogs with developing myocardial infarction. *Am. J. Cardiol.* 38:301-321.

Orci, L., M. Ravazolla, M. Amherdt, O. Madsen, J-D. Vassalli, and A. Perrelet. 1985. Direct identification of prohormone conversion site in insulin sectreting cells. *Cell* 42:671-681.

PABST Laboratories. Circular 0R-10. 1967. Ultraviolet absorption of 5'-ribonucleotides.

Pai, E. F., W. Kabsch, U. K. Krengel, K. C. Holmes, J. John, and A. Wittinghofer. 1989. Structure of the guanine-nucleotide-binding domain of the *Ha-ras* oncogene product p21 in the triphosphatase conformation. *Nature* 341:209-214.

Palmer, D. J. and D. L. Christie. 1990. The primary structure of glycoprotein III from bovine adrenal medullary chromaffin granules. *J Biol. Chem.* 265:6617-6623.

Palmgren, M. G. 1991. Acridine orange as a probe for measuring pH gradients across membranes: mechanisms and limitations. *Anal. Biochem.* 192:316-321.

Pan, Y-X., J. Xu, J. E. Strasser, M. Howell, and G. E. Dean. 1991. Structure and expression of subunit A from the bovine chromaffin cell vacuolar H^+-ATPase. *FEBS Lett.* 293:89-92.

Parry, R. V., J. C. Turner, and P. A. Rea. 1989. High purity preparations of higher plant vacuolar H^+-ATPase reveal additional subunits. . *J Biol. Chem.* 264:20025-20032.

Pedersen, P. L. 1994. The machine that makes ATP. *Current Biology* 4:1138-1141.

Pedersen, P. L. and L. M. Amzel. 1993. ATP Synthases. Structure, reaction centre, mechanism, and regulation of one of nature's most unique machines. *J Biol. Chem.* 268:9937-9940.

Pedersen, P. L. and E. Carafoli. 1987. Ion motive ATPases 1. Ubiquity, properties and significance to cell function. *Trends Biochem. Sci.* 12:146-150.

Penefsky, H. S. and R. L. Cross. 1991. Structure and mechanism of F_OF_1-type ATP synthases and ATPases. *Adv. Enzymol.* 64:173-214.

Peng, S-B. 1995. Nucleotide labelling and reconstitution of the recombiant 58kDa subunit of the vacuolar proton-translocating ATPase. *J Biol. Chem.* 270:16926-16931.

Peng, S-B., B. P. Crider, X-S. Xie, and D. K. Stone. 1994a. Alternative mRNA splicing generates tissue-specific isoforms of 116kDa polypeptides of vacuolar proton pump. *J Biol. Chem.* 269:17262-17266.

Peng, S-B., Y. Zhang, B. P. Crider, A. E. White, V. A. Fried, D. K. Stone, and X-S. Xie. 1994b. Reconstitution of the recombinant 70kDa subunit of the clathrin-coated vesicle H^+-ATPase. *J Biol. Chem.* 269:27778-27782.

Percy, J. M. and D. K. Apps. 1986. Proton-translocating adenosine triphosphatase of chromaffin-granule membranes; the active site is in the largest (70 kDa) subunit. *Biochem. J.* 239:77-81.

Percy, J. M., J. G. Pryde, and D. K. Apps. 1985. Isolation of ATPase I, the proton-pump of chromaffin granule membranes. *Biochem. J.* 231:557-564.

Perin, M. S., V. A. Fried, C. A. Slaughter, and T. C. Südhof. 1988. The structure of cytochrome b_{561}, a secretory vesicle-specific electron transfer protein. *EMBO J.* 9:2697-2703.

Perin, M. S., V. A. Fried, D. K. Stone, X. -S. Xie, and T. C. Südhof. 1991. Structure of the 116-kDa subunit of the clathrin-coated vesicle/synaptic vesicle proton pump. *J. Biol. Chem.* 266:3877-3881.

Perlin, D. S., K. Kasamo, R. J. Brooker, and C. W. Sayman. 1984. Electrgenic proton translocation by the plasma membrane ATPase of *Neurospora*. *J Biol. Chem.* 259:7884-7892.

Peterson, G. L. 1977. A simplification of the protein assay method of Lowry *et al.* which is more generally applicable. *Anal. Biochem.* 83:346-356.

Phillips, R. 1966. Adenosine and the adenine nucleotides. Ionization, metal complex formation and conformation in solution. *Chem. Rev.* 66:501-527.

Poole, B. and S. Ohkuma. 1981. Effect of weak bases on the intralysosomal pH in mouse peritoneal macrophages. *J. Cell Biol.* 90:665-669.

Pryde, J. G. and J. H. Phillips. 1986. Fractionation of membrane proteins by temperature-induced phase separation in triton X-114: application to subcellular fractions of the adrenal medulla. *Biochem. J.* 233:525-533.

Puopolo, K., C. Kumamoto, I. Adachi, and M. Forgac. 1991. A single gene encodes the catalytic A subunit of the bovine vacuolar H^+-ATPase. . *J Biol. Chem.* 266:24564-24572.

Pérez-Castiñeira, J. R. and D. K. Apps. 1990. Vacuolar H+-ATPase of adrenal secretory granules. Rapid partial purification and reconstitution into proteoliposomes. *Biochem. J.* 271:127-131.

Rabon, E., R. D. Gunther, A. Soumarmon, S. Bassilian, M. Lewin, and G. Sachs. 1985. Solubilisation and reconstitution of the gastric H^+,K^+-ATPase. *J Biol. Chem.* 260:10200-10207.

Randall, S. K. and H. Sze. 1986. Properties of the partially purified tonoplast H^+-ATPase from oat roots. *J Biol. Chem.* 261:1364-1371.

Randall, S. K. and H. Sze. 1987. Probing the catalytic subunit of the tonoplast H^+-ATPase from oat roots. *J Biol. Chem.* 262:7135-7141.

Rea, P. A., C. J. Griffith, and D. Sanders. 1987. Purification of the N,N'-dicycolhexylcarbodiimide-binding proteolipid of a higher plant tonoplast H^+-ATPase. *J Biol. Chem.* 262:14745-14752.

Reenstra, W. W., L. Patel, H. Rottenberg, and H. R. Kaback. 1980. Electrochemical proton gradient in inverted membrane vesicles from *Escherichia coli*. *Biochemistry* 19:1-9.

Rottenberg, H. 1989. Proton electrochemical potential gradient in vesicles, organelles and prokaryotic cells. *Methods. Enzymol.* 172:63-84.

Rottenberg, H. and R. Morenosanchez. 1993. The proton pumping activity of H^+-ATPases - an improved fluorescence assay. *Biochim. Biophys. Acta* 1183:161-170.

Runswick, M. J. and J. E. Walker. 1983. The amino acid sequence of the b-subunit of ATP synthase from bovine heart mitochondria. *J Biol. Chem.* 258:3081-3089.

Saika, K. and M. Yoshida. 1995. A minimum catalytic unit of F_1-ATPase shows non-cooperative activity inherent in a single catalytic site with a K_m of 70μM. *FEBS Lett.* 368:207-210.

Saraste, M., P. R. Sibbald, and A. Wittinghofer. 1990. The P-loop - a common motif in ATP- and GTP-binding proteins. *Trends Biochem. Sci.* 15:430-434.

Schmid, S. L. R., P. Fuchs, and I. Mellman. 1988. Two distinct subpopulations of endosomes involved in membrane recycling and transport to lysosomes. *Cell* 52:73-83.

Schmid, S. R., M. Fuchs, A. Kielian, and I. Mellman. 1989. Acidification of endosome populations in wild-type chinese hamster ovary cells and temperature-sensitive acidification-defective mutants. *J. Cell Biol.* 108:1291-1300.

Schmidle, T., R. . Weiler, C. Desnos, D. Scherman, R. Fischer-Colbrie, E. Floor, and H. Winkler. 1991. Synaptin/synaptophysin, p65 and SV2: their presence in adrenal chromaffin granules and sympathetic large dense core granules. *Biochim. Biophys. Acta* 1060:251-256.

Schneider, D. L. 1981. ATP-dependent acidification of intact and disrupted lysosomes. Evidence for an ATP-drien proton pump. *J Biol. Chem.* 256:3858-3864.

Schneider, E. and K. Altendorf. 1985. All three subunits are required for the reconstitution of an active proton channel (F_O) of *Escherichia coli* ATP synthase (F_1F_O). *EMBO J.* 4:515-518.

Schneider, E. and K. Altendorf. 1987. Bacterial ATP synthase (F_1F_O): purification and reconstitution of F_O complexes and biochemical and functional characterisation of their subunits. *Microbiol.Rev.*51:477-497.

Schuldiner, S., H. Rottenburg, and M. Avron. 1972. Determination of ΔpH in chloroplasts. Fluorescent amines as a probe for the datermination of ΔpH in chloroplasts. *Eur. J. Biochem.* 25:64-70.

Schägger, H., W. A. Cramer, and G. von Jagow. 1994. Analysis of molecular masses and oligomeric states of protein complexes by blue native electrophoresis and isolation of membrane protein complexes by two-dimensional native electrophoresis. *Anal. Biochem.* 217:220-230.

Schägger, H. and G. von Jagow. 1987. Tricine-sodium dodecyl sulphate-polyacrylamide gel electrophoresis for the separation of proteins in the range from 1 to 100kDa. *Anal. Biochem.* 166:368-379.

Selwyn, M. J., A. P. Dawson, M. Stockdale, and N. Gains. 1970. Chloride-hydroxide exchange across mitochondrial, erythrocyte and artificial lipid membranes mediated by trialkyl and triphenyltin compounds. *Eur. J. Biochem.* 14:120-126.

Senior, A. E. 1988. ATP synthesis by oxidative phosphorylation. *Physiol. Rev.* 68:177-231.

Serrano, R. 1988. Strucure and function of proton translocating ATPase in plasma membranes of plants and fungi. *Biochim. Biophys. Acta* 947:1-28.

Siebert, A., F. Lottspeich, N. Nelson, and H. Betz. 1994. Purification of the synaptic vesicle-binding protein physophilin. Identification as 39kDa subunit of vacuolar H^+-ATPase. *J Biol. Chem.* 269:28329-28334.

Sista, H., M. A. Wechser, and B. J. Bowman. 1994. The proteolipid subunit of the *Neurospora crassa* vacuolar ATPase: isolation of the protein and the *vma-3* gene. *Mol. Gen. Genet.* 243:82-90.

Stockdale, M., A. P. Dawson, and M. J. Selwyn. 1971. Effects of trialkyltin and triphenyltin compounds on mitochondrial respiration. *Eur. J. Biochem.* 15:342-351.

Stokes, D. L., W. R. Taylor, and N. M. Green. 1994. Structure, transmembrane topology and helix packing of P-type ion pumps. *FEBS Lett.* 346:32-38.

Sun, S-Z., X-S. Xie, and D. K. Stone. 1987. Isolation and reconstitution of the dicyclohexylcarbodiimide-sensitive proton pore of the clathrin-coated vesicle proton translocating complex. *J Biol. Chem.* 262:14790-14794.

Sundquist, K., P. Lakkakorpi, B. Wallmark, and K. Väänänen. 1990. Inhibition of osteoclast proton transport by Bafilomycin-A_1 abolishes bone resorption. *Biochem. Biophys. Res. Comm.* 168:309-313.

Supattapone, S., L. D. Fricker, and S. H. Snyder. 1984. Purification and characterization of a membrane-bound enkephalin-forming carboxypeptidase, "enkephalin convertase". *J. Neurochem.* 42:1017-1023.

Supek, F., L. Supekova, S. Mandiyan, Y-C. E. Pan, H. Nelson, and N. Nelson. 1994. A novel accessory subunit for vacuolar H^+-ATPase from chromaffin granules. *J Biol. Chem.* 269:1-5.

Supek, F., L. Supekova, H. Nelson, and N. Nelson. 1995. Organelle specific subunits of V-ATPases and cross talk between the enzyme and uptake processes in chromaffin granules. In Conference abstracts, 8^{th} international symposium on chromaffin cell biology. Edinburgh. pp49.

Sutton, R. and D. K. Apps. 1981. Isolation of a DCCD-binding protein from bovine chromaffin-granule membranes. *FEBS Lett.* 130:103-106.

Südhof, T. C., M. Baumert, S. Perin, and R. Jahn. 1989. A synaptic vesicle membrane protein is conserved from mammals to Drosophila. *Neuron* 2:1475-1481.

Taiz, L., J. P. Gogarten, H. Kibak, I. Struve, P. Bernasconi, T. Rausch, and S-L. Taiz. 1989. Studies on the structure and evolution of the vacuolar H^+-ATPase. In Plant membrane transport. V. Dainty, editor. 131-137.

Takase, K., I. Yamato, and Y. Kakinuma. 1993. Cloning and sequencing of the genes encoding for the A and B subunits of vacuolar-type Na^+-ATPase from *Enterococcus hirae. J. Biol. Chem.* 268:11610-11616.

Taljanidisz, J., L. Stewart, A. J. Smith, and J. P. Klinman. 1989. Structure of bovine adrenal dopamine b-monooxygenase as deduced from cDNA and protein sequencing: evidence that the membrane bound form of the enzyme is anchored by an uncleaved signal peptide. *Biochemistry* 29:10054-10061.

Thevenod, F., T. P. Kemmer, A. L. Christian, and I. Schulz. 1989. Characterisation of a MgATP-driven uptake into a microsomal vesicle fraction from rat pancreatic acinar cells. *J. Membr. Biol.* 107:263-275.

Thom, M. and E. Komar. 1994. Effect of magnesium and ATP on ATPase of sugarcane vacuoles. *Planta* 161:361-365.

Tirrell, J. G. and E. W. Westhead. 1979. The uptake of ascorbate acid and dehydroascorbic acid by chromaffin granules of the adenal medulla. *Neurosci.* 4:181-186.

Towbin, H., T. Staehelin, and J. Gordon. 1979. Electrophoretic transfer of proteins from polyacrylamide gels to nitrocellolose sheets: procedure and some applications. *Proc. Nat. Acad. Sci. USA* 76:4350-4354.

Turina, P. and R. A. Capaldi. 1994. ATP binding causes a conformational change in the g subunit of *Escherichia coli* F_1-ATPase which is reversed on bond cleavage. *Biochemistry* 33:14275-14280.

Tycko, B. and F. R. Maxfield. 1982. Rapid acidification of endocytic vesicles containing a_2-macroglobulin. *Cell* 26:643-651.

Uchida, E., Y. Ohsumi, and Y. Anraku. 1988. Characterization and function of catalytic subunit a of H^+-translocating adenosine triphosphatase from vacuolar membranes of *Saccharomyces cerevisiae* . *J. Biol. Chem.* 263:45-51.

Uchida, E., Y. Oshuma, and Y. Anraku. 1985. Purification and properties of the H^+-translocating, Mg^{2+}-ATPase from vacuolar membranes of *Saccharomyces cerevisiae*. *J Biol. Chem.* 260:1090-1095.

Usta, J. and D. E. Griffiths. 1992. Organotin-flavone complexes: a new class of fluorescent probes for F_1F_O-ATPase. *Biochem. Biophys. Res. Comm.* 188:365-371.

Usta, J. and D. E. Griffiths. 1993. Dibutyltin-3-hydroxyflavone bromide: a fluorescent inhibitor of F_1F_OATPase. *J. App. Organometall. Chem.* 7:193-200.

van Hille, B., M. Vanek, H. Richener, J. R. Green, and G. Bilbe. 1993. Cloning and tissue distribution of subunits C, D and E of the human vacuolar H^+-ATPase. *Biochem. Biophys. Res. Comm.* 197:15-21.

Väänänen, H. K., E. K. Karhukorpi, K. Sundquist, B. Wallmark, I. Roininen, T. Hentunen, J. Tuukkanen, and P. Lakkakorpi. 1990. Evidence for the presence of a proton pump of the vacuolar H^+-ATPase type in the ruffled borders of osteoclasts. *J. Cell Biol.* 111:1305-1312.

Wakefield, L. M., A. E. G. Cass, and G. K. Radda. 1986. Electron transfer across the chromaffin granule membrane. *J Biol. Chem.* 261:9746-9752.

Walker, J. E., I. M. Fearnley, N. J. Gay, B. W. Gibson, F. D. Northrop, S. J. Powell, M. J. Runswick, M. Saraste, and V. L. Tybulewicz. 1985. Primary structure and subunit stoichiometry of F_1-ATPase from bovine mitochondria. *J. Mol. Biol.* 184:677-701.

Walker, J. E., M. Saraste, and N. J. Gay. 1984. The *unc* operon. Nucleotide sequence, regulation and structure of ATP-synthase. *Biochim. Biophys. Acta* 768:164-200.

Walker, J. E., M. Saraste, M. J. Runswick, and N. J. Gay. 1982. Distantly related sequence in the a subunit and b subunit of ATP synthase, myosin kinase, and other ATP-requiring enzymes and a common nucleotide binding fold. *EMBO J.* 1:945-951.

Wang, S-Y., Y. Moriyama, M. Mandel, J. D. Hulmes, Y-C. E. Pan, W. Danho, H. Nelson, and N. Nelson. 1988. Cloning of cDNA encoding a 32-kDa protein. An accessory polypeptide of the H^+-ATPase from chromaffin granules. *J Biol. Chem.* 263:17638-17642.

Wang, Z. -Q. and S. Gluck. 1990. Isolation and properties of bovine kidney brush border vacuolar H^+-ATPase. *J. Biol. Chem.* 265:21957-21965.

Ward, J. H., A. Renders, H. T. Hsu, and H. Sze. 1992. Dissociation and reassembly of the vacuolar H^+-ATPase complex from oat roots. *Plant Physiol.* 99:161-169.

Warren , M., J. A. C. Smith, and D. K. Apps. 1992. Rapid purification and reconstitution of a plant vacuolar ATPase using triton X-114 fractionation: subunit composition and substrate kinetics of the H^+-ATPase from the tonoplast of *Kalanchoë daigremontiana. Biochim. Biophys. Acta* 1106:117-125.

Wieczorek, H. 1992. The insect V-ATPase, a plasma membrane proton pump energizing secondary active transport: Molecular analysis of electrogenic potassium transport in the tobacco hornworm midgut. *J. Exp. Biol.* 172:335-343.

Wieczorek, H., M. Putzenlechner, W. Zeiske, and V. Klein. 1991. Vacuolar type proton pump energises K^+/H^+ antiport in an animal plasma membrane. *J Biol. Chem.* 266:15340-15347.

Wieczorek, H., S. Weerth, M. Schindlbeck, and U. Klein. 1989. A vacuolar-type proton pump in a vesicle fraction enriched with potassium transporting plasma membranes from tobacco hornworm midgut. *J. Biol. Chem.* 264:11143--32768.

Williamson, J. R. and B. E. Corkey. 1979. Assay of citric acid cycle intermediates and related compounds - update with tissue metabolite levels and intracellular distribution. *Met. Enzymol.* LV:200-222.

Winkler, H. 1976. The composition of adrenal chromaffin granules: an assessment of controversial results. *Neurosci.* 1:65-80.

Winkler, H., D. K. Apps, and R. Fischer-Colbrie. 1986. The molecular function of adrenal chromaffin granules: estabished facts and unresolved topics. *Neurosci.* 18:261-290.

Winkler, H. and E. Westhead. 1980. The molecular organisation of adrenal chromaffin granules. *Neurosci.* 5:1803-1823.

Wray, W., T. Boulikas, V. P. Wray, and R. Hancock. 1981. Silver staining of proteins in polyacrylamide gels. *Anal. Biochem.* 118:197-203.

Xie, X-S. and D. K. Stone. 1986. Isolation and reconstitution of the clathrin-coated vesicle proton translocating complex. *J Biol. Chem.* 261:2492-2495.

Xie, X-S. and D. K. Stone. 1988. Partial resolution and reconstitution of the subunit of the the clathrin-coated vesicle proton ATPase responsible for Ca^{2+}-activated ATP hydrolysis. . *J Biol. Chem.* 263:9859-9867.

Xie, X-S., D. K. Stone, and E. Racker. 1984. Activation and partial purification of the ATPase from clathrin-coated vesicles and reconstitution of the proton pump. *J Biol. Chem.* 259:11676-11678.

Yokoyama, K., Y. Akabane, N. Ishii, and M. Yoshida. 1994. Isolation and properties of prokaryotic V_OV_1-ATPase from a thermiphilic eubacterium, *Thermus thermophilus*. *J Biol. Chem.* 269:12248-12253.

Zachowski, A. 1993. Phospholipids in animal eukaryotic membranes: transverse asymmetry and movement. *Biochem. J.* 294:1-14.

Zachowski, A., J-P. Henry, and P. F. Devaux. 1989. Control of transmembrane lipid asymmetry in chromaffin granules by an ATP-dependent protein. *Nature* 340:75-76.

Zhang, J., Y. Feng, and M. Forgac. 1994. Proton conduction and bafilomycin binding by the V_O domain of the coated vesicle V-ATPase. *J Biol. Chem.* 269:23518-23523.

Zhang, J., M. Myers, and M. Forgac. 1992. Characterization of the V_O domain of the coated vesicle (H^+)-ATPase. *J. Biol. Chem.* 267:9773-9778.

Zhang, J., E. Vasilyeva, Y. Feng, and M. Forgac. 1995. Inhibition and labelling of the coated vesicle V-ATPase by 2-Azido-[^{32}P]ATP. *J Biol. Chem.* 270:15494-15500.

Zimniak, L., P. Dittrich, J. P. Gogarten, H. Kibak, and L. Taiz. 1988. The cDNA sequence of the 69-kDa subunit of the carrot vacuolar H^+-ATPase. Homology to the b-chain of F_OF_1-ATPases. *J Biol. Chem.* 263:9102-9112.

Eur. J. Biochem. 232, 586–595 (1995)

Allosteric regulation of proton translocation by a vacuolar adenosinetriphosphatase

Lorna C. WEBSTER, José R. PÉREZ-CASTIÑEIRA, Gordon L. ATKINS and David K. APPS

Department of Biochemistry, University of Edinburgh, Edinburgh, Scotland

(Received 8 May 1995) – EJB 95 0732/6

The kinetics of nucleoside-triphosphate-dependent proton translocation by a vacuolar-type adenosinetriphosphatase have been studied, using the enzyme from bovine chromaffin-granule membranes, purified and reconstituted into proteoliposomes. The reaction was followed by recording the quenching of the fluorescence of the permeant weak base 9-amino-6-chloro-2-methoxyacridine; fluorescence data were collected and stored in digital form, and the initial reaction rates estimated by linear regression. In the absence of nucleoside diphosphate, the dependence of initial rates of proton translocation on substrate concentration were fitted well by the Michaelis-Menten equation, as were the kinetics of ATP hydrolysis. ADP and other nucleoside diphosphates were potent inhibitors of the ATPase, effecting a reduction in the maximum velocity of the reaction, and producing sigmoid substrate-saturation curves which could be fitted by the empirical Hill equation, the Hill coefficient approaching 2 at high inhibitor concentrations. Data sets containing initial-rate estimates were collected over a wide range of independently varied concentrations of substrate and inhibitor and were modeled, using rate equations derived from several different models based on the concerted-transition model of allosteric inhibition proposed by Monod, Wyman and Changeux. These equations were fitted to the data by weighted non-linear regression, using an iterative computer program to obtain the best estimates of kinetic parameters. One model consistently fitted all of the data sets better than all the others, and this model was based on the following assumptions: that the ATPase exists in two conformational states, R and T; that only the R state is catalytically active; that each state contains three kinetically equivalent catalytic sites, and one regulatory site; that nucleoside triphosphates bind only to the catalytic sites, and that nucleoside diphosphates bind both to the catalytic sites and to the regulatory site. The optimized values of the kinetic parameters indicate that in the absence of nucleoside diphosphate, the enzyme is almost completely in the R state; that nucleoside triphosphates bind more tightly to the R than to the T state; that binding of nucleoside diphosphates to the regulatory site is very tight, but occurs only in the T state; and that competitive binding of nucleoside diphosphates at the catalytic sites is stronger in the T state than in the R state. Experiments conducted with varying total magnesium concentrations indicated that the magnesium complexes of nucleoside diphosphates are much stronger inhibitors than the free nucleotides, and that free nucleoside triphosphates are weakly inhibitory, probably competing with the magnesium complexes for binding at the catalytic sites. The results of these experiments indicate that the effects of nucleoside diphosphates, particularly ADP, occur at concentration ranges that are likely to be physiologically significant, and they make predictions about ligand-induced conformation changes in the ATPase that can be tested by other means.

Keywords: adenosinetriphosphatase; allosteric; fluorescence; proton; vacuolar.

Three distinct classes of H^+-translocating ATPases have been recognized, and termed the F, P and V types [1]. Of these, the V-type H^+-ATPases, which are widely distributed in endomembranes and also occur in some plasma membranes, are the most recently described and the least well characterized. Recently, considerable progress has been made in establishing the number of different subunit types and their arrangement, and the functions of a few of these subunits have been tentatively assigned [2, 3]; this has resulted in a recognition of some structural similarities between V-ATPases and ATPases (more properly, ATP-synthases) of the F type [3, 4].

In comparison with the large amount of structural information available, there has been relatively little work published on the kinetics of the V-ATPases. Studies have been carried out on ATP hydrolysis by plant vacuolar membranes [5, 6], by the V-ATPase purified from brain clathrin-coated vesicles [7] and by the V-ATPase of bovine chromaffin granules, either in resealed chromaffin granule ghosts [8] or as a purified, reconstituted preparation [9]. These results are complicated in some cases by the use of unfractionated membranes (this is a particular problem with chromaffin-granule membranes, which contain, in addition to the proton pump, a second ATPase, of unknown function [10, 11]) and in every case by the use of discontinuous assays for ATP hydrolysis, which makes it difficult to measure initial reaction rates accurately, especially at low substrate con-

Correspondence to D. K. Apps, Department of Biochemistry, University of Edinburgh, Hugh Robson Building, George Square, Edinburgh EH8 9XD, Scotland

Fax: +131 650 3711.

Abbreviations. ACMA, 9-amino-6-chloro-2-methoxyacridine; ADP[S], adenosine 5′-*O*-(2-thiodiphosphate); AIC, Akaike's information theoretic criterion.

Note. The present address of J. R. Pérez-Castiñeira is IBMCP, Universidad Politecnica de Valencia, E-46022, Valencia, Spain.

centrations. Alternatively, it is possible to measure rates of ATP-dependent proton translocation into resealed membrane vesicles or proteoliposomes, using suitable probes to provide a continuous spectrophotometric or fluorimetric record of intravesicular acidification; results of this type have been published for the H^+-ATPases of plant vacuoles [12] and for chromaffin-granule ghosts [13]. This approach has yielded interesting information about the properties of these enzymes in membranes of physiological lipid composition, although, because of the complexity of the systems used, the results are hard to interpret in terms of mechanistic or regulatory features of the H^+-ATPases.

In previous studies [14, 15] we have reported the development of a rapid method for the purification and reconstitution of V-type H^+-ATPases, using fractionation of membrane proteins with Triton X-114, resolubilization of the ATPase with octyl β-glucoside and liposome formation using exclusion chromatography to remove detergents, after the addition of phospholipids and cholesterol. This procedure was applied to the enzymes from bovine chromaffin granule membranes and from the tonoplast of the crassulacean acid metabolism plant *Kalanchoë daigremontiana*. ATP-dependent proton translocation into ATPase-proteoliposomes can be measured by the quenching of the fluorescence of permeant weak bases derived from acridine, providing a sensitive means of determining initial reaction rates. We now report more detailed kinetic studies on the bovine enzyme, suggesting that it is regulated by an allosteric mechanism. The objective of this work was to produce data over a wide range of substrate and inhibitor concentrations, that could be fitted by rate equations derived from theoretical models of allosteric regulation. It should be possible to correlate the features of these models (numbers of binding sites, binding affinities, etc.) with the results of parallel work on nucleotide binding by the ATPase, and on ligand-induced protein conformational changes. A preliminary report of some of this work has appeared [16].

MATERIALS AND METHODS

Materials. Triton X-114 was obtained from Fluka AG and purified by three cycles of solution and condensation [17]. The concentration of the final stock solution of Triton X-114 was measured as described [18]. Phosphatidylserine (bovine spinal cord) and phosphatidylethanolamine (egg) were from Lipid Products. Cholesterol, *n*-octyl β-glucoside and nucleotides were from Boehringer. The pH of nucleotide solutions was adjusted to 7.0 with NaOH where necessary, and the nucleotide concentrations of these stock solutions were calculated from their measured ultraviolet absorbance, at the appropriate wavelength. [γ-^{32}P]ATP (specific radioactivity 110 TBq/mmol) was obtained from Amersham. 9-amino-6-chloro-methoxyacridine (ACMA) was the generous gift of Dr R. Kraayenhof, Free University of Amsterdam, Netherlands. Calbiosorb™ absorbent was from Calbiochem.

ATPase proteoliposomes. The H^+-ATPase of bovine chromaffin-granule membranes was purified and reconstituted by the procedure described previously [14], with the following modifications.

After Triton X-114 fractionation of membranes, the ATPase-containing pellet (P1) was resolubilized in buffer (0.15 M KCl, 10 mM Hepes, pH 7.4, 1 mM dithiothreitol, 0.1 mM EDTA) containing *n*-octyl β-glucoside (18 mg/ml) and dissolved lipids (5 mg/ml total).

The composition of the lipid mixture was phosphatidylethanolamine (69% by mass), phosphatidylserine (11% by mass), cholesterol (20% by mass).

Proteoliposomes were formed by removal of the detergent with Calbiosorb, rather than by passage through Bio-Gel P-6DG.

These modifications optimized the rates of H^+ translocation and gave more consistent activity than the procedure originally decribed. The final specific activity was 1.6−2.0 μmol ATP hydrolysed · min^{-1} · mg $protein^{-1}$ at 30°.

Assays. H^+ translocation by proteoliposomes was assayed by recording the quenching of ACMA fluorescence (emission measured at 480 nm on excitation at 420 nm) at 30° in a specially modified Perkin-Elmer 3000 fluorimeter, the output of which was connected in parallel to a PCL-718 LabCard data acquisition card (Advantech) and a Servoscribe chart recorder. The assay mix (final volume 500 μl) contained 0.3 M sucrose, 10 mM Hepes/NaOH, pH 7.4, 1.0 mM $MgSO_4$, 0.8 μM ACMA and 0.45 μM valinomycin (ACMA and valinomycin were added as stock solutions in ethanol; the final concentration of ethanol was 0.4% by vol.). When required MgADP (or another nucleoside diphosphate, as its magnesium complex) was added to the required final concentration before the addition of proteoliposomes. About 30 s after the addition of proteoliposomes (10 μl, approximately 2 μg protein) to the continuously stirred cuvette, the fluorescence had stabilized and the enzymic reaction was initiated by the rapid injection of MgATP (or another nucleoside triphosphate, as its magnesium complex) to the required final concentration through a light-tight port, using a 25-μl Hamilton syringe fitted with a 7-cm needle.

ATP hydrolysis was measured by determining the rate of liberation of ^{32}P from [γ-^{32}P]ATP. Incubation mixes (200 μl) contained [γ-^{32}P]ATP (approximately 2.4×10^3 Bq), various concentrations of MgATP, 0.3 M sucrose, 10 mM Hepes/NaOH, pH 7.4, 1.0 mM $MgSO_4$ and 0.45 μM valinomycin. Each incubation mix was warmed to 30°, and the reaction was started by the addition of 10 μl ATPase proteoliposomes. After 5 min the reaction was stopped with ice-cold trichloroacetic acid (3% mass/vol.); inorganic phosphate was extracted as its phosphomolybdate complex [19] and counted in Ultima Gold liquid scintillant.

Data collection. The digitised signal from the fluorimeter was collected at 10 Hz on an IBM286 computer, using software written by Dr M. B. Dutia, Department of Physiology, University of Edinburgh; it was also displayed on a monitor in graphical form. Optional three-point smoothing of noisy quench-curves could be applied if necessary; the range of points for initial-rate estimation was then selected, and a straight line fitted by linear regression using the Apple Macintosh version of Regression (Blackwell Scientific Publications). Individual data points were not weighted and regression was based on a least-squares routine with a Marquardt algorithm. This procedure produced the estimates of the initial rates of proton translocation that were fed into the model-fitting programme.

Error function. Five experimental protocols were chosen so that the predicted values of the initial reaction velocity, v, covered the entire experimental range. Ten replicate rate measurements were performed with each of the five protocols, and for each set of values the mean initial velocity and its SD were calculated. An error function

$$var = SD^2 = a + b \cdot v^2$$

was fitted to the data by linear regression to give estimates for the two constants a and b.

Fitting of the Michaelis, Hanes and Hill equations. At the pH of the assay, and with the concentrations of free Mg^{2+} used, ATP was essentially all present as its magnesium complex, $MgATP^{2-}$. This was not true of ADP, which was present as 20−24% ADP^{3-}, and up to 80% $MgADP^-$. The actual concentration of MgADP was calculated using a dissociation constant for the complex of 2.4×10^{-4} M [20].

Reaction rates measured in the absence of inhibitor were first plotted as Michaelis-Menten, Hanes or Hill plots by weighted regression, with v as the dependent variable and [S] as the independent variable. Each point was weighted as $1/var$ and the weights were normalized. Fitting of the Michaelis equation was assessed by calculating the determination coefficient, d:

$$d = 1 - \frac{\Sigma(v - v_{calc})^2}{\Sigma(v - \bar{v})^2}$$

and for the Hanes and Hill plots goodness of fit to a straight line was assessed from the correlation coefficient, r:

$$r = \frac{n\,\Sigma xy - \Sigma x\,\Sigma y}{\sqrt{([n\,\Sigma x^2 - (\Sigma x)^2]\,[n\,\Sigma y^2 - (\Sigma y)^2])}}.$$

Model fitting. The models were fitted using weighted nonlinear regression with substrate concentration (S) and inhibitor concentration (I) as the independent variables and v as the dependent variable. Each point was weighted as $1/var$. The values of var were calculated from the above error function using the experimentally determined value of v and the constants a and b as determined above. All of the data points from one experiment were used in each model-fitting run.

Strategy. The number of parameters to be estimated was 6, 7, 8 and 9, respectively, for the four models tested. This was too many for the amount and quality of the available data to bear, and early attempts to determine the complete set proved unreliable. However, by fixing four of the parameters beforehand, model fitting could be carried out successfully in most cases. This was done by giving n and m integer values (the combinations 3 and 1, 2 and 1 and 3 and 2 proved to be the most successful) and fitting the Michaelis-Menten equation to the first curve (nucleoside triphosphate concentration varied in the absence of inhibitor), thus obtaining the values of V_{max} and K_r.

Computer program. The program for model fitting is written in C. The least-squares routine for regression calls the NAG FORTRAN library routines EO4FCF, which uses a combined Gauss-Newton and modified Newton algorithm, and EO4CCF, which uses the Simplex method. Several lesser routines are also called from the NAG library. The program was run on a Sequent computer, under UNIX, at the Edinburgh University Computing Service.

Model discrimination. The questions posed were (a) which of the four proposed models and (b) which of the three combinations of n and m produced the best fit of the data? The two major statistical tests used for this purpose were (a) a Runs test, which analysed the distribution of residuals about a fitted curve and (b) Akaike's information theoretic criterion (AIC).

The number of runs (Tables 3 and 4) is the number of times that the sign of the residual changed, from one point to the next along a curve; its theoretical maximum is the number of data points in that particular data set (the sum of the + and − values in Tables 3 and 4). Obviously the number of positive and negative residuals should approach equality for the best fit.

The AIC uses the residual sum of squares adjusted for the number of parameters estimated [21], and is defined as

$$\text{AIC} = (-2 \log [\text{residual}])^2 + 2\,(\text{no. of independently-adjusted parameters}).$$

A third, subjective criterion was that each of the curves in one experiment should fit equally well.

Theoretical models. The four models considered are all variants of the general two-state concerted-transition model of allosteric regulation, which was first proposed by Monod, Wyman and Changeux [22]. They have the following features in common. The ATPase exists as an equilibrium mixture of two conformational states, called R and T. The equilibrium constant for the conformation change is L:

$$L = [\text{T}]/[\text{R}].$$

The value of L is assumed to be independent of the number of nucleotide-binding sites filled.

The enzyme contains n catalytic sites and m regulatory, nucleotide-binding sites.

Free nucleotides are assumed to be in equilibrium with nucleotides bound at the catalytic and regulatory sites, i.e., ligand-binding reactions and protein conformational changes are much faster than the catalytic step, which is rate limiting.

The dissociation constants for binding of nucleotides to the catalytic and to the regulatory nucleotide-binding sites are altered by the protein conformational change, and are therefore different in the R and T states.

In either conformational form, the affinities of all sites within a particular class (catalytic or regulatory) are assumed to be equal.

The R and T states of the ATPase differ in their catalytic activities; in three of the models the T state is assumed to be inactive.

We had also to consider that inhibitors such as MgADP could possibly bind in two modes, i.e., as allosteric inhibitors (binding at the regulatory sites) and as competitive inhibitors (binding at the catalytic sites).

Mathematical models. Four models, of increasing complexity, were considered.

Model 1. The substrate (S) and inhibitor (I) bind exclusively to the R and T states of the enzyme, respectively. The R state is catalytically active, but the T state is inactive. There are just two binding reactions, plus the conformational equilibrium and the catalytic reaction. Solution of the algebraic equations describing them gives the rate equation

$$v/V_{max} = \frac{([\text{S}]/K_r)\,(1 + [\text{S}]/K_r)^{n-1}}{L\,(1 + [\text{I}]/K_i)^m + (1 + [\text{S}]/K_r)^n}$$

where v is the initial rate of the reaction; V_{max} is the maximum velocity of the reaction; [S] the concentration of substrate, and K_r its dissociation constant from catalytic sites; [I] is the concentration of inhibitor and K_i its dissociation constant from regulatory sites.

Model 2. The inhibitor binds only to the T state of the enzyme; the substrate binds to both the R and the T states, although the latter is inactive. There are three binding reactions, the conformational equilibrium and the catalytic reaction. The rate equation is

$$v/V_{max} = \frac{([\text{S}]/K_r)\,(1 + [\text{S}]/K_r)^{n-1}}{L\,(1 + [\text{I}]/K_i)^m\,(1 + [\text{S}]/K_t)^n + (1 + [\text{S}]/K_r)^n}$$

where K_t is the dissociation constant of the substrate from catalytic sites in the T state.

Model 3. As for model 2, but both the R and the T states of the enzyme are catalytically active, with different V_{max} values. There are three binding reactions, two catalytic reactions and the conformational equilibrium. The rate equation is

$$v = \frac{V_r([\text{S}]/K_r)\,(1 + [\text{S}]/K_r)^{n-1} + V_t L'([\text{S}]/K_t)\,(1 + L' \cdot [\text{S}]/K_t)^{n-1}}{L'(1 + [\text{S}]/K_t)^n + (1 + [\text{S}]/K_r)^n}$$

where $L' = L\,(1 + [\text{I}]/K_i)^m$ and V_r and V_t are the maximum velocities of the reactions catalysed by the R and T states, respectively.

Model 4. The substrate binds to catalytic sites in both the R and the T states, with different affinities; and the inhibitor binds

competitively at these sites. Binding of the inhibitor to distinct regulatory sites occurs only in the T state. Only the R state is catalytically active. There are five ligand-binding reactions, the conformational equilibrium and the catalytic reaction, and the rate equation is

$$v/V_{max} = \frac{[[S]/\{K_r(1 + [I]/K_a)\}] \cdot [1 + [S]/\{K_r(1 + [I]/K_a)\}]^{n-1}}{[1 + [S]/\{K_r(1 + [I]/K_a)\}]^n + L(1 + [I]/K_i)^m [1 + [S]/\{K_t(1 + [I]/K_b)\}]^n}$$

where K_a and K_b are the dissociation constants of the inhibitor from catalytic sites in the R and T state, respectively, and K_i is its dissociation constant from the regulatory site in the T state.

RESULTS

Time-course of ACMA fluorescence quenching. Fig. 1a shows a typical fluorimeter recording of a fast reaction, and Fig. 1b shows points collected from the initial part of the fluorescence-quenching curve, which were used to estimate the initial reaction rate of proton-translocation by the reconstituted chromaffin-granule H^+-ATPase.

The kinetic data were collected as sets of measurements of initial rates; for each set the concentration of the substrate MgATP (or the magnesium complex of another nucleoside triphosphate) was varied between 1 μM and 1000 μM (up to 15 points) at a number of concentrations of the inhibitor MgADP (or of the magnesium complex of another nucleoside diphosphate). Usually six inhibitor concentrations were used, between 0 and 150 μM. With the highest MgADP concentrations, the rates were unmeasurably low with very low [MgATP], but were measured down to the lowest practicable substrate concentration. The data sets therefore each contained some 60−70 rate measurements, over the range 0.3−100 U/s; this was the maximum that could be conveniently performed in one day.

Kinetics in the absence of inhibitors. In the absence of inhibitors the H^+-ATPase exhibits Michaelis-Menten kinetics, i.e., initial-rate/substrate concentration curves are fitted well by the Michaelis equation (Fig. 2a), and a Hanes plot of the same data is linear (Fig. 2b). Values of the determination coefficient for the Michaelis-Menten plot and of the correlation coefficient for the Hanes plot are very close to unity with all three nucleoside triphosphates examined, confirming that the proton pump exhibits Michaelian kinetics in the absence of inhibitors. The order of apparent affinities is MgATP > MgGTP > MgITP; with MgGTP as substrate, V_{max} is lower than with MgATP or MgITP (Table 1).

When the same data are expressed as Hill plots (Fig. 3) a Hill coefficient (n_H) of 1.07 is obtained in the absence of ADP (Table 2), consistent with a good fit by the Michaelis-Menten equation.

Kinetics of ATP hydrolysis. The kinetics of phosphate release from ATP, in the absence of inhibitors, are shown in Fig. 4. As with proton translocation, the velocity/substrate curve is accurately fit by the simple Michaelis-Menten equation. The K_m obtained, 71 μM, is close to that estimated for proton translocation (54 μM). The V_{max} values cannot be compared directly, since rates of fluorescence quenching do not yield absolute rates of H^+ translocation.

Inhibition by nucleoside diphosphates. All of the nucleoside diphosphates tested produced similar types of inhibition: with increasing inhibitor concentration, there was a change from hyperbolic to sigmoid dependence of the H^+-translocation rate on ATP concentration, with a decrease in V_{max}. The value of n_H rises progressively from 1.07 to 1.75 as the MgADP concentration is raised to approximately 200 μM (Table 2). This produces characteristic sigmoid Michaelis-Menten plots (see, for example, Figs 5 and 6), indicating that the inhibitor induces cooperative binding of MgATP.

Inhibition was studied with various total Mg^{2+} concentrations; increasing the free [Mg^{2+}] to 5 mM made no significant difference to the kinetics, and the conditions chosen for subsequent detailed study were with 1 mM free Mg^{2+}, ensuring that about 80% of the nucleoside diphosphate, and virtually all of the nucleoside triphosphate, were present as their magnesium complexes. Some experiments were carried out in which the total concentration of ATP exceeded that of Mg^{2+}, so that the concentration of the substrate MgATP was determined by the total magnesium concentration, and there was significant free ATP but only low levels of free Mg^{2+}. Under these conditions the K_m for MgATP was progressively increased (to about 200 μM, in the presence of 5 mM free ATP), but inhibition by added free ADP was very slight (data not shown).

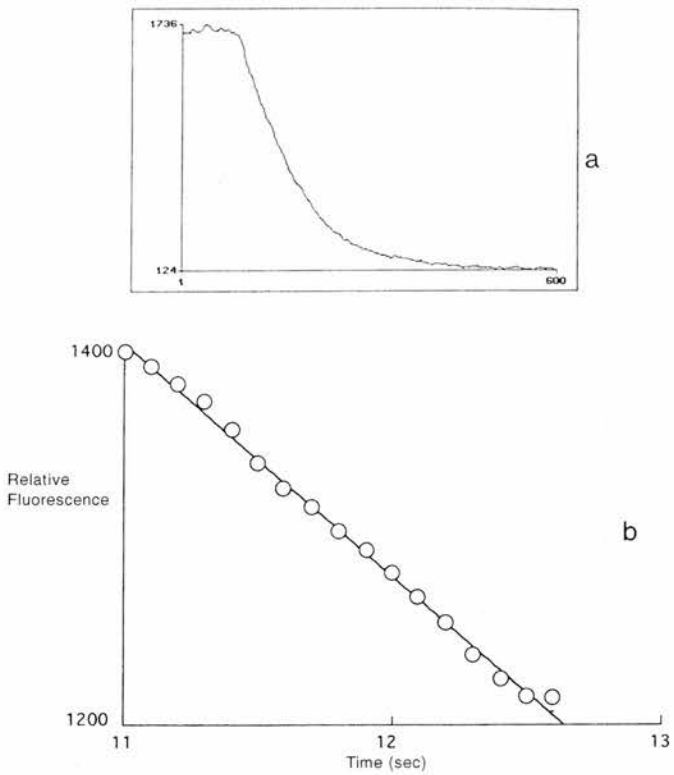

Fig. 1. ACMA fluorescence quenching. (a) Record of an ATP-induced fluorescence quench trace: output of digitally stored data from the computer. The concentration of MgATP was 1.0 mM. The vertical scale is of relative fluorescence; the horizontal scale records the number of data points (10/s), so the entire record covers 1 min. (b) Determination of the initial rate of fluorescence quenching from the same trace, by linear regression of data points collected over approximately 1.5 s.

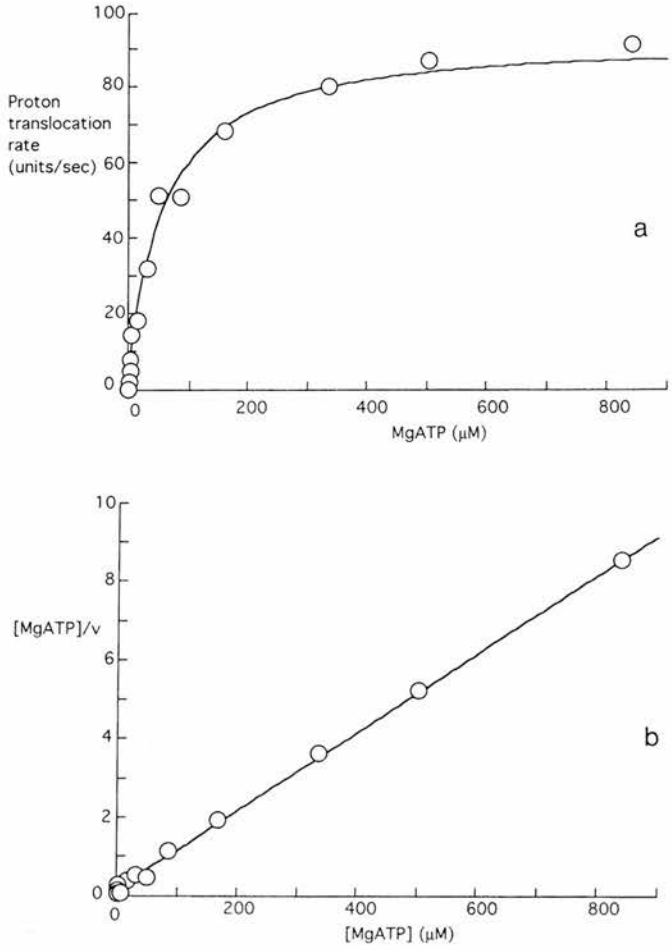

Fig. 2. Initial rates of ACMA fluorescence quenching by ATPase-proteoliposomes, as a function of the concentration of the substrate MgATP. (a) Michaelis plot; the points are experimental, and the line is that predicted by the best fit of the Michaelis Menten equation, with V_{max} = 94 U/s, K_m = 54 μM. (b) Hanes plot; the line was fitted to the experimental points by linear regression, with V_{max} = 94 U/s, K_m = 51 μM.

Table 1. Kinetic parameters for the ATPase in the absence of inhibitors. Parameters were obtained either by using non-linear regression to fit the Michaelis-Menten equation, or by linear regression in the Hanes plot. In the latter case the criterion $1 > r > 2/\sqrt{(n-1)}$, where r is the correlation coefficient and n is the number of data points, is met in each case.

Plot	Addition	V_{max}	K_m	d	n
		U/s	μM		
Michaelis plot	MgATP	94 ± 5	54 ± 5	0.991	13
	MgITP	82 ± 11	413 ± 77	0.981	10
	MgGTP	16 ± 1	161 ± 25	0.968	8
Hanes plot	MgATP	94 ± 5	51 ± 3	0.996	13
	MgITP	83 ± 12	372 ± 35	0.966	10
	MgGTP	17 ± 2	161 ± 18	0.979	8

We also confirmed the report of Moriyama and Nelson [23] that CTP and UTP activate the enzyme; this activation was most marked in the absence of MgADP. Both Mg CTP and MgUTP were found to support low rates of H^+ translocation in the absence of ATP.

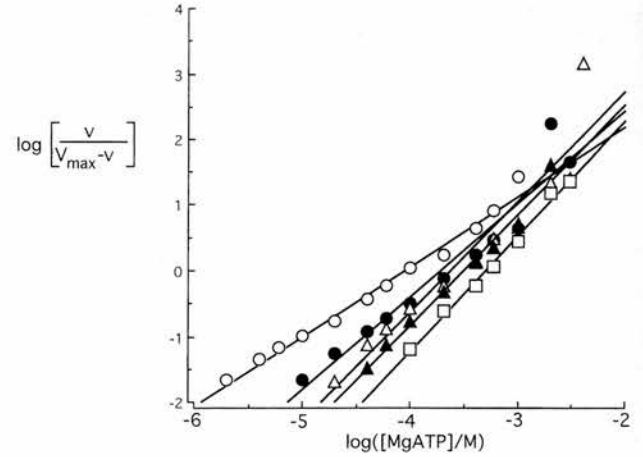

Fig. 3. Hill plots for initial rates of ACMA fluorescence quenching as a function of the concentration of the substrate MgATP, at various concentrations of the inhibitor MgADP. (○), 0; (●), 25; (△), 50; (▲), 100; (□), 200 μM.

Table 2. Hill coefficients for MgATP, with different concentrations of the inhibitor MgADP. Parameters were obtained using weighted linear regression to fit the Hill equation.

[MgADP]	$K_{0.5}$	n_H	r
μM			
0	85	1.07 ± 0.04	0.985
25	186	1.42 ± 0.13	0.933
50	230	1.68 ± 0.18	0.909
100	303	1.68 ± 0.07	0.984
200	491	1.75 ± 0.07	0.992

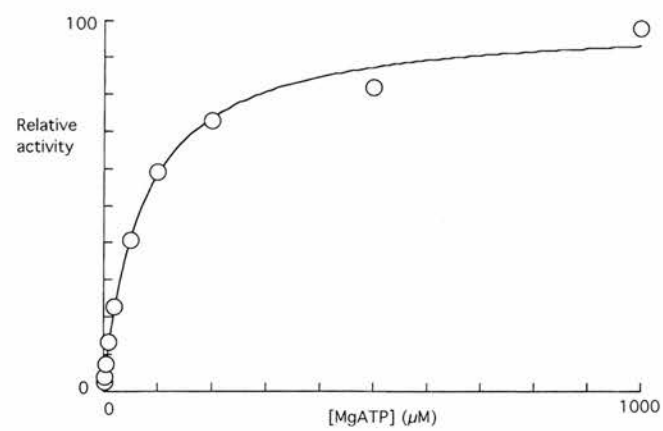

Fig. 4. Michaelis plot of ATP hydrolysis. Data points are experimental, and the line is that predicted by the best fit of the Michaelis equation with K_m = 71 μM. V_{max} was approximately 1 μmol · mg^{-1} · min^{-1}.

DISCUSSION

Validity of the approach. We chose to assay H^+ translocation by the ATPase, rather than ATP hydrolysis, for several reasons: first, this is the primary function of the enzyme, and its kinetic characteristics should therefore reflect important features of the enzyme's behaviour in the cell; second, the assay for H^+ translocation is very sensitive, is capable of measuring initial reaction rates over a very wide range, and is therefore suitable for mechanistic studies; third, the technique provides a direct, continuous

Table 3. Statistical comparison of fitting the different models to data sets with MgATP as substrate, different nucleoside diphosphates as inhibitors and various values of *m* and *n*. SSQ, sum of squares of residuals. +/−, numbers of points with positive and negative residuals. AIC, Akaike's Information Theoretic Criterion.

Model	*n*, *m*	Parameters determined using substrate, inhibitor															
		MgATP, MgADP				MgATP, MgGDP				MgATP, MgIDP				MgATP, ADP[S]			
		SQ	runs	±	AIC	SQ	runs	±	AIC	SQ	runs	±	AIC	SQ	runs	±	AIC
2	3,1	137	19	22/26	57	123	24	30/27	50	263	23	24/24	89	168	26	27/35	68
2	2,1	155	19	22/26	63												
2	3,2	411	13	18/30	110												
3	3,1	124	19	23/25	55	115	24	31/26	49	246	23	20/28	87	151	29	29/33	64
3	2,1	151	20	23/25	64												
3	3,2	312	11	18/30	98												
4	3,1	74	21	24/24	32	98	25	29/28	42	223	25	21/27	85	151	30	39/33	66
4	2,1	99	21	23/25	45	121	25	25/32	54	252	27	20/28	90	202	22	28/34	84
4	3,2	160	17	19/29	66	196	18	27/30	80	341	16	18/30	103	236	25	22/40	93

record of the reaction, the addition of inhibitors such as ADP does not interfere with the operation of the assay, and any changes in reaction rate can confidently be attributed to effects on the ATPase itself. A final and important point is that only the activity of the V-ATPase is recorded by this assay. We have previously shown that contamination of our reconstituted V-ATPase preparation, for example by mitochondrial F_1F_0-ATPase or by chromaffin granule ATPase II, is negligible, but it is important to exclude the possibility that any deviations from ideal kinetic behaviour, particularly at low substrate levels, are not due to contamination by small amounts of other ATPases.

To be useful for detailed kinetic analysis and model fitting, the recorded rate of fluorescence quenching must accurately report the rate of H^+ translocation by the enzyme. A theoretical justification of the use of fluorescence probes for kinetic measurements has been published [12], and computer analysis of the quenching of the fluorescence of probes such as acridine orange has been used to quantify H^+ fluxes [24]. ACMA has been shown to be the probe of choice for the measurement of relatively small ΔpH values [25], and we have shown previously [14] both that the response of ACMA fluorescence to changes in ΔpH in ATPase proteoliposomes is very rapid, and that the rate of fluorecence quenching is proportional to reaction rate over a very wide range.

In previously reported work [14, 15] the initial rates of fluorescence quenching were estimated manually, from chart-recorder traces. This approach was difficult to apply to reactions with low substrate concentrations, because the traces were curved, and with high substrate concentrations the fast reaction rates tended to be underestimated. The digital data-collection system gave more reproducible rate estimates, and a much wider range of substrate concentrations could be used. We found that at the highest substrate concentrations the initial rate of reaction was only maintained for a few seconds, but that the digital data-collection system permitted accurate determination of the quench rate over this short time period.

Although we have concentrated on measuring H^+ translocation, we also studied the concentration dependence of MgATP hydrolysis in the absence of inhibitors (Fig. 4). These kinetics are essentially identical to those of H^+ translocation. The small difference in K_m may be due to the difficulty in measuring truly initial reaction rates by a discontinuous assay, particularly at low substrate concentrations.

Models of cooperative substrate binding. We attempted to model the allosteric regulation of the chromaffin-granule H^+-ATPase by fitting the initial-rate data with equations derived from a series of models based on the postulates of Monod, Wyman and Changeux [22]. The four models explored differed in the assumptions made about which of the two states of the enzyme are active, and which bind nucleotides at either the catalytic or the regulatory sites. A summary of the results of model-fitting attempts appears in in Tables 3 and 4. No data appear for model 1, in which the substrate and inhibitor bind exclusively to the R and T states respectively, because with this model no convergence of the fitting program was obtained even after several hundred iterations.

Table 4. Statistical comparison of fitting the different models to data sets with different nucleoside triphosphates as substrate, MgADP as inhibitor and various values of *m* and *n*.

Model	*n*, *m*	Parameter determined with substrate, inhibitor							
		MgITP, MgADP				NgGTP, MgADP			
		SSQ	runs	±	AIC	SSQ	runs	±	AIC
2	3,1	95	19	17/18	41	11	15	15/14	−20
2	2,1								
2	3,2								
3	3,1	44	21	18/17	17	11	15	15/14	−20
3	2,1								
3	3,2								
4	3,1	23	20	17/18	−3	10	18	14/15	−21
4	2,1	28	17	19/16	4	14	13	15/14	−10
4	3,2	85	14	19/16	41	21	15	13/16	2

Convergence was obtained with each of the three other models tested. Comparisons of the fits achieved by the different models was made using the AIC value, which takes into account the number of independently adjusted parameters, and by comparison of the number of runs, i.e. the distribution of the experimental points about the velocity/substrate curve calculated from the best fit of the model to the data as a whole. The sum of squares of residuals (SSQ) can only be used for evaluation of results obtained with different values of parameters within a particular model (i.e., with the fit obtained using different values of *m* and *n*) and should not be used for comparisons between models with different numbers of parameters.

In all data sets, model 4 produced the best fit to the experimental data points as indicated by the lowest AIC values and

Table 5. Kinetic parameters obtained by fitting the rate equation derived from model 4 to a number of data sets, with different substrates and inhibitors. In each case the values of m and n were 1 and 3, respectively.

Substrate	Inhibitor	K_r	K_t	L	K_i	K_a	K_b	V_{max}
		μM			μM			U/s
MgATP	MgADP	63 ±2.1	147 ±8	5.7×10^{-7} $\pm2.7\times10^{-6}$	3.4×10^{-7} $\pm3.7\times10^{-8}$	232 ±1	17.1 ±1.1	97 ±2.5
MgITP	MgADP	384 ±27	395 12	0.015 ±0.009	0.002 ±0.001	44 ±5.4	0.8 ±0.06	81 ±3.7
MgGTP	MgADP	142 0	778 79	0.047 ±0.036	0.002 ±0.002	7×10^{5} $\pm1.0\times10^{9}$	1.6 ±0.4	15 ±0
MgATP	MgIDP	63 ±2.6	127 ±7.5	0.008 ±0.02	0.3 ±0.8	1.8×10^{6} $\pm8.5\times10^{7}$	425 ±64	128 ±3.3
MgATP	MgGDP	63 ±2.0	176 ± 5.7	0.019 ±0.014	0.6 ±0.4	7.4×10^{5} $\pm7.2\times10^{6}$	780 ±75	103 ±2.0
MgATP	MgADP[S]	37 ±0.9	253 ± 9.2	0.053 ±0.016	1.2 ±0.4	4.1×10^{3} 0.4×10^{3}	1.2×10^{6} $\pm8.2\times10^{7}$	121 ±1.7

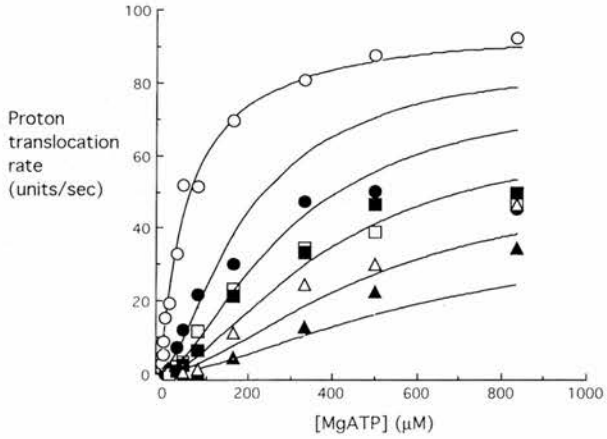

Fig. 5. Fitting of model 2 to a data set. Initial rates of ACMA fluorescence quenching over a range of concentrations of the substrate MgATP, at various concentrations of the inhibitor MgADP. (○), 0; (●), 6.6; (□), 16.5; (■), 33; (△), 66; (▲), 132 μM. The points are experimental; the lines are calculated from the best fit of the rate equation derived from model 2, with $m = 1$, $n = 3$ (Table 3).

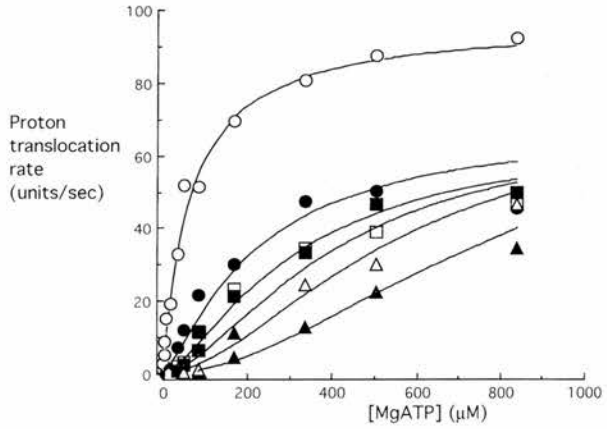

Fig. 6. Fiting of model 4 to a data set. Initial rates of ACMA fluorescence quenching over a range of concentrations of the substrate MgATP, at various concentrations of the inhibitor MgADP: (○), 0; (●), 66; (□), 16.5; (■), 33; (△), 66; (▲), 132 μM. The points are experimental; the lines are calculated from the best fit of the rate equation derived from model 4, with $m = 1$, $n = 3$ (Table 3).

better run statistics. In most cases model 3 approaches the statistical performance of model 4; for example with MgATP as substrate and MgIDP as inhibitor the AIC values for the best fit for models 3 and 4 are very close, at 87 and 85, respectively (Table 3). The runs are also very similar for this data set. Thus these data do not descriminate between models in which the T state was active (model 3) and inactive (model 4). However on inspection of optimized parameters it is apparent that the best fits of model 3 to all of our data indicated values of the catalytic activities of the T state that were very small or even negative. This strongly suggests that model 3 is not applicable, and that the T state of the enzyme is not catalytically active.

Graphical representations of the best fits of models 2 and 4, with MgATP as the substrate and MgADP as the allosteric inhibitor, appear in Figs 5 and 6, respectively. Although there is only a relatively small difference between the AIC values (Table 3) it is apparent that model 4 produces a superior fit to the experimental data, particularly in predicting the significant decrease in V_{max} produced even by low concentrations of MgADP, an aspect of the enzyme's behaviour that model 2 does not predict. The reason that the AIC values appear to underestimate the superiority of model 4 may be due to the weighting factor, in that model 2 tends to produce a better fit of points at low [MgATP], which are more heavily weighted than those at high substrate concentration. Although the model we have developed produces a good fit to the data, we cannot exclude the possibility that the enzyme has other features that are not included in the model, such as the binding of MgATP to the regulatory site; however it is doubtful whether a more elaborate model can be distinguished from the existing ones simply by its steady-state kinetics.

Number of nucleotide-binding sites. The same data set with MgATP as substrate and MgADP as inhibitor was fitted to all three models, using fixed values of n and m of 1, 2, 3 or 4. In every case, including models that gave a generally less satisfactory fit than model 4, the best convergence was obtained with n and m set at 3 and 1, respectively (Tables 3 and 4). This was also the case for the fitting of model 4 to data sets obtained with various other combinations of substrate and inhibitor. Values of m and n above 3 gave poor fits and the data are not shown.

If there are 3 nucleoside-triphosphate-binding sites, the value of n_H is expected to approach 3 at high concentrations of MgADP, which displace the conformational equilibrium so far that all of the enzyme is in the T state. The highest value of n_H

Table 6. Interdependence of the kinetic parameters L and K_i. The equation derived from model 4 was fitted to a data set with MgATP and MgADP, with $m = 1$ and $n = 3$. V_{max} and K_r were fixed at 97 U/s and 63 μM, respectively, L at one of the values shown in the table and the other parameters allowed to float. The parameters obtained by the overall best fit to this data set appear in Table 5, in which $L/K_i = 1.68\ \mu M^{-1}$.

L	K_i	K_t	K_a	K_b	L/K_i
	μM				μM^{-1}
0.01	0.006	148	233	18	1.67
0.02	0.012	141	221	16	1.67
0.05	0.031	142	221	16	1.61

obtained in this work was 1.75 (Table 2); but the simple Hill analysis is complicated by the fact the MgADP acts as a competitive, as well as an allosteric, inhibitor.

Values of constants in the rate equation. A major aim of this work was to determine the dissociation constants for the regulation of the H^+-ATPase by allosteric inhibitors. Unfortunately the complexity of the rate equation means that although we have succeeded in developing models that adequately describe the kinetic features of the ATPase, such as sigmoidal velocity/substrate curves in the presence of ADP, and an effect of ADP on the apparent V_{max}, it was not possible to determine the value of the dissociation constant of MgADP from its regulatory site with any degree of confidence.

This is illustrated by considering the values of L and K_i, constants which describe the allosteric regulation by nucleoside diphosphates and which always appear in the same term. The value of L, the conformational equilibrium constant, is predicted to be small. This follows from the lack of cooperativity in the absence of inhibitor, with a good fit to the simple Michaelis-Menten equation and a Hill coefficient close to 1, indicating that the enzyme is almost fully in the R state in the absence of MgADP. As it is a property of the free enzyme, the value of L should be independent of the substrate or inhibitor studied, and as shown in Table 5 in most cases it takes a value of 0.01−0.05. The optimized values of both constants obtained with the first data (MgATP and MgADP) are very low, and inconsistent with those in other sets; however the ratio L/K_i is similar. We therefore tried fitting a data set with the equation derived from model 4, with m and n fixed at 1 and 3, respectively, K_r and V_{max} fixed, and L fixed at 0.01, 0.02 or 0.05; the other constants were allowed to float. There was no significant change in the goodness of fit with the different values of L, nor were the values of K_t, K_a or K_b altered; only K_i was changed (Table 6). Since K_i is of the order of 10^{-8} M, under the experimental conditions employed ($[I] \gg K_i$) the denominator term $L\ (1 + [I]/K_i)$ approximates to $[I]$. L/K_i, and L/K_i remained approximately constant.

The value of K_r, the dissociation constant of the substrate from catalytic sites in the R state, is around 60 μM for MgATP (Fig. 1 and Table 5); the affinity for other purine nucleoside triphosphates is lower (MgATP > MgGTP > MgITP). In all cases the substrate binds more tightly to the catalytic sites in the R state than in the T state ($K_r < K_t$), although for MgATP the difference in affinity is less than twofold. In contrast, nucleoside diphosphates bind to the catalytic site more tightly in the T state than in the R state (the exception to this being ADP[S], for which the large value of K_b suggests that binding to the T state is very weak). From the effects of varying the total magnesium concentration it appears that the inhibitory form of ADP, which binds at both the catalytic and the regulatory sites, is its magnesium complex ($MgADP^-$).

It is noteworthy that the values of K_a and K_b, which should be characteristic of the inhibitor used but independent of the substrate, are different in the first three data sets reported in Table 5, all of which are for MgADP; this is a reflection of the difficulty of fitting such a complex rate equation to a data set containing a relatively low number of data points. In any case, the values of K_a are larger than the concentrations of MgADP actually used in the experiments, so they are not significant. We tried fitting the data with a rate equation derived from a modified version of model 4, in which binding of MgADP to the R state was ignored (i.e. $K_a = \infty$), but the overall fit by this model was significantly inferior to that by model 4 (data not shown).

Comparison with previous kinetic studies. Although some studies of the kinetics of V-type ATPases have been reported elsewhere, in most cases comparison with the present work is difficult either because rates of ATP hydrolysis, rather than of H^+ translocation, were measured, or because the ATPase preparations were different (for example, many workers have used unfractionated membranes or sealed membrane vesicles, rather than purified H^+-ATPase). Johnson et al. [8] studied ATP hydrolysis by chromaffin-granule membranes, and reported simple kinetics with a K_m value of 69 μM for MgATP. Inhibition by ADP of proton translocation into chromaffin-granule ghosts, however, indicated complex binding of MgATP in the presence of the inhibitor [26]; in this study proton translocation was measured from the change in the spectrum of acridine orange, so the presence in the membranes of a second ATPase which does not pump protons should not have affected the results. Studies on ATP hydrolysis by plant V-type ATPases [5, 6] have generally shown simple kinetics, although we have found inhibition by MgADP of the reconsituted H^+-ATPase from the tonoplast of *K. daigremontiana* [16], similar to that reported here.

The data of Moriyama and Nelson [23] on ATP hydrolysis by purified, reconstituted chromaffin-granule ATPase show simple kinetics (K_m = 83 μM) in the absence of inhibitors, while 100 μM ADP produced a sigmoid ATP saturation curve, with a Hill coefficient approaching 2.2; these results are very similar to those reported here. However Hanada et al. [9] reported more complex kinetic behaviour of a similar preparation; graphical analysis suggested three different K_m values for ATP (5 μM, 30 μM and 300 μM). Rather similar results were reported with the ATPase of bovine brain clathrin-coated vesicles [7], which is presumably derived from neurosecretory vesicles and likely to be similar or identical to the chromaffin-granule enzyme; in this case two different K_m values were obtained. However when H^+ translocation was measured in this preparation it was found that high concentrations of MgATP were inhibitory. Kinetic behaviour suggesting two or more types of catalytic site, with different affinities for ATP, might reflect inhomogeneity in the ATPase preparation, with two or more separate types of ATPase showing different K_m values, or it could be the result of negative cooperativity between different classes of catalytic site within the same enzyme. We obtained similar results when using a coupled assay to study ATP hydrolysis by the reconstituted chromaffin-granule ATPase [16], and in this case modeling gave a good fit to the data of a double Michaelis function; however we have not found multiple K_m values, nor Hill coefficients significantly less than 1.0, in the present work, when measuring either proton translocation or ATP hydrolysis. A possible explanation for these discrepancies is that the reconsituted preparation contains several types of ATPase molecule, of different subunit composition or in different environments, not all of which are capable of proton translocation. The ATPase activity of our reconsituted preparation is insensitive to vanadate, so contamination with ATPase II can be excluded; similarly the Triton X-114

fractionation procedure, used in the first stage of purification, removes F_1F_0-ATPase [10]. In any case results such as those shown in Fig. 1, with Hill coefficients greater than 1.0, cannot arise through enzyme inhomogeneity, and we conclude that the cooperativity induced by ADP is a real effect, occurring in the form of the ATPase seen in the assay for proton translocation. That such effects occur when ATP hydrolysis is studied are confirmed by the data of Moriyama and Nelson [23], but a more detailed study of the effects of ADP on ATP hydrolysis is clearly necessary.

Mechanistic implications. The kinetic model (model 4) that best fits the kinetic data has a number of features that should be amenable to testing by other experimental means. There are three catalytic nucleotide-binding sites, which bind ATP, GTP or ITP (as their magnesium complexes), and at which MgADP binds competitively. There is one regulatory nucleotide-binding site, which binds nucleoside diphosphates very tightly ($K_d < 1$ μM). The enzyme undergoes a ligand-induced conformational change; in the absence of ADP it is almost completely in the R (active) state.

Analysis of the closely similar V-ATPase isolated from bovine brain clathrin-coated vesicles has suggested that it contains three copies each of subunits A (72 kDa) and B (57 kDa) [27]. It is established that the 72-kDa subunits contain the catalytic sites [2], and our kinetic results, suggesting three nucleoside-triphosphate-binding sites, are therefore in agreement with the proposed subunit stoichiometry. The sequence similarity between the A and B subunits, and their evolutionary relationship to the β and α, subunits, respectively, of F-type ATPases [4], suggest that the B subunits might contain the regulatory nucleotide-binding site, and the 57-kDa B subunit of the V-ATPase from beet tonoplast was shown to be labelled by a covalently reacting ATP analogue [28]. Since there are apparently three copies of subunit B, our kinetic results would imply either that the T state of the enzyme, at least, is highly asymmetric and able to bind only one nucleotide in its regulatory sites, or that some of the regulatory sites are already filled when the enzyme is isolated. We have not attempted to measure bound nucleotide in the enzyme, but the latter explanation seems unlikely in view of the Michaelis-Menten kinetics observed in the absence of added ADP, and the effects of added ADP at low concentration. It is noteworthy that the 39-kDa subunit, probably present in a single copy [27], can also be labeled by ATP analogues [23]. We have been unable to assign tight MgADP binding to a particular subunit, but the kinetics of protection of the catalytic site by MgADP from alkylation by *N*-ethylmaleimide are consistent with a MgADP-induced conformation change that reduces the reactivity of the essential cysteine, with complete protection at higher MgADP concentrations; furthermore the kinetics of *N*-[^{3}H]ethylmaleimide incorporation into the 72-kDa subunit A show that the three copies behave identically, confirming that the R state of the enzyme is symmetrical (Webster, L. C., unpublished results).

Important assumptions are made in all of the models tested: that equilibrium binding of the substrates applies; that the rate of the reaction is proportional to the fraction of catalytic sites occupied by nucleoside triphosphate; and that within a given state of the enzyme the (three) catalytic sites are equivalent. We do not have an accurate estimate of k_{cat} (see [9]), but given that nucleotide binding is likely to be diffusion controlled, with a k_{on} around 10^8 M^{-1} s^{-1}, it should be much faster than catalysis even at the lowest concentrations used here. The assumption of symmetry is supported by the alkylation work mentioned above, but is clearly not applicable to the related F-type ATPases [29], and the situation in the V-ATPases requires direct investigation by other means. The observations [23], confirmed by us, of activation by MgCTP and MgUTP, and of tight and loose binding sites for 2′,3′-*O*-(2,4,6-trinitrophenyl) adenosine triphosphate [30], may be relevant here, but the subunit locations of the binding sites for these nucleotides have not been determined.

The physiological significance of the inhibition by MgADP is at present unclear. The value of K_i deduced from model fitting is very small (< 0.1 μM) but since the value of L is also small ADP only becomes an effective inhibitor at much higher concentrations (> 1 μM) which are in the physiological range. This regulatory feature is not confined to the mammalian V-ATPase: preliminary results with an enzyme from plant tonoplast were similar [16].

This work was supported by a grant from the Wellcome Trust, and by the award of a Spanish Government Postgraduate Studentship to J. R. P.-C. We thank Dr M. B. Dutia, Department of Physiology, University of Edinburgh, for help in setting up the data-collection system.

REFERENCES

1. Pedersen, P. L. & Carafoli, E. (1987) Ion motive ATPases. I. Ubiquity, properties and significance to cell function, *Trends Biochem. Sci. 12*, 146–150.
2. Forgac, M. (1989) Structure and function of vacuolar class of ATP-driven proton pumps, *Physiol Rev. 69*, 765–796.
3. Nelson, N. (1992) Organellar proton-ATPases, *Curr. Opin. Cell Biol. 4*, 654–660.
4. Kibak, H., Taiz, L., Starke, T., Bernasconi, P. & Gogarten, J. P. (1992) Evolution of structure and function of V-ATPases, *J. Bioenerg. Biomembr. 24*, 415–424.
5. Thom, M. & Komor, E. (1994) Effect of magnesium and ATP on ATPase of sugarcane vacuoles, *Planta (Heidelb.) 161*, 361–365.
6. Bennet, A. P., O'Neill, S. A., Eilman, M. & Spanswick, R. M. (1985) H^+-ATPase activity from storage tissue of *Beta vulgaris*, *Plant Physiol. (Bethesda) 78*, 495–499.
7. Arai, M., Pink, S. & Forgac, M. (1989) Interactions of anions and ATP with the coated vesicle proton pump, *Biochemistry 28*, 3075–3082.
8. Johnson, R. C., Beers, M. F. & Scarpa, A. (1982) H^+-ATPase of chromaffin granules, *J. Biol. Chem. 257*, 10701–10707.
9. Hanada, H., Moriyama, Y., Maeda, M. & Futai, M. (1990) Kinetic studies of chromaffin granules H^+-ATPase and effects of Bafilomycin A_1, *Biochem. Biophys. Res. Commun. 170*, 873–878.
10. Percy, J. M., Pryde, J. G. & Apps, D. K. (1985) Isolation of ATPase I, the proton pump of chromaffin granule membranes, *Biochem. J. 231*, 557–564.
11. Moriyama, Y. & Nelson, N. (1988) Purification and properties of a vanadate- and *N*-ethylmaleimide-sensitive ATPase from chromaffin granule membranes, *J. Biol. Chem. 263*, 8521–8527.
12. Bennett, A. B. & Spanswick, R. M. (1983) Optical measurement of ΔpH and $\Delta\Psi$ in corn root membrane vesicles: kinetic analysis of Cl^- effects on a proton-translocating ATPase, *J. Membr. Biol. 71*, 95–107.
13. Flatmark, T., Grønberg, M., Husebye, E. Jr & Berge, S. V. (1985) The assignment of the Ca^{2+}-ATPase activity of the chromaffin granule to the proton pump, *FEBS Lett. 182*, 25–30.
14. Pérez-Castiñeira, J. R. & Apps, D. K. (1990) Vacuolar H^+-ATPases of adrenal secretory vesicles. Rapid partial purification and reconstitutiton into proteoliposomes, *Biochem. J. 271*, 127–131.
15. Warren, M., Smith, J. A. C. & Apps, D. K. (1992) Rapid purification and reconstitution of a plant vacuolar ATPase using Triton X-114 fractionation: subunit composition and substrate kinetics of the H^+-ATPase from the tonoplast *of Kalanchoë daigremontiana*, *Biochim. Biophys. Acta 1106*, 117–125.
16. Apps, D. K., Pérez-Castiñeira, J. R., Warren, M. & Atkins, G. L. (1992) Reconstitution and kinetics of vacuolar H^+-translocating ATPases from plants and animals, *Biochem. Soc. Trans. 20*, 245S.
17. Pryde, J. G. & Phillips, J. H. (1986) Fractionation of membrane proteins by temperature-induced phase separation in Triton X-

114. Application to subcellular fractions of the adrenal medulla, *Biochem. J. 233*, 525–533.
18. Garewal, H. S. (1973) A procedure for estimation of microgram quantities of Triton X-100, *Anal. Biochem. 54*, 319–324.
19. Nelson, N. (1980) Coupling factors from higher plants, *Methods Enzymol. 69*, 301–313.
20. Phillips, R. (1966) Adenosine and the adenine nucleotides. Ionization, metal complex formation and conformation in solution, *Chem. Rev. 66*, 501–527.
21. Gardner, M. L. G. & Atkins, G. L. (1982) Kinetic analysis of transport processes in the intestine and other tissues, *Clin. Sci. (Lond.) 63*, 405–414.
22. Monod, J., Wyman, J. & Changeaux, J. P. (1965) On the nature of allosteric transitions: a plausible model, *J. Mol. Biol. 12*, 88–118.
23. Moriyama, Y. & Nelson, N. (1987) Nucleotide binding sites and chemical modification of the chromaffin granule proton ATPase, *J. Biol. Chem. 262*, 14723–14729.
24. Jennings, I. R., Rea, P. A., Leigh, R. A. & Sanders, D. (1988) Quantitative and rapid estimation of H^+ fluxes in membrane vesicles: software for analysis of fluorescence quenching and relaxation, *Plant Physiol. (Bethesda) 86*, 1257–1263.
25. Fregni, V. & Casadio, R. (1993) Kinetic characterization of the ATP-dependent proton pump in bacterial photosynthetic membranes: a study with the probe 9-amino-6-chloro-2-methoxyacridine, *Biochim. Biophys. Acta 1143*, 215–222.
26. Grønberg, M. & Flatmark, T. (1987) Studies on Mg^{2+}-dependent ATPase in bovine adrenal chromaffin granules, *Eur. J. Biochem. 164*, 1–8.
27. Arai, H., Terres, G., Pink, S. & Forgac, M. (1988) Topography and subunit stoichiometry of the coated vesicle proton pump, *J. Biol. Chem. 263*, 8796–8802.
28. Manolson, M. F., Rea, P. A. & Poole, R. J. (1985) Identification of 3-*O*-(4-benzoyl)benzoyladenosine 5′-triphosphate- and *N*,*N*′-dicyclohexylcarbodiimide-binding subunits of a higher plant H^+-translocating tonoplast ATPase, *J. Biol. Chem. 260*, 12273–12279.
29. Boyer, P. D. (1993) The binding change mechanism for ATP synthase – some probabilities and possibilities, *Biochim. Biophys. Acta 1140*, 215–250.
30. Adachi, I., Arai, H., Pimental, R. & Forgac, M. (1990) Proteolysis and orientation on reconstitution of the coated vesicle proton pump, *J. Biol. Chem. 265*, 960–966.

Interaction of vacuolar-type H^+-ATPases with fluorescent organotin-flavone complexes

LORNA C WEBSTER,*DAVID E GRIFFITHS and DAVID K APPS

Department of Biochemistry, University of Edinburgh, Hugh Robson Building, George Square, Edinburgh EH8 9XD and *Department of Chemistry, University of Warwick, Coventry CV4 7AL

Although regarded as a distinct class of proton-pumps, the vacuolar (V-type) H^+-ATPases have considerable structural homology with F-type ATP synthases (F_1F_O-ATPases) [1] and are inhibited by several agents in common, including DCCD and trialkyltins [2]. Recently the synthesis of a novel series of pentacoordinate organotin flavone complexes was described [3]; these are potent inhibitors of mitochondrial ATPase, and in some cases the fluorescence of the complex is enhanced on binding to the enzyme. They appear to bind to the F_O segment of the ATPase, although to which subunit is as yet unknown, and can be used to titrate this component in mitochondrial membranes and in derived preparations of F_1F_O-ATPase and of F_O [4].

We now report the interaction of dibutyltin-3-hydroxy - flavone bromide (Bu_2Sn(of)) with membranes containing V-type ATPases, and with the purified, reconstituted V-type H^+-ATPase of bovine chromaffin granule membranes.

Fig.1 shows the enhancement of fluorescence of a fixed concentration of Bu_2Sn(of) when various gradient-purified membranes are added. The wavelengths of excitation and emission were 395nm and 450 nm, respectively, and fluorescence readings are corrected for light-scattering. The specific enhancement (ΔF/mg protein) correlates with the expected content of V-type ATPase and is 89 (tonoplast of *Kalanchoe daigremontiana*), 28 (bovine chromaffin granule membranes), 12 (bovine kidney microsomes), 10 (rat insulinoma granule membranes), 5.5 (bovine pituitary dense granule membranes), and 6.5 (rat liver microsomes). Bovine erythrocyte 'ghosts', used as a control in this experiment, have only a low specific enhancement (1.9).

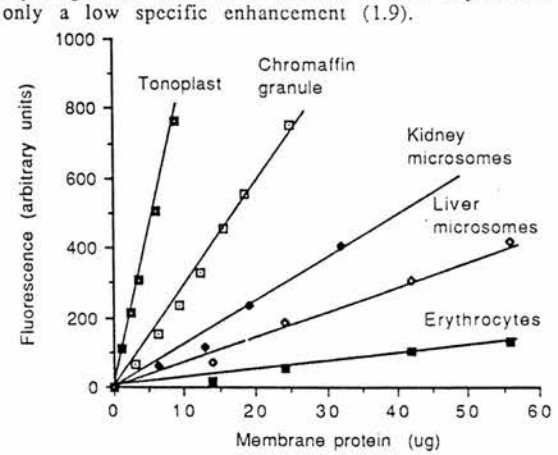

Fig.1. Titration of dibutyltin-3-hydroxyflavone bromide with purified membranes.

The specific fluorescence enhancement by proteo-liposomes containing the purified chromaffin granule H^+-ATPase [5] was some fivefold greater than that by the purified membranes (data not shown), strongly suggesting that Bu_2Sn(of) binds to the ATPase. Control liposomes, containing phospholipid and cholesterol but no ATPase, produce only a minimal enhancement of fluorescence.

Titration of these proteoliposomes (2.0 µg protein) with Bu_2Sn(of) showed that the fluorescence of the complex was enhanced approximately 55-fold on interaction with the enzyme, which was half-saturated at approximately 0.7 µM Bu_2Sn(of). This enhancement is decreased in the presence of alkyl-tin complexes such as tributyltin chloride (Fig.2) suggesting competion between this inhibitor and the fluorescent tin complex, for the binding-site; furthermore back-titration with tributyltin chloride after saturation of the membranes with Bu_2Sn(of) produces a progressive and complete abolition of the fluorescence enhancement, confirming the reversibility of binding.

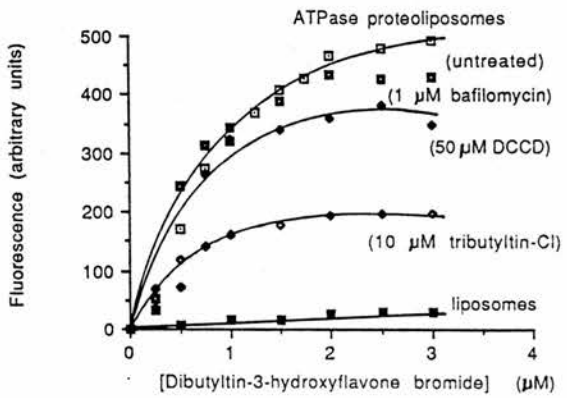

Fig.2 Titration of ATPase proteoliposomes with dibutyltin-3-hydoxyflavone bromide.

As other F_O inhibitors, paricularly venturicidin, affect the interaction of Bu_2Sn(of) with F-type ATPases (Griffiths and Usta, unpublished), various inhibitors of V-type ATPases were tested for their effects on the interaction of the enzyme with tin complexes. Bafilomycin A_1 (at 1 µM, a concentration far above that required for complete inhibition) had no significant effect on Bu_2Sn(of) fluorescence enhancement, while pretreatment of the proteoliposomes with DCCD (50 µM, pre-incubated for 12 h) had only a slight, though reproducible, effect (Fig.2). The site of interaction of the fluorescent tin complexes with V-ATPases is therefore unclear.

Dibutyltin-3-hydoxyflavone may be a useful probe in analysing the structure/function relationship of the V-ATPases. Its site of interaction remains to be demonstrated: we have failed to find any binding to isolated V_O segments of chromaffin granule ATPase (unpublished work). The large fluorescence enhancement on binding may be useful in quantifying the enzymes in membrane preparations or during purification, but is not specific to this class of ATPases, and provides further evidence of structural homology between V-type and F-type proton pumps.

This work was supported by a grant from the Wellcome Trust to D.K.A.

1. Nelson, N. (1992) Curr. Op. Cell Biol. **4**, 654-660
2. Apps, D.K., Pryde, J.G., Sutton, R. & Phillips, J.H. (1980) Biochem. J. **190**, 273-282
3. Usta, J. & Griffiths, D.E. (1992) Biochem. Biophys. Res. Comm. **188**, 365-371
4. Usta, J. & Griffiths, D.E. (1993) Appl. Organomet. Chem. **7**, (in press)
5. Pérez-Castiñeira, J.R. & Apps, D.K. (1988) Biochem. J. **271**, 127-131